

THE EFFECT OF PROPYLENE PRESSURE ON SHAPE-SELECTIVE ISOPROPYLATION OF BIPHENYL OVER H-MORDENITE

Y. Sugi, X. Tu^{a)}, T. Matsuzaki, T. Hanaoka, Y. Kubota, J.-H. Kim^{b)}, and M. Matsumoto^{a)}

National Institute of Materials and Chemical Research, AIST, Tsukuba, Ibaraki 305, Japan

^{a)}Research and Development Center, Osaka Gas Co., Ltd., Osaka 554, Japan

^{b)}Department of Materials Science, Tottori University, Tottori 680, Japan

Keywords: shape-selectivity, acid site, isomerization

INTRODUCTION

Catalytic alkylation of aromatics using zeolites has been the subject of much research, because it is essential to match the dimensions between reactants, products, and zeolite pore to achieve highly shape-selective catalysis [1,2]. H-Mordenites have been found as potential catalysts for the shape-selective alkylation of polynuclear aromatics such as biphenyl [3-9], naphthalene [10-14], and terphenyl [15]. We previously described the activity and the selectivity of the slimmest DIPB isomers, 4,4'-DIPB, were enhanced by the dealumination because of reactions inside pores, and discussed the participation of external acid sites for the H-mordenite with the low SiO₂/Al₂O₃ ratio because the pores were choked by coke-deposition [3-7]. However, mechanisms of the catalysis by acid sites and of the steric requirement of substrate and products in mordenite pores have not been fully understood.

In this paper, we describe the effect of propylene pressure on the isopropylation of biphenyl over a highly dealuminated H-mordenite, and discuss the role of acid sites at intracrystalline and external surfaces.

EXPERIMENTAL

Catalysts and reagents. H-Mordenite (HM(220), SiO₂/Al₂O₃ = 220) was obtained from Tosoh Corporation, Tokyo, Japan, and calcined at 500 °C just before use for the reactions. Biphenyl and propylene were purchased from Tokyo Kasei Co. Ltd., Tokyo, Japan, and used without further purifications.

Alkylation. The alkylation was carried out without solvent using a 100 or 200 ml autoclave. Oxygen in the autoclave containing biphenyl and HM(220) was purged out with flashing N₂ before heating. After reaching reaction temperature, propylene was supplied to the autoclave and kept at a constant pressure throughout the reaction. A standard set of the reaction included: 200 mmol of biphenyl, 2 g of HM(220), 0.8 MPa of propylene pressure, and 250 °C of temperature. Propylene pressure was expressed by the difference between before and after the introduction of propylene.

Isomerization of 4,4'-DIPB. The isomerization of 4,4'-DIPB was examined under the condition as follows: 100 mmol of 4,4'-DIPB, 1 g of HM(220), 0-0.8 MPa of propylene pressure, 250 °C of temperature, and 4 h of period.

Product analysis. The products were analyzed with a HP-5890 GC equipped with a 25 ml Ultra-1 capillary column, and identified with a HP-5978 GC-MS. The yield of every product was calculated on the basis of biphenyl used for the reaction, and the selectivities of each IPBP and DIPB isomers are expressed as:

$$\text{Selectivity of DIPB (IPBP) isomers} = \frac{\text{Each DIPB (IPBP) isomer (mmol)}}{\text{Total DIPB (IPBP) isomers (mmol)}}$$

RESULTS and DISCUSSION

Effects of propylene pressure on the isopropylation

The isopropylation over HM(220) reached to above 80 % of conversion within 800 min at 250 °C under every propylene pressure among 0.1-0.8 MPa as shown in Fig. 1. No significant effect of propylene pressure was observed in the initial rate of the isopropylation although there were some differences in the late stage. These results showed that primarily principal reaction was the alkylation over HM(220) under every pressure. Figure 2 shows the profile of the formation of isopropylbiphenyl (IPBP), diisopropylbiphenyl (DIPB), and trisopropylbiphenyl (TriPB) isomers expressed on the basis of the conversion of biphenyl under various propylene pressures. The yield of products under every pressure was on the same plot. These profiles show that the alkylation proceeds by the same reaction paths under every propylene pressure.

Figure 3 shows the effect of pressure on the yield of 4- and 3-IPBP. No significant effects of propylene pressure on the yields were observed. The yield of 4-IPBP reached the maximum at 50-60 % conversion, and decreased as further alkylation proceeded. On the other hand, the yield of 3-IPBP increased monotonously with the conversion of biphenyl. The predominant formation of 4-IPBP in the isopropylation of biphenyl to IPBP isomers occurs through the shape selective catalysis inside the pores at any propylene pressures. The isomerization of IPBP isomers was not observed under these conditions. The difference of the formation of 4- and 3-IPBP isomers can be understood on the difference of their participation to form DIPB isomers. The profiles of 3- and 4-IPBP shows that 4-IPBP is a sole precursor to produce DIPB isomers, and that 3-IPBP does not participate to the formation of 3,4'-DIPB, at least, except the late stage of the reaction. Highly selective formation of 4,4'-DIPB is also ascribed to the shape selective catalysis inside H-mordenite pores. The higher selectivity of 4,4'-DIPB compared to that of 4-IPBP shows that the isopropyl group of 4-IPBP gives more severe restriction than the hydrogen group of biphenyl at the transition states between propylene, biphenyl, and acid sites in the pores.

The formation of 4,4'-DIPB over HM(220) was much influenced by propylene pressure as shown in Fig. 4. The selectivities were as high as 80 % under all pressure conditions at early stages, and kept almost constant during the reaction under higher pressures than 0.3 MPa. However, the decrease of the selectivity was observed under lower pressures than 0.2 MPa, although no significant effects of pressure on the selectivities were observed in the formation of IPBP isomers. The decrease of the selectivity of 4,4'-DIPB corresponded to the increase of that of 3,4'-DIPB. The yields of 4,4'- and 3,4'-DIPB were in linear relations to the yield of combined DIPB isomers under higher pressure than 0.3 MPa. These results show that the alkylation occurs in steady state under high propylene pressures. The yield of 4,4'-DIPB under such a low pressure as 0.1 MPa was deviated downwards from the linear plot under higher pressures, and the upward deviation occurred for the yield of 3,4'-DIPB. The amount of 4,4'-DIPB decreased after reaching the maximum at higher conversion. The increase of the yield of 3,4'-DIPB corresponded to the decrease of the case of 4,4'-DIPB. These results show that the decrease of the selectivity of 4,4'-DIPB is not due to the change of shape-selectivity of the pore, but to its isomerization to 3,4'-DIPB because 3,4'-DIPB is more thermodynamically stable isomer than 4,4'-DIPB. The analysis of the products encapsulated inside the pores after the reaction showed that the distribution of 4,4'-DIPB was as high as 90 % under every propylene pressure [16].

Further isopropylation of 4,4'-DIPB occurred only in a small amount even under high propylene pressure. This means that alkylation of 4,4'-DIPB is prevented in the pore. H-mordenite pore allows the formation of 4- and 3-IPBP, and 4,4'- and 3,4'-DIPB, while the formation of TriPB is forbidden in the pore.

Takahata and his co-workers found also the increase of the selectivity of 4,4'-DIPB with raising propylene pressure over H-mordenite with the low $\text{SiO}_2/\text{Al}_2\text{O}_3$ ratio [17]. Fellmann proposed that the increase of the selectivity was ascribed to the steric crowding with accumulation of propylene at the active sites [18]. However, our results show that the change of the selectivity of 4,4'-DIPB with propylene pressure is due to the isomerization of 4,4'-DIPB by preferential adsorption of propylene at the external surface as discussed above.

The behavior of 4,4'-DIPB under propylene pressure

The behavior of 4,4'-DIPB during the reaction is one of the essential factors for product distributions. Figure 5 shows the stability of 4,4'-DIPB in the presence of propylene pressure over HM(220). Without propylene or under low propylene pressure, 4,4'-DIPB was isomerized significantly to 3,4'-DIPB accompanying IPBP isomers formed by the dealkylation. However, the formation of 3,4'-DIPB decreased with the increase of propylene pressure. These tendencies correspond well with the influences of propylene pressure in the alkylation. 4,4'-DIPB was found as exclusive isomer encapsulated in H-mordenites under these conditions [16]. These results lead us to conclude that active sites for the isomerization of 4,4'-DIPB are not inside the pores, but at external surface. The inhibition of the isomerization under high propylene pressure show that propylene adsorbs more preferentially than 4,4'-DIPB does. Adsorbed propylene prevents the adsorption of 4,4'-DIPB, and retards its isomerization. However, the adsorption of 4,4'-DIPB predominates over that of propylene under low propylene pressure to result in the enhancement of its isomerization.

Further isopropylation of 4,4'-DIPB under the conditions was observed only in small amounts even under high propylene pressure; i.e., the alkylation of 4,4'-DIPB is prevented inside the pores. This is one of the reasons why shape-selective isopropylation occurs in the catalysis of H-mordenite. H-mordenite pore allows the formation of 3- and 4-IPBP, and 4,4'- and 3,4'-DIPB, while the formation of TriPB is forbidden in the pores. The higher steric restriction of 3,4'-DIPB compared with that of 4,4'-DIPB results in the lowly formation of 3,4'-DIPB because molecular diameter of the former isomer is bigger than that of the latter. The relatively high amount of TriPB was observed in the isomerization of 4,4'-DIPB under 0.1 MPa. TriPB is formed by the alkylation of DIPB isomers at the external surface because of low propylene pressure.

Mechanistic aspects on the catalysis

The isopropylation of biphenyl over H-mordenite occurred inside the pores by successive addition of propylene to biphenyl. Principal factor controlling the catalysis is ascribed to steric restriction at the transition state composing biphenyl, propylene, and acid sites. Predominant formation of 4-IPBP in the isopropylation of biphenyl to IPBP isomers proceeds through the shape selective catalysis inside the pores. The difference of 4- and 3-IPBP isomers for their formation and for their alkylation to DIPB isomers is ascribed to the difference of their accommodations inside the pores. 4-IPBP is a sole precursor to form DIPB isomers, and that 3-IPBP does not participate in the formation of 3,4-DIPB. Higher selectivity of 4,4'-DIPB compared with that of 4-IPBP is due to the bulkiness of 4'-isopropyl group in 4-IPBP.

Propylene pressure changed significantly the selectivity of DIPB isomers in the isopropylation of biphenyl over H-mordenite. The isomerization of 4,4'-DIPB occurred under low pressure of propylene. However, total formations of IPBP and DIPB isomers were on the same profiles under any propylene pressure. This means that the isomerization occurs after the formation of 4,4'-DIPB. The distribution of 4,4'-DIPB encapsulated in the pores was highly selective under any pressures [16]. These results support that the isomerization of 4,4'-DIPB occurs at the external acid sites. The isomerization under high propylene pressures is prevented by the preferential adsorption of propylene on the acid sites, whereas under low propylene pressure, the adsorption of 4,4'-DIPB predominates over that of propylene, and thus, the isomerization of 4,4'-DIPB occurs at external acid sites.

The high selectivity of 4,4'-DIPB during the isopropylation suggests that the difference of the rate among acid sites at intracrystalline and external surface is not so significant. It also reflects the amount of acid sites at the surfaces.

REFERENCES

1. S. Csicsery, *Zeolites*, 4 (1984) 203.
2. Y. Sugi and M. Toba, *Catal. Today*, 19 (1994) 187.
3. T. Matsuzaki, Y. Sugi, T. Hanaoka, K. Takeuchi, T. Tokoro, and G. Takeuchi, *Chem. Express*, 4 (1989) 413.
4. Y. Sugi, T. Matsuzaki, T. Hanaoka, K. Takeuchi, T. Tokoro, and G. Takeuchi, *Chemistry of Microporous Crystals (Stud. Surf. Sci. Catal., vol. 60)*, T. Inui, S. Namba, T. Tatsumi (eds.), Kodansha, Tokyo, and Elsevier, Amsterdam, 1991, pp. 303-330.
5. X. Tu, M. Matsumoto, T. Matsuzaki, T. Hanaoka, Y. Kubota, J.-H. Kim, and Y. Sugi, *Catal. Lett.*, 21 (1993) 71.
6. Y. Sugi, T. Matsuzaki, T. Hanaoka, Y. Kubota, J.-H. Kim, X. Tu, and M. Matsumoto, *Catal. Lett.*, 27 (1994) 315.
7. Y. Sugi, T. Matsuzaki, T. Takeuchi, T. Hanaoka, T. Tokoro, X. Tu, and G. Takeuchi, *Sekiyu Gakkaishi*, 37 (1994) 376.
8. G.S. Lee, J.J. Maj, S.C. Roake, and J.M. Garces, *Catal. Lett.*, 2 (1989) 243.
9. T. Matsuda and E. Kikuchi, *Zeolites and Microporous Crystals (Stud. Surf. Sci. Catal., vol. 83)*, T. Hattori and T. Yashima (eds.), Kodansha, Tokyo, and Elsevier, Amsterdam, 1994, pp. 295-302.
10. A. Katayama, M. Toba, G. Takeuchi, F. Mizukami, S. Niwa, and S. Mitamura, *J. Chem. Soc., Chem. Commun.*, (1991) 31.
11. P. Moreau, A. Finiels, P. Geneste, and J. Solofo, *J. Catal.*, 136 (1992) 487.
12. Y. Sugi, J.-H. Kim, T. Matsuzaki, T. Hanaoka, Y. Kubota, X. Tu, and M. Matsumoto, *Zeolite and Related Microporous Materials: State of the Art 1994 (Stud. Surf. Sci. Catal., vol. 84)*, J. Weitkamp, H.G. Karge, and W. Hölderich (eds.), Elsevier, Amsterdam, 1994, pp. 1837-1844.
13. C. Song and S. Kirby, *Microporous Materials*, 2 (1994) 467.
14. J.-H. Kim, Y. Sugi, T. Matsuzaki, T. Hanaoka, Y. Kubota, M. Matsumoto, and X. Tu, *Microporous Materials*, in press.
15. G. Takeuchi, H. Okazaki, M. Yamae, and K. Kito, *Appl. Catal.*, 76 (1991) 49.
16. unpublished results.
17. K. Takahata, M. Yasuda, and H. Miki, *Jpn. Tokkyo Kokai*, 88-122635.
18. J. Fellmann, *Catalytica Highlights*, 17 (1991) 1.

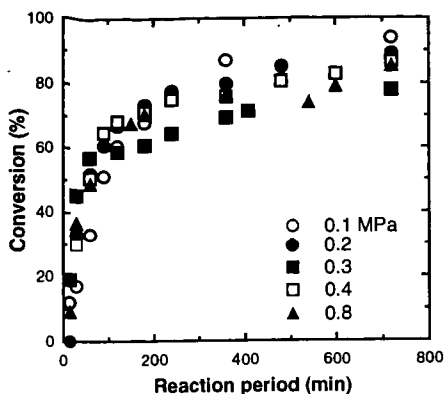


Fig. 1 Effect of propylene pressure on catalytic activity of HM(220) in the isopropylation of biphenyl. Reaction conditions: biphenyl 400 mmol, HM(220) 2 g, propylene pressure 0.1-0.8 MPa, temperature 250 °C.

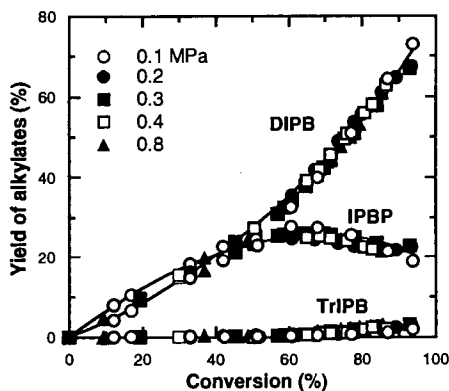


Fig. 2 Product Profile of the isopropylation of biphenyl. Reaction conditions were the same as Fig. 1.

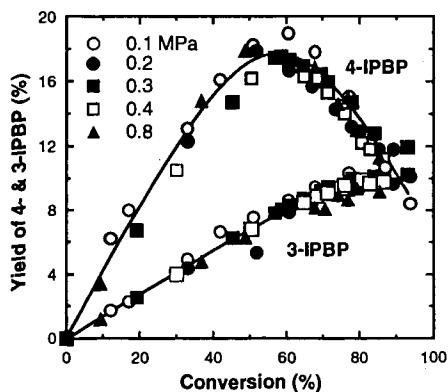


Fig. 3 Effect of propylene pressure on the yield of 4- and 3-IPBP over HM(220). Reaction conditions were the same as Fig. 1.

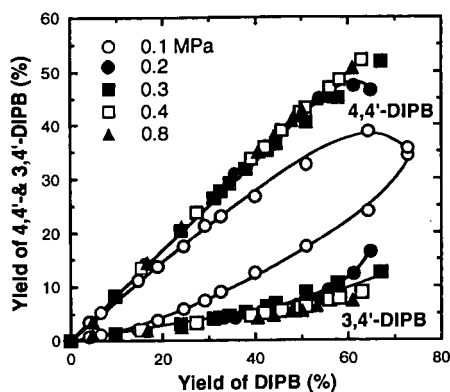


Fig. 4 Effect of propylene pressure on the yield of 4,4'- and 3,4'-DIPB over HM(220). Reaction conditions were the same as Fig. 1.

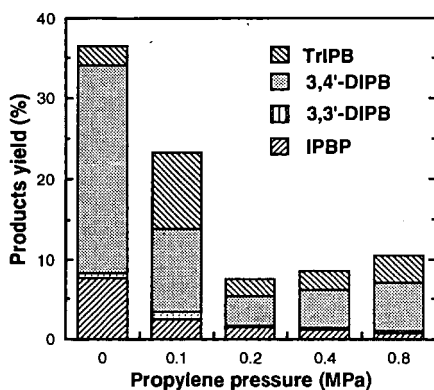


Fig. 5 Effect of propylene pressure on the isomerization of 4,4'-DIPB over HM(220). Reaction conditions: 4,4'-DIPB 100 mmol, HM(220) 1 g, temperature 250 °C, period 4 h.

SELECTIVE DIALKYLATION OF NAPHTHALENE WITH HINDERED ALKYLATING AGENTS OVER HM AND HY ZEOLITES UNDER LIQUID PHASE CONDITIONS.

Patrice Moreau, Annie Finiels, Patrick Geneste, Frédéric Moreau and Jonis Solofo.

Laboratoire de Matériaux Catalytiques et Catalyse en Chimie Organique, URA CNRS 418, Ecole Nationale Supérieure de Chimie, 8 rue de l'Ecole Normale, 34053 MONTPELLIER Cedex 1, FRANCE.

Keywords: zeolites, shape-selective alkylation, naphthalene, heterogeneous catalysis.

INTRODUCTION

Whereas the use of zeolite catalysts has been widely investigated for the shape-selective conversions of mononuclear aromatic hydrocarbons, such as alkylation of toluene or isomerization of xylenes¹⁻³, in contrast relatively few reports are available on the conversion of polynuclear aromatics, such as naphthalene derivatives. Among the latter, 2,6-dialkylnaphthalenes are the most valuable compounds, since, as precursors of 2,6-naphthalene dicarboxylic acid, they are potentially useful raw materials for production of high quality polyester fibers and plastics⁴ and of thermotropic liquid crystal polymers⁵.

The interest of such derivatives was shown, in the recent years, by the increasing number of patents relevant to their preparation and separation. Following the pioneering work of Fraenkel et al.⁶ on the alkylation of naphthalene with methanol over various zeolites, much attention has been paid, in the early nineties, to studies on the activity and selectivity of zeolites in the isopropylation of naphthalene⁷⁻⁹. The interest of the use of bulky substituents in such reactions over zeolites has been clearly demonstrated by recent papers¹⁰⁻¹².

The present communication is concerned with the results obtained in the alkylation of naphthalene over a series of HM and HY zeolites, using isopropyl bromide, cyclohexyl bromide and cyclohexene as alkylating agents, under liquid-phase conditions, leading to a better regulation of the reaction pathway.

EXPERIMENTAL

Materials. Analytical grade cyclohexane, isopropyl bromide, cyclohexyl bromide, cyclohexene and naphthalene (Aldrich Chemical) were used as supplied.

Catalysts. H mordenite (Zeolon 100-H, Si/Al = 6.9 from Norton) and three dealuminated mordenites were used for the isopropylation reactions. The dealuminated mordenites were prepared, according to the published procedure¹³, from Zeolon 100-H (HM) by treatment in 1M HCl solution at 100°C for 3 h or refluxing in 3 M HCl solution for 6 h or in 6 M HCl solution for 12 h. The resulting powders, washed and oven dried at 110°C, had Si/Al atomic ratios of 9 (HM₁), 13.1 (HM₂), and 20.6 (HM₃). The HY catalyst was derived from the thermal decomposition of NH₄Y (Linde SK 41, Si/Al = 2.5 from Union Carbide). The US-HY was supplied by Chemisch Fabrik Uetikon, Zürich (Z6-05-01, Si/Al = 2.5). The CVD-modified zeolites were obtained according to the silanation procedure⁹, and fully characterized by various technics¹⁴.

For the cyclohexylation reactions, the US-HY used was the same as above. The dealuminated HY (Si/Al = 19.5) and HM (Si/Al = 10.8) were from Zeocat, Montoir de Bretagne (ZF 520 and ZM 510).

Catalytic runs. The isopropylation of naphthalene was carried out in a 0.1 liter stirred autoclave reactor (Sotelem). In a typical run, the autoclave was charged with 1 g of zeolite freshly calcined in air at 500°C, a mixture of 5 mmol naphthalene and 10 mmol isopropyl bromide in 50 ml of cyclohexane and heated to 200°C. Samples were withdrawn periodically and analyzed by GLC (Altech OV1 capillary column, 10 m or 25 m x 0.25mm).

The same procedure and analysis technic were used for cyclohexylation reactions with cyclohexyl bromide. When cyclohexene was used, the procedure was the following: the autoclave was charged with naphthalene (5 mmol), cyclohexane (50 ml) and the catalyst (1 g), and heating was started; cyclohexene (10 mmol) was then added, drop by drop, by means of a stainless steel pressurized funnel, and the

mixture was stirred in the same conditions as above.

For the isolation and purification of 2,6-dicyclohexylnaphthalene, the procedure was the following: after cooling, the catalyst was filtered and cyclohexane evaporated; the crude product solidified at room temperature, the solid was then filtered and recrystallized from ethanol (mp 152°C after two recrystallizations). The structure was confirmed by GC-MS, ^1H and ^{13}C NMR spectroscopy together with X-ray crystallography¹⁵.

RESULTS AND DISCUSSION

Isopropylation reaction over HM and HY zeolites. The isopropylation of naphthalene with isopropyl bromide over a series of mordenites and Y zeolites show that both conversion and selectivity depend largely upon the nature and the structure of the catalyst. The main results, obtained in this study and reported in Table 1, can be summarized as follows:

- mordenites are less active than Y zeolites;
- in both cases, a high β -selectivity is found, leading to the selective formation of 2-isopropylnaphthalene and a mixture of 2,6- + 2,7-diisopropylnaphthalenes;
- the formation of trialkylnaphthalenes cannot be avoided over untreated zeolites.

The origin of the high β -selectivity observed is different depending on the zeolite. Over H-mordenites, such a selectivity is explained as the result of transition-state shape selectivity, due to the constrained environment in the channels of the mordenite; the steric hindrance of the 1-isopropylnaphthalene (α -isomer) does not allow its formation inside the tight one-dimensional tunnels of the zeolite. Over Y zeolites, the β -selectivity has been shown to be due to a thermodynamic equilibrium favorable to the 2-isopropylnaphthalene; the 1-isopropylnaphthalene (kinetic product) is initially formed inside the three-dimensional large-pore structure of Y zeolites, and it is then rearranged into the 2-isomer (thermodynamic product) at high temperatures.

Over the two kinds of zeolites, 2,6- and 2,7-diisopropylnaphthalenes are the main disubstituted derivatives. Such a result is expected taking into account the β -selectivity observed in the monoisopropylation step, whatever the origin of this selectivity.

In both cases, in our experimental conditions, the same distribution between the 2,6- and 2,7- isomers (2,6-/2,7- ratio = 1) is observed; such a result seems not surprising, if we consider that these two isomers have the same kinetic diameter (6.5Å), and that their production and subsequent diffusion in the pores or cavities of zeolites occur in the same way. Nevertheless, a higher 2,6-/2,7- ratio is generally observed over mordenites by some authors^{7,8,10}; various assumptions, such as differences in diffusion rates or in the ease of transition-state formation for the two isomers, might explain these higher ratios, obtained in different experimental conditions.

These results are very encouraging regarding the efficiency of the catalytic activity of zeolites in isopropylation of naphthalene and their shape selectivity properties. Nevertheless, the selective formation of the 2,6-isomer is not possible in any case. The possibility of an improvement of such a selectivity has then been considered by the use of either modified zeolites or more hindered alkylating agents.

Isopropylation over CVD-modified zeolites. Shape-selectivity of zeolites may be improved by reducing the number of active sites of the external surface. It is known that silanation of zeolites leads not only to such a deactivation of the outer active sites but also to a uniform control of the pore-opening size of the zeolite^{16,17}. The "chemical vapor deposition" silanation method¹⁸ leads, in particular, to a remarkable enhancement of the reactant and product shape-selectivity^{19,20}.

Over such CVD-modified zeolites, the formation of the bulky trialkylnaphthalenes is totally suppressed in the case of mordenites, and considerably reduced with the HY zeolites (2% compared with 14% over the untreated zeolite) (Table 1). Such a result clearly demonstrates that the trialkylation reaction occurs on the acidic sites located on the external surface of mordenites. The acidic outer sites of the HY zeolites are also largely involved in the formation of the triisopropyl derivatives, which can be, nevertheless, produced also inside the cavities of these three-dimensional large-pore Y zeolites.

The results obtained in the isopropylation of the 2-isopropylnaphthalene over CVD-modified HY zeolite, i.e. a drastic decrease in the amount of triisopropylnaphthalenes (4% instead of 18% over the untreated HY), leading to an

enhancement of the β -selectivity over the CVD-modified HY for this reaction (85%), confirm such an involvement.

With CVD-modified HM, the 2-isopropylnaphthalene is the major product (90% at 10% conversion); despite the low conversion, this result must be taken into account because 2-isopropylnaphthalene can be easily separated from the reaction mixture by simple distillation, and then isopropylated as starting material for diisopropylnaphthalene production. With CVD-modified HY zeolites, a high β -selectivity (>90%) is obtained, corresponding to 63% of 2-isopropylnaphthalene and 30% of 2,6- + 2,7-diisopropylnaphthalenes at 70% conversion.

The overall results show that, from a synthetic point of view, the CVD-modified zeolites appear to be the best catalysts with which it is possible to selectively obtain β - and $\beta\beta$ - isomers.

Cyclohexylation reaction over HY zeolites. As already said above, no selectivity in 2,6-diisopropylnaphthalene could be found despite the hindrance of the isopropyl group; moreover, the separation of 2,6- and 2,7-diisopropyl isomers is very difficult. It was reported that, in the cyclohexylation reaction of naphthalene under conventional conditions (i.e. over Friedel-Crafts catalysts, such as aluminum chloride), the 2,6-dicyclohexylnaphthalene could be isolated, in a very low yield, from the reaction mixture by crystallization^{21,22}.

Taking into account such a property and the steric hindrance of the cyclohexyl group, we studied the catalytic activities of a sample of H-mordenite and two samples of HY zeolites in the cyclohexylation reaction of naphthalene with cyclohexyl bromide and cyclohexene respectively (Table 2).

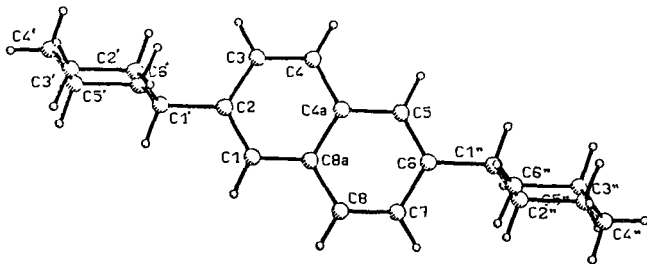
The H-mordenite presents a weak activity in the reaction with the cyclohexyl bromide, as shown by the low conversion of naphthalene (6%) at 200°C, whereas the HY zeolites appear to be very efficient even at lower temperatures. The ultrastable zeolite HY (Si/Al = 2.5) and the dealuminated sample (Si/Al = 20) exhibit similar activity and selectivities at the same temperatures, as shown on Table 2. When cyclohexene is used as the alkylating agent instead of cyclohexyl bromide, a slight difference is observed if the reaction is carried out under the same conditions (naphthalene and alkylating agent put together in the autoclave), due to dimerisation of cyclohexene. When cyclohexene is added drop by drop to the stirred mixture, the same results are then obtained, both in conversion and selectivity.

The comparison of cyclohexylation with isopropylation of naphthalene over the ultrastable zeolite US-HY under the same conditions is given on Table 3. In both reactions, a high conversion of naphthalene is obtained after short reaction times (10 min with cyclohexyl bromide, 1 h with isopropyl bromide).

The cyclohexylation reaction yields an increasing amount of 2,6- and 2,7-dicyclohexylnaphthalenes, together with a significant decreasing amount of trialkyl derivatives due to the steric hindrance of the cyclohexyl group, leading to an improvement of the β - β selectivity (82% compared with 71%). Nevertheless, the relative distribution of the 2,6- and 2,7- isomers does not dramatically change (2,6-/2,7- = 0.95 for isopropyl and 1.1 for cyclohexyl). Such a result confirms that Y zeolites increase the $\beta\beta$ selectivity, but do not lead to the predominant formation of one given dialkyl isomer.

The advantage of the cyclohexylation in comparison with the isopropylation is directly related to the physical properties of the 2,6-dicyclohexylnaphthalene, which is separated from the mixture by crystallization.

Pure 2,6-dicyclohexylnaphthalene (white crystals, mp = 152°C) is isolated in moderate yields (19 to 27%) depending on the zeolites²³.



As shown above, this crystalline 2,6-dicyclohexylnaphthalene contains a crystallographic symmetry centre; the cyclohexyl substituents adopt a chair conformation, and the presence of the two bulky substituents involves only a slight deviation from flatness for the naphthalene ring¹⁵.

CONCLUSION

The liquid-phase alkylation of naphthalene with hindered alkylating agents such as isopropyl and cyclohexyl derivatives can be carried out efficiently over HM and HY zeolites. High conversions and efficient β - β' selectivities are obtained after very short reaction times at 200°C. In the case of isopropylation with isopropyl bromide, the use of zeolites modified by silanation of the external surface leads to an improvement of such a selectivity by suppressing or reducing the formation of the triisopropyl derivatives. The use of cyclohexyl derivatives, cyclohexyl bromide or cyclohexene, as alkylating agents, yields, over HY zeolites, an increasing amount of 2,6- and 2,7-dicyclohexylnaphthalenes, together with a significant decreasing of the trialkyl derivatives. Moreover, the 2,6-dicyclohexylnaphthalene, a crystalline compound, is easily separated from the reaction mixture by crystallization, which is, to our knowledge, the first example of the production of a pure 2,6-dialkylnaphthalene.

REFERENCES

- 1 Venuto, P.B. *Microporous Materials* 1994, 2, 297 and references therein.
- 2 Chen, N.Y.; Kaeding, W.W.; Dwyer, F.G. *J. Am. Chem. Soc.* 1979, 101, 6783.
- 3 Kaeding, W.W.; Chu, C.; Young, L.B.; Weintein, B.; Butter, S.A. *J. Catal.* 1981, 67, 159.
- 4 Gaydos, R.M. in "Kirk Othmer Encyclopaedia of Chemical Technology" (Kirk, R.E.; Othmer, D.F., Eds.); Wiley: New York, 1981, vol 15, p 698.
- 5 Song, C.; Schobert, H.H. *Fuel Proc. Tech.* 1993, 34, 157.
- 6 Fraenkel, D.; Cherniavsky, M.; Iltah, B.; Levy, M. *J. Catal.* 1986, 101, 273.
- 7 Katayama, A.; Tobe, M.; Takeuchi, G.; Mizukami, F.; Niwa, S.; Mitamura, S. *J. Chem. Soc., Chem. Comm.*, 1991, 39.
- 8 Fellmann, J.D.; Saxton, R.J.; Weatrock, P.R.; Derouane, E.G.; Massiani, P. U.S. Patent n° 5,026,942, 1991.
- 9 Moreau, P.; Finiels, A.; Geneste, P.; Solofo, J. *J. Catal.* 1992, 136, 487.
- 10 Song, C.; Kirby, S. *Microporous Materials* 1994, 2, 467.
- 11 Sugi, Y.; Kim, J.H.; Matsuzaki, T.; Hanaoka, T.; Kubota, Y.; Tu, X.; Matsumoto, M. *Stud. Surf. Sci. Catal.* 1994, 84, 1837.
- 12 Chu, S.J.; Chen, Y.W. *Appl. Catal. A* 1995, 123, 51.
- 13 Fajula, F.; Ibarra, R.; Figueras, F.; Gueguen, C. *J. Catal.* 1984, 89, 60.
- 14 Chamoumi, M.; Brunel, D.; Fajula, F.; Geneste, P.; Moreau, P.; Solofo, J. *Zeolites* 1994, 14, 282.
- 15 Moreau, P.; Solofo, J.; Geneste, P.; Finiels, A.; Rambaud, J.; Declercq, J.P. *Acta Crystallogr.* 1992, C48, 397.
- 16 Niwa, M.; Kato, S.; Hattori, T.; Murakami, Y. *J. Chem. Soc., Faraday Trans I* 1984, 80, 3135.
- 17 Niwa, M.; Kawashima, Y.; Murakami, Y. *J. Chem. Soc., Faraday Trans I* 1985, 81, 2757.
- 18 Niwa, M.; Itoh, H.; Kato, S.; Hattori, T.; Murakami, Y. *J. Chem. Soc., Chem. Comm.* 1982, 819.
- 19 Niwa, M.; Kato, S.; Hattori, T.; Murakami, Y. *J. Phys. Chem.* 1986, 90, 6233.
- 20 Bein, T.; Carver, R.F.; Farlee, R.D.; Stucky, G.D. *J. Am. Chem. Soc.* 1988, 110, 4546.
- 21 Bodroux, E. *Ann. Chim. Phys.* 1929, 11, 535.
- 22 Pokrovskaya, E.S.; Stepanitseva, T.G. *J. Gen. Chem.* 1939, 9, 1953.
- 23 Solofo, J.; Moreau, P.; Geneste, P.; Finiels, A. PCT Int. Appl. WO 91 0159, 1991.

Table 1. Isopropylation of Naphtalene over a Series of Untreated and CVD Modified Zeolites at 200°C with Isopropyl bromide

Catalyst	time, h	naphth. conv., %	product distribution, %					selectivity, %	
			MIEN 2-IPN	DIPN 2,6- 2,7- others			TIPN	2,6-+2,7- DiPN	overall 8-select.
HM	24	18	81	4	4	3	8	72	89
HM ₁	24	60	74	7	6	5	10	70	87
HM ₂	24	20	61	13	11	9	9	74	85
HM ₃	24	16	55	14	13	7	9	80	82
HY	1	86	42	16	17	12	14	73	74
US-HY	1	97	28	19	20	16	17	71	67
CVD-HM	1	10	90	3	4	3	0	70	97
CVD-HY	1	70	63	15	15	5	2	85	93

Table 2. Cyclohexylation of Naphtalene over Zeolites at 200° C with Cyclohexyl bromide (CB) and Cyclohexene (CH)

Catalyst	Alkylat. agent	time, min	naphth. conv., %	product distribution, %			selectivity, %		
				MCN	DCN	TCN	2-MCN MCN	2,6-DCN DCN	2,6-+2,7-DCN DCN
HM	CB	70	6	56	44		46	16	27
HY _{2.5}	CB	10	96	31	67	2	6	43	82
HY ₂₀	CB	10	94	53	46	1	8	43	79
	CH ^a	10	90	85	15		53	20	36
	CH ^b	25 ^c	98	44	54	2	7	41	77

^a CH charged together with naphthalene in the autoclave before heating. ^b CH added drop by drop. ^c time corresponding to the end of addition of naphthalene.

Table 3. Isopropylation and Cyclohexylation of Naphtalene over US-HY Zeolite at 200°C with Isopropyl bromide (IB) and Cyclohexyl bromide (CB)

Alkyl. agent	time min	naphth. conv., %	product distribution, %					selectivity, %	
			MAN ^a	DAN ^b 2,6- 2,7- 2,6-+2,7- others				TAN ^c	2,6-+2,7-DAN DAN
IB	60	97	28	19	20	39	16	17	71
CB	10	96	31	29	26	55	12	2	82

^a MAN: monoalkylnaphthalenes.

^b DAN: dialkylnaphthalenes.

^c TAN: trialkylnaphthalenes.

REGIOSELECTIVE ISOPROPYLATION OF DINUCLEAR AROMATICS OVER DEALUMINATED MORDENITE CATALYSTS

Andrew D. Schmitz and Chunshan Song

Department of Materials Science and Engineering
Fuel Science Program, 209 Academic Projects Building
Pennsylvania State University, University Park, PA 16802

Keywords: naphthalene, biphenyl, shape-selective alkylation

Summary

Selective addition of propylene to naphthalene or biphenyl over dealuminated H-mordenite (HM) catalysts is being used to produce 2,6-diisopropyl-naphthalene (2,6-DIPN) and 4,4'-diisopropylbiphenyl (4,4'-DIPB), respectively. When oxidized, these selectively substituted dinuclear aromatics become monomers for liquid crystalline polymers and engineering plastics.¹⁻⁵ We, and others, have shown that HM dealumination increases alkylation regioselectivity for isopropylation of binuclear aromatics.⁶⁻¹⁶ In this paper, we more closely examine the effects of HM dealumination on catalyst activity and regioselectivity, as well as effects on catalyst physical properties.

Two different mordenites were dealuminated by mineral acid leaching, HM14 and HM38, having $\text{SiO}_2/\text{Al}_2\text{O}_3$ (mol ratio) of 14 and 38, respectively. For naphthalene isopropylation, dealumination of HM14 increases the 2,6-DIPN isomer selectivity from 30 to 60%. Dealumination of HM38 gives similar results but with lower regioselectivity. For comparison, 4,4'-DIPB regioselectivity was examined in biphenyl isopropylation over a series of mordenites with $\text{SiO}_2/\text{Al}_2\text{O}_3$ 14-230. Selectivity for the 4,4'-isomer increased from 66 to 87%. Therefore, increased selectivity for the slimmest diisopropyl-isomer with dealumination is a general property: it occurs with different mordenite starting materials and different, but similar in size and shape, reactant molecules.

Selectivity for β -substitution of naphthalene seems to correlate with changes in HM mesopore volume brought about by dealumination. An increase in the mesopore volume is mirrored by an increase in 2,6-DIPN isomer selectivity. HM micropore volumes do not change appreciably. It has been shown that the two $\beta\beta$ -disubstituted naphthalenes have nearly identical critical diameters, but 2,6-DIPN has a somewhat more linear structure than 2,7-DIPN.^{3,6} Consequently, 2,6-DIPN has a lower activation energy for diffusion in HM.⁶ This explains why HM catalysts typically give 2,6/2,7 DIPN isomer ratios greater than unity. We have used X-ray powder diffraction to measure the decrease in HM unit cell volumes caused by dealumination. The 2,6/2,7 DIPN ratio shows an approximate inverse relationship with the unit cell volumes. A probable explanation is that the unit cell contractions caused by dealumination decrease the channel diameter, slightly, resulting in more snug fit for the $\beta\beta$ -disubstituted isomers in the channels. As a consequence, the difference in diffusion rates for 2,6- and 2,7-DIPN is magnified.

Experimental

Catalyst Preparation. The procedures used in this work have been described earlier.⁵ Mordenite catalysts CBV 10A (NaM14), CBV 20A (HM21) and CBV 30A (HM38) were supplied as 10 μm average particle size powders (PQ Corporation). HM14 was generated from NaM14 by sodium-exchanged with 1 M NH_4Cl . Dealumination was accomplished by stirring HM in aqueous hydrochloric or nitric acid at reflux temperature. Time and acid concentration were varied to control the extent of aluminum removal. All catalysts were calcined 5.5 h at 465 °C except HM230. HM230 was prepared according to a procedure described by Lee et al. for extensive aluminum removal.¹⁶ Accordingly, NaM14 was first treated at reflux with 1 M HCl to generate the HM54 sample. In the second step, HM54 was calcined at 700 °C and treated with 6 M HNO_3 , followed by final calcination at 700 °C. Samples were dissolved using lithium metaborate fusion and analyzed for silicon, aluminum and sodium by ICP-AES. Sorption data and residual sodium content for the catalysts are listed in Table 1.

Catalyst Evaluation. As described previously, catalyst testing was done in a tubing-bomb batch reactor charged with 0.10 g catalyst, 1.0 g (7.8 mmol) naphthalene, and 0.66 g (15.6 mmol) propylene.⁵ Naphthalene and biphenyl (Aldrich, 99% grades) and propylene (Matheson, 99.5 % minimum, polymer purity) were used as supplied. Solution products were analyzed by GC-MS and GC-FID for qualitative and quantitative analyses, respectively, using a 30m x 0.25mm DB-17 (J&W Scientific) column.

X-ray powder diffraction (XRD) was done on a Scintag 3100 diffractometer using nickel-filtered $\text{Cu K}\alpha$ radiation. The $\text{Cu K}\alpha_2$ component was stripped from the patterns using the standard Scintag algorithm, so the wavelength used in the calculations is 1.540598 Å. Samples were mixed with ca. 10 wt% -325 mesh silicon internal standard for 2 θ corrections. The scan rate was 0.5° 2 θ /min with 0.02° steps. XRD pattern indexing and determination of lattice constants for HM (CMC2₁ space group) was done using the JCPDS-NBS*LSQ82 unit cell refinement computer program.¹⁷ This program minimizes the sum S defined in equation 1, where θ^{corr} are

$$S = \sum w_{hkl} (\theta_{hkl}^{\text{corr}} - \theta_{hkl}^{\text{calc}})^2 \quad (1)$$

the observed Bragg angles, corrected for instrumental and physical peak shifts, and θ^{calc} are calculated from the current unit cell parameters and the weighting factors w_{hkl} . Starting values for θ^{calc} are determined from the input unit cell parameters which are then adjusted, using a nonlinear least-squares method, to minimize S . This approach can lead to cell parameters accurate to a few parts in 10,000.¹⁷

Sorption analyses were done on either of two automated instruments: a Coulter SA 3100, or Quantachrome Autosorb. Samples were outgassed at 400 °C. Multipoint surface areas were calculated by the BET method. Micropore volumes were calculated using the T-plot method.

Results and Discussion

Isopropylation of Naphthalene. Catalyst test data for the two series of dealuminated HM catalysts is presented in Table 2. Greater than 98% of the products are isopropynaphthalenes (IPN's). The predominant side reactions result in small amounts of alkylnaphthalenes that are not solely isopropyl-substituted. Mass balances are greater than 96% in all cases, with material losses being primarily attributed to carbonaceous deposits on the catalyst.

The effects of dealumination on catalyst performance are shown in graphically in Figures 1-3. HM54 has abnormally low activity so its data for were omitted from these graphs because. HM230 has higher activity than expected, apparently due the higher activation temperature used in its preparation. Both HM14- and HM38 derived catalysts show similar activity patterns: naphthalene conversion first increases, then decreases as aluminum is removed from the lattice (volcano plots, Figure 1). This type of activity trend is quite common for HM and is due to the decreasing acid site density and increasing acid site strength that occurs with dealumination as discussed elsewhere.^{6,18-19} Both series of catalysts show a severe loss in activity at high $\text{SiO}_2/\text{Al}_2\text{O}_3$ ratios, probably due to gross depletion of acid sites. HM38-derived catalysts retain reasonable activity to higher ratios, indicative of higher acid site concentrations. HM93 (from HM38) shows a moisture loss on ignition 2.5 times the amount desorbed from HM90 (from HM14). This also suggests that HM38-derived catalysts have higher acid site concentrations than HM14-derived catalysts at the same $\text{SiO}_2/\text{Al}_2\text{O}_3$ ratio.

As shown in Figure 2, DIPN yield and selectivity are increased by dealumination up to the same maxima defined in Figure 1. Beyond these maxima, monoalkylation dominates and TriPN+ production falls to near zero. However, β -substitution selectivity (%2-MIPN and %2,6-DIPN) continues to increase with more extensive aluminum removal (Figure 3). This means that a larger fraction of the naphthalene and 2-MIPN molecules are reacting within the confines of the HM channels where α -substitution is sterically blocked. Less reaction occurs on the external surface acid sites which are non-selective. The first alkylation step is much more rapid than the second. Furthermore, since ortho-substitution of naphthalene by propylene is sterically prevented, formation of TriPN+ products must involve α -substitution. Consequently, TriPN+ product concentrations also decrease considerably at higher levels of dealumination. Sugi et al. made similar observations on this reaction.⁹ They also showed that the external-surface acid sites of HM128 could be preferentially deactivated to improve β -substitution selectivity, while still maintaining the activity for selective substitution inside the channels. Figure 3 also shows that the ultimate attainable β -substitution selectivity depends on the choice of HM starting material.

The HM catalysts have, on average, 38% of their total pore volume in the mesopore region (20-600 Å diameter). Using XRD line-broadening, we determined the mean crystallite dimensions for HM14, HM74 and HM110 to be $0.23 \pm 0.02 \mu\text{m}$, and for HM230, $0.14 \pm 0.01 \mu\text{m}$.⁵ Laser-scattering measurements reported by the manufacturer show that the mordenite starting materials have average particle sizes of about $10 \mu\text{m}$. It is likely that most of the mesopore volume is in the interstices between crystals in the catalyst particles, and dealumination increases the interstitial (mesopore) volume.

The constraints of the microporous channels not only gives rise to the desired regioselective alkylations, but also impede diffusion of the desired products. If formation of the β -substituted products is diffusion limited, an increase in the mesopore volume should increase the rate of their production. Figure 4 shows that the β -substitution selectivity does, in fact, closely parallel HM mesopore volume. Lee et al. showed a similar trend for isopropylation of biphenyl.¹⁶ To account for concurrent, but less pronounced, increase in micropore volumes, it has been proposed that lattice-bound aluminum is removed from the 4-membered rings that separate the 12-membered rings of the main channels from the neighboring 8-membered ring side-pockets.¹⁸ Lee et al. have suggested that propylene may preferentially diffuse through these 8-membered ring channels that run perpendicular to the main channels, and are inaccessible to naphthalene.¹⁶

Pore volume changes do not seem to explain why the 2,6/2,7 DIPN isomer ratio increases with dealumination, considering these two isomers have nearly identical critical diameters.^{3,6} Horsley et al. used molecular graphics screening and molecular mechanics calculations to provide convincing evidence that 2,6-DIPN, with its slightly more linear structure, has a lower activation energy for diffusion than 2,7-DIPN in the microchannels of HM.⁶ With its isopropyl groups on the same side of the molecule, steric repulsions are maximum when 2,7-DIPN diffuses into the pore windows; whereas, diffusion of 2,6-DIPN is significantly less hindered.⁶ Since the channel diameter is obviously a critical parameter in determining the 2,6/2,7 DIPN ratio, we used X-ray powder diffraction to measure the changes in HM unit cell volumes caused by dealumination. These data are listed in Table 3, where the cited errors limits are the standard errors calculated by the LSQ82 program. Mordenite was the only phase detected in the patterns. HM79 seems to be an anomaly because its cell parameters are much lower than expected. The XRD pattern for this catalyst is of low intensity suggesting that some structural collapse may have occurred during

its dealumination. Still, there is a general trend of unit cell contraction with dealumination, with the largest change being in the *b*-direction. HM71 shows the following magnitudes of contraction relative to HM14: a, 0.59%; b, 0.77%; c, 0.65%; and volume, 2.0%. As shown in Figure 5 for the six samples, excluding the anomalous HM79 data, the 2,6/2,7 DIPN ratio shows an approximate reciprocal relation to the changes in unit cell volume. A probable explanation is that HM dealumination causes a slight shrinkage in the channel diameter that results in more snug fit of the 2,6- and 2,7-DIPN isomers in the channels. Diffusion of 2,7-DIPN becomes even more hindered than in the non-dealuminated HM case.

Isopropylation of Biphenyl. General applicability of the dealumination procedure for improvement of regioselectivity was evaluated by examining biphenyl isopropylation over selected dealuminated mordenites. The experimental results are shown in Table 4 and in Figures 6-7. Greater than 99% of the products are isopropylbiphenyls with a small percentage of other alkylbiphenyls which are not *solely* isopropyl-substituted. Tetra-substitution of biphenyl is not observed. The trends in alkylation regioselectivity are remarkably similar to those observed for the naphthalene reaction. Conversion and DIPB yield increase with initial dealumination, then both decrease at higher $\text{SiO}_2/\text{Al}_2\text{O}_3$ ratios. Formation of 3-MIPB is not effected much by dealumination; whereas, the concentration of 2-MIPB in the product goes to near zero. Neglecting isomers with isopropyl groups ortho to each other, there are 10 possible DIPB isomers. We observe 9 peaks in the GC-MS having *m/z* of 238. At present, only the three DIPB isomers listed in Table 4 can be identified with certainty. Of the remaining 7 isomers, there is the 3,5-isomer, and 6 isomers involving substitution at the 2-position(s). Consequently, it is not so surprising that the concentrations of compounds labeled *other-DIPB* closely parallel the 2-MIPB concentrations.

Overall, isopropylation of biphenyl is a more efficient process than isopropylation of naphthalene. Separation of mono-, di- and polysubstituted products from each other is easy in comparison to separation of positional isomers. Dealuminated HM can give 4,4'-DIPB isomer selectivity over 80%, and an isomer ratio with the next most concentrated isomer, 3,4'-DIPB, of about 8. On the other hand, selectivity for the target 2,6-DIPN isomer is only about 60% with a 2,6/2,7 DIPN not exceeding 2.3 in this work. It should be noted that 2,6-DIPN isomer selectivity of over 65%, with 2,6/2,7 DIPN exceeding 2.6, can be achieved by adding a small amount of water to the reactor or by increasing the reaction temperature,⁵ or by using isopropanol as the alkylating agent.³

Conclusions

Dealumination of HM14 increases the 2,6-DIPN isomer selectivity from 30 to 60%. While a similar trend is observed for dealumination of HM38, lower regioselectivity is obtained. However, HM38 retains reasonable activity to higher $\text{SiO}_2/\text{Al}_2\text{O}_3$ ratios than HM14 does. Both factors demonstrate that performance of the dealuminated catalysts is dependent upon the choice of starting material. In comparison biphenyl isopropylation experiments, it was found that 4,4'-DIPB regioselectivity can be increased from 66 to 87% by HM dealumination. Therefore, increased selectivity for the slimmest diisopropyl-isomer with dealumination is a general property: it occurs with different mordenite starting materials and different, but similar in size and shape, reactant molecules.

Comparing regioselectivity and sorption data, we found that a higher percentage of reaction occurs in the confines of the mordenite channels when the density of non-selective external surface acid sites is diminished by dealumination. Relative diffusion rates seem to be a major controlling factor in determining selectivity. Reducing diffusion resistance by increasing the mesoporous volume in the catalyst particle interstices results in an increase in DIPN yield and 2,6-DIPN isomer selectivity.

As reported elsewhere, 2,6-DIPN has a slightly smaller critical diameter and lower activation energy for diffusion in HM than 2,7-DIPN.^{3,6} We used a careful analysis of the unit cell parameters to show that the 2,6/2,7 DIPN ratio increases as the unit cell volumes decrease with aluminum removal. A probable explanation is that HM dealumination causes a slight shrinkage of the channel diameter, increasing the difference in diffusion rates for 2,6- and 2,7-DIPN.

Acknowledgements

We would like to acknowledge the encouragement and support of Prof. Harold Schobert at the Pennsylvania State University. We would also like to thank the PQ Corporation, Inc. for graciously providing the mordenite starting materials with detailed analytical data, and Prof. Deane K. Smith at the Pennsylvania State University for his assistance in the XRD work.

References

1. Song, C.; Schobert, H. H. Specialty Chemicals and Advanced Materials from Coals: Research Needs and Opportunities *Am. Chem. Soc. Div. Fuel Chem. Prepr.* **1992**, *37*(2), 524-532.
2. Song, C.; Schobert, H. H. Opportunities for Developing Specialty Chemicals and Advanced Materials from Coals *Fuel Process. Technol.* **1993**, *34*, 157-196.
3. Song, C.; Kirby, S. Shape-Selective Alkylation of Naphthalene with Isopropanol Over Mordenite Catalysts *Microporous Materials* **1994**, *2*, 467-476.
4. Song, C.; Schobert, H. H. Non-Fuel Uses of Coals and Synthesis of Chemicals and Materials *Am. Chem. Soc. Div. Fuel Chem. Prepr.* **1995**, *40*(2), 249-259.
5. Schmitz, A. D.; Song, C. Shape-Selective Isopropylation of Naphthalene Over Dealuminated Mordenites *Am. Chem. Soc. Div. Fuel Chem. Prepr.* **1994**, *39*(4), 986-991.

6. Horsley, J. A.; Fellmann, J. D.; Derouane, E. G.; Freeman, C. M. Computer-Assisted Screening of Zeolite Catalysts for the Selective Isopropylation of Naphthalene *J. Catal.* **1994**, *147*, 231-240.
7. Loktev, A. S.; Chekriy, P. S. Alkylation of Binuclear Aromatics with Zeolite Catalysts in "Zeolites and Related Microporous Materials: State of the Art 1994," *Stud. Surf. Sci. Catal.* **1994**, *84*, 1845-1851.
8. Chu, S.-J.; Chen, Y.-W. Isopropylation of Naphthalene Over β Zeolite *Ind. Eng. Chem. Res.* **1994**, *33*, 3112-3117.
9. Sugi, Y.; Kim, J.-H.; Matsuzaki, T.; Hanaoka, T.; Kubota, Y.; Tu, X.; Matsumoto, M. The Isopropylation of Naphthalene Over Cerium-Modified H-Mordenite in "Zeolites and Related Microporous Materials: State of the Art 1994," *Stud. Surf. Sci. Catal.* **1994**, *84*, 1837-1844.
10. Sugi, Y.; Matsuzaki, T.; Hanaoka, T.; Kubota, Y.; Kim, J.-H. Shape-Selective Alkylation of Biphenyl Over Mordenites: Effects of Dealumination on Shape-Selectivity and Coke Deposition *Catal. Lett.* **1994**, *26*, 181-187.
11. Sugi, Y.; Toba, M. Shape-Selective Alkylation of Polynuclear Aromatics *Catalysis Today* **1994**, *19*, 187-212.
12. Tu, X.; Matsumoto, M.; Matsuzaki, T.; Hanaoka, T.; Kubota, Y.; Kim, J.-H.; Sugi, Y. *Catal. Lett.* **1993**, *21*, 71-75.
13. Moreau, P.; Finiels, A.; Geneste, P.; Solofo, J. Selective Isopropylation of Naphthalene Over Zeolites *J. Catal.* **1992**, 487-492.
14. Katayama, A.; Toba, M.; Takeuchi, G.; Mizukami, F.; Niwa, S.-i.; Mitamura, S. Shape-Selective Synthesis of 2,6-Diisopropyl-naphthalene Over H-Mordenite Catalyst *J. Chem. Soc., Chem. Commun.* **1991**, 39-40.
15. Fellmann, J. D.; Saxton, J.; Wentreck, P. R.; Derouane, E. G.; Massioni, P. Process for Selective Diisopropylation of Naphthyl Compounds Using Shape Selective Acidic Crystalline Molecular Sieve Catalysts U. S. Patent No. 5,026,942, 1991.
16. Lee, G. S.; Maj, J. J.; Roche, S. C.; Garcés, J. M. *Catal. Lett.* **1989**, *2*, 243-248.
17. Hubbard, C. R.; Lederman, S. M.; Pyrras, N. P., "A Least Squares Unit Cell Refinement Program;" National Bureau of Standards: Washington, D.C., and JCPDS—International Centre for Diffraction Data: Swarthmore, PA, July 1983.
18. Mishin, I. V.; Bremer, H.; Wendlandt, K.-P. Synthesis and Properties of High-Silica Zeolites with Mordenite Structure in "Catalysis on Zeolites," (Kalló, D.; Minachev, Kh. M., Eds.); H. Stillman Publishers, Inc.: Boca Raton, FL, 1988, pp 231-275.
19. Seddon, D. The Conversion of Aromatics Over Dealuminised Mordenites *Appl. Catal.* **1983**, *7*, 327-336.

Table 1. Sorption Data and Residual Sodium Content for Mordenite Catalysts

catalyst	Na ₂ O, wt%	surface area, m ² /g			pore volume, cm ³ /g		
		total	micro	meso	total	micro	meso
NaM14 ^a	6.24	466	457	10	0.312	0.174	0.138
HM21 ^a	0.02	606	536	70	0.317	0.207	0.110
HM38 ^a	0.07	512	429	82	0.293	0.167	0.126
HM14	0.19	na ^{b,c}	na	na	na	na	na
HM54	0.15	na	na	na	na	na	na
HM62	<0.01	504	413	91	0.250	0.163	0.087
HM70	<0.01	556	395	161	0.280	0.180	0.099
HM71	<0.01	572	497	75	0.349	0.191	0.125
HM74	<0.01	583	509	74	0.385	0.196	0.148
HM79	0.14	na	na	na	na	na	na
HM90	<0.01	540	471	69	0.313	0.188	0.125
HM93 ^d	0.01	na	na	na	na	na	na
HM110	<0.01	539	480	59	0.362	0.184	0.138
HM140 ^d	0.02	na	na	na	na	na	na
HM230	<0.01	498	437	60	0.342	0.168	0.136

^a Data as reported by supplier. ^b Not available. ^c HM14 and NaM14 are assumed to have very similar sorption properties. ^d Produced by dealumination of HM38.

Table 2. Isopropylation of Naphthalene Test Data for HM14- and HM38-Derived Dealuminated Mordenites

catalyst	conv., %	product distribution, mol%			isomer distribution, mol%			
		MIPN	DIPN	TriPN ^a	2-MIPN ^b	2,6-DIPN ^c	2,7-DIPN ^c	2,6/2,7
HM14	76	63	32	3.6	60	33	19	1.76
HM54	43	75	22	1.2	68	50	24	2.11
HM62	78	61	34	3.9	54	29	16	1.78
HM70	82	52	40	5.6	58	44	20	2.17
HM71	74	59	37	2.3	64	51	22	2.29
HM74	47	75	23	0.6	71	55	25	2.24
HM79	69	65	29	3.6	59	39	21	1.86
HM90	36	79	19	0.9	70	53	24	2.21
HM110	15	84	14	0.4	83	61	30	2.05
HM230 ^d	41	72	25	1.1	74	58	25	2.32
HM38	73	60	34	4.4	58	39	19	1.99
HM93	84	48	43	6.5	62	48	22	2.21
HM140	38	77	21	0.4	73	56	25	2.20

^a Tri- and tetraisopropylnaphthalenes. ^b Mole percent in MIPN products. ^c Mole percent in DIPN products. ^d Calcined at 700 °C.

Table 3. Unit Cell Parameters for HM14-Derived Dealuminated Mordenites Determined from XRD Data Using the JCPDS-NBS*LSQ82 Cell Refinement Program

unit cell parameter	HM14	HM54	HM71	HM74	HM79	HM110	HM230
<i>a</i> , Å	18.163 ± 0.005	18.051 ± 0.004	18.056 ± 0.006	18.091 ± 0.009	17.947 ± 0.016	18.075 ± 0.006	18.047 ± 0.008
<i>b</i> , Å	20.314 ± 0.004	20.162 ± 0.005	20.157 ± 0.007	20.217 ± 0.009	19.866 ± 0.012	20.233 ± 0.006	20.197 ± 0.009
<i>c</i> , Å	7.490 ± 0.002	7.447 ± 0.003	7.441 ± 0.003	7.460 ± 0.003	7.383 ± 0.004	7.463 ± 0.002	7.452 ± 0.003
volume, Å ³	2764 ± 1	2710 ± 1	2708 ± 1	2730 ± 1	2632 ± 2	2730 ± 1	2717 ± 2

Table 4. Isopropylation of Biphenyl Test Data for Selected Dealuminated H-Mordenites

catalyst	conv., %	product distribution, mol%			MIPB isomer distribution, mol%			DIPB isomer distribution, mol%			
		MIPB	DIPB	TriPB	2-	3-	4-	3,3'-	3,4'-	4,4'-	other
HM14	49	74	25	0.5	9.2	24	66	3.9	17	66	13.8
HM21	60	64	33	1.5	8.1	26	66	3.0	15	72	10.8
HM38	71	54	42	3.0	10.2	28	62	2.7	13	72	12.2
HM71	46	62	37	1.1	3.1	24	73	1.3	11	83	4.9
HM230	23	67	32	0.5	2.0	18	80	0.9	10	87	2.5

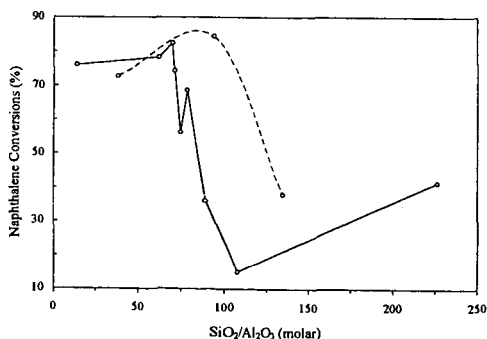


Figure 1. Naphthalene conversions for HM14-derived (solid line) and HM38-derived (broken line) catalysts as a function of SiO₂/Al₂O₃ ratio.

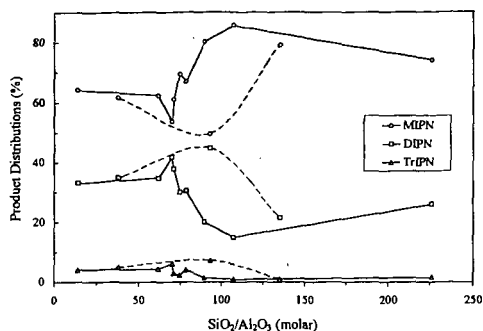


Figure 2. Naphthalene isopropylation product distributions for HM14-derived (solid lines) and HM38-derived (broken lines) catalysts as a function of $\text{SiO}_2/\text{Al}_2\text{O}_3$ ratio.

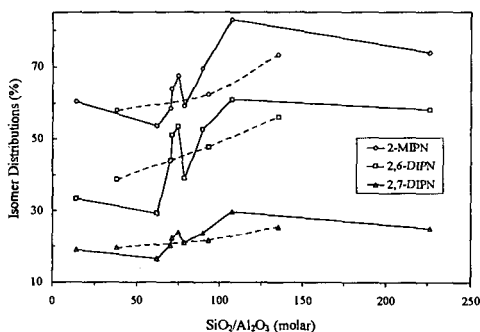


Figure 3. Naphthalene isopropylation isomer distributions for HM14-derived (solid lines) and HM38-derived (broken lines) catalysts as a function of $\text{SiO}_2/\text{Al}_2\text{O}_3$ ratio.

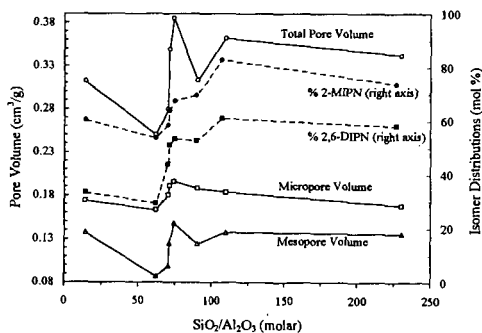


Figure 4. Comparison of pore volumes (solid lines) and β -substitution selectivities (broken lines) for dealuminated HM14 catalysts as a function of $\text{SiO}_2/\text{Al}_2\text{O}_3$ ratio.

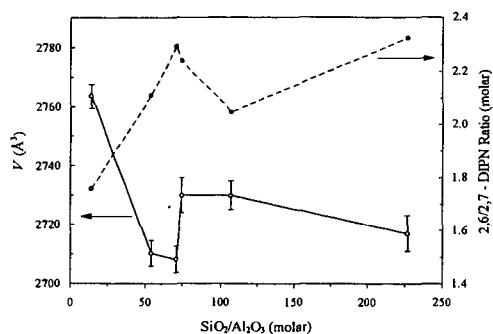


Figure 5. Comparison of unit cell volumes (solid line, left axis) with 2,6/2,7 DIPN ratios (broken line, right axis) for dealuminated HM14 catalysts as a function of $\text{SiO}_2/\text{Al}_2\text{O}_3$ ratio. Error bars represent four-times the standard error in unit cell volumes from Table 3.

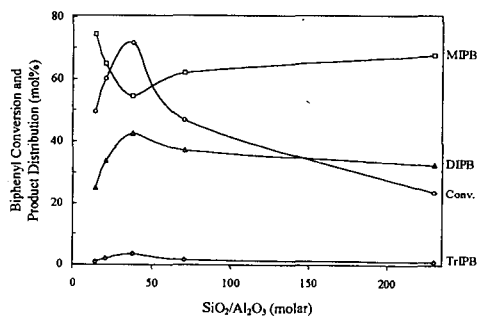


Figure 6. Isopropylation of biphenyl conversion and product distribution as a function of $\text{SiO}_2/\text{Al}_2\text{O}_3$ ratio.

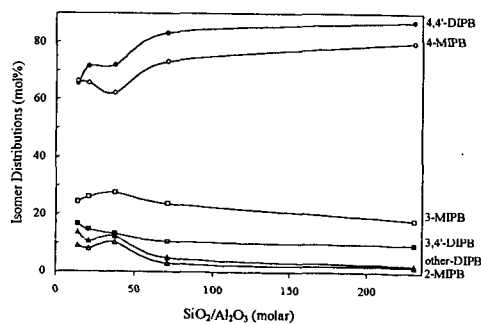


Figure 7. Biphenyl isopropylation isomer distributions as a function of $\text{SiO}_2/\text{Al}_2\text{O}_3$ ratio.

SYNTHESIS OF POLYESTERS WITH RIGID BIPHENYL SKELETON BY CARBONYLATION-POLYCONDENSATION WITH PALLADIUM-PHOSPHINE CATALYSTS

Y. Kubota, K. Takeuchi, T. Hanaoka, and Y. Sugi

National Institute of Materials and Chemical Research, AIST, Tsukuba, Ibaraki 305, Japan

Keywords: polyester, carbonylation-polycondensation, DBU

INTRODUCTION

Stiff macromolecules are expected, when properly processed, to produce materials with high degrees of molecular orientation and order which should result in superior mechanical strength [1,2]. Biphenyl derivatives are promising components for advanced materials such as heat-resistant polymers and liquid crystalline polymers. Copolyesters based on terephthalic acid, isophthalic acid, and bisphenol A have already been used because they are heat-resistant and transparent. Wholly aromatic polyesters containing biphenyl-4,4'-dicarboxylate moiety in place of terephthalate and isophthalate moiety must be highly potential for heat-resistance. For this reason, we tried to synthesize biphenyl-containing polyesters. Among several synthetic methods, carbonylation-polycondensation method originally developed by Imai and his co-workers [3], and subsequently by Perry and his co-workers [4] on the basis of Heck reaction [5] seemed to be the most straightforward way to get target polyesters.

We report herein the successful synthesis of polyesters which contain rigid biphenyl skeleton by palladium-catalyzed carbonylation-polycondensation. Especially, introduction of 9,10-dihydrophenanthrene moieties was found to afford highly soluble polyesters in organic solvent. This is advantageous for polyester formation by carbonylation-polycondensation in solution and for molding resulting polyesters.

EXPERIMENTAL

Materials. 4,4'-Dibromobiphenyl (DBBP) and 4,4'-diiodobiphenyl (DIBP) were obtained from Aldrich Japan, Tokyo, Japan, and purified by recrystallization from toluene. 2,7-Dibromo-9,10-dihydrophenanthrene (DBDHP) and 2,7-diiodo-9,10-dihydrophenanthrene (DIDHP) were prepared from 9,10-dihydrophenanthrene by known methods [6,7]. All other materials were obtained commercially, and used with appropriate purifications.

Molecular weight measurements. The weight average molecular weight (M_w) and the number average molecular weight (M_n) were determined by means of gel permeation chromatography on the basis of a polystyrene calibration on a Yokogawa HPLC Model LC100 System (column, Tosoh TSK-Gel G4000HHR; eluent, chloroform or chloroform/1,1,1,3,3,3-hexafluoro-2-propanol (HFIP) = 3/1 (v/v); detection, UV (wavelength: 254 nm)). Thermal characteristics were studied with a Mettler FP800 Thermal Analysis System and a MAC Science TG-DTA 2000 apparatus.

Typical procedure for carbonylation-polycondensation. In a 50 ml stainless steel autoclave equipped with a magnetic stirrer was placed 845.1 mg (2.5 mmol) of DBDHP, 570.7 mg (2.5 mmol) of bisphenol A, 17.7 mg (0.1 mmol) of $PdCl_2$, 104.9 mg (0.4 mmol) of PPh_3 , 10 ml of chlorobenzene, and 0.82 ml (5.5 mmol) of 1,8-diazabicyclo[5.4.0]undec-7-ene (DBU). Carbon monoxide was introduced at 1.1 MPa of an initial pressure and then heated with vigorous stirring at 130 °C in an oil bath for 3 h. After excess carbon monoxide was purged, reaction mixture was poured into 100 ml of methanol. Precipitated polymer was separated from methanol by decantation, dissolved in 50 ml of chloroform, and then poured into 100 ml of methanol again with stirring. Polymer was filtered, washed with 100 ml of methanol, and dried *in vacuo* to afford poly[oxy-1,4-phenylene(1-methylethylidene)-1,4-phenyleneoxycarbonyl(9,10-dihydro-2,7-phenanthrenediyl)-carbonyl] (**1**) as white or pale green yellow solid. The yield was 1.09 g (95%). M_w and M_w/M_n determined by GPC were 102,600 and 2.5, respectively. The 10 % weight loss temperature (T_{10}) was 414 °C and the 5 % weight loss temperature (T_5) was 394 °C in air. Found: C, 79.93; H, 5.09; Br, 1.35 %. Calcd. for $(C_{31}H_{24})_n$: C, 80.85; H, 5.25 %. IR and 1H and ^{13}C -NMR spectral data were satisfactory for polyester **1**.

The other polyesters were obtained by analogous procedures.

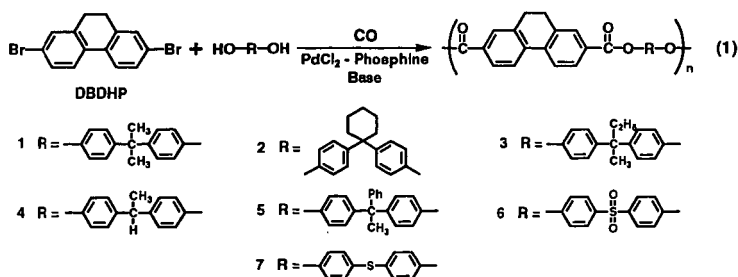
RESULTS AND DISCUSSION

Effect of reaction parameters on the carbonylation-polycondensation

The synthesis of polyesters by the carbonylation-polycondensation is shown in Eq. 1. To make clear factors controlling the synthesis, parameters such as temperature, CO pressure, solvent, and base were studied for polyester **1** from DBDHP and bisphenol A.

Figure 1 summarizes the effect of temperature on the molecular weight of **1** by the use of PPh_3 as a ligand and DBU as a base. The carbonylation-polycondensation was dependent on temperature, and the molecular weight was the highest at 120-130 °C. Low molecular weight is due to low reaction rate at low temperatures, and to side reactions at high temperatures.

Effects of solvent on the molecular weight of **1** by the use of 1,3-bis(diphenylphosphino)propane (dppp) as a ligand and DBU as a base are shown in Table 2. Although the alcoholysis of acyl-palladium intermediate is expected to be favorable in polar solvent, the solubility of product is more important factor than the polarity of solvent in our case. Polyester **1** was found to be easily dissolved in chlorobenzene, nitrobenzene, dichloromethane, and chloroform. Among them, only chlorobenzene mediated effectively the carbonylation-polycondensation. The efficiency of chlorobenzene may be due to good solubility of polyesters in it. Table 2 summarizes the effect of base on the molecular weight of **1**. The highest molecular weight was obtained for DBU. DBU was efficient under wide variety of conditions because it is a strong base ($pK_a = 11.5$). Because the salt from DBU and HBr liberated by the carbonylation was highly soluble in organic solvents, it is easier to remove HBr than the salt of other bases such as Et_3N and $i-Pr_2NEt$. Under optimum



condition, **1** was obtained in 95% yield with high molecular weight ($M_w = 1.0 \times 10^5$) as described in experimental part.

Catalytic activity of palladium-phosphine complex on the carbonylation-polycondensation is important for the molecular weight of polyesters. The effect of phosphine on the molecular weight of **1** is summarized in Table 3. The use of four moles of PPh_3 per mole of palladium was necessary to prevent catalyst decomposition, probably by a cluster formation [8]. However, large excess of PPh_3 ($\text{PPh}_3/\text{Pd} = 10$) inhibited polymer formation because excess ligands coordinated to metal center reduce the coordination of substrate and carbon monoxide. This is a different feature from the case of the ethoxycarbonylation of DBBP, where catalytic activity kept high even at high PPh_3/Pd ratio [9]. Bidentate phosphine such as dppp has been described to be more effective ligand for the carbonylation than monodentate phosphine such as PPh_3 [9-12]. In our previous work [9], high catalytic activities were observed for bidentate phosphines, α, ω -bis(diphenylphosphino)alkanes ($\text{Ph}_2\text{P}(\text{CH}_2)_n\text{PPh}_2$ ($n=2-5$)), especially for dppp ($n=3$) and dppb ($n=4$) in palladium catalyzed ethoxycarbonylation of DBBP and DBDHP. The catalysts with these ligands have been much more active than those with PPh_3 . The effectiveness of bidentate ligand is due to the formation of chelated complex with palladium, such as six-membered chelate ring for dppp . In the carbonylation-polycondensation, dppp gave the highest molecular weight of **1** among them. Two fold excess of dppp for palladium was also required for the carbonylation and for high molecular weight, however, large excess of dppp prevented them. Figure 2 shows the effect of CO pressure on the molecular weight of **1** for PPh_3 and dppp . The molecular weight was the highest under CO pressure around 1 MPa, and then gradually decreased with further increase of CO pressure. Both PPh_3 and dppp were effective ligands in the carbonylation-polycondensation, especially under relatively low pressure of 0.6-1.5 MPa. However, PPh_3 was more excellent than dppp for the formation of high molecular weight polyester **1** under these conditions. The effect of CO pressure on the molecular weight of **1** for DIDHP was different from the case for DBDHP as shown in Fig. 2. The molecular weight of **1** for DIDHP was low under every pressure.

The structure of dihalide and bisphenol affected the carbonylation-polycondensation. Table 4 shows the effect of dihalide on the molecular weight of **1** by the use of dppp and DBU. Polyester **1** from DBDHP or DIDHP has higher solubility than poly[1,4-phenylene(1-methyl-ethylidene)-1,4-phenylene-carbonyl(4,4'-biphenylene-carbonyl)] (**8**) from DBBP or DIBP and accompanied the enhancement of its molecular weight. Such an increase of solubility is owing to the effect of bulkiness of 9,10-dihydrophenanthrene moiety. The molecular weight of **1** from DBDHP was higher than that from DIDHP. The difference between bromide and iodide should be explained by the difference of rate determining steps in successive reactions. Significant increase of the molecular weight of **8** was observed by the use of DIBP instead of DBBP. This was due to the enhanced reactivity of DIBP, which was compensated for negative factor of insolubility. When *p*-dibromobenzene was used as a dihalide, polyester **9** was obtained with low molecular weight due to the low solubility of the resulting polyester. Table 5 summarizes the effect of bisphenol on the molecular weight of polyesters. Bisphenols having sufficiently bulky alkyl spacers resulted moderately high molecular weight. Especially, bisphenol A gave the best results among them. Bisphenols with phenyl groups gave relatively poor results. Polyester **6** from bis(4-hydroxyphenyl)sulfone had low molecular weight. Polyester **7** from 4,4'-thiobisphenol was insoluble in the solvent. These low molecular weight is due to their low solubility.

Mechanistic aspects of the carbonylation-polycondensation

According to previous paper by Moser and his co-workers [8], active species for the carbonylation of aromatic halide is expected to be $\text{Pd}(0)\text{L}_n$ complex (L: phosphine moiety; $n: 1-4$), which is formed *in situ* from $\text{Pd}(\text{II})\text{Cl}_2$ and phosphine or from $\text{Pd}(\text{II})\text{L}_2\text{Cl}_2$ complex with phosphine. Oxidative addition of aryl halide to $\text{Pd}(0)\text{L}_n$ species, followed by CO insertion, and base mediated the alcoholysis to yield ester with regeneration of $\text{Pd}(0)\text{L}_n$. This mechanism is plausible and applicable to the carbonylation-polycondensation.

We found several characteristic features in our carbonylation-polycondensation. The molecular weight of **1** depended on the type of base. Strong organic bases such as DBU, TMEDA, and DABCO preferred to typical amines such as Et_3N and *i*-Pr₃NEt. These results suggest the alcoholysis step is a key step for the increase of molecular weight. Similar effects of base were observed in the carbonylation of 4-bromobiphenyl [12]. The molecular weight of **1** for DIDHP was inferior to that for DBDHP. The effects of CO pressure on the molecular weight of **1** for DIDHP were quite different from the case for DBDHP. These results mean that the oxidative addition of halide to $\text{Pd}(0)\text{L}_n$ is not so important for the increase of the molecular weight of resulting polyesters.

Figure 3 shows time dependence curves on CO consumption by the use of dppp and PPh_3 , respectively, under atmospheric pressure. The periods, for which half amount of carbon monoxide was consumed for the reaction, were 16 min and 32 min in the case of dppp and of PPh_3 ,

respectively. This means that catalytic activity for dppp is apparently higher than that for PPh₃. Figure 4 shows time dependence on the M_w by use of dppp and PPh₃, respectively, under the same condition as in Fig. 3. Initial rate of the increase of M_w for dppp is obviously larger than that for PPh₃, whereas final M_w for PPh₃ is higher than that for dppp. These results mean that catalytic activity is not parallel to final molecular weight of resulting polyesters, and that some inhibiting reactions may occur during the growth of the polyester in the case of dppp. We should note the side reactions because the rate of polyester formation should not affect the final molecular weight of polyester. To know whether side reactions take place or not, the phenoxycarbonylation of DBBP using the catalyst with dppp or PPh₃ was examined. Diphenyl biphenyl-4,4'-dicarboxylate was observed as a sole product from DBBP in high yield in both cases. Only a detectable product except the esters from DBBP was phenyl benzoate judging from GC analysis. This product should form via the carbonylation of chlorobenzene used as a reaction solvent. Amount of phenyl benzoate was 0.115 mmol with dppp and 0.044 mmol with PPh₃, respectively, from phenol (6.0 mmol) and chlorobenzene (10 ml) in the presence of DBBP (2.5 mmol). The amount of phenyl benzoate arising during the carbonylation-polycondensation with dppp was about three times larger than that with PPh₃. It is evident that the benzoyl complex as an intermediate of the carbonylation of chlorobenzene can act as a terminator of the carbonylation-polycondensation. This is a possible reason why the molecular weight of **1** with dppp is lower than that with PPh₃ in spite of higher catalytic activity of palladium-dppp complex. These results show that in order to obtain the polyesters with high molecular weight, the selectivity of the catalyst for the carbonylation is more important factor than catalytic activity.

Thermal properties of polyesters

Wholly aromatic polyesters **1-9** did not have melting point and glass transition temperature up to 400 °C. The 10 % weight loss temperature (T_{10}) values of them were above 380 °C in air. On the basis of TG profiles, polyesters **1** and **8** were more stable than **9** at 300-390 °C, although they lost their weights faster than **9** above 400 °C. Polyesters **1** and **5** were soluble in chloroform and dichloromethane. Soluble polyesters with M_w larger than 10,000 easily formed transparent casting films.

REFERENCES

- 1) J.-I. Jin, S. Antoun, C. Ober, and R. W. Lenz, *Brit. Polym. J.*, **12** (1990) 132.
- 2) M. Ballauff, *Angew. Chem. Int. Ed. Engl.*, **28** (1989) 253.
- 3) M. Yoneyama, M. Kakimoto, and Y. Imai, *Macromolecules*, **21** (1988) 1908; **22** (1989) 2593, 4152.
- 4) R.J. Perry, S.R. Turner, R.W. Blevins, *Macromolecules*, **26** (1993) 1509.
- 5) R.F. Heck, *Adv. Catal.*, **26** (1977) 323.
- 6) D.E. Pearson, U.S. Patent, 3988369 (1976).
- 7) Von H.O. Wirth, K.H. Gönner, and W. Kern, *Makromol. Chem.*, **63** (1963) 53.
- 8) W.R. Moser, A.W. Wang, N.K. Kildahl, *J. Am. Chem. Soc.*, **110** (1988) 2816.
- 9) Y. Sugi, K. Takeuchi, T. Hanaoka, T. Matsuzaki, S. Takagi, and Y. Doi, *Sekiyu Gakkaishi*, **37** (1994) 70.
- 10) Y. Ben-David, M. Portnoy, D. Milstein, *J. Am. Chem. Soc.*, **111** (1989) 8742.
- 11) R.E. Dolle, S.J. Schmidt, L.I. Kruse, *J. Chem. Soc., Chem. Commun.*, (1987) 904.
- 12) Y. Kubota, T. Hanaoka, K. Takeuchi, and Y. Sugi, *Synlett*, (1994) 515.

Table 1. Effects of solvent on the synthesis of **1**^{a)}

Run	Solvent	Yield (%)	M_w ($\times 10^3$)	(M_w/M_n)
1	Chlorobenzene	99	35	(3.6)
2	Anisole	99	25	(4.0)
3	Fluorobenzene	98	6.7	(2.3)
4	Benzene	94	5.8	(2.1)
5	Nitrobenzene	0	-	-

a) Reaction conditions: DBDHP 2.5 mmol, bisphenol A 2.5 mmol, PdCl₂ 0.1 mmol, dppp 0.2 mmol, DBU 5.5 mmol, solvent 10 ml, CO pressure 2.1 MPa, temperature 120 °C, period 3 h.

Table 2. Effects of base on the synthesis of **1**^{a)}

Run	Base	Yield (%)	M_w ($\times 10^3$)	(M_w/M_n)
6	DBU	95 ^{b)}	92	(2.5)
7	TMEDA ^{d)}	99	16	(3.3)
8	DABCO ^{c)}	96 ^{b)}	12	(4.1)
9	Et ₃ N	92 ^{b)}	4.5	(3.0)
10	<i>i</i> -Pr ₃ NEt	22	0.9	(1.4)

a) Reaction conditions: DBDHP 2.5 mmol, bisphenol A 2.5 mmol, PdCl₂ 0.1 mmol, PPh₃ 0.4 mol, DBU 5.5 mmol, chlorobenzene 10 ml, CO pressure 2.1 MPa, temperature 120 °C, period 3 h. b) dppp 0.2 mmol, was used as a ligand. c) Palladium precipitate was observed. d) *N,N,N',N'*-tetramethylethylenediamine. e) 1,4-Diazabicyclo[2.2.2]octane.

Table 3. Effects of catalyst on the synthesis of **1**^{a)}

Run	Catalyst	Yield (%)	M _w (x10 ³)	(M _w /M _n)
11	PdCl ₂ /2PPh ₃	39	1.2	(1.6)
12	PdCl ₂ /4PPh ₃	92	37	(3.0)
13	Pd(PPh ₃) ₄ ^{b)}	96	19	(3.8)
14	PdCl ₂ /2dppe ^{c)}	94	12	(3.6)
15	PdCl ₂ /dppp ^{d)}	97	6.2	(2.5)
16	PdCl ₂ /2dppp	99	35	(3.6)
17	PdCl ₂ /5dppp	39	1.2	(1.6)
18	PdCl ₂ /2dppb ^{e)}	95	21	(3.4)
19	PdCl ₂ /2dppe ^{f)}	91	17	(3.2)

a) Reaction conditions: DBDHP 2.5 mmol, bisphenol A 2.5 mmol, PdCl₂ 0.1 mmol, phosphine 0.1-0.5 mmol, DBU 5.5 mmol, chlorobenzene 10 ml, CO pressure 2.1 MPa, temperature 120 °C, period 3 h. b) Pd(PPh₃)₄, 0.1 mmol. c) 1,2-bis(diphenylphosphino)ethane. d) 1,3-bis(diphenylphosphino)propane. e) 1,4-bis(diphenylphosphino)butane. f) 1,5-bis(di-phenylphosphino)hexane.

Table 4. Polyesters of dihalides with bisphenol A^{a)}

Run	Dihalobiphenyl	Polyester	Yield (%)	M _w (x10 ³)	(M _w /M _n)
20	DBDHP	1	99	35	(3.6)
21	DIDHP	1	98	24	(2.8)
22	DBBP	8	94	5.6	(6.3)
23	DIBP	8	94	12	(2.5)
24	<i>p</i> -Dibromobenzene	9	96	2.6	(2.5)

a) Reaction conditions: dihalide 2.5 mmol, bisphenol A 2.5 mmol, PdCl₂ 0.1 mmol, dppp 0.2 mmol, DBU 5.5 mmol, chlorobenzene 10 ml, CO pressure 2.1 MPa, temperature 120 °C, period 3 h.

Table 5. Polyesters of bisphenols with DBDHP^{a)}

Run	Bisphenol	Polyester	Yield (%)	M _w (x10 ³)	(M _w /M _n)	Remarks
26	Bisphenol A	1	99	35	(3.6)	-
27	4,4'-Cyclohexylidenebisphenol	2	93	20	(3.1)	-
28	4,4'-(<i>s</i> -Butylidene)bisphenol ^{b)}	3	97	13	(3.0)	-
29	4,4'-Ethylidenebisphenol	4	98	12	(2.7)	+
30	4,4'-(1-Phenylethylidene)bisphenol	5	99	25	(3.7)	-
31	4,4'-Sulfonylbisphenol	6	77	1.2	(2.0)	++
32	4,4'-Triobisphenol	7	99	insoluble		++

a) Reaction conditions: DBDHP 2.5 mmol, bisphenol 2.5 mmol, PdCl₂ 0.1 mmol, dppp 0.4 mmol, DBU 5.5 mmol, chlorobenzene 10 ml, CO pressure 2.1 MPa, temperature 120 °C, period 3-5 h. b) CO pressure 1.1 MPa. c) Outlook of reaction mixture just after the reaction. -: homogenous. +: slightly suspended. ++: suspended.

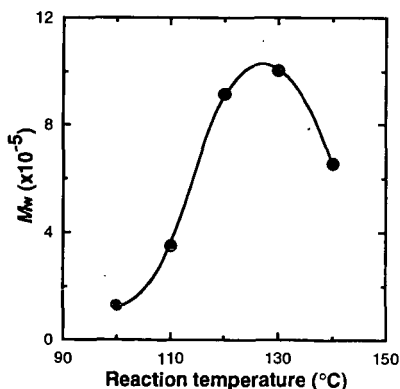


Fig. 1. Effect of reaction temperature on the molecular weight of **1**. Reaction conditions: DBDHP 2.5 mmol, bisphenol A 2.5 mmol, PdCl₂ 0.1 mmol, PPh₃ 0.2 mmol, DBU 5.5 mmol, chlorobenzene 10 ml, CO pressure 1.1 MPa, period 3 h.

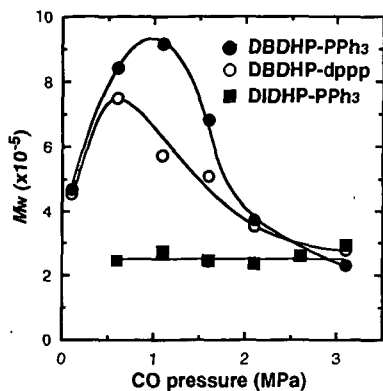


Fig. 2. Effect of CO pressure on the molecular weight of **1**. Reaction conditions: dihalide 2.5 mmol, bisphenol A 2.5 mmol, PdCl₂ 0.1 mmol, PPh₃ 0.2 mmol or dppp 0.1 mmol, DBU 5.5 mmol, chlorobenzene 10 ml, temperature 120 °C, period 3 h.

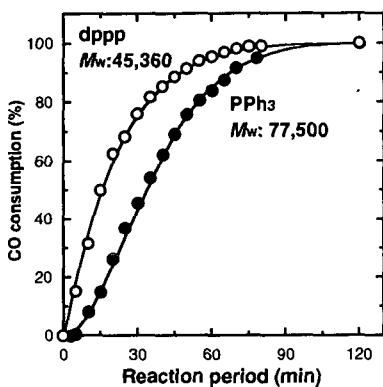


Fig. 3. CO consumption during the carbonylation-polycondensation. Reaction conditions: DBDHP 2.5 mmol, bisphenol A 2.5 mmol, PdCl₂ 0.1 mmol, PPh₃ 0.4 mmol or dppp 0.2 mmol, DBU 5.5 mmol, chlorobenzene 10 ml, CO pressure 0.1 MPa.

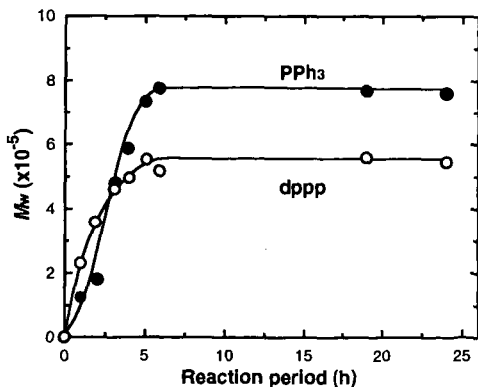


Fig. 4. Time dependence of the molecular weight on the synthesis of **1**. Reaction conditions: DBDHP 2.5 mmol, bisphenol A 2.5 mmol, PdCl₂ 0.1 mmol, PPh₃ 0.4 mmol or dppp 0.2 mmol, DBU 5.5 mmol, chlorobenzene 10 ml, CO pressure 0.1 MPa.

SHAPE-SELECTIVE HYDROGENATION OF NAPHTHALENE OVER ZEOLITE-SUPPORTED Pt AND Pd CATALYSTS

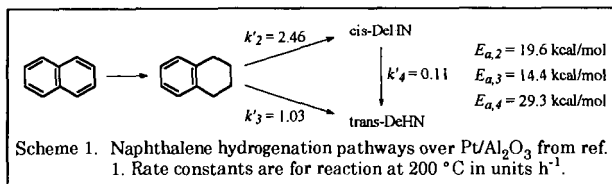
Andrew D. Schmitz, Grainne Bowers and Chunshan Song

Department of Materials Science and Engineering
Fuel Science Program, 209 Academic Projects Building
Pennsylvania State University, University Park, PA 16802

Keywords: hydrogenation, bifunctional catalysts, shape-selectivity

Introduction

Per-hydrogenation of naphthalene produces both *cis*-decalin (*c*-DeHN) and *trans*-decalin (*t*-DeHN). Huang and Kang reported the rate data shown in Scheme 1 for this reaction catalyzed by $\text{Pt}/\text{Al}_2\text{O}_3$.¹ Isomerization of *c*-DeHN was treated as irreversible, and it was assumed that dehydrogenation of DeHN could be neglected. We have found it possible to achieve high selectivity



for one DeHN isomer by appropriate catalyst selection. For example, Pt/HY gives 100% naphthalene conversion to decalins with 80% selectivity for *c*-DeHN. There numerous potential industrial applications for *c*-DeHN; such as, the production of sebacic acid which can be used in the manufacture of Nylon 6,10 and softeners. Conversely, catalysts that promote the thermodynamically favored *c*-DeHN to *t*-DeHN isomerization can be made to give nearly 95% *t*-DeHN. This reaction can be used in fuel upgrading applications, to increase the thermal stability of the fuel.

Considerable effort has been invested in this laboratory to develop jet fuels with improved thermal stability, particularly for high-performance jet aircraft (see ref. 2, for example). In this application, the fuel is also used as the primary heat sink for cooling. As the fuel temperature is raised, fuel degradation leads to the formation of solid particulates in the fuel.² Over time, the particulates agglomerate and are deposited, plugging filters, fuel lines and fuel injectors. A jet fuel's overall carbon-forming propensity can be reduced by limiting its aromatic content as in the complete hydrogenation of naphthalene. In thermal stressing of jet fuels, Song et al. have shown that cyclic alkanes have higher thermal stability than normal alkanes.²⁻³ Cycloalkane conformation also effects high temperature stability, and it has been shown that *t*-DeHN is more stable than *c*-DeHN.²⁻³ Tests on the thermal stressing of petroleum-derived fuels and model compounds have shown that addition of *t*-DeHN can significantly retard the rate of carbon deposition.³

Two types of zeolites were used in this work: H-mordenite (HM) and HY. Mordenite has a two-dimensional channel structure with elliptically shaped channels of diameter 6.7 x 7.0 Å. Since naphthalene's critical diameter is very close to the HM channel dimension, transition state selectivity is induced on reactions of naphthalene occurring in the channels. Relative diffusion rates of the products can also effect selectivity. HY has large cavities in its interior and narrow channel openings. A reactant that has entered the channel structure may reorient itself and react at catalyst sites on the walls of the cavities. However, because of restricted diffusion at the channel openings, only molecules of appropriate diameter will be produced at an appreciable rate.

The final *t*-DeHN/*c*-DeHN (*t/c*) ratio in the product is governed by several factors related to the bifunctionality of the catalysts. While the initial *t/c* ratio may be governed by several factors, zeolite acid character significantly influences *c*-DeHN isomerization. It has been found that catalysts based on dealuminated HM give the highest *t*-DeHN selectivity. Choice of the noble metal, Pt or Pd, is also important. In accord with previously reported data for naphthalene hydrogenation using noble metal catalysts on non-zeolite supports,⁴ our data show that Pd/zeolite has higher initial selectivity for *t*-DeHN, and also isomerize *c*-DeHN at higher rates than platinum on the same zeolite. Metal particle sizes determined from X-ray powder diffraction (XRD) line-widths show large variations on the different zeolites.

Experimental

Catalyst Preparation. The zeolites were supplied in NH_4 -form and used as received. Table 1 lists their properties. Two portions of each zeolite were loaded with metal, one with Pt, the other Pd, to generate a total of eight catalysts. Incipient wetness impregnation of either aqueous $\text{H}_2\text{PtCl}_6 \cdot x\text{H}_2\text{O}$ (Aldrich, 99.995% Pt, metal basis) or PdCl_2 (Aldrich, 99.999% Pd, metal basis) dissolved in dilute hydrochloric acid (sufficient to form soluble PdCl_4^{2-}) was used to achieve a nominal metal concentration of 6 wt%. Following drying in vacuo, the catalysts were calcined in

air at 450 °C for 2 h. Noble metal reduction occurs during the catalyst test, in the hydrogen pressurized reactors.

Catalyst Evaluation. A 30 mL, stainless steel tubing-bomb batch reactor was used for catalyst tests. A tee-shaped design was used where most of the reactor internal volume is in the horizontal member that contains the catalyst and reactants. The horizontal member is connected by a 10" length of 1/4" o.d. tubing to a pressure gauge and valve. The reactor was charged with 0.4 g catalyst, 1.0 g (7.8 mmol) naphthalene (Aldrich, 99%), 4.0 g n-tridecane reaction solvent, and 0.35 g n-nonane internal standard. The charged reactor was flushed with H₂ then sealed and leak-tested with H₂. Finally, the hydrogen pressure was adjusted to 1500 psig cold (ca. 0.2 g) to start the test. Naphthalene begins to react immediately, even at room temperature, so a consistent procedure was established to minimize the time between reactor pressurization and the start of the run.

The reactor was affixed to a holder and placed in a fluidized sand-bath heater so that approximately two-thirds of the total length was immersed. Vertical agitation at 240 cycle/min was used to provide mixing. The reactions were done at 200 °C for 6-60 min. At the end of each test, the reaction was quenched in cold water. After cooling, the gas headspace was collected for analysis and the reactor was opened. Acetone was used to wash the reactor contents onto a filter and the filtrate was analyzed by GC/GC-MS (30m x 0.25mm DB-17 column, J&W Scientific), while the solid was dried for XRD examination.

X-ray powder diffraction analyses (XRD) were done on a Scintag 3100 diffractometer using Cu K α radiation and a scan rate of 1° 2 θ /min with 0.02° steps. Diffraction line widths were measured using a profile-fitting program which assumes a peak shape intermediate between Gaussian and Cauchy. Manual measurements were always used to check the calculated results, especially for very diffuse lines where the computer routine fails. Mean metal crystallite size was calculated by application of the Scherrer equation (wavelength 1.54056 Å, Scherrer constant 0.89).⁵ Silicon powder (-325 mesh) was used as an external standard for measuring instrumental and spectral broadening. K α_2 -doublet broadening corrections, and pure line profile determination for low-angle reflections were done as described elsewhere.⁵ For most of the catalysts, only the Pt or Pd (111) diffraction line was suitable for profile analysis. The lower intensity lines of the metals were interfered with by zeolite patterns.

Results and Discussion

XRD Observations. XRD for the Pt and Pd catalysts removed from the reactors following the 60 min runs are shown in Figures 1-2. In each case, only diffraction lines corresponding to the zero-valency state of the metals are observed. Several catalysts from the 30 min runs were also examined, and only metallic phase is observed. Therefore, in situ hydrogen treatment is adequate for complete metal reduction. Differences between the samples are striking, especially for the Pt catalysts. Pt/HY shows very sharp and intense metal diffraction lines (large Pt particles), but Pt/HM38 and Pt/HM17 show very broad, diffuse lines indicative of small Pt particles. Pt/M21 is intermediate. Closer examination of Pt/HM38 shows that the Pt-phase is bidisperse. A sharp line appears superimposed over a very broad band, both arising from reduced platinum. Pd catalysts (Figure 1) all show significant line-broadening. The trend in line width increase on going from metal/HY to metal/HM17 is also observed for Pd, but is less pronounced. Average metal particle sizes for the Pt and Pd catalysts are compared in Table 2 and Table 3, respectively.

Accuracy of the XRD particle size technique is generally accepted to be \pm 10-20%. When XRD lines become very broad and diffuse, accurate line-width measurements are difficult, however. This was more of a problem for Pd which has a lower scattering power ($z = 46$) than Pt ($z = 78$). Baseline zeolite signals from HM38 and HM17 cloud the Pd (111) reflection enough that accurate measurements are not possible. Conservatively narrow best-guesses at the line widths were used to determine the values cited in the tables.

Effects of Catalyst Composition. Test data for 60 min runs at 200 °C for the eight Pt- and Pd-loaded zeolite catalysts are compared in Table 2 and Table 3, respectively. The products of Nap hydrogenation are almost exclusively isomeric DeHN's. In some cases, a small amount of tetrahydronaphthalene (TeHN) is observed. Gas headspace analyses show 5-50 ppm levels of C₁-C₄ hydrocarbons. Every catalyst gives ca. 100% Nap conversion in 1 h, so it is not possible to rank catalyst activity based on these data. Yet, the *trans/cis* DeHN ratio is highly dependent on both the zeolite and the metal. Palladium gives higher *t*-DeHN selectivity than platinum on the same zeolite. Catalysts based on HM38 gave the highest *t*-DeHN selectivity. There is a definite upward trend in *t/c* ratio with HM SiO₂/Al₂O₃ ratio. Pt/HY shows amazingly high selectivity for *c*-DeHN.

Comparing catalyst with the same metal, there does not seem to be any correlation between metal crystallite size and DeHN isomer selectivity. Neither naphthalene hydrogenation nor *c*-DeHN isomerization involve C-C σ -bond breaking. Consequently, the overall reaction should be structure insensitive and independent of metal particle size.

Effects of Run Duration. In order to determine the practical equilibrium *t/c* ratio, four tests were done with Pd/HM21 at extended reaction times (Table 4). An approximately constant *t/c* of 13.6 is obtained within 6 h reaction time. This value is somewhat lower than the calculated equilibrium constant for *c*-DeHN to *t*-DeHN isomerization of 20.5 at 200 °C.⁶ However, ca. 14 is the practical limit as confirmed using other Pt/zeolite and Pd/zeolite catalysts.⁷ Some decalin may reside in the portion of the reactor that extends above the sand level in the fluidized sand bath, the *cold zone*, and may not react. According to calculations, if even 5% of the decalin doesn't react to form an equilibrium amount of *t*-DeHN, the equilibrium constant value falls to 13.0.⁶

It was already known that complete naphthalene conversion to a mixture of decalins occurred within the first hour of each test. We wanted to find out if the initial product distribution was significantly different than what we had observed in 60 min runs. Additional runs were done with Pt/HM38, Pd/HM38, Pt/HY and Pd/HY at 15 and 30 min. The metal/HY catalysts were also tested at 6 min. It should be noted that 6 min is the approximate time required for the interior of the reactor to equilibrate to the reaction (sand bath) temperature. Greater than 99% naphthalene conversion occurred within the shortest run period for each test. Decalins were the only hydrogenation products with the exception of the 6 min run with Pt/HY, where 48% TeHN was also observed. However, less than 3 % TeHN was observed in the longer runs with Pt/HY. Plots of $\log(c\text{-DeHN})$ vs time are linear (Figure 3) showing that the isomerization of c-DeHN is first-order. Considering Scheme 1, when all of the TeHN has been consumed, the rate expression for disappearance of c-DeHN simplifies to a simple first-order expression in c-DeHN concentration. This simplification does not hold when the TeHN concentration is non-zero, so the 6 min data point for Pt/HY is not included in the determination of k_d . Values determined for the rate constant in this work are compared with literature values in Table 5. It can be seen that not only does Pd have a higher initial selectivity for t-DeHN, but it also isomerizes t-DeHN faster than Pt. The values of k_d determined in this work are considerably higher than those reported by Huang and Kang,¹ and Lai and Song for direct isomerization of c-DeHN.⁶ Huang and Kang did not report the mass of catalyst used, so it is not possible to compare values on a per-gram catalyst basis. Lai and Song used the same Pt/HM38 catalyst that was used here. We are still not certain what causes the discrepancy between these data and the results of Lai and Song. Other detailed kinetic studies on hydrogenation of aromatics have recently been published.⁸⁻⁹

The Pt/HY catalyst is highly selective for c-DeHN and does not promote the isomerization. We are unable to explain this result at present but suspect that it may be due, in some way, to the large Pt particle size (1700 Å). It is possible that a unique type of shape-selectivity may arise from partial blockage of the channel openings by the large metal particles. Further understanding may be gained by electron microscopy and H₂ chemisorption to determine metal dispersions.

Conclusions

It has been established that the naphthalene hydrogenation process can be tailored to produce either c-DeHN or t-DeHN by appropriate choice of the zeolite and metal species. Selectivity for t-DeHN increases with SiO₂/Al₂O₃ ratio in the HM catalysts, so that catalysts based on HM38 gave the highest t-DeHN selectivity. Compared to Pt on a given zeolite, Pd shows a higher initial selectivity for t-DeHN, and a higher rate for c-DeHN to t-DeHN isomerization. The practical equilibrium t/c ratio is 14 at 200 °C. Metal crystallite sizes are highly dependent on the zeolite. Pd generally had a higher dispersion than did platinum on a given zeolite. Naphthalene hydrogenation and c-DeHN isomerization are structure insensitive reactions. Therefore, DeHN isomer selectivity does not show a correlation with particle size. Uniquely high selectivity for c-DeHN has been obtained with Pt/HY. It has been proposed that partial channel blockage by the large metal particles of this catalysts give rise to a unique type of shape-selectivity.

Acknowledgements

We wish to thank the following persons at the Pennsylvania State University: Prof. Harold Schobert for his encouragement and support, and W.-C. Lai for his thoughtful comments on this work. This work was jointly supported by the U.S. Dept. of Energy, Pittsburgh Energy Technology Center, and the Air Force Wright Propulsion Laboratory. We would also like to thank Mr. W. E. Harrison III of USAF and Dr. S. Rogers of DOE for their support.

References

- Huang, T.-C.; Kang, B.-C. Kinetic Study of Naphthalene Hydrogenation Over Pt/Al₂O₃ Catalyst *Ind. Eng. Chem. Res.* **1995**, *34*, 1140-1148. The authors neglected to divide the slopes from activation energy plots by the gas constant (1.987 cal/mol·K) for reporting activation energies. The data cited in Scheme 1 are the correct values.
- Song, C.; Eser, S.; Schobert, H. H.; Hatcher, P. G. Pyrolytic Degradation Studies of a Coal-Derived and a Petroleum-Derived Aviation Fuel *Energy & Fuels*, **1993**, *7*, 234-243.
- Song, C.; Lai, W.-C.; Schobert, H. H. Hydrogen-Transferring Pyrolysis of Cyclic and Straight-Chain Hydrocarbons. Enhancing High Temperature Thermal Stability of Aviation Jet Fuels by H-Donors *Am. Chem. Soc. Div. Fuel Chem. Prepr.* **1992**, *37*, 1655.
- Weitkamp, A. W. Stereochemistry and Mechanism of Hydrogenation of Naphthalenes on Transition Metal Catalysts and Conformational Analysis of the Products *Adv. Catal.* **1968**, *18*, 1-110.
- Klug, H. P.; Alexander, L. E., "X-ray Diffraction Procedures for Polycrystalline and Amorphous Materials;" Wiley: New York, 1974. See example calculations on p 699.
- Lai, W.-C.; Song, C. Zeolite Catalyzed Conformational Isomerization of cis-Decahydronaphthalene. Reaction Pathways and Kinetics *Am. Chem. Soc. Div. Fuel Chem. Prepr.* **1995**, *40*, in press.
- Schmitz, A. D.; Song, C. unpublished results.
- Korre, S. C.; Klein, M. T.; Quann, R. J. Polynuclear Aromatic Hydrocarbons Hydrogenation. I. Experimental Reaction Pathways and Kinetics *Ind. Eng. Chem. Res.* **1995**, *34*, 101-117.

9. Stanislaus, A.; Cooper, B. H. Aromatic Hydrogenation Catalysis: A Review *Catal. Rev.—Sci. Eng.* 1994, 36, 75-123.

Table 1. Properties of the Zeolite Starting Materials

zeolite id.	zeolite type	supplier	SiO ₂ /Al ₂ O ₃ , molar	Na ₂ O, wt %	surface area, m ² /g
HY	zeolite Y	Linde LZ-Y62	5.0	2.5	948
HM17	mordenite	Linde LZ-M-8	17.0	0.05	480
HM21	mordenite	PQ Corp., Inc. CBV 20A	21.1	0.02	606
HM38	mordenite	PQ Corp., Inc. CBV 30A	37.5	0.07	512

Table 2. Naphthalene Hydrogenation Data for Platinum Catalysts in 60 min Runs at 200 °C

catalyst	conv., %	Product Distribution (mole %)				average metal particle size, Å
		TeHN	trans- DeHN	cis- DeHN	total DeHN	trans/cis DeHN
Pt/HM17	100	0.0	37	63	100	0.58
Pt/HM21	100	0.0	45	55	100	0.83
Pt/HM38	100	0.0	70	30	100	2.34
Pt/HY	100	2.6	15	82	97	0.18

^a Bidisperse metal. Particle sizes for the broad (and sharp) components of the Pt (111) are indicated.

Table 3. Naphthalene Hydrogenation Data for Palladium Catalysts in 60 min Runs at 200 °C

catalyst	conv., %	Product Distribution (mole %)				average metal particle size, Å
		TeHN	trans- DeHN	cis- DeHN	total DeHN	trans/cis DeHN
Pd/HM17	100	0.0	65	35	100	1.84
Pd/HM21	100	0.0	75	25	100	3.00
Pd/HM38	100	0.0	82	18	100	4.42
Pd/HY	100	0.0	73	27	100	2.69

^a Diffuse diffraction line makes accurate width measurement difficult. Metal particles are no larger than the indicated size.

Table 4. Equilibrium DeHN Isomer Distribution from Naphthalene Hydrogenation Over Pd/HM21 Catalyst at 200 °C

time (h)	conv., %	Product Distribution (mole %)				trans/cis DeHN
		TeHN	trans- DeHN	cis- DeHN	total DeHN	
1	100	0.0	76.5	23.5	100	3.26
6	100	0.0	93.1	6.92	100	13.46
10	100	0.0	93.2	6.78	100	13.74
24	100	0.0	93.2	6.85	100	13.59

Table 5. Comparison of c-DeHN Isomerization Rate Constants from This Work and the Literature

	Pt/HM38	Pd/HM38	Pt/HY	Pd/HY	Pt/HM38 ^a	Pt/Al ₂ O ₃ ^b
k_d, h^{-1}	0.78	0.84	0	0.35	0.30	0.11
$k_d, \text{mmol/g-cat}\cdot\text{h}$	15.2	16.4	0	6.9	10.9	—

^aIsomerization of c-DeHN from ref. 6. ^bNaphthalene hydrogenation from ref. 1.

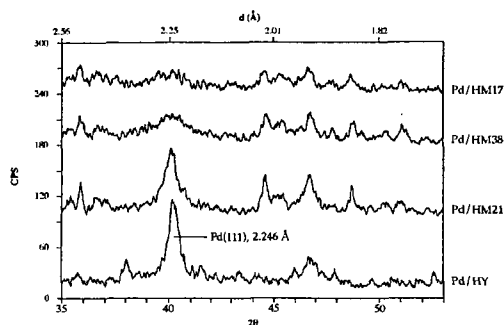


Figure 1. XRD patterns for palladium catalysts in the region of the Pd (111) and (200) lines.

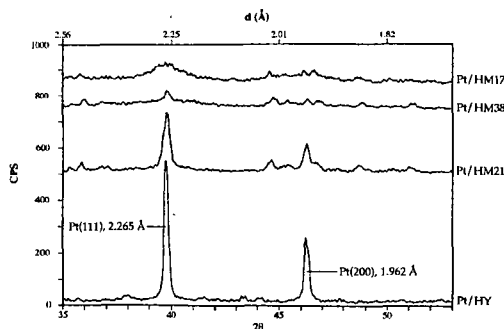


Figure 2. XRD patterns for platinum catalysts in the region of the Pt (111) and (200) lines.

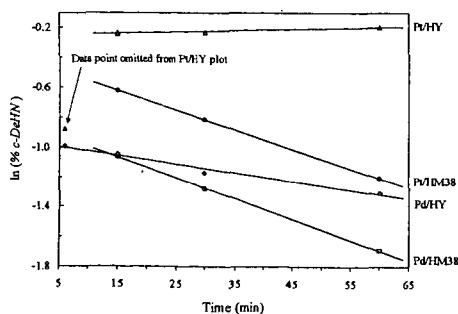


Figure 3. First-order rate constant plots for c-DeHN to t-DeHN isomerization at 200 °C.

CATALYTIC HYDROGENATION OF POLYAROMATIC COMPOUNDS USING COKE-OVEN GAS INSTEAD OF PURE HYDROGEN.

C.E.Brackman-Danheux, A.H.Fontana, Ph.M.Laurent and Ph.Lolivier

Service de Chimie Générale et Carbochimie, Faculté des Sciences Appliquées, Université Libre de Bruxelles, CP 165, Av. F.D. Roosevelt, B-1050, Bruxelles, Belgium.

Keywords: catalytic hydrogenation, polyaromatic, coke-oven gas.

ABSTRACT

In order to improve the economy of the conversion process of polyaromatic molecules to their hydroaromatics analogs, catalytic hydrogenation of phenanthrene has been carried out under pressure of different simulated coke-oven gases instead of pure hydrogen. The influence of reaction time, temperature and pressure on the hydrogenation yields and on the nature of the obtained products has been studied. Comparisons have been made with reaction with pure hydrogen in the same conditions. The influence of the different components of a real coke-oven gas has also been pointed out. The results indicate that coke-oven gas can be used if the goal is not to obtain perhydroaromatics compounds for a thermal cracking, but to give partly hydrogenated compounds to be used as hydrogen donor solvent in a coal liquefaction process. The results have been applied to coal-tar highly aromatic fractions.

INTRODUCTION

Coal derived heavy oils contain principally polyaromatics hydrocarbons (P.A.H.). Previously published studies^{1,2} showed that these molecules must be hydrogenated to their perhydrogenated analogs in order to obtain high yields of light aromatics (B.T.X.) and ethylene by thermal cracking. Moreover, these perhydrogenated molecules could provide one of the best solution to the requirement of modern jet plane fuels³⁻⁵. If the hydrogenation is not complete, the partly hydrogenated oils could also be used as hydrogen donor solvent in a coal liquefaction process.

An important economic factor in hydrogenation processes is the hydrogen cost. To reduce this cost will be beneficial. In this perspective, Doughty and al.^{6,7} studied the hydrocracking of coal derived liquids using bimetallic catalyst and a gas mixture of 90% H₂ / 10% CO instead of pure hydrogen. They showed that the conversion to low boiling point materials was lower in presence of 10% CO, probably because the CO molecules occupy the H₂ sites at the catalyst surface. Fu and al.⁸ performed the hydrogenation of model compounds in presence of petroleum solvent using syngas (H₂ : CO = 1:1). The experiments were carried out in a microreactor during 45 minutes. The results showed that the hydrogenation of anthracene at 350°C under H₂ pressure gave 90% conversion. The reaction with syngas at the same temperature gave only 65.9% anthracene conversion. The most important product was dihydroanthracene.

The use of H₂/CO mixtures may introduce other competing reactions which lead to undesirable products. For example, if the experimental conditions are similar to those used in the methanation reaction, hydrogen and carbon monoxide will be consumed, producing unwanted methane and water. Even with low levels of CO, catalyst poisoning may be increased. The loss in catalytic activity would lead to reduced conversions, which have to be compared to the gain in cost due to the use of a coke-oven gas. Moreover, industrial gases used directly may contain H₂S which could poison the catalyst.

The aim of this work is to hydrogenate polyaromatics hydrocarbons using the coke-oven gas instead of pure hydrogen. Coke oven-gas contains approximatively 55% H₂, 30% CH₄, the balance being made by CO₂, CO, C_nH_m, N₂. Phenanthrene has been chosen as a model compound for the P.A.H. in the heavy oils. Many works over catalytic hydrogenation of P.A.H. were published, but anyone study the possibility of using coke-oven gas instead of pure hydrogen.

EXPERIMENTAL

Procedure

Experiments were performed in a 250 ml stainless steel PARR 4570 autoclave. 10 g of phenanthrene and 2 g of catalyst are introduced in the reactor, without solvent. The installation is purged with the reactive gas and pressurised at ambient temperature. Temperature is then raised as quickly as possible to the desired one. The reaction system is continuously stirred at 250 rpm. After reaction, the autoclave is cooled at ambient temperature and depressurised. The gases and the liquids are collected and analyzed.

Catalysts

A commercial nickel-molybdenum catalyst (3% NiO, 15% MoO₃ on alumina, surface area : 300 m²/g) was used in all experiments. For comparison, some experiments were carried out with a cobalt-molybdenum catalyst and also with a palladium catalyst.

Analyses

Gases and liquids products are analyzed by gas chromatography. The g.c. conditions are described elsewhere⁶. The products, first identified by gc/ms, are dihydrophenanthrene (DHP), tetrahydrophenanthrene (THP), sym-octahydrophenanthrene(sOHP), asym-octahydrophenanthrene (asOHP), and perhydrophenanthrene (PHP). Mass balances are controlled after each experiment. The compositions of the different simulated coke-oven gases used in this work are given in table 1.

RESULTS AND DISCUSSION

Hydrogenation of phenanthrene with pure hydrogen (gas 1)

The hydrogenation of phenanthrene under H₂ pressure was studied as a function of reaction time. Temperature and pressure were kept constant (370°C-21 MPa). The results are summarized in table 2 and confirms these of Colglough¹⁰ at the same temperature and pressure. It can be seen also that the yield of cracking products remains low. These results will be used for the comparison with the hydrogenation performed with the other gases mixtures.

Hydrogenation of phenanthrene with simulated coke-oven gases.

Influence of reaction time.

The hydrogenation of phenanthrene was studied as a function of time, at 370°C and under 21 MPa of a gas containing the two main components of a coke-oven gas, the balance being made by nitrogen (gas 3). The results are presented in table 2. As in pure hydrogen, the conversion of phenanthrene is high, more than 90% after 2 hours. The PHP yield increases regularly but cannot reach the value obtained under pure hydrogen, even after 16 hours of reaction.

Influence of temperature

The hydrogenation of phenanthrene with gas 3 was studied between 300 °C and 450°C. Pressure and reaction time were kept constant (21MPa-16 hours). The results are shown in table 2. It can be seen that a rise in temperature favour the hydrogenation reactions. The maximum yield of PHP is obtained at 370°C. At higher temperature, the yield of PHP decreases while the yields of cracking products and phenanthrene increase. Higher temperatures introduce ring opening reactions, leading to the formation of lower molecular weight products. The formation of aromatics compounds by deshydrogenation reactions is also favoured by increasing temperature and explain the high yield of phenanthrene.

Influence of pressure.

The hydrogenation of phenanthrene was studied between 11 and 25 MPa of gas 3. Temperature and reaction time were kept constant (370°C-16 hours). Table 2 gives the yield of the products as a function of pressure. At the lower pressure, the conversion of phenanthrene is low and the hydroaromatics species are the major products. The hydrogenation of phenanthrene is favoured at higher pressure. These results are also in agreement with these of previous works.

Influence of the components of the coke-oven gas.

In order to learn more about the influence of each components, catalytic hydrogenation of phenanthrene was studied under pressure of different simulated coke-oven gases. Temperature, pressure and reaction time were kept constant (370°C-21MPa-16 hours). Results are shown in table 2. The results are also compared to the one obtained under 11.5 MPa of hydrogen, this pressure corresponding to the H₂ partial pressure in the coke-oven gas.

- Hydrogen influence

Under pure H₂ pressure, the conversion of phenanthrene is 99%. The yield of PHP is more than 80% and the yield of cracking products is small. The conversion and the yield of PHP decrease in presence of nitrogen (gas 2). However, the yield of cracking products become important. The comparison between the results obtained under 11.5 MPa of hydrogen and under 21 MPa of gas 2 permitted to distinguish between the influence of total pressure and hydrogen partial pressure. It can be seen that for the same hydrogen pressure, the yield of cracking products is less important if the total pressure is higher.

- Methane influence

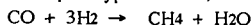
The comparison of the results of reaction with gas 2 and gas 3 showed that the yields of the different hydrogenated products are not significantly influenced by the presence of methane. In our experimental conditions, methane does not handicap the catalytic hydrogenation of phenanthrene.

- Influence of the other components

The presence of ethane, ethylene and carbon dioxide (gas 5) modifies slightly the composition of the hydrogenation products. On the other hand, the presence of CO lead to an important drop of the yields of hydrogenated compounds and specially the PHP. The cracking becomes also important; it raises from 10% to 30%.

The influence of the carbon monoxide can be explained by the following hypotheses:

- formation of alkanes by Fisher-Tropsch type reactions, consuming hydrogen, for example:



- partial deactivation of the catalysts, the carbon monoxide occupying preferentially some active sites^{6,7}.

In our experimental conditions, these reactions occur as shown by the following experiments. The composition of the hydrogenating gas (gas 4) has been compared before and after reaction in 3 cases: Exp1 : the autoclave contains coke-oven gas (gas 4) alone;

Exp2 : the autoclave contains coke-oven gas (gas 4) and the NiMo catalyst;

Exp3: the autoclave contains coke-oven gas (gas 4), the NiMo catalyst and the phenanthrene. The results are shown in table 3. The experiments 2 and 3 confirm the reactivity of carbon monoxide: the yield of methane increases while the yield of hydrogen decreases when coke-oven gas is treated in presence of the catalyst. The formation of propane could also be explained by Fischer-Tropsch reaction. Partial hydrogenation of ethylene occurs also, even in the absence of the catalyst.

Thermal cracking of the hydrogenated compounds.

In order to verify the thermal behaviour of the hydrogenated compounds, thermal cracking experiments have been performed on the mixtures obtained after hydrogenation of the phenanthrene with gas 4 and with pure hydrogen. The crackings are made at atmospheric pressure under nitrogen at 800°C and with a residence time of 1 s. As shown in table 4, the BTX yields obtained by thermal cracking are directly related to the amount of perhydrogenated compounds present in the hydrogenation products, as explained previously¹².

Hydrogenation of heavy oils.

Two different industrial oils have been hydrogenated : an heavy naphtha fraction of petroleum (HLN) and a chrysénic fraction of a coal tar (HC). The experimental conditions are: T°: 370°C, P : 21 MPa, t : 16 h, cat.: sulfided Ni-Mo. The hydrogenating gas used is gas 4 and the results are compared with hydrogenation under pure hydrogen. Due to the complexity of the oils, the thermal cracking of the mixtures obtained after hydrogenation has been directly performed, mainly to compare the BTX yields. It has to be pointed out that the untreated heavy oils do not contain BTX. The results, summarized in table 5, indicate clearly that the amounts of perhydrogenated compounds are lower when the simulated coke-oven gas is used for the hydrogenation, confirming the results obtained on the model substance.

CONCLUSIONS

The results obtained during this research have shown, the possibility to use a coke-oven gas to perform the hydrogenation of PAH with a commercial catalyst. But it was not possible, even by increasing the reaction time, to obtain with a gas containing 55% H₂ the same yield of PHP as the one obtained with pure hydrogen.

The influence of the various components of the coke-oven gas on the hydrogenation yields has been investigated: CH₄ does not handicap the catalytic hydrogenation of the phenanthrene; the presence of C₂H₄, C₂H₆, and CO₂ modifies slightly the composition of the hydrogenation products; the presence of CO leads to an important drop of the yields of hydrogenated compounds and specially the perhydrogenated.

It can be concluded that, if the goal of the hydrogenation is not to obtain perhydrogenated compounds for a chemical upgrading by thermal cracking, but to give partly hydrogenated compounds to be used as hydrogen donor solvent in coal liquefaction processes, then the hydrogen can be economically replaced by a coke-oven gas.

AKNOWLEDGEMENTS.

The authors wish to thank the Commission of the European Communities, Coal Directorate, for their financial support for the project (ECSC Project 7220-EC/208).

REFERENCES.

1. Cyprès R. and Bredael P., *Fuel Process. Technol.*, 1980, **3**, 297.
2. Bernhardt R.S., Ladner W.R., Newman J.O. and Page P.W., *Fuel*, 1981, **60**, 139.
3. Perry M.B., Pukanic G.W. and Ruether J.A., *Preprints Amer.Chem.Soc.Div.Fuel Chem.*, 1989, **34**, 1206.
4. Sullivan R.F., *Preprints Amer.Chem.Soc.Div.Fuel Chem.*, 1986, **31**, 280.
5. Greene M., Huang S., Strangio V., Reilly J., *Preprints Amer.Chem.Soc.Div.Fuel Chem.*, 1989, **34**, 1197.
6. Doughty P.W., Harrison G. and Lawson G.J., *Fuel*, 1989, **68**, 298.
7. Doughty P.W., Harrison G. and Lawson G.J., *Fuel*, 1989, **68**, 1257.
8. Fu Y.C., Akiyoshi M., Tanaka F. and Fiyika K., *Preprints Amer.Chem.Soc.Div.Fuel Chem.*, 1991, **36**, 1887.
9. Brackman-Danheux C., Cyprès R., Fontana A., Laurent Ph. and Van Hoegaerden M., *Fuel*, 1992, **71**, 251.
10. Colclough P., *Proceedings of ECSC Round-Table on Coal Valorization*, 1982, 36.

Table 1. Composition (vol.%) of the gases used for hydrogenation.

Gas 1 : 100% H₂
 Gas 2 : 55% H₂, 45% N₂.
 Gas 3 : 55% H₂, 15% N₂, 30% CH₄
 Gas 4 : 55% H₂, 1% N₂, 30% CH₄, 6% CO, 3% C₂H₄, 3% C₂H₆, 2% CO₂
 Gas 5 : 55% H₂, 7% N₂, 30% CH₄, 0% CO, 3% C₂H₄, 3% C₂H₆, 2% CO₂

Table 2. Hydrogenation of phenanthrene (catalyst : sulfided Ni-Mo)

Gas	T° (°C)	t (h)	P (MPa)	Phen. (Wt%)	DHP (Wt%)	THP (Wt%)	OHP (Wt%)	PHP (Wt%)	Others (Wt%)
1	370	1	21	5.8	8.3	5.9	26.8	48.0	0.9
		2		1.2	7.3	1.9	24.8	60.2	1.2
		4		0.7	4.9	1.6	23.6	67.9	1.1
		16		0.7	1.9	0.6	20.7	81.2	1.1
		16	11.5	3.9	5.8	6.0	16.5	55.6	2.4
3	370	2	21	6.8	11.1	13.1	33.7	26.6	0.5
		4		6.2	10.0	10.5	25.9	38.9	1.3
		8		5.4	7.5	8.2	18.7	47.9	2.3
		12		5.2	6.0	6.8	17.9	54.3	7.1
		16		2.8	5.4	5.2	14.6	61.0	8.9
3	300	16	21	3.4	0.5	1.9	72.5	12.7	2.6
	350			2.7	5.7	4.8	24.1	58.0	1.3
	400			5.3	8.3	7.9	20.1	40.5	7.3
	450			25.0	5.4	5.2	3.5	33.9	18.0
3	370	16	11	25.3	7.3	13.6	13.5	21.4	3.5
			15	12.2	6.1	11.4	19.1	37.8	5.3
			25	0.9	3.2	1.9	9.7	72.8	7.2
2 4 5	370	16	21	3.7	5.6	5.8	13.9	59.8	0.8
				7.4	5.2	8.0	16.4	26.6	29.2
				3.1	5.2	5.0	14.6	57.8	9.0

Table 3. Behaviour of the hydrogenating gas (gas 4) during the reactions (vol.%)

	H ₂	CH ₄	CO	CO ₂	C ₂ H ₄	C ₂ H ₆	C ₃ H ₈	N ₂
Gas 4	55.0	30.0	6.0	2.0	3.0	3.0	0.0	1.0
Exp.1	54.3	30.9	5.8	2.4	1.3	4.3	0.0	1.0
Exp.2	52.4	36.7	1.1	2.1	0.3	5.2	1.3	1.0
Exp.3	39.4	46.0	1.7	2.1	0.3	8.1	1.4	1.0

Table 4. Thermal cracking of the phenanthrene hydrogenation products.

Cracking conditions : T°: 800°C, residence time : 1 s, P : 0.1 MPa N₂.

Hydrogenation conditions : T° : 370°C, t : 16 h, P : 21 MPa.

Product 1 : hydrogenated with gas 1.

Product 2 : hydrogenated with gas 4.

Wt% of the main compounds.

	Product 1		Product 2	
	Before cracking	After cracking	Before cracking	After cracking
Benzene	-	10.6	-	2.6
Toluene	-	4.8	-	1.7
Xylenes	-	1.7	-	0.8
Total BTX	-	17.1	-	5.1
Phenanthrene	0.7	3.9	7.4	15.4
DHP	1.9	-	5.2	0.4
THP	0.6	-	8.0	0.8
OHP	20.7	0.8	16.4	1.2
PHP	81.2	1.9	26.6	0.5

Table 5. Thermal cracking of the heavy oils hydrogenation products.

Hydrogenation and thermal cracking conditions are the same as in table 4.

BTX yields (in wt%)

	HLN		HC	
	gas 1	gas 4	gas 1	gas 4
Benzene	6.7	3.6	5.1	2.1
Toluene	5.5	2.9	2.8	0.7
Xylenes	2.3	1.9	1.5	0.5
Total BTX	14.8	8.4	9.4	3.3

Role of Iron Catalyst on Hydroconversion of Aromatic Hydrocarbons

Eisuke Ogata, Xain-Yong Wei^a, Akio Nishijima^b, Tomo Hojo^c and Kazuyuki Horie
Department of Chemistry and Biotechnology, Graduate School of Engineering,
The University of Tokyo; 7-3-1, Hongo, Bunkyo-ku, Tokyo 113, Japan ^{***}

1. Introduction

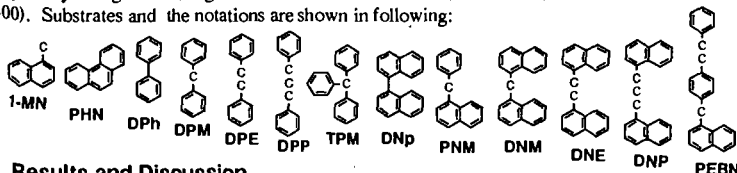
A symposium on iron-based catalysts for coal liquefaction was held at the 205th ACS National Meeting[1], and some of the papers have been published in *Energy & Fuels*[2]. Reviews of the development of catalysts for coal liquefaction were also published in *Journal of the Japan Institute of Energy*[3], and Ozaki reviewed the results of the studies of upgrading residual oils by means of thermal cracking and coking under reduced pressures, catalytic cracking over nickel ores and iron oxides, and hydrodesulfurization, as well as hydrodemetalization[4]. We reported that catalysis of metallic iron and iron-sulfide catalysts were affected by the S/Fe ratio; the activity increased with pyrrhotite formation and the activity was accelerated by the presence of excess sulfur[5-8]. Activity of pyrite FeS₂ for phenanthrene hydrogenation[9] and activity of natural ground pyrites for coal liquefaction[10] decreased with storage under air. On the other hand, the NEDOL process for a coal liquefaction pilot plant of 150 t/d which is one of the national projects in Japan, will use pyrites as one of the catalysts for the first-stage because FeS₂ has high activity and is low in price. In this paper, we describe in detail the role of iron catalysts in hydroconversion of aromatic hydrocarbons such as diphenyl (DPh), dinaphthyl (DNp) and diarylalkanes (DAAs) constructed with monocyclic aromatic-units and/or bicyclic aromatic-units and both monocyclic and bicyclic aromatic units and linked with from one to three methylene-groups.

2. Experimental

Materials: (1-Naphthyl)phenylmethane (NPM) and di(1-naphthyl)methane (DNM) were synthesized by heating naphthalene (NpH) with benzyl chloride and 1-chloromethylnaphthalene in the presence of metallic zinc powder catalyst, respectively[11], and 1,2-di(1-naphthyl)ethane (DNE) was synthesized by the reaction of 1-bromomethylnaphthalene with metallic iron powder catalyst in boiling water [12]. 1,3-Di(1-naphthyl)propane (DNP) was synthesized by a coupling reaction of 1-naphthylmagnesium bromide with 1,3-dibromopropane in the presence of copper(I) bromide catalyst in hexamethylphosphoric triamide (HMPA) solvent [13]. These diarylalkanes (DAAs) were purified using conventional methods such as vacuum distillation, separation with silica and alumina column chromatography and recrystallization from the solutions. The other substrates such as 1-methylnaphthalene (1-MN), diphenyl (DPh), 1,1'-dinaphthyl (DNp), diphenylmethane (DPM), 1,2-diphenylethane (DPE), 1,3-diphenylpropane (DPP), triphenylmethane (TPM), 1-[4-(2-phenylethyl)benzyl]naphthalene (PEBN); hydrogen-donors such as tetralin (THN), 9,10-dihydrophenanthrene (DHP) and 9,10-dihydroanthracene (DHA); and the solvent decalin (DHN), were purchased commercially and further purified, if necessary, by conventional methods. **Catalysts:** Pyrite FeS₂ and metallic iron ultra fine powder Fe were synthesized by Asahi Chemical Industry Co. Ltd. and Vacuum Metallurgical Co. Ltd., respectively. **Procedure:** In typical reactions, 1.0 g of 1-MN or PEBN or 7.7 mmol of DAAs, the prescribed amount of FeS₂ or Fe catalysts and 30 ml of DHN, as well as the prescribed amount sulfur (S/Fe ratio = 2.0) if necessary, were placed in 90 ml or 150 ml stainless steel, magnetically stirred autoclaves. After pressurization with 10 MPa of hydrogen, nitrogen or argon, the

^{***} Present Address: ^aDepartment of Coal Preparation and Utilization, China University of Mining and Technology, Xuzhou (221008), Jiangsu, China; ^bSurface Characterization Laboratory, National Institute of Materials and Chemical Research, 1-1, Higashi, Tsukuba-shi, Ibaraki 305, Japan; ^cDepartment of Industrial Chemistry, College of Science and Technology, Nihon University, 1-8, Surugadai, Kanda, Chiyoda-ku, Tokyo 101, Japan.

autoclave was heated to the desired reaction temperature from 300°C to 400°C within 20 min and maintained for 1 hr. It was then immediately cooled in an ice-water bath. **Analyses:** The reaction products were identified by GC-MS (Shimadzu GCMS QP-1000, equipped with a 0.24 mm (I.D.) x 50 m (L.) glass capillary column chemically bonded with OV-1) and quantified by GC (Shimadzu GC-15A, equipped with the same capillary column). **Oxidation of FeS₂ Catalyst:** FeS₂ was oxidized at room temperature, 80°C, 150°C and 200°C for the desired time under atmospheric air. The bulk structure of iron catalysts oxidized and recovered after the reaction was analyzed by using XRD (Rigaku Denki Model RINT 2400) and XPS (Perkin-Elmer Model PHI 5500). Substrates and the notations are shown in following:



3. Results and Discussion

Thermolysis of aromatic hydrocarbons was strongly affected by the bridged-methylene length, aromatic-ring size in the arylalkane structure, and the presence of molecular hydrogen (H₂) in the reaction system as shown in Table 1. Under reaction conditions of 400°C for 1 hr, DPM was very stable in both the absence and presence of H₂. The reactivity of diarylalkanes (DAAs) constituted of two phenyl-rings increased in the following order: DPM << DPE << DPP. These conversions were slightly increased by the presence of H₂. Generally, the reactivities of DAAs constituted of two naphthyl-rings were higher than those of diphenylalkanes (DPAs). It is particularly remarkable that many radical-adducts between species formed from C_{alk}-C_{alk} bond cleavage and solvent DHN molecule was recovered, and many phenylethyldecalins and naphthylethyldecalins were produced especially in the case of diarylpropane thermolyses and the formation was slightly depressed by the presence of gas phase H₂ molecule. From other experiments it was shown that the reaction between styrene and DHN under the same reaction conditions formed many phenylethyldecalins as solvent adducts, suggesting that these solvent adducts were produced when arylethylenes were formed in the reaction system. These results ultimately indicate that C-C bond scission was proceeded by a radical chain reaction and the reactivity of DAAs was governed by dissociation energy of C_{alk}-C_{alk} and C_{alk}-C_{ar} bonds in the absence of catalyst.

Tables 2 and 3 show the effect of bridged methylene length in the diarylalkane structure on the hydroconversion with pyrite FeS₂ catalyst at 300°C for 1 hr, and the effect of aromatic ring-size and number in the arylalkane structure. DPE and DPP were not converted even after 10 hrs. The reaction of DPh yielded only cyclohexylbenzene via the hydrogenation of one benzene-ring. DPM hydrocracking also proceeded via the C_{ar}-C_{alk} bond scission, but DPM was much less reactive than triphenylmethane (TPM). DNp hydrocracking resulted in the corresponding tetra-hydrogenated 1,1'-dinaphthyls as main products. Reactivity of DNM was the highest in this hydroconversion series. DNM hydrocracking mainly produced naphthalene (NpH) and 1-MN, via hydrogen addition to the ipso-carbon of DNM. Only a small amount of hydrogenated di(1-naphthyl)methanes (H-DNMs) was produced. DNM hydrocracking was much easier than that of DPM and TPM. Drastically different from DNM, the reactions of DNE and DNP mainly yielded the hydrogenated 1,2-di(1-naphthyl)ethanes (H-DNEs) and the hydrogenated 1,3-di(1-naphthyl)propanes (H-DNPs) rather than decomposed products, respectively. The result shows that the cleavage of the C_{ar}-C_{alk} linkage in DNE and DNP is much more difficult than that in DNM. The total selectivity of decomposed products in the case of DNP was higher than that in DNE hydroconversion. Reaction of DNP mainly produced hydrogenated 1,3-di(1-naphthyl)propanes (H-DNPs), and a small amount of hydrocracked products such as NpH and (1-naphthyl)

propane (1-NP). Table 4 shows the effects of Fe and FeS₂ catalysts and reaction temperature on the hydroconversion of DPM. FeS₂ catalyst has more hydrocracking sites than hydrogenation sites, while Fe catalyst has highly active sites and mainly produced hydrogenated diphenylmethanes (H-DPMs).

Table 5 shows the additive effects of hydrogen-donors (H-donors) on DPP thermolysis and the additive effects of metallic Fe and FeS₂ catalysts on DPP hydroconversion at 400°C for 1 hr. DPP conversion decreased with H-donor addition in the order: none > THN >> DHP > DHA. These results are easily understood because the resulting PhCH₂· abstracts hydrogen atoms from the H-donors readily more than it does from DPP. In other words, the H-donors inhibited the radical chain reaction in DPP thermolysis by donating their benzylic hydrogen to PhCH₂·. Table 5 also demonstrates the catalytic effects of FeS₂ and Fe on the DPP thermolysis when compared with the non-catalytic reaction of DPP under H₂ of 10 MPa at 400°C. FeS₂ greatly promoted C_{alk}-C_{alk} bond scission as DPP hydrocracking. Under H₂, the rate for DPP hydrocracking in the presence of FeS₂ was ca. 2-fold faster than that in the absence of the catalyst and dramatically decreased the formation of solvent adducts. Fe catalyst promoted DPP hydrogenation, but DPP conversion was low, about the same as that under N₂. This result suggests that Fe catalyst promoted DPP hydrogenation and inhibited thermolysis. The inhibiting effect of Fe on DPP thermolysis remains to be investigated. It appears remarkably that the formation of solvent adducts such as phenylethyldecals (PEDs) was drastically inhibited by FeS₂ and metallic Fe catalysts.

FeS₂ was oxidized to ferrous sulfate FeSO₄·H₂O even at room temperature under atmospheric air, and the catalytic activities of oxidized FeS₂ on 1-MN hydrogenation were decreased with increases in the storage time. Recently, Linehan and co-workers [14,15] reported the C-C bond scission activity of PEBN on well-characterized eleven synthesized iron-oxygen compound catalysts in the presence of elemental sulfur and a hydrogen-donating solvent in detail. As shown in Figs. 1 and 2, thermolysis of PEBN under Ar was stable, but the conversion of PEBN was effectively accelerated in the presence of 10 MPa H₂ and the main reaction was changed from C_{alk}-C_{alk} bond scission (*Route [A]*) to C_{ar}-C_{alk} bond scission (*Route [C]*). Metallic Fe catalyst mainly accelerated the hydrogenation (*Route [B]*), and FeS₂ catalyst promoted C-C bond scission of *Route [C]*. FeS₂ catalyst activity was decreased with the oxidation of FeS₂ by oxygen in the air. However, the deactivated FeS₂ catalysts were reactivated by the presence of excess elemental sulfur in the system, and the reaction proceeded along *Route [C]*.

4. Concluding Remarks

Hydroconversion of aromatics and arylalkanes as a model reaction of coal liquefaction and heavy petroleum residue degradation was carried out in the absence or presence of metallic iron Fe and pyrite FeS₂. Thermolysis of some diarylalkanes proceeded slowly by the radical chain reaction. The reaction rate was reduced by the addition of hydrogen-donating solvents and was slightly accelerated in the presence of hydrogen molecules. Metallic Fe catalyst accelerated the hydrogenation of aromatic-rings, especially bicyclic-rings, more than that of monocyclic-rings. FeS₂ catalysts, which is converted to pyrrhotite Fe₁₋₂S under reaction conditions, promoted C_{ar}-C_{alk} bond cleavage of diarylalkanes only, and also promoted the hydrogenation of diarylethanes and diarylpropanes. C-C bond cleavage of arylalkanes was related to the hydrogen-accepting ability, C-C bond dissociation energy and resonance energy of the species after C-C bond scission. Oxidation of pyrites and its catalysis were also investigated. It was found that the catalytic activity of pyrites in the hydrogenation of 1-methylnaphthalene and 1-[4(2-phenylethyl)benzyl]naphthalene decreased with oxidation under air, and deactivated pyrites was reactivated by addition of sulfur to the reaction system.

Acknowledgment

The authors wish to thank to the New Sunshine Program Promotion Headquarters, Agency

of Industrial Science and Technology, Ministry of International Trade and Industry of Japan for financial support.

References

1. Prepr. "Symposium on Iron-Based Catalysts for Coal Liquefaction", Div. Fuel Chem., 205th ACS National Meeting (Denver), Vol. 38 (No.1), pp-1-238 (1993).
2. *Energy & Fuels*, **8**, (1), (Special issue), p-2-123 (1994).
3. *J. Jpn. Inst. Energy*, **73**, (1), (Special issue), p-2-49 (1994).
4. H. Ozaki, Sekiyu Gakkaishi, **36**, (3), 169 (1993).
5. E. Ogata, E. Niki, Proc. 27th Conf. Coal Sci. Jpn. Soc. Fuel (Tokyo), pp-115 (1990).
6. X.-Y. Wei, E. Ogata, E. Niki, *Chem. Lett.*, 2199 (1991).
7. X.-Y. Wei, E. Ogata, Z.-M. Zong, E. Niki, *Energy & Fuels*, **6**, 868 (1992).
8. E. Ogata, K. Ishiwata, X.-M. Wei, E. Niki, Proc. 7th Inter. Conf. Coal Sci. (Banff), Vol. II, pp-349 (1993).
9. E. Ogata, T. Suzuki, K. Kawamura, Y. Kamiya, 26th Conf. Coal Sci. Jpn. Soc. Fuel (Sapporo), pp-121 (1989).
10. K. Hirano, T. Hayashi, K. Hayakawa, 30th Conf. Coal Sci. Jpn. Soc. Fuel (Tokyo), pp-161 (1993).
11. S. Futamura, S. Koyanagi, Y. Kamiya, *Fuel*, **63**, 1660 (1984).
12. N. P. Buu-Hoi and N. Hoan, *J. Org. Chem.*, **14**, 1023 (1949).
13. J. Nishijima, N. Yamada, Y. Horiuchi, E. Ueda, A. Ohbayashi, and A. Oku, *Bull. Chem. Soc. Jpn.*, **52**, 2035 (1986).
14. J. C. Linehan, D. W. Matson, and J. G. Darab, *Energy & Fuels*, **8**, 56 (1994).
15. D. W. Matson, J. C. Linehan, J. G. Darab, and M. F. Buehler, *Energy & Fuels*, **8**, 10 (1994).

Table 1 Effect of Chain-length and Ring-size in the Diarylalkane Structure and 10 MPa of Hydrogen on the Thermolysis at 400°C for 1 hr.

Substrate	DPM		DPE		DPP		DNM		DNE		DNP	
Gas Phase	N ₂	H ₂	N ₂	H ₂	N ₂	H ₂	N ₂	H ₂	N ₂	H ₂	N ₂	H ₂
Conv. (%)	0	0	2.3	3.5	32.9	46.5	2.1	45.8	73.0	35.6		
Selectivity (mol %)												
Benzene	0	0	0	98.2	0	3.4	0	0	0	0	0	0
Naphthalene	0	0	0	0	0	0	61.7	1.5	12.6	0	0	0
Arylmethane	0	0	200 ^a	101.8 ^a	100 ^a	96.6 ^a	61.7 ^b	174.4 ^b	132.2 ^b	105.0 ^b		
Arylethane	0	0	0	98.2 ^c	2.9 ^c	16.5 ^c	0	1.4 ^d	9.7 ^d	6.4 ^d		
Arylethylene	0	0	0	0	9.8 ^e	6.2 ^e	0	0	0	14.9 ^f		
Arylpropane	0	0	0	0	0	3.4 ^g	0	0	0	0		
Arylalkyldecalins	0	0	0	0	87.4 ^h	73.4 ^h	38.3	4.7	14.9	73.7 ⁱ		

a: Toluene; b: Methyl-naphthalene; c: Ethylbenzene; d: Ethyl-naphthalene; e: Styrene; f: Vinyl-naphthalene; g: Propylbenzene; h: Phenylethyldecalins; i: Naphthylethyldecalins.

Table 2 Effects of Chain-length in the Diarylalkane Structure on Hydroconversion with Pyrite FeS₂ Catalyst at 300°C for 1 hr.

Substrate	DPh	DPM	DPE	DPP	DNp	DNM	DNE	DNP
Conv. (%)	0.5	3.1	0	0	11.4	91.7	50.7	51.1
(10 hrs.) ^a	(6.2)	(36.1)	(0)	(0)	---	---	---	---
Selectivity (mol %)								
Benzene	0	100	0	0	0	0	0	0
Naphthalene	0	0	0	0	17.3	95.7	1.8	10.3
Arylmethane	0	100 ^b	0	0	0	89.0 ^c	2.3 ^c	tr ^c
Arylethane	0	0	0	0	0	0	0.4 ^d	tr ^d
Arylpropane	0	0	0	0	0	0	0	7.0
HDAAs ^e	100 ^f	0	0	0	43.3 ^g	2.9	86.8	88.1

a: Reaction Time 10 hrs; b: Toluene; c: 1-Methylnaphthalene; d: Ethylnaphthalene; e: Hydrogenated Diarylalkanes; f: Cyclohexylbenzene; g: Hydrogenated Dinaphthyls.

Table 3 Effects of Ring-size and Number in the Diarylmethane Structure on Hydrogenation with Pyrite FeS₂ Catalyst at 300°C for 1 hr.

Substrate	DPM	TPM	NPM	DNM
Conversion (%)	3.1	36.1 ^a	21.4	86
Selectivity (mol %)				
Benzene	100	99	102.6	tr
Naphthalene	0	0	0	64
Arylmethane	100 ^b	99 ^b	2.6 ^b	71 ^b
Diarylmethane	---	---	97.4 ^c	12 ^c
Tetralins	0	0	0	9.3
H-DAAs	0	1.5	tr	15
				2.9

a: Reaction Time 10 hrs; b: Toluene; c: 1-Methylnaphthalene; d: Diphenylmethane; e: (2-Naphthyl)-phenylmethane; f: Hydrogenated diarylalkanes.

Table 4 Effects of Iron Catalysts and Reaction Temperature on Hydroconversion of Diphenylmethane for 1 hr.

Temp. (°C)	Catalyst (g)	Conv. (%)	Selectivity (mol %)					
			CH ₃ ^a	PhH ^b	MCH ^c	Tol ^d	DCHM ^e	BCH ^f
300	Fe (0.23)	58.4	0	0	0	0	13.4	86.6
300	FeS ₂ (0.50) ^g	3.1	0	100	0	100	0	0
400	Fe (0.02)	79.3	3.2	0	9.8	0	42.1	57
400	FeS ₂ (0.50) ^g	59.1	0	98	0	97.2	2.4	0

a: Cyclohexane; b: Benzene; c: Methylcyclohexane; d: Toluene; e: Dicyclohexylmethane; f: Benzylcyclohexane; g: Addition of Sulfur 0.05 g.

Table 5 Additive Effect of Hydrogen-Donating Solvents and Iron Catalysts on Conversion Reaction of Diphenylpropane at 400°C for 1 hr.

Additive (g)	Gas	React. Phase	Time (hr)	Conv. (%)	Selectivity (mol %)							
					PhH ^b	Tol ^c	EtPh ^d	Sty ^e	CHPF ^f	BCHP ^g	PEDs ^h	
None	0	N ₂	1	39.9	0	100	2.9	9.8	0	0	0	87.4
THN	7.5 ⁱ	N ₂	1	28.6	0	100	3.8	19.5	0	0	0	76.7
DHP	7.5 ⁱ	N ₂	1	7.4	0	100	6.4	39.8	0	0	0	53.8
DHA	7.5 ⁱ	N ₂	1	3.8	0	100	60.9	20.8	0	0	0	0
None	0	H ₂	1	46.5	3.4	96.6	16.5	6.2	0	0	0	73.4
None	0	H ₂	2	70.7	5.1	94.9	29.1	2.0	0	0	0	68.9
Fe	0.02	H ₂	1	40.0	6.6	63.4	56.2	0	24.7	5.3	13.8	
Fe	0.02	H ₂	2	65.9	10.7	53.9	48.8	0	26.9	8.5	15.8	
FeS ₂	0.50 ^j	H ₂	1	69.7	8.7	87.6	87.2	2.6	3.7	0	0	
FeS ₂	0.50 ^j	H ₂	2	86.2	9.9	86.8	86.5	1.9	3.3	0	0	

a: Reaction Condition DPP 7.5 mmol, DHN 30 ml, PH₂ 10 MPa; b: Benzene; c: Toluene; d: Ethylbenzene; e: Styrene; f: Cyclohexylphenylpropane; g: Bicyclohexylpropane; h: Phenylethyldecals; i: mmol; j: Addition of Sulfur 0.05 g.

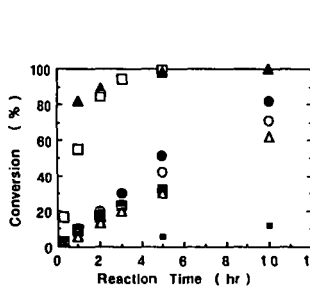


Fig. 1 Effect of Reaction Time on the Conversion Reaction of 1-[4-(2-Phenylethyl)benzyl]naphthalene.

Reaction Conditions: PEBN 1.0 g, DHN 30 ml, PH₂ 10 MPa, ○: H₂ - 350°C, ●: H₂ - 380°C, □: H₂ - 400°C, ■: Ar - 380°C, ▲: Ar - 400°C, △: H₂ - 380°C - DHA Addition (DHA/PEBN = 3.0), ▲: H₂ - 380°C - Fe Cat. (0.05 g).

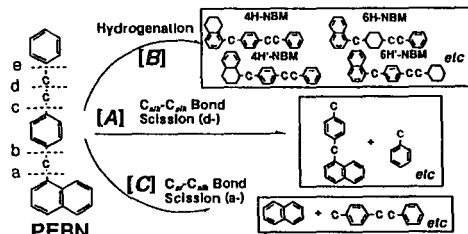


Fig. 2 Reaction of 1-[4-(2-Phenylethyl)benzyl]naphthalene

CATALYSIS OF ALKENE AND ARENE HYDROGENATION BY THERMALLY ACTIVATED SILICA

Venkatasubramanian K. Rajagopal

Robert D. Guthrie
Department of Chemistry
University of Kentucky
Lexington, KY 40506

Burton H. Davis
Kentucky Center for Applied Energy Research
3572 Iron Works Pike, Lexington, KY 40511

Keywords: Deuterium Incorporation, Diphenylacetylene, Hydrogenation Stereochemistry

INTRODUCTION

In a recent study we described the hydrogenation of stilbene, α -methylstyrene and anthracene at 410 °C under 14 MPa of hydrogen or deuterium gas in the absence of added catalysts to give diphenylethane, cumene and 9,10-dihydroanthracene respectively.¹ As we were simultaneously working on the hydrolifuefaction of coal-model compounds attached to silica,² we became aware of work by Bittner, Bockrath and Solar³ which demonstrated catalytic effects of thermally activated silica in reactions involving H₂ and D₂. Using a pulse-flow microreactor, Bittner showed that after fumed silica is heated at 330 °C for 16 h in an argon stream it catalyzes the reaction H₂ + D₂ → 2 HD at temperatures as low as 120 °C. Moreover, this material catalyzes the hydrogenation of ethene to ethane at 150 °C and produces ethane-d₆ when D₂ is used as a flow gas. We became curious to see whether silica activated in this way would serve as a hydrogenation catalyst in a static reactor. Our results and additional information about the catalytic behavior of this material are described below.

EXPERIMENTAL

Hydrogenation Procedure. Approximately 300 mg of fumed silica (Cab-O-Sil M-5, Cabot Corporation) was placed in a length of (16 mm o. d.) glass tubing with a section of 1 - 2 mm capillary (ca. 16 cm long) attached to one end. Plugs of glass wool were placed between the silica powder and the tube exits. This assembly was heated in a tube furnace either at 330 °C or at 430 °C for 16 or more hours with argon flowing in the capillary tube and out through a ca. 2 mm hole in a stopper placed in the wide end. After this activation time, the tube was cooled to room temperature and a substrate was introduced maintaining the argon atmosphere during the addition process. The argon flow was then discontinued, the assembly evacuated, and the noncapillary end of the tube sealed under vacuum. Argon was readmitted and the reaction vessel was placed in a steel tube reactor under H₂ or D₂ pressure. The assembly was heated for the desired time period in a fluidized sand bath as described earlier.⁴ When the heating period was complete, the apparatus was cooled, the pressure released, the glass reactor section cracked open and the silica hydrolyzed with ca. 30 mL of 1 M aqueous NaOH for ca. 15 h. At this point a measured aliquot of an external standard (biphenyl in CH₂Cl₂) was added. The aqueous solution was acidified and extracted three times with CH₂Cl₂. The glass reaction vessel was washed with CH₂Cl₂ and the washings combined with the extracts. The solvent was removed by rotary evaporation and the products analyzed by GC and GC/MS.

Exchange Experiments. Experiments to assess surface exchange were carried out in the same way as for the D₂ experiments described above except that instead of cracking the tube open after the D₂ treatment, a sample of phenol in benzene was added to the tube through the capillary opening using small diameter polyethylene tubing. Most of the benzene was pumped out and the capillary section sealed. The entire assembly was then placed in a tube furnace at 400 °C for 60 min. We have shown in other experiments that phenol-d₆ undergoes replacement of three of its ring deuterium atoms by hydrogen atoms on heating with Cab-O-Sil at temperatures above 140 °C.² After heating, the sealed tube was opened and the contents hydrolyzed in NaOH solution as described in the previous section. Control experiments showed that phenol could be recovered quantitatively from the hydrolysis workup and that the workup did not remove ring deuterium atoms.

RESULTS AND DISCUSSION

The results from hydrogenation of several alkenes in the presence of thermally-activated silica are given in Table I. The compound examined most extensively was stilbene (1,2-diphenylethene), **STB**.

Table I. Reaction of Unsaturated Compounds with D₂ or H₂ in the Presence and Absence of Thermally-Activated Silica.

Compound	T (°C)	Time (min)	D ₂ /H ₂	Silica ^a	% H-C-C-H	% C=C
<i>trans</i> - STB	300	30	D ₂	A	31	65
	300	50	D ₂	NA	7.2	90
	350	90	D ₂	A	91.2	7.3
	350	60	D ₂	none	1	98
	350	15	H ₂	none	<1	99 ^b
	350	100	H ₂	none	<1	99 ^c
Naphthalene	300	30	D ₂	A	1.2 ^d	98.5
	350	90	D ₂	A	1.5 ^d	98.5
1-Nonene	300	30	D ₂	A	36.3 ^e	35.3 ^e
Anthracene	350	80	D ₂	A	30	61
	350	60	D ₂	none	0.5	99.5
DPA ^f	350	40	D ₂	A	3.3 + 38.9 ^g	57.5 ^g
	300	90	D ₂	A	29 + 69 ^h	<1 ^h

^a A = Activated, NA = not activated. ^b *cis/trans* = 0.085. ^c *cis/trans* = 0.087. ^d Product appears to be mixture of dihydronaphthalene-*d*₂ and tetralin-*d*₄. ^e Remainder appears to be alkene isomers. ^f **DPA** = Diphenylacetylene. ^g Product contains 3.3% diphenylethane, **DPE**, and 38.8% mixed *cis*- and *trans*-**STB**, *cis/trans* = 0.26. This run was carried out with a different procedure, however, and it is not certain that all of the **DPA** was available for reaction. ^h Product is a mixture of **DPE** (29%) and **STB** with no significant amount of residual **DPA**. The **STB** shows *cis/trans* = 0.18.

It is clear that for **STB** there is no reaction with D₂ at 350 °C in the absence of silica and nearly complete hydrogenation to **DPE** after 90 min in the presence of activated silica. For the three runs carried out in the presence of silica, the deuterium distribution in the **DPE** produced was *d*₂ = 85.4%, *d*₃ = 6.0% *d*₄ = 3.5% in the first run, *d*₂ = 83.7%, *d*₃ = 10.6% *d*₄ = 2.0% in the second run, and *d*₂ = 63.3%, *d*₃ = 25.4% *d*₄ = 7.2% in the third run. The balance was a small amount of *d*₀ **DPE** present as an impurity in the **STB**. Thus, the product was mainly *d*₂ material which underwent additional deuteration at longer times and higher temperatures. ²H NMR showed that neither the **DPE** nor the **STB** remaining contained any significant amount of aromatic D whereas there was a prominent signal for the aliphatic D in the **DPE** produced. It will be noted that unactivated silica does catalyze the reaction to a lesser extent, but this might be expected in view of the fact that reaction temperatures are similar to activation temperatures. With naphthalene, there appears to be a small amount of dihydronaphthalene and tetralin being formed and these contain mainly 2 and 4 atoms of D respectively. However, we have not been able to increase the yield much above 1% by increases in time or temperature. Possible reasons for this situation are discussed below.

Nonene was picked as a prototypical nonaromatic alkene and it shows hydrogenation to nonane. The saturated material produced under these conditions is a mixture of ca. 64% nonane-*d*₀ and 36% nonane-*d*₃. The unreacted 1-nonene is mainly undeuterated, but the precision required to determine small amounts of D was unavailable due to extensive mass spectral fragmentation. Both of the nonene isomers, presumably *cis*- and *trans*-2-nonene are mainly *d*₁ material but contain about 30 % *d*₀ material. It thus seems likely that 1-nonene can isomerize under these circumstances and that at least part of the process does not involve the intermediacy of nonane-*d*₂.

The reaction is not limited to alkenes as anthracene can be reduced to dihydroanthracene, mainly with two atoms of D. Diphenylacetylene (**DPA**) is also

hydrogenated. At 350 °C, the STB produced is largely converted to DPE- d_4 . At 300 °C, substantial amounts of intermediate STBs are observed, mainly d_2 . The STB from these experiments seemed to be slightly enriched in the *cis*-isomer but the analysis was inherently imprecise due to the GC overlap between *cis*-STB and DPE. In order to provide more convincing evidence that the initial product of hydrogenation of DPA is *cis*-STB, the reaction temperature was lowered to 250 °C. Data for hydrogenation of DPA (with H₂) under these conditions is presented in Table II.

Table II. Yields of Products from Reaction of Diphenylacetylene with H₂ at 250 °C Over Thermally-Activated Cab-O-Sil.

	Time (min)				
	5	15	30	60 ^e	60 (<i>trans</i> -STB ^a)
DPA ^b	98.8	87.7	55.8	35.1	
<i>cis</i> -STB ^a	0.9	5.5	20.3	47.9	1.5
<i>trans</i> -STB	0.3	1.7	3.5	10.9	52.8
<i>cis/trans</i> ^c	3	3.3	5.8	4.4	
DPE ^d	<0.3	5.1	20.3	6.0	45.7

^a STB = Stilbene. ^b DPA = Diphenylacetylene. ^c Thermal equilibration gives a ratio of 0.1 at 350 °C. ^d DPE = Diphenylethane. ^e Reasons for the dramatic decrease in DPE formation in the 60 min run are uncertain. But, for this run the silica was activated at 430 °C rather than the 330 °C used for all of the other runs. This result is being checked.

It is clear from the data in Table II that the predominant product of hydrogenation of DPA at 250 °C is *cis*-STB by a ratio of at least 3 to 1. The equilibrium ratio of *cis*-/*trans*-STB has not been established at 250 °C, but the 5th and 6th runs of Table I show that at 350 °C the ratio is 0.086 and a lower value might be expected at 250 °C. Thus there seems little doubt that *cis*-STB is the kinetic product of DPA hydrogenation. This would seem to clearly rule out radical processes in which the two hydrogen atoms are transferred independently. The fact that we see none of the products expected from 1,2-diphenylethyl radicals: tetraphenylbutane or 1,1-diphenylethane also supports this conclusion. It appears that, whatever the active site for silica-catalyzed hydrogenation might be, it is similar to a metal-surface type catalyst in that H atoms are transferred in pairs and transferred in a stereoselectively *syn* fashion. It seems likely that the *trans*-STB produced in this reaction results from the thermal isomerization of the *cis*-isomer. Comparison of the STB runs in Table I carried out at 300 and 350 °C to the run in the last column of Table II shows that a temperature change of 100 °C does not have the effect on the conversion of STB to DPE that would be expected for a thermally activated reaction. For the thermal hydrogenation of STB studied earlier, reaction proceeds at a kinetically convenient rate at 410 °C but is not measurable after comparable times at 350 °C. It would thus seem a reasonable hypothesis that the rate-limiting step in the catalytic process has a low enthalpy of activation and may be controlled by geometric restrictions for access to the site.

It seemed logical that if D₂ is combining with silica in order to be activated for addition to unsaturated molecules, that the formation of OD bonds must be involved and, this being the case, that the process would provide a mechanism for exchange of the Si-OH groups on the silica surface with the D₂ atmosphere. In their microreactor process, Bittner did not observe formation of HD when D₂ was passed over the thermally-activated silica.³ Nevertheless, it seemed possible that this would happen under the higher pressures used in our experiments. To this end we carried out a series of experiments in which silica was activated then heated with D₂ followed by removal of the D₂ under vacuum and heating with phenol. Earlier work had shown that the *ortho* and *para*-positions of phenol undergo exchange with OH groups on the silica surface at temperatures above 140 °C.² After recovery from an aqueous workup the deuterium content of the phenol was determined by GC/MS analysis. Data are presented in Table III.

Although there is some scatter in the data, it is clear that heating with D₂ at temperatures above 200 °C introduces SiOD groups on the silica surface. Calculations based on the expected⁵ 4.5 SiOH groups per nm² of surface area suggest that roughly

75% of the surface SiOH groups are replaced by SiOD groups in the high temperature runs. The threshold temperature for the exchange reaction with D₂ appears to be between 200 and 250 °C. In the four runs carried out at 250 °C, the exchange with D₂ seemed about twice as great with silica which had undergone prior activation, however, the effect of activation on exchange was not as great as that on the STB reduction.

Table III. Deuterium Content of Phenol Exchanged^a with Cab-O-Sil (300 mg) Previously Treated with D₂ at 14 MPa at Various Temperatures.

Run	Activation?	Rxn. Time (min)	Rxn. Temp. °C	mg. PhOH	D/molecule
1	yes	20	350	40	0.30
2	yes	60	350	45	0.27
3	yes	120	350	42	0.38
4	yes	180	350	43	0.23
5	no	20	350	40	0.29
6	no	60	350	33	0.26
7	no	180	350	37	0.45
8	yes	60	250	16 (12)	0.31 (0.34)
9	no	60	250	19 (11)	0.18 (0.18)
10	yes	60	200	22	0.03
11	no	60	200	21	0.06

^a See Experimental section for details of the exchange experiments.

It remains uncertain at this point whether the mechanism for deuterium exchange of the silica surface hydroxyl groups and the mechanism for hydrogenation of alkenes are linked. At least for the alkene reaction, we can roughly estimate the concentration of active sites by the following experiment. Activated silica is heated with D₂, a process which Table III demonstrates will convert most of the surface SiOH groups to SiOD groups. The resultant deuterated silica (300 mg) which then has at least 0.33 mmole of D on the surface (after pumping off excess D₂) is heated with excess STB. The STB then contains a small amount of DPE-d₂. This amount is less than 0.015 mmole or roughly 10 % of the equivalents of D₂ present on the surface.

We find in some experiments that the thermally activated silica also is capable of catalyzing the hydrogenation of aromatic rings. The circumstances of this occurrence and the type of compound which is susceptible are under continuing investigation. As shown in Table I, a small amount of naphthalene is hydrogenated under the conditions described. To our astonishment, DPE is more extensively hydrogenated than naphthalene provided that the silica is thermally activated either for several days at 330 °C or at 430 °C for 16 h. We have found that the latter procedure gives reasonably reproducible results. Representative experiments are listed in Table IV. The reaction gives two products with gas chromatographic retention times which are very similar to DPE. With H₂ these products have mass spectra which match 1-cyclohexyl-2-phenylethane (CPE) and 1,2-dicyclohexylethane (DCE). Each is extensively deuterated and the ²H NMR spectrum of the mixture shows an envelope of purely aliphatic D atoms in the range of 1 to 1.5 ppm from TMS. The D content of the two reduction products suggests that much of the material arises from the replacement of the four benzylic H atoms in DPE as well as the addition of three D₂ molecules per reduced benzene ring. However, evidence for exchange at the aliphatic sites of the saturated rings is provided by the presence of up to CPE-d₁₈ and up to DCE-d₂₆. The DPE which is recovered is mainly DPE-d₄ but there is evidence for some exchange in the aromatic rings as well.

Astonishingly, when naphthalene is mixed with DPE and subjected to the conditions of Table IV, neither compound is hydrogenated and, moreover, the presence of naphthalene prevents even the exchange of the benzylic hydrogens as the DPE recovered contains very little deuterium. From a thermodynamic standpoint, it should be easier to hydrogenate one ring in naphthalene than the isolated phenyl rings of DPE. It

seems possible that naphthalene somehow blocks sites on the silica preventing its catalytic action, at least toward hydrogenation of DPE. Naphthalene does not block the hydrogenation of stilbene.

Table IV. Yields of Products from Reaction of Diphenylethane (DPE) with D₂ in the Presence of Thermally Activated Cab-O-Sil.

	Run 1	Run 2	Run 3
Activation Time	42 h	16 h	16 h
Activation Temp.	330 °C	430 °C	430 °C
Run Time	1 h	1 h	7 h
Run Temp.	350 °C	350 °C	350 °C
Yield CPE ^a	30.4%	22.6% ^e	37 % ^e
Yield DCE ^b	5%	5% ^f	13 % ^f
Recovery DPE ^c	64%	72% ^g	50 % ^g

^a CPE = 1-cyclohexyl-2-phenylethane. ^b DCE = 1,2-dicyclohexylethane. ^c DPE = 1,2-diphenylethane. ^e This was not completely resolved from DPE by GC, but its presence was clearly indicated by an envelope of ions in the mass spectrum ranging from d_6 to d_{18} with maximum intensity at d_{11} . The relative intensities of the ions in this envelope were similar for runs 2 and 3. ^f DCE was well resolved from DPE and CPE. Its mass spectrum showed an envelope of ions from d_{12} to d_{26} with maximum intensity at d_{19} . Again, relative intensities were similar for runs 2 and 3. ^g Recovered DPE showed an envelope of ions ranging from d_0 to d_{12} with maximum intensity at d_4 . In run 2, a substantial amount of d_0 material remained (slightly more than d_4). In run 3, the d_0 material had been largely consumed. However, the D distribution in the d_4 to d_{12} material was similar in the two runs.

SUMMARY

We have shown that even in bulk reactions, thermally-activated silica is a viable catalyst for the hydrogenation of alkenes and even of some arenes. Evidence for the stereoselectively *syn* nature of this process is found in the preferential formation of *cis*-hydrogenation of *cis*-STB from DPA. We have also shown that heating silica with D₂ at temperatures above 200 °C leads to exchange of surface OH groups in what may be a related process. Although mechanistic speculation may be premature, it seems reasonable that siloxane bonds formed when silica is heated are hydrogenated open by H₂ (or D₂) in a manner similar to that proposed for the reaction of ZnO with H₂.⁶ D₂ reacts with Si-(O)₂-Si to form DO-Si-O-Si-D which could possibly be the reactive species toward unsaturated carbon compounds. The strange effect of naphthalene suggests that the situation may be more complicated than this, however.

ACKNOWLEDGEMENTS

The authors gratefully acknowledge a grant from the United States Department of Energy, Pittsburgh, DE-FG22-91-PC91291, supporting this work.

REFERENCES

1. Rajagopal, V.; Guthrie, R. D.; Shi, B.; Davis, B. H. *Prepr., Div. Fuel Chem., Am. Chem. Soc.* **1994**, *39*, 673.
2. Guthrie, R. D.; Ramakrishnan, S.; Britt, P. F.; Buchannan, III., A. C.; Davis, B. H. *Prepr., Div. Fuel Chem., Am. Chem. Soc.* **1994**, *34*, 668.
3. Bittner, E. W.; Bockrath, B. C.; Solar, J. M. *J. Catal.* **1994**, *149*, 206
4. Guthrie, R. D.; Shi, B.; Sharipov, R.; Davis, B. H. *Prepr. Div. Fuel Chem., Am. Chem. Soc.* **1993**, *38*, 526-533.
5. Information provided in product bulletin by Cabot Corporation for Cab-O-Sil M-5.
6. Dent, A. L.; Kokes, R. J. *J. Am. Chem. Soc.* **1970**, *92*, 6709-6718.

HYDROGENATION/DEHYDROGENATION OF MULTICYCLIC COMPOUNDS USING ATTM AS CATALYST PRECURSOR

Richard P. Dutta and Harold H. Schobert
Fuel Science Program
Pennsylvania State University
University Park, Pa 16802.

Keywords: Hydrogenation/dehydrogenation; kinetics; thermodynamics.

Introduction

Coal liquefaction can be considered a viable technical alternative for production of advanced fuels if the coal macromolecule can be broken up into low molecular weight fragments and hydrogenated to decrease the concentration of aromatics in the final product. Previous studies have shown that the initial breakdown of coal can be achieved using various catalysts and various conditions. However, if the final product is to be a very high quality distillate, the coal liquids still need further hydrotreatment if they are to be satisfactory. One way to improve the quality is to add another step to the liquefaction process. This would employ a very active catalyst to hydrogenate the products from the first liquefaction stage. However if operating costs are to be kept to a minimum, it would be advantageous to hydrogenate the coal fragments as they are being released during the first stage of liquefaction. Burgess has shown that ammonium tetrathiomolybdate (ATTM) can be used as a catalyst precursor in a process for conversion of coal to a "proto-jet fuel" [1]. Coal conversion up to 95% were observed but the products were aromatic and contained some phenols.

Various temperature strategies have been formulated for coal liquefaction. The majority of these strategies are concerned with the depolymerisation of coal and the avoiding of retrogressive reactions. Another important aspect of temperature strategies is the thermodynamic behavior of released coal fragments. With careful 'fine tuning' of the reaction conditions, it could be possible to have advantageous thermodynamics in the system along with reasonably fast kinetics of depolymerisation of the coal macromolecule. Basically, a trade-off between kinetics and thermodynamics is possible.

Model compound studies can be used to understand the fundamental behavior of coal fragments during coal liquefaction and coal liquids upgrading. The literature on hydrogenation of model compounds is vast and has been recently reviewed by Girgis [2].

For the past several years we and our colleagues have been investigating the hydrogenation and dehydrogenation chemistry of a variety of polycyclic compounds. This work has aimed at investigating some of the fundamental chemical processes involved in various aspects of fuel utilization. The compounds investigated have included decalin and tetralin [3], anthracene [4], phenanthrene [5, 6], pyrene [6, 7] and chrysene [6].

This paper will discuss the hydrogenation and dehydrogenation behavior of naphthalene and pyrene. Kinetic and thermodynamic parameters will be calculated from product distribution trends. From these parameters it should be possible to outline a possible reaction strategy that allows all these compounds to remain in their hydroaromatic states during a coal liquefaction operation.

Experimental

All reactions were carried out in 25ml microautoclave reactors (made of type 316 stainless steel). In all runs, 3 ± 0.01 g naphthalene or pyrene (Aldrich, 99%, used as received) and 0.075 ± 0.005 g ammonium tetrathiomolybdate (Aldrich, used as received) were weighed into the reactor. The reactor was then evacuated and pressurized with hydrogen to 7MPa. Heating was accomplished by lowering the reactor into a fluidized sand bath preheated to the desired temperature. After a measured reaction time, the reactor was quenched to room temperature by immersing it in a cold water bath. The products from the reaction were removed from the reactor using THF. The THF was removed by rotary evaporation and the product was weighed. It was found that in all cases the weight of the products equaled the weight of the original compound before reaction. The products were dissolved in acetone and analysed using a Perkin-Elmer 8500GC.

In order to determine the dehydrogenation behavior of the hydrogenated pyrenes, the products from pyrene hydrogenated at 350°C and 60 minutes, 400°C and 80 minutes, and 450°C and 40 minutes, were catalytically dehydrogenated under N₂. This was accomplished using the same reactors as in the hydrogenation step. The products from the three hydrogenations listed above were weighed into the reactor along with a 1wt% (metal) loading of ATTM. The reactor was pressurized with approx. 3MPa N₂ and immersed in a sand bath at the desired temperature and for the desired reaction time. After this time, the reactor was quenched as before, and the products were removed using THF. The products were analysed using GC as before. The dehydrogenation behavior of tetralin was investigated in a similar way to the hydrogenated pyrenes.

Results and discussion

1. Naphthalene

Thermodynamics.

Figure 1 shows the product distributions of naphthalene hydrogenation at 350, 400 and 450°C for various reaction times up to 3hrs. In all cases only tetralin was detected as a

hydrogenation product of naphthalene. No decalin was observed. Cracking/isomerisation products of tetralin were observed at 450°C, but total concentration did not exceed 5wt%. At 450°C, conversion of naphthalene to tetralin reaches a maximum at 51%. At 400°C, conversion is 62% and at 350°C the reaction does not reach equilibrium, but after 3hrs conversion is 72% (to calculate K_p for 350°C reaction, extrapolation used to assume 95% conversion). Figure 2 shows how the product distribution at equilibrium varies with temperature. From these equilibrium compositions, K_p values were calculated as below:

$$K_p = \frac{[\text{tetralin}]_{eq}}{[\text{naphthalene}]_{eq} [\text{H}_2 \text{ pressure}]^2}$$

Table 1 reports the K_p values for naphthalene hydrogenation. As expected, K_p decreases with increasing temperature. This is because thermodynamics controls the extent of the reaction as the temperature increases.

The variation in K_p with temperature can be used to find the enthalpy of the reaction. This is done using the van't Hoff isochore equation:

$$d \ln K_p / dT = \Delta H / RT^2$$

A van't Hoff plot gives a value of -32 kcal/mol. This is in agreement with values given in the literature (-29-32 kcal/mol) [8, 9].

Kinetics.

1. Reversible reaction kinetics

This can be modeled as a first order process with an effective rate constant equal to the sum of the forward and reverse rate constants:

$$-dC_A/dt = k_f C_A P H_2^n - k_r C_N$$

where C_A = concentration aromatic at time t , C_N = concentration hydroaromatic at time t , k_f = forward rate constant and k_r = reverse rate constant.

On integration, the following expression is derived:

$$\ln C_A - C_{Ae} / C_{A0} - C_{Ae} = -(k_f + k_r) t$$

where C_{A0} is the initial aromatic concentration and C_{Ae} is the equilibrium aromatics concentration.

2. Irreversible reaction kinetics.

If equilibrium effects are negligible, a simple pseudo-first order kinetic model can be used to obtain the forward rate constant:

$$\ln C_A / C_{A0} = -k_f t$$

If values of the above equation are plotted upto the time where equilibrium effects the reaction, a good approximation of k_f can be obtained.

Table 1 shows the calculated values of the rate constants calculated from plots of the above kinetic equations. Figure 7 shows an Arrhenius plot of the calculated rate constants. An activation energy of 14.7 kcal/mol for the forward reaction, and 25.5 kcal/mol for the reverse reaction were calculated. From this plot, dehydrogenation would be favored over hydrogenation at a temperature of 416°C.

Kinetics vs Thermodynamics.

If hydroaromatics are to be produced from aromatics, two factors have to be considered.

1. Conversion.
2. Length of time to get to the desired conversion level.

As can be seen from the data, conversion decreases with increasing temperature, but the kinetics of the reaction are slower at lower temperatures. From the data, it can be concluded that high temperatures are desirable for the first 40 minutes of reaction, but after this time thermodynamics limit the conversion. At this point, it is then advisable to drop the temperature to below 400°C, and continue to convert naphthalene to tetralin as seen in the 350°C reaction. To hydrogenate only at 350°C would take too long to achieve respectable conversions, i.e. conversion at 350°C and 120 minutes is the same as 450°C and 60 minutes. Therefore in hydrogenating naphthalene to tetralin a reverse temperature stage reaction is proposed.

Stage 1. 400°C and 40 minutes reaction time.

Stage 2. 350°C and 60 minutes reaction time.

Dehydrogenation reactions of tetralin

Figure 3 shows the product distribution of tetralin dehydrogenation at 350, 400, and 450°C for various reaction times up to 30 minutes. As temperature increases, the rate of dehydrogenation increases, and the conversion of tetralin to naphthalene also increases. At 350 and 400°C, conversion to naphthalene does not exceed 13%, but at 450°C conversion is 42%. This explains

the rapid approach to equilibrium seen in the hydrogenating reactions and the relatively low conversions seen at the high temperature of 450°C.

2. Pyrene

Thermodynamics.

Product distribution of pyrene, dihydropyrene, tetrahydropyrene and hexahydropyrene are shown in figures 4 and 4b. From these product distributions it can be seen that temperature is affecting the conversion of pyrene to hydrogenated pyrenes. At 450°C, equilibrium is reached after 20 minutes, with 28% conversion of pyrene. At 400°C, equilibrium is reached after 80 minutes, with 45% conversion of pyrene. At 350°C, equilibrium is not observed, even after 120 minutes of reaction. Conversion at this point is 55% pyrene to hydrogenated pyrenes. These product distribution trends are similar to that observed for naphthalene hydrogenation in that as temperature increases, conversion decreases but the rate of reaction to equilibrium increases. Figure 5 shows the equilibrium composition of pyrene and total hydrogenated pyrenes. Kp values are reported in table 1. Kp decreases with increasing temperature. These values can be used to determine the enthalpy of reaction as described earlier. A value of -6.4 kcal/mol is obtained from a van't Hoff plot. This value is a reasonable comparison to the value obtained by Johnston (-10 kcal/mol)[10].

Kinetics.

A similar model is used for evaluation of pyrene kinetic data as was used for naphthalene. Rate constants are reported in table 1. Figure 8 shows an Arrhenius plot for the calculated rate constants. An activation energy of 6.83 kcal/mol for the forward reaction, and 21.5 kcal/mol for the reverse reaction were calculated. From this plot, dehydrogenation would be favored over hydrogenation at temperatures above 350°C.

Kinetics vs thermodynamics.

The same arguments apply for pyrene as they did for naphthalene. A reverse temperature stage reaction is proposed for pyrene hydrogenation:

Stage 1. 400°C and 20 minutes reaction time.

Stage 2. 350°C and reaction time set for the desired conversion.

Dehydrogenation of hydropyrenes.

Figure 6 show the dehydrogenation product distributions of dihydropyrene, tetrahydropyrene and hexahydropyrene. It can be seen that dehydrogenation is rapid and complete at 450°C. At the lower temperatures, dehydrogenation is slower and complete dehydrogenation to pyrene is not seen in the 30 minutes reaction used in this study.

Comparisons between naphthalene and pyrene

Table 1 shows a comparison of the parameters for the two compounds. It can be seen that as ring size increases, enthalpy of reaction increases and activation energy decreases.

Future Work

The work will be expanded to include 3-ring systems and other 4-ring compounds. When the parameters are calculated for these compounds and plotted vs ring size, molecular weight etc., it should be possible to make predictions as to how other compounds behave under hydrogenating/dehydrogenating conditions. Ideal temperature strategies will be estimated from the product distribution curves and compared for the different compounds.

References

1. Burgess, C. *PhD Thesis* 1994, Pennsylvania State University.
2. Girgis, M. J. and Gates, B. C. *Ind. Eng. Chem. Res.* **1991**, 30, 2021.
3. Song, C. and Hatcher, P. G. *Prepr. Pap.- Am. Chem. Soc., Div. Pet. Chem.* **1992**, 37, 529.
4. Song, C., Ono, T. and Nomura, M. *Bull. Chem. Soc. Jpn.* **1989**, 62, 680.
5. Song, C., Schobert, H. H., Matsui, H., *Prep. Pap.- ACS, Div. Fuel. Chem.*, **1991**, 36(4), 1892.
6. Dutta, R., *BSc Thesis*. **1991**, Nottingham Polytechnic.
7. Tomic, J., *PhD Thesis*. **1993**, Pennsylvania State University.
8. Frye, C. G. *J. Chem. Eng. Data*. **1962**, 7, 592.
9. Frye, C. G. and Weitkamp, A. W. *J. Chem. Eng. Data*. **1969**, 14, 372.
10. Johnston, K. P. *Fuel*. **1984**, 63, 463.

Table 1. Kinetic and thermodynamic parameters for naphthalene and pyrene hydrogenation

	Kp 350C	Kp 400C	Kp 450C	k/min ⁻¹ 350C	k/min ⁻¹ 400C	k/min ⁻¹ 450C	ΔH kcal/mol	Ea (kf) kcal/mol
Naphthalene	0.0045	0.00037	0.00027	kf 0.0059 kr 0.0027	kf 0.0150 kr 0.0125	kf 0.0301 kr 0.0194	-32	14.7
Pyrene	0.0078	0.0058	0.0038	kf 0.0088 kr 0.0100	kf 0.0139 kr 0.0342	kf 0.0187 kr 0.1103	-6.4	6.8

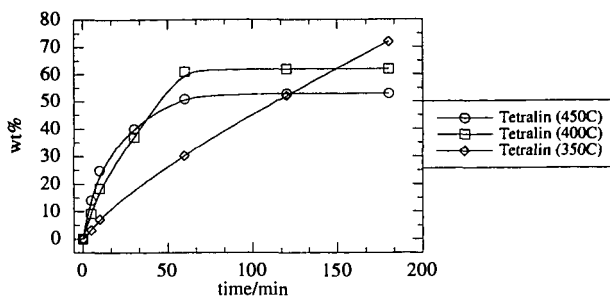


Figure 1. Naphthalene-tetralin product distribution vs time

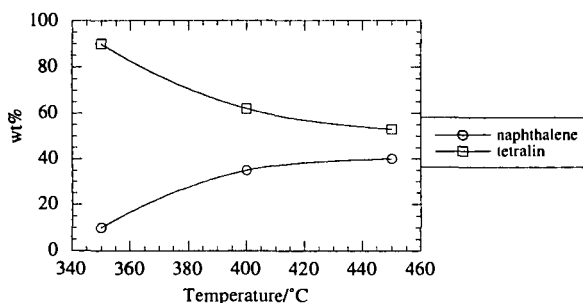


Figure 2. Naphthalene hydrogenation product distribution at equilibrium

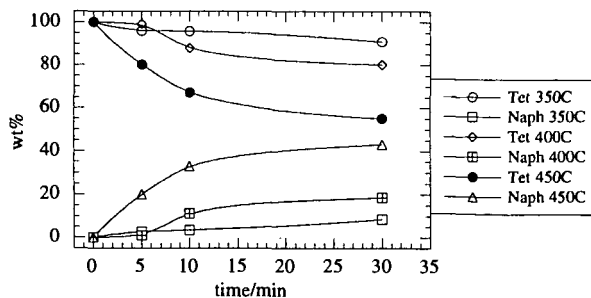


Figure 3. Tetralin dehydrogenation product distribution vs reaction time

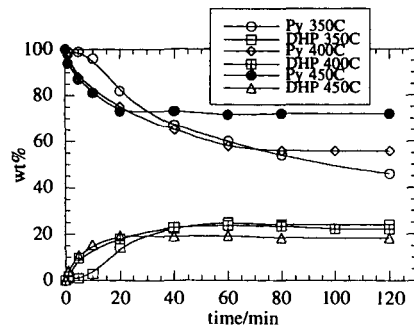


Figure 4. Pyrene-dihydropyrene product distribution vs time

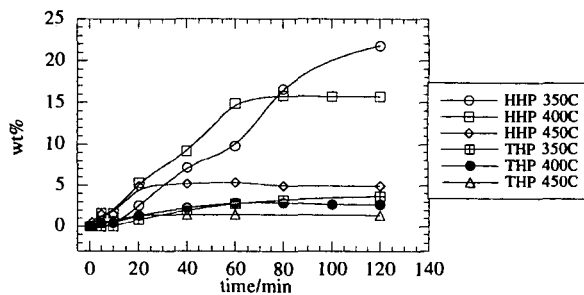


Figure 4b. Tetrahydropyrene-hexahydropyrene product distribution vs time

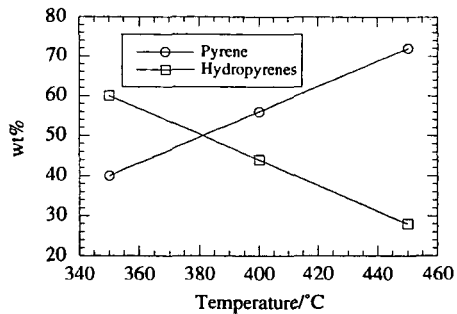


Figure 5. Pyrene hydrogenation product distribution at equilibrium

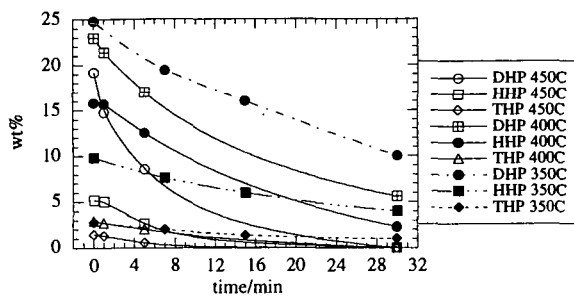


Figure 6. Hydropyrenes dehydrogenation product distribution vs time

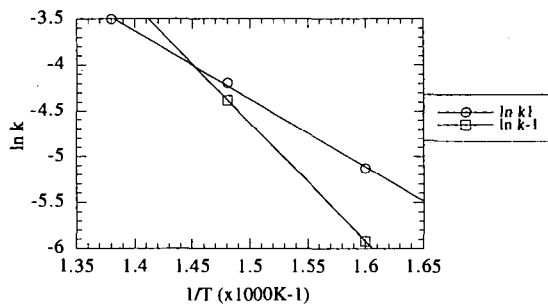


Figure 7. Arrhenius plot- naphthalene hydrogenation

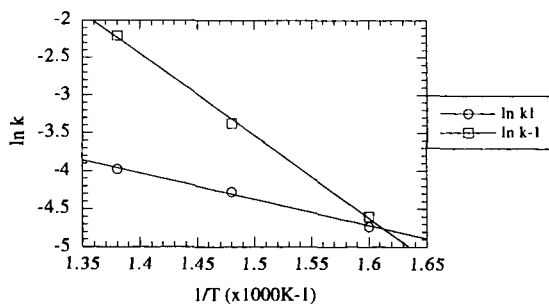


Figure 8. Arrhenius plot- pyrene hydrogenation

Effect of Temperature on Quantitative Structure/Reactivity Relationships for Hydrocracking Polynuclear Aromatics

by

Stella C. Korre and Michael T. Klein
Center for Catalytic Science and Technology
Department of Chemical Engineering
University of Delaware
Newark, DE 19716

Introduction

The increased interest in the molecular modeling of hydrocarbon conversion processes is motivated by the need to predict both the performance and environmental properties of the products. A molecular description of the hydrocarbon mixture is the logical starting point for these predictions, which has motivated considerable interest in the development of molecular reaction models.

The construction of such models is complicated by the enormous need for rate, adsorption and equilibrium parameters. This staggering need can be reduced considerably when the homologous patterns of both compound types and their reactions in these mixtures can be recognized. This has motivated the development of a lumping approach that organizes the kinetics information in potentially thousands of rate, adsorption and equilibrium constants into the parameters of a handful ($O(10)$) of Quantitative Structure/Reactivity Relationships (QSRR) using the formalism of Linear Free Energy Relationships.

The application of these ideas to hydrocracking is quite recent. For example, Landau (1991) verified the applicability of the QSRRs to dealkylations of butyl tetralins. Neurock (1992) showed that the standard enthalpy of reaction of the controlling elementary step could be used to correlate the kinetics of both dealkylations and isomerizations. Korre (1995) developed QSRRs for hydrogenation of polynuclear aromatics using the same principles. All of the foregoing work was limited to a set of "isothermal correlations", i.e., one correlation was developed for each temperature. Clearly, a more universal, temperature-independent correlation would be desirable.

The present work aimed to exploit this concept and explore 1) the applicability of QSRRs to the acid center transformations during hydrocracking, and 2) the dependence of QSRRs on temperature for both metal- and acid- catalyzed reactions. The tangible result of such correlations would be the organization of energetic and entropic quantities for both overall reaction and activation for a wide range of hydrocracking reactions.

Experimental Results

A batch autoclave equipped with reactant injection and sample procurement systems was used. Naphthalene and phenanthrene hydrocracking were studied over the temperature range of 300-370°C. The reactant mixture consisted of 30 g of a 50% wt mixture of naphthalene and phenanthrene, dissolved in 15 g of cyclohexane. The reactant mixture was introduced in 400 g of cyclohexane as a solvent at the arbitrary $t=0$ time with hydrogen back pressure. The solvent was in a supercritical phase at all conditions, and the hydrogen pressure was varied from 62 atm (300°C) to 70 atm (370°C) in order to ensure constant hydrogen concentration of 1.33 g/mol/l during all experiments.

The evolution of phenanthrene and naphthalene conversion with time is presented in Fig. 1. Conversion rates for both reactants were accelerated with increasing temperature. The effect of temperature was more pronounced at temperatures lower than 350°C. At the temperatures of 350°C, 365°C and 370°C, the influence of thermodynamic equilibrium on the hydrogenation rates began to appear.

Naphthalene and phenanthrene hydrocracking product yields vs. reactant conversion are presented in Fig. 2. Fig. 2f indicates that virtually all naphthalene was converted to tetralin at all temperatures, up to naphthalene conversion of approximately 0.6. At higher naphthalene conversions, the maximum in tetralin yield decreased with increasing temperature. This implies that tetralin consumption rates had a stronger temperature dependence than its formation rate from naphthalene hydrogenation. For irreversible reactions, a stronger temperature dependence is associated with a higher activation energy.

The effect of temperature on the yields of di- and tetra- hydrophenanthrene with respect to phenanthrene conversion is presented in Fig. 2a and Fig. 2b, respectively. The maximum yields for di- and tetra- hydrophenanthrene did not significantly diverge from 0.08 and 0.14 respectively, for all reaction temperatures. This indicates that their production and consumption reactions had similar temperature dependence.

These experiments led to the reaction network of Fig. 3. This allowed parameter estimation to the dual-site LHHW (Langmuir-Hinshelwood-Hougen-Watson) rate expression of Eq. 1.

$$-\frac{dC_i}{dt} = \frac{\sum_j k_{ij}(C_i - C_j/K_{ij})}{D_H} + \frac{\sum_l k_{il}(C_i - C_l/K_{il})}{D_A} \quad (1)$$

In Eq. (1), C_i, C_j, C_l were component concentrations (mol l^{-1}), k_{ij}, k_{il} were combined numerator rate parameters ($\text{l kg}_{\text{cat}}^{-1} \text{s}^{-1}$), and K_{ij}, K_{il} were the equilibrium ratios ($\text{mol i/mol j/P}_{\text{H}_2^0}$). D_H, D_A were the adsorption groups for the metal (hydrogenation, H) and zeolite (acid, A) sites respectively, defined in Eq. (2).

$$D_H = 1 + \sum_i K_i^H C_i, \quad D_A = 1 + \sum_i K_i^A C_i \quad (2)$$

In Eq. (2), K_i^H, K_i^A (l mol^{-1}) represented individual component adsorption constants on the metal and acid sites, respectively.

A total of 21 numerator rate parameters (k_{ij}) and 17 equilibrium parameters (K_{ij}) were regressed for each of the eight reaction temperatures, corresponding to the naphthalene and phenanthrene hydrocracking networks of Fig. 3. Thus a total of 304 numerator rate parameters and equilibrium ratios were required to represent the kinetics of naphthalene and phenanthrene hydrocracking in the temperature interval 300–370°C. In this first-pass parameter estimate, the 34 adsorption constants for the metal and acid sites were not included; their addition for each temperature would have brought the total parameter number to 576. The overall agreement between experimental and calculated concentration profiles was very good. The sum-of-squares error on concentrations was less than $5 \cdot 10^{-3}$ at all temperatures.

Reactivity Indices

The foregoing parameter estimation information shows that even the relatively simple hydrocracking networks of naphthalene and phenanthrene required 21 rate, 17 equilibrium and 34 adsorption constants at each temperature. Extrapolation to the demands of a heavy oil suggests that a lumping strategy aimed at representing this information in terms of fewer parameters would be very useful. To this end, it seemed cogent to attempt to organize the hydrocracking reactions into reaction families, which could in turn be characterized by quantitative structure/reactivity relationships.

The present development of QSRRs for each reaction family essentially is a model of the variation of the activation energies (E^* , kcal/gmol) and pre-exponential factors (A , $l/kg_{cat}/s$) within a reaction family. The concept of a reaction family exploits either a constant pre-exponential factor, or one that compensates with changes in E^* . The latter approach, adding flexibility, was used to relate changes in pre-exponential factors within a family to changes in activation energies. The activation energies for the acid center reactions were correlated with the enthalpy of formation of the carbocation intermediate (ΔH_c^+ , kcal/gmol). The activation energies for the metal center transformations were correlated with the enthalpy of reaction (ΔH_R^0 , kcal/gmol). Similarly, equilibrium constants for all reactions were correlated with ΔH_R^0 , using the compensation notion to constrain the overall reaction and adsorption entropies. The adsorption constants for both metal and acid sites were correlated with the number of aromatic rings (N_{AR}) and the number of saturated carbons (N_{SC}). All thermochemical quantities were calculated with semi-empirical molecular orbital calculations (MOPAC/AM1).

Parameter Estimation Results

The parameter estimation was performed to the concentration vs. time experimental data from naphthalene/phenanthrene hydrocracking in the temperature interval 300-370°C. This represented approximately 1600 experimental concentration measurements. The quantitative structure/reactivity relationships were imposed for the relevant reaction family to summarize a total of 304 numerator rate and equilibrium constants and 272 adsorption constants on metal and acid sites. The final quantitative structure/reactivity relationships summarize the results. These are given in the following Eq. (3) - Eq. (12):

Hydrogenations:

$$\text{Adsorption: } \ln K_{ads} = 1.324 + (0.887N_{AR} + 0.123N_{SC})/RT \quad (3)$$

$$\text{Equilibrium: } \ln K = -7.017 n^+ + (1/RT - 0.54707) \Delta H_R^0 \quad (4)$$

$$\text{Rate: } \ln k = \ln K_{ads} + n \ln P_{H_2} + \ln A_H - E_H^*/RT \quad (5)$$

$$\ln A_H = -(6.613 + 5.767 n); E_H^* = 0.228 \Delta H_R^0 \quad (6)$$

Acid Center Transformations:

$$\text{Adsorption: } \ln K_{ads} = 0.182 + (1.934N_{AR} + 0.187N_{SC})/RT \quad (7)$$

$$\text{Equilibrium: } \ln K = -1.775 + (1.469 - 1/RT) \Delta H_R^0 \quad (8)$$

Isomerization Rate:

$$\ln k = -2.89 - 305. (0.585 - 1/RT) + (1 - 1/0.585RT) \Delta H_c^+ \quad (9)$$

$$(E_i^* = -305. + 1.709 \Delta H_c^+; \ln A_i = -2.89 + 0.585 E_i^*) \quad (10)$$

Ring Opening Rate:

$$\ln k = \ln P_{H_2} - 4.64 - 271 (0.585 - 1/RT) + (1 - 1/0.585RT) \Delta H_c^+ \quad (11)$$

$$(E_{RO}^* = -271. + 1.709 \Delta H_c^+; \ln A_{RO} = -4.64 + 0.585 E_{RO}^*) \quad (12)$$

Fig. 2 summarizes these parameter estimation results in terms of a set of a yield-vs.-conversion plots for key products. The sum-of-squares error on concentrations was less than 0.05. The predictions follow the experimental data very closely, considering the reduction in the number of parameters from 576 to 17.

Summary

The number of parameters needed to describe hydrocracking kinetics was reduced by the development of temperature-independent quantitative structure/reactivity relationships for the activation and reaction enthalpies and entropies. This approach can be summarized in the quantitative structure/reactivity relationships of Eq. (3)–Eq. (12) for the calculation of rate, equilibrium, and adsorption constants. In turn this allowed the kinetics of naphthalene and phenanthrene to be represented very satisfactorily, over a wide temperature range, in terms of just 17 QSRR parameters. These 17 parameters summarized the chemical information in 576 rate, equilibrium, and adsorption constants, which shows that the QSRR approach reduced the number of modeling parameters by about 97%.

References

- Landau, R.N. (1991) *Chemical Modeling of the Hydroprocessing of Heavy Oil Feedstocks*. (Ph.D. Dissertation, University of Delaware.)
- Neurock, M.T. (1992) *A Computational Chemical Reaction Engineering Analysis of Complex Heavy Hydrocarbon Reaction Systems*. (Ph.D. Dissertation, University of Delaware.)
- Korre, S. C., Neurock, M., Klein, M.T., and Quann, R.J. (1995) *Hydrogenation of Polynuclear Aromatic Hydrocarbons. 2. Quantitative Structure/Reactivity Correlations*. Chem. Eng. Sci., 49, 4191-4210.

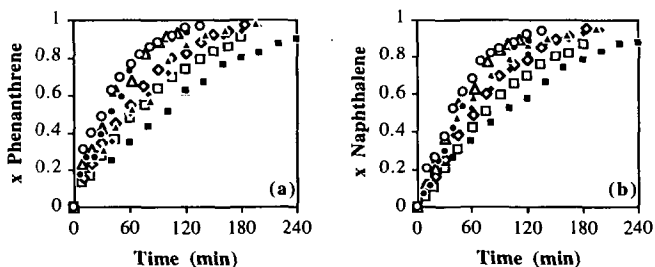


Fig. 1 Evolution of phenanthrene (a) and naphthalene (b) hydrocracking conversion with time as a function of reaction temperature.

(■): 300°C; (□): 310°C; (◆): 320°C; (◇): 330°C; (▲): 340°C; (△): 350°C; (●): 365°C; (○): 370°C.

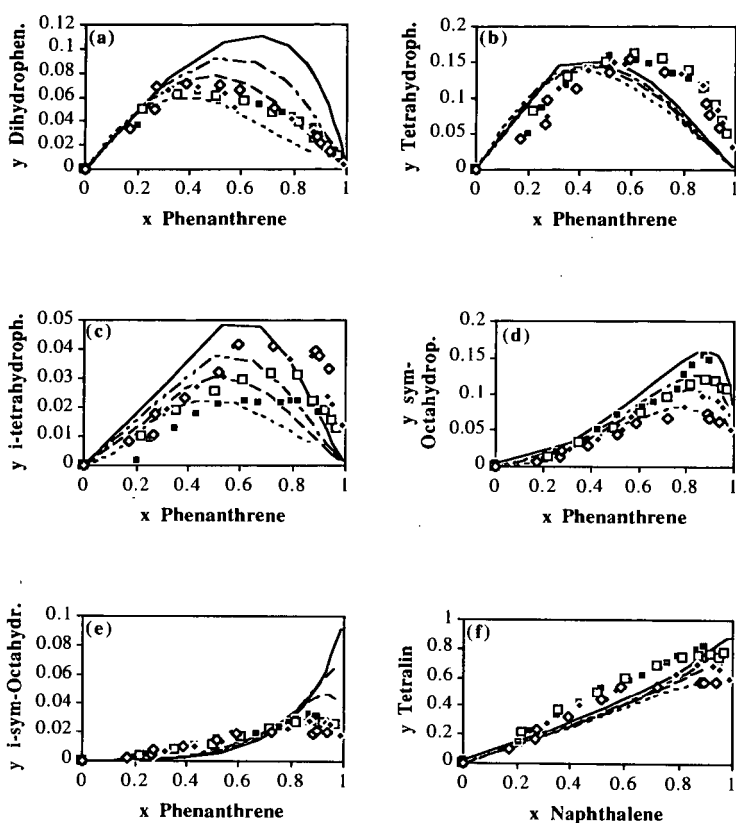


Fig. 2 Comparison between experimental and QSRR calculated yields of phenanthrene and naphthalene hydrocracking products.

(a) Dihydrophenanthrene. (b) Tetrahydrophenanthrene.

(c) *sym*-octahydrophenanthrene. (d) *i*-tetrahydrophenanthrene.

(e) *i*-*sym*-octahydrophenanthrene. (f) Tetralin.

Lines represent parameter estimation results (Eq. (1) – Eq. (12)).

(■): 300°C; (□): 320°C; (◆): 340°C; (◇): 365°C.

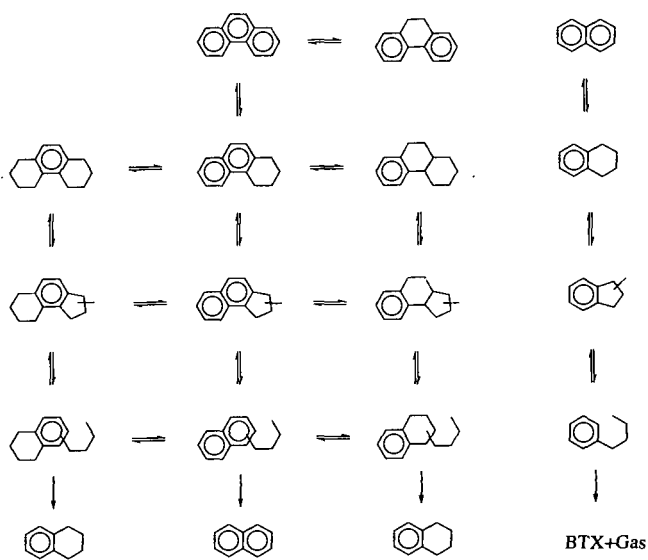


Fig. 3 Proposed network for phenanthrene and naphthalene hydrocracking.

NOBLE METAL CATALYSTS FOR LOW-TEMPERATURE NAPHTHALENE HYDROGENATION IN THE PRESENCE OF BENZOTHIOPHENE

Shawn D. Lin¹ and Chunshan Song*

¹Department of Chemical Engineering,

Yuan-Ze Institute of Technology, Neili, Taiwan 320, R.O.C.

*Fuel Science Program, Department of Material Science and Engineering,
Pennsylvania State University, University Park, PA16802, U.S.A.

Keywords: Naphthalene hydrogenation, Benzothiophene, Noble metal catalysts

INTRODUCTION

The hydrogenation of aromatic and polyaromatic compounds are typically exothermic [1,2]; therefore, a lower reaction temperature is thermodynamically favorable. However, in considering the hydrotreating process of heavy liquids where polycyclic aromatic compounds are abundant, a reaction temperature above 623K is typical which consequently requires a high concentration of hydrogen to offset the limitation of thermodynamic equilibrium conversion. Noble metal catalysts are active for the hydrogenation of aromatics even at a temperature below 473K [2-4], but they were not used for hydrotreating purpose owing to the cost and their susceptibility to the poisoning by sulfur-containing compounds [5]. However, recent studies showed that noble metal catalysts may not be as sensitive to sulfur as what has been recognized [6-10]. This study is therefore attempted to probe the possibility of using noble metal catalysts for low-temperature hydrotreating reaction in the presence of sulfur-containing compounds, and the model reaction of naphthalene hydrogenation in the presence of benzothiophene was used.

EXPERIMENTAL

Pt/Al₂O₃, Pd/Al₂O₃, and Pd/TiO₂ catalysts were all prepared by incipient wetness method using H₂PtCl₆ (Aldrich, 99.995%) and PdCl₂ (Aldrich, 99.995%, dissolved in ultra pure HCl before use) as the precursors. The pore volume and surface area of the support are 0.8 cc/g and 200 m²/g for γ -Al₂O₃ (Sumitomo Metal Mining, S-1, grounded to 80-120 mesh size before use) and 0.5 cc/g and 50 m²/g for TiO₂ (Degussa, P25). The supports were calcined at 773K under dried air flow for 2 h before catalyst preparation. A nominal loading of 2% metal was used for all three catalysts. A commercially available NiMo/Al₂O₃ hydrotreating catalyst (Shokubai Kasei, P-modified and presulfided) was used without further pretreatment and as a reference for comparison in this study. Pretreatment of catalysts were carried out in a flow-type glass reactor which has a side arm to connect to a catalyst transfer tube with which the reduced catalyst powders can be poured into the transfer tube without exposing to the air. The transfer tube loaded with pretreated catalyst was usually stored under N₂ environment in a home-made glove box. The pretreatment conditions for these noble metal catalysts were H₂ reduction at 723K for Pt/Al₂O₃, 20% O₂ calcination at 673K for Pd/Al₂O₃, and H₂ reduction at 473K for Pd/TiO₂; these conditions were found to cause relatively higher activities for naphthalene hydrogenation at 553K with these three noble metal catalysts.

Hydrogenation was studied using tubing bombs made from weld connectors (Swagelok®, ss316), and a 1/4" tube as the side arm for connection to a pressure gauge and a close-off valve. The total inner volume of the bomb was approximately 25 cc. Bombs were typically loaded with 4 g tridecane (Aldrich, 99%), 1 g naphthalene (Fischer, certified grade), and benzothiophene (Fluka, 99%) in some cases, transferred into the home-made glove box, loaded with pretreated noble metal catalyst, capped using wrenches, transferred out of glove box, and further tightened. Thereafter, the bomb was connected to a gas manifold via its side-arm and the atmosphere inside the bomb was replaced by hydrogen (MG Ind., 99.999%) using dilution purge, i.e., at least 8 cycles of pressurizing with H₂ to 1000 psig followed by a careful venting to approximately 50 psig. At the completion of dilution purge, the bomb was charged with H₂ to either 1000 psig or 1500 psig, disconnected from the manifold, sinked into a fluidized sandbath (Tecam) preset to the desired reaction temperature, and the reaction was timed. After the reaction time was reached, the bomb was removed from the sandbath and quenched in water. The reaction temperature was typically controlled to an accuracy of $\pm 10^\circ\text{C}$.

After reaction, the pressure in the tubing bomb was carefully released to prevent from any entrainment of liquid in the vent gas; part of the vent gas was collected in a gas bag for later composition analysis. The bomb was then opened and the liquid content was poured into a funnel with filter paper, and the bomb was rinsed and flushed with acetone (Aldrich, 99.9%); the filtrate and the wash solution are separately stored in small vials for later analysis. The solid residue on the filter paper was dried in an oven at 120°C for at least 3 h and then weighed.

The composition of vent gas was analyzed with GC (Perkin-Elmer 5800) using Chemipack C18 (Alltech, 1/8", 6ft) column with FID and Carboxene 1000 (Supelco, 1/8", 15ft) column with TCD. The gas yield and the amount of H₂ reacted were calculated from the average molecular weight of vent gas, the bomb pressure after reaction, and the weight change before and after the bomb was vented. Liquid samples were quantized by adding known amount of n-nonane (Aldrich, 99.9%) followed by GC (HP5890II) analyses with either a DB-17 (J&W, 30mx0.25mm) or a Rtx-50 (Restek, 30mx0.25mm) capillary column and the FID; the response factors of individual species were determined by injection of mixtures of known composition. GC-MS (HP5890II GC with HP5971A MSD) equipped with the same capillary column was used to obtain structural information of unknown species from time to time. The sum of the liquid products in both the filtrate and the wash solution samples were used as the overall yields of liquid products. The yield of solid product was taken as the weight difference between the solid residue and the catalyst loaded in the reactor. An overall mass balance of $\pm 10\%$ was obtained with this kind of analysis; most experiments show an overall mass balance within $\pm 5\%$.

RESULTS AND DISCUSSION

The results of naphthalene hydrogenation at 553K over these three noble catalysts and the NiMo/Al₂O₃ catalyst are shown in Table 1. The naphthalene conversions over Pt/Al₂O₃, Pd/Al₂O₃, and Pd/TiO₂ were all above 70% in the one-hour run, comparing to a 17% conversion over NiMo/Al₂O₃ at a 50% higher catalyst loading; it is clear that the three noble metal catalysts are much more active than the NiMo/Al₂O₃ hydrotreating catalyst at this reaction condition. Also included in Table 1 are the hydrogenation results of TiO₂ and HCl treated Al₂O₃; it is clear that the high activities of these three noble metal catalysts cannot be attributed to the support or the Cl⁻ residue in the catalysts. Beside the higher naphthalene conversions with the three noble metal catalysts, the selectivities to hydrogenated naphthalene products (dihydronaphthalene, tetralin, and decalins) and the ratios of the moles of hydrogen reacted to that of naphthalene reacted, $\Delta H/\Delta N$, are also significantly higher than the NiMo/Al₂O₃ catalyst. The calculated $\Delta H/\Delta N$ ratio for the three noble metal catalysts roughly agrees with the amount of hydrogen added to form the hydrogenated products based on the product analysis. This indicates that the hydrogen reacted was almost all used for hydrogenation with the noble metal catalysts; whereas, for NiMo/Al₂O₃ part of the hydrogen reacted was used to form gas products. This implication agrees with the low yields to solid and gas products with the noble metal catalysts. It is clear that the noble metal catalysts are more suitable for the hydrogenation of naphthalene and, likely, more suitable for the hydrotreating purposes at 553K.

It is interesting to note that the main product of the naphthalene hydrogenation is tetralin at 553K even when the naphthalene conversion is above 90% (Table 1). As the naphthalene hydrogenation and the tetralin hydrogenation are both exothermic reactions, a higher equilibrium yield to deeper hydrogenated products is expected from thermodynamics when a lower reaction temperature is used. Therefore, the naphthalene hydrogenation at 473K was studied and the results are shown in Table 2 for the three noble metal catalysts. It appears that the selectivities to decalins increase only when high naphthalene conversion was achieved at 473K; it seems that a more detailed study is needed if a high selectivity to decalins is desired. However, the hydrogenation abilities of these noble metal catalysts are clearly shown from the high selectivities to hydrogenated products, high $\Delta H/\Delta N$ ratios, and the low selectivities to gases and solids in Table 2. This indicates that noble metal catalysts can be useful for low-temperature polyaromatic hydrogenation.

The results of naphthalene hydrogenation in the presence of benzothiophene are also included in Table 2. The addition of 0.2% (wt) of sulfur in the form of benzothiophene caused a 87, 53, and 39% decrease in the naphthalene conversion respectively for the Pt/Al₂O₃, Pd/Al₂O₃, and Pd/TiO₂ catalysts in the one-hour runs; whereas, a 90, 84, and 57% decrease was observed respectively when 0.5% (wt) of sulfur was added. It is clear that organic sulfur compounds can significantly hinder the hydrogenation activities of noble metal catalysts and a higher sulfur content resulted in a lower conversion during the same period of reaction. However, the above percentages of decrease in naphthalene conversion indicate that palladium catalysts are less sensitive to sulfur compound than the platinum catalyst and that the TiO₂ support can be beneficial in regards to the catalytic hydrogenation activity in the presence of benzothiophene.

Experiments with an extended reaction period (8 h) showed that the naphthalene hydrogenation in the presence of benzothiophene can proceed to a conversion as high as 89 and 78% respectively for Pd/TiO₂ and Pd/Al₂O₃. As no benzothiophene was identified in the liquid products from all the runs with the addition of benzothiophene, it implies that benzothiophene was adsorbed favorably to naphthalene and reacted slower than the naphthalene under the reaction conditions of this study. As the benzothiophene was gradually converted to another sulfur species not held

on the catalytic surface, the naphthalene hydrogenation started and gradually went to completion. Since no other form of sulfur compound was identified in the liquid products except small amount of dihydrobenzothiophene and since the yield to ethylbenzene which is included in R-(1-ring) category in Table 2 increased with the reaction time, it is speculated that the conversion of the benzothiophene over these noble metal catalysts proceeds via a hydrodesulfurization reaction to ethylbenzene and hydrogen sulfide with dihydrobenzothiophene as the intermediate. Accordingly, the hydrogen sulfide formed should not be a poison, at least to the palladium catalysts used in this study. It should be noted that hydrogen sulfide was not included in the products because it could not be identified with the analytical tools used in this study. Although the possibility of the formation of SO_2 species over TiO_2 [6] could not be excluded from this study, the above speculation is preferred because $\text{Pd}/\text{Al}_2\text{O}_3$ also catalyzed the naphthalene hydrogenation to 78% conversion in the 8-h run with the addition of benzothiophene. It is also interesting to note that the selectivities to hydrogenated naphthalene products were not significantly affected by the presence of benzothiophene, as shown in Figure 1; this again agrees with the speculation that naphthalene hydrogenation could occur simultaneously with the benzothiophene hydrodesulfurization. These results suggest that noble metal catalysts can be useful for low-temperature hydrotreating purpose even when the feed contains sulfur.

In an effort to obtain a quantitative analysis of the effect of benzothiophene on the naphthalene hydrogenation over these noble metal catalysts, a pseudo-first order kinetics [1] is assumed applicable to the results of this study. As a consequence, the apparent rate constants can be estimated by the slopes from a graph like Figure 2, where the results reported for the naphthalene hydrogenation at 553K (Table 1) and the hydrogenation at 473K in the presence of 0.5% (wt) sulfur (Table 2) are presented according to the pseudo-first order kinetics. The effect of sulfur compound on the rate of naphthalene hydrogenation is then estimated by the ratio of the apparent rate constant in the presence of benzothiophene to that with no addition of benzothiophene, i.e., k_s/k . After correcting for the amounts of catalysts used in different runs, the $k_s(473\text{K})/k(553\text{K})$ ratio was found to be 0.1, 0.12, and 0.02 for Pd/TiO_2 , $\text{Pd}/\text{Al}_2\text{O}_3$, and $\text{Pt}/\text{Al}_2\text{O}_3$ respectively. If the activation energy that Nieuwstad *et al.* reported for 2-methylnaphthalene hydrogenation over Pd/C catalyst [4], 10 kcal/mol, is used to correct for the effect of reaction temperature, then the $k_s(473\text{K})/k(473\text{K})$ ratio becomes 0.46, 0.56, and 0.1 respectively for Pd/TiO_2 , $\text{Pd}/\text{Al}_2\text{O}_3$, and $\text{Pt}/\text{Al}_2\text{O}_3$. This again indicates that the palladium catalysts are less affected by the presence of benzothiophene. The ratios for the two palladium catalysts are comparable to the calculated k_s/k ratio of 0.73 for $\text{NiMo}/\text{Al}_2\text{O}_3$ at 623K based on the equation reported by Lo [1,11] and the benzothiophene concentration used in this study. This indicates that the palladium catalysts are comparable to $\text{NiMo}/\text{Al}_2\text{O}_3$ for simultaneous hydrogenation and hydrodesulfurization even at a lower reaction temperature where $\text{NiMo}/\text{Al}_2\text{O}_3$ catalyst shows little activity.

From Tables 1 and 2, the three noble metal catalysts studied showed their potentials for applications in the polyaromatic hydrogenation and hydrotreating purposes. The high activities of group VIII metal catalysts toward hydrogenation of alkylbenzenes and of polycyclic aromatic compounds have been known for some times [2-4]; their activities toward hydrogenation of polyaromatic compounds can be orders of magnitude higher than the conventional hydrotreating catalysts such as $\text{NiMo}/\text{Al}_2\text{O}_3$ [2]. Even the presulfided Pt and Pd catalysts showed significantly higher hydrogenation activities and C-N hydrogenolysis activities than sulfided Mo catalyst [12]; this indicates that sulfur-poisoned noble metal catalysts might still have comparable activities to the conventional hydrotreating catalysts. Thus, as the energy efficiency and the activity of the hydrotreating catalyst are concerned, the use of noble metal catalysts for lower-temperature hydrotreating purposes seems to be a reasonable choice. However, the preparation of optimal supported noble metal catalyst for these applications still waits for more detailed studies.

ACKNOWLEDGMENT

We thank Dr. H. H. Schobert and Dr. W.-C. Lai for all of their assistance and the helpful discussion.

REFERENCES:

1. Girgis, M. J. and Gates, B. C., *Ind. Eng. Chem. Res.*, **1991**, 30, 2021.
2. Stanislaus, A. and Cooper, B.H., *Catal. Rev.- Sci. Eng.*, **1994**, 36, 75.
3. Sakarishi, K., Ohira, M., Mochida, I., Okazaki, H., and Soeda, M., *Bull. Chem. Soc. Jpn.*, **1989**, 62, 3994.
4. Nieuwstad, Th. J., Klapwijk, P., and van Bekkum, H., *J. Catal.*, **1973**, 29, 404.
5. Bartholomew, C.H., Agrawal, P. K., and Katzer, J. R., *Advan. Catal.*, **1982**, 31, 135.
6. Chen, Y., Chen, Y., Li, W., and Sheng, S., *Appl. Catal.*, **1990**, 63, 107.
7. Hayes, L. E., Snape, C. E., and Affrossman, S., *Prepr. Am. Chem. Soc. Div. Fuel. Chem.*,

- 1991, 36, 1817.
8. Berube, M. N., Sung, B., and Vannice, M. A., *Appl. Catal.*, 1987, 31, 133.
9. Koussathana, M., Vamvouka, D., Economou, H., and Verykios, X., *Appl. Catal.*, 1991, 77, 283.
10. Koussathana, M., Vamvouka, N., Tsapatsis, M., and Verykios, X., *Appl. Catal. A*, 1992, 80, 99.
11. Lo, H. S., *Ph. D. Dissertation*, 1981, University of Delaware, Newark.
12. Shabtai, J., Guohe, Q., Balusami, K., Nag, N. K., and Massoth, F. E., *J. Catal.*, 1988, 113, 206.

Table 1. Naphthalene Hydrogenation over Various Catalysts at 553K using Tridecane as the Solvent

	NiMo/Al ₂ O ₃	Pt/Al ₂ O ₃	Pd/Al ₂ O ₃	Pd/TiO ₂	TiO ₂	HCl/Al ₂ O ₃
Feed						
Catalyst(mg)	207	127	136	132	137	144
H ₂ ¹ (psig)	1000	1000	1000	1000	1000	1000
N ² (mg)	1001	1001	1003	1002	1011	1002
Reaction						
T ² (°C)	280	280	280	280	280	280
Time (h)	1	1	2	1	2	1
x _N ⁴ (%)	17	72	86	77	90	84
ΔH ₂ ⁵ (mmol)	2	10	15	10	16	12
ΔH ₂ /ΔN ⁶	1.5	1.8	2.2	1.7	2.2	1.8
Yield ⁷ (mg)	122	804	949	829	992	863
Product (wt%)						
di-H-N ⁸	0.2	0	0	0	0	0
Tetralin	55	92	85	90	90	92
t-Decalin	0	3	7	2	2	1
c-Decalin	0	2	5	0.7	0.4	0.2
R-(1-ring) ⁹	6	0.6	0.6	2	0.5	0.6
R-(2-ring) ¹⁰	1	0.1	0.2	0.1	0.1	0.2
R-(3+ring) ¹¹	0	0	0	0	0	0
Solid	0	0.2	0.5	0.3	0.2	0
Gas	38	3	1	5	7	6

¹ H₂ feed at room temperature to an accuracy of ±20 psig.

² Naphthalene.

³ Temperature setting of the sandbath; the accuracy of actual reading is ±10°C.

⁴ Naphthalene conversion, calculated from the amount of N remained and the amount of N fed.

⁵ Number of moles of H₂ reacted.

⁶ Molar ratio of H₂ reacted to N reacted.

⁷ Overall yield of products listed below.

⁸ Dihydronaphthalene.

⁹ R-(1-ring) includes alkylbenzenes and alkylcycloparaffins.

¹⁰ R-(2-ring) includes indenenes, indanes, alkyltetralins, alkylindaphthalenes, and biphenyls.

¹¹ R-(3+ring) includes species having at least 3-ring structures.

Table 2¹. Naphthalene Hydrogenation over Pd/Al₂O₃, Pd/Al₂O₃, and Pd/TiO₂ Catalysts at 473K using Tridecane as the Solvent

Feed	Pd/Al ₂ O ₃						Pd/Al ₂ O ₃						Pd/TiO ₂					
	124	207	191	184	196		135	208	199	195	202		138	214	197	194	191	202
Catalyst(mg)	1500	1500	1500	1500	1500		1500	1500	1500	1500	1500		1500	1500	1500	1500	1500	1500
H ₂ (psig)	1002	1004	1003	1004	1001		1001	1004	1001	1002	1002		1002	1002	1002	1001	1000	1001
N (mg)	0	0	9	21	21		0	0	9	21	21		0	0	9	21	21	21
BT ² (mg)																		
Reaction																		
T (°C)	200	200	200	200	200		200	200	200	200	200		200	200	200	200	200	200
Time (h)	2	2	2	2	8		2	2	2	2	8		2	2	2	2	4	8
x _N (%)	11	100	13	10	10		42	100	47	16	78		37	100	61	43	61	89
ΔH ₂ (mmol)	4	34	3	2	6		8	29	9	4	10		8	33	7	7	11	17
ΔH ₂ /ΔN	4.8	4.3	2.9	2.6	7.7		2.5	3.7	2.4	3.2	1.6		2.8	4.2	1.5	2.1	2.3	2.4
Yield (mg)	115	1072	149	120	133		434	1060	500	187	828		388	1068	636	462	656	949
Product (wt%)																		
di-H-N	0	0	0	0	0		0	0	0	0	0		0	0	0.1	0	0	0
Tetralin	44	1	63	20	47		82	36	83	62	93		84	0.5	88	81	89	89
t-Decalin	0	44	0	0	0		0	43	0.5	0	0.3		0.4	76	0.4	0.3	0.2	0.8
c-Decalin	0	49	0	0	0		0	17	0	0	0		0.1	18	0	0.1	0	0.1
R-(1-ring)	3	0	0.2	7	9		1	0	0.8	4	2		2	0	0.8	2	2	1
R-(2-ring)	2	0	0.1	3	1		0.5	0.1	0.1	2	0.3		0.4	0.1	0.2	0.4	0.4	3
R-(3*ring)	0	0	0	0	0		0	0	0	0.4	0		2	0	0.1	0	0	0
di-H-BT ³	0	0	0	1	0		0	0	0.2	5	0.1		0	0	0	0.8	0.2	0
Solid	6	1	1	11	0		1	0.2	0	0	0.1		0	0	0	0.1	0.1	0.5
Gas	46	6	35	59	43		16	5	15	28	5		12	5	10	15	9	6

¹ See footnotes of Table 1.

² Benzothiophene.

³ Dihydrobenzothiophene.

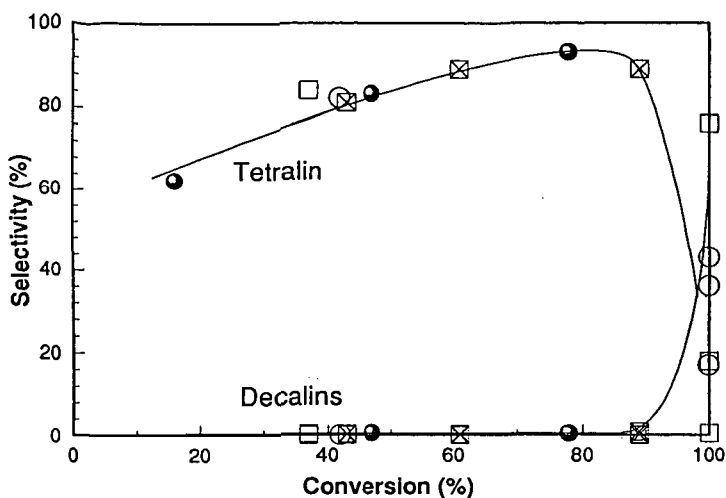


Figure 1. Selectivity to tetralin and decalins as a function of naphthalene conversion during the naphthalene hydrogenation at 473K over Pd/Al₂O₃ (○, ●) and Pd/TiO₂ (□, ⊠). Open symbols: runs with no addition of benzothiophene; filled symbols: runs with the addition of benzothiophene.

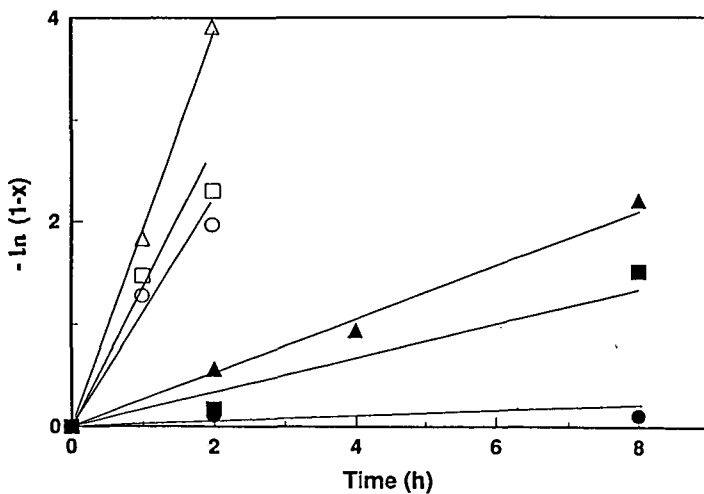


Figure 2. Pseudo-first-order plot of the naphthalene hydrogenation over Pt/Al₂O₃ (○, ●), Pd/Al₂O₃ (□, ■) and Pd/TiO₂ (△, ▲). Open symbols: runs at 553K with no addition of benzothiophene; filled symbols: runs at 473K with the addition of benzothiophene.

EFFECTS OF DISPERSED Mo CATALYSTS AND H₂O ADDITION ON HYDROGENATION AND HYDROCRACKING OF 4-(1-NAPHTHYLMETHYL)BIBENZYL

Eckhardt Schmidt* and Chunshan Song

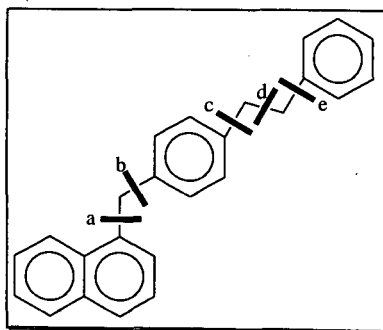
Fuel Science Program, Department of Materials Science and Engineering, 209 Academic Projects Building, The Pennsylvania State University, University Park, PA 16802

This paper reports our results on the effects of dispersed Mo catalysts and H₂O addition on hydrogenation and C-C bond hydrocracking of 4-(1-naphthylmethyl)bibenzyl, abbreviated as NMBB. Batch studies in micro reactors (initial cold H₂ pressure of 6.9 MPa) revealed that active catalysts can be generated in situ from either ammonium tetrathiomolybdate (ATTM) or Mo(CO)₆ under the reaction conditions (350 or 400 °C, 30 min) with the main catalysis of the latter for NMBB hydrogenation, but the former for C-C bond cleavage. At 350 °C hydrocracking of NMBB proceeds with ATTM, with the bond cleavage occurring at the C-C bond between naphthyl and bibenzylmethyl groups to produce naphthalene and 4-methylbibenzyl. Runs at 350 °C using Mo(CO)₆ lead to tetrahydro-NMBB-derivatives and few cleavage products. Water added to Mo(CO)₆ suppressed hydrogenation. The combination Mo(CO)₆ and S lead to almost complete conversion of NMBB. A run with Mo(CO)₆/S/H₂O gave similar results. It appears that water can increase NMBB conversion with ATTM at 350 °C but decreases conversion for runs at 400 °C.

Keywords: Model reactions, hydrocracking, dispersed catalysts, Mo-based catalysts.

INTRODUCTION

Ever since Bergius (1) demonstrated the feasibility of dispersed coal liquefaction, numerous studies have been made to make the process more cost effective. Suitable catalytic systems contain Co, Ni, Mo or its combinations (2), either as inorganic complexes, or organometallic species in a concentration of 1 wt % or lower. Good solubility of catalyst precursors generally leads to better catalyst dispersion and greater effectiveness for liquefaction reactions (3). It has been demonstrated (4) that highly dispersed catalysts from organometallic precursors can be effective for hydrogenating the coal with molecular hydrogen without relying upon a donor solvent. One way to achieve better dispersion is the use of soluble organometallic precursors which produce in situ finely dispersed active catalyst particles at elevated temperatures. Greater catalyst surface area increases the yield of products dramatically, due to greater hydrogen activation by augmented reactive catalyst sites. The beneficial effect of S on conversion has been demonstrated (5) for a variety of transition metal-based catalysts. Recent research in our group (6) has demonstrated a strong synergistic effect between a Mo sulfide catalyst and water in low severity coal liquefaction reactions. This finding seems to be contrary to conventional wisdom. Under normal liquefaction conditions, water deactivates Mo-based catalysts (7). In order to help understand the mechanism of water promoted liquefaction reactions, we also examined the effect of water on the catalytic reactions of the model compound NMBB which represents a simplified model of coal. This paper reports our work on hydrocracking experiments of NMBB over different Mo-based metal catalyst precursors. The effects of Mo-based catalyst precursors on conversion and product selectivity, as well as the influence of the sulfur and water addition and reaction temperature on the product distribution will be discussed.



Scheme 1: Potential cleavage sites in 4-(1-naphthylmethyl)bibenzyl.

EXPERIMENTAL SECTION

Preparation of Catalyst Precursors

Sulfur and ammonium tetrathiomolybdate were purchased from Aldrich, Mo(CO)₆ from Alfa and the model compound NMBB from TCI America. GC-MS confirmed sufficient purity of NMBB

(> 99 %) and it was used without further purification.

Model compound reactions

A reactor with a capacity of 33 mL was loaded with ca. 0.25 g NMBB, 1 wt % catalyst precursor (1 wt % Mo based on NMBB) and 0.14 g solvent (tridecane). When water was added, the molar ratio of H_2O to NMBB was 10, corresponding to a wt ratio of H_2O /NMBB of 0.56. The reactor was purged three times with H_2 and then pressurized with 6.9 MPa H_2 at room temperature for all experiments. A preheated fluidized sand bath was used as the heating source and the horizontal tubing bomb reactor was vertically agitated to provide mixing (about 240 strokes/min). After the reaction the hot tubing bomb was quenched in cold water. The liquid contents were washed with 15 ml $CHCl_3$ through a low speed filter paper for qualitative and quantitative GC analysis of the filtrate. All runs were carried out at least twice to confirm reproducibility. When sulfur was added, the atomic ratio of S:Mo was 4:1.

The products were identified by GC-MS using a Hewlett-Packard 5890 II GC coupled with a HP 5971A mass-selective detector operating at electron impact mode (EI, 70 eV). The column used for GC-MS was a J&W DB-17 column; 30-m X 0.25-mm, coated with 50 % phenyl 50 % methylpolysiloxane with a coating film thickness of 0.25 μm . For quantification, a HP 5890 II GC with flame ionization detector and the same type of column (DB-17) was used. Both GC and GC-MS were temperature programmed from 40 to 280 $^{\circ}C$ at a heating rate of 4 $^{\circ}C$ /min and a final holding time of 15 min. The response factors for 10 of the products were determined using pure compounds. More experimental details may be found elsewhere (8).

RESULTS AND DISCUSSION

NMBB Reaction at 350 $^{\circ}C$

Effect of Precursor Type and S Addition

Table 1 presents the results of non-catalytic and catalytic runs of NMBB with dispersed catalysts at 350 $^{\circ}C$. NMBB is essentially inert at 350 $^{\circ}C$ under H_2 pressure in a non-catalytic run. ATTM showed remarkable catalytic effect on NMBB conversion at 1 wt % Mo loading. The main products are 4-methylbiphenyl (4-MBB) and naphthalene, which were formed from cleavage of bond **a** in NMBB. It is clear that the molybdenum sulfide in situ generated from ATTM at 350 $^{\circ}C$ is catalytically active, and can promote the cleavage of C-C bond **a** in NMBB. ATTM decomposition also generates extra sulfur. However, our results in Table 1 shows that adding sulfur alone, or H_2O alone, had little effect on NMBB conversion.

The material in situ generated from $Mo(CO)_6$ at 350 $^{\circ}C$ acted as a hydrogenation catalyst. The dominant product with $Mo(CO)_6$ is tetrahydro-NMBB (TH-NMBB). Sulfur addition to $Mo(CO)_6$ increased NMBB conversion significantly, from 50.8 to 94.3 %. Adding sulfur also changed the product distribution pattern. The major products with $Mo(CO)_6 + S$ are 4-MBB and naphthalene arising from cleavage of bond **a**. The run with $Mo(CO)_6 + S$ also produced considerable amounts of biphenyl and methylnaphthalene, probably via cleavage of bond **b** in NMBB.

Figure 1 compares the product distribution for runs at 350 $^{\circ}C$. An interesting result was found in the run with $Mo(CO)_6$ at 350 $^{\circ}C$. Most of the total conversion of 50.8 % can be attributed to the formation of TH-NMBB derivatives (45.5 mol %). This finding suggests that under low severity reaction conditions the initial step in hydrocracking of NMBB is the addition of hydrogen. Several TH-NMBB derivatives (MW 326) can be detected in the GC-MS analysis, indicating hydrogenation of different aromatic moieties in the model compound. At elevated temperatures activated $Mo(CO)_6$ cleaves NMBB completely; no more TH-NMBB derivatives can be detected, as described later.

Effect of H_2O Addition

The addition of H_2O to ATTM enhanced NMBB conversion and increased the yields of 4-MBB and naphthalene. Therefore, the co-use of ATTM and water appears to be beneficial for NMBB hydrocracking at 350 $^{\circ}C$. However, adding H_2O to $Mo(CO)_6$ decreased NMBB conversion to the level close to a non-catalytic run. This indicates that added H_2O either inhibited the formation of a catalytically active phase or passivated the active sites on the surface of the active phase, or reacted to form some kind of catalytically inactive material. However, adding H_2O to $Mo(CO)_6 + S$ system did not have significant effects on NMBB conversion or product distribution.

It is interesting to note that H_2O addition to the catalytic runs with either ATTM or $Mo(CO)_6 + S$ system did not alter the product distribution pattern, suggesting that the added water did not alter the reaction pathways in these cases.

NMBB Reaction at 400 $^{\circ}C$

Table 2 shows the results for non-catalytic and catalytic runs of NMBB at 400 $^{\circ}C$. NMBB is not very reactive in a non-catalytic run at 400 $^{\circ}C$ under H_2 pressure, as its conversion is below 4 %. Sulfur, however, began to show catalytic effect when the temperature is increased from 350 to 400 $^{\circ}C$.

Both ATTM and $Mo(CO)_6$ afforded higher conversion of NMBB at 400 $^{\circ}C$ than the corresponding runs at 350 $^{\circ}C$. ATTM alone is a more effective catalyst precursor than $Mo(CO)_6$ alone, in terms of higher NMBB conversion (93.0 vs. 79.6 %). Addition of water to ATTM in the run at 400 $^{\circ}C$, however, had negative impact on NMBB conversion. These results are consistent

with those for catalytic hydroliquefaction of coal, where H_2O addition had a strong promoting effect for runs at 350 °C, but inhibiting effect for runs at 400 °C (6).

It appears from our results that water has two opposing effects on NMBB conversion at 350 and 400 °C. Possibility exists that the ratio of water to catalyst is also influential. Farcașiu et al. (9) reported that NMBB cleavage at 420-430 °C with various dried iron oxide precursors were different from rehumidified catalysts. Addition of small quantities of water increases, to some extent, the catalytic activity. Completely rehumidified iron oxides showed very low catalytic activity compared to partially hydrated iron oxide. The activity of the system as an acidic catalyst is destroyed by larger amounts of water (longer rehumidification time).

Figure 2 further compares the product distribution for runs at 400 °C. For the runs with ATTM and $ATTM+H_2O$, 4-MBB and naphthalene are the major products. In the case of $Mo(CO)_6$, the yield of tetralin is higher than that of naphthalene. Apparently, the activity and selectivity of a dispersed Mo catalyst for NMBB hydrocracking depends on the catalyst precursor type and reaction conditions. Since it is the precursor that was charged into the reactor, an activation into catalyst is involved during the heat up and the subsequent reaction.

It is known (3,5,10) that the S-free catalyst precursors like metal carbonyls require the addition of sulfur for sufficient activity in coal liquefaction; activation of ATTM into the catalytically active species (close in composition to MoS_2) occurs at a temperature of 325-350 °C. This temperature range was used in our model reactions. Sulfur addition to $Mo(CO)_6$ generates MoS_2 after high temperature activation. The resulting product distribution at 350 °C is very similar to runs with ATTM (Table 1). We assume that the active catalytic species is similar to that from ATTM. Unlike ATTM, the organometallic complex $Mo(CO)_6$ decomposes at much lower temperatures. The active catalyst particles will be readily available under the conditions employed. This may rationalize why the NMBB conversion is higher with $Mo(CO)_6$ than with ATTM at 350 °C. However, for runs at 400 °C, the NMBB conversions with ATTM and $Mo(CO)_6$ are similar to each other (8).

With respect to the effect of the catalyst loading level, we have reported some results on NMBB hydrocracking over dispersed catalysts at 2.11 wt % metal loading (8). Decreasing Mo loading level from 2.11 wt % to 1 wt % (this work) did not have negative impacts on NMBB conversion with ATTM, but caused some changes in product distribution from NMBB with $Mo(CO)_6$.

CONCLUSIONS

Dispersed fine particles in situ generated from either water-soluble precursors such as ATTM or oil-soluble precursors such as $Mo(CO)_6$, can be effective Mo catalysts for promoting the cleavage of certain C-C bonds such as bond a in NMBB at 350-400 °C. When the sulfur-free precursor is used, adding sulfur helps to improve catalytic activity, particularly hydrocracking activity. When ATTM is used at low temperature (350 °C), adding water seems to be beneficial in improving NMBB conversion.

ACKNOWLEDGMENTS

We wish to thank Dr. H. Schobert for his encouragement and support. This project was supported by the U.S. Department of Energy, Pittsburgh Energy Technology Center under contract DE-AC22-92PC92122. We are grateful to Dr. U. Rao of PETC for his support. We also thank Mr. R. Copenhagen for the fabrication of reactors.

REFERENCES

1. Bergius, F. and Billiviller, J. *German Patent No. 301.231*, Coal Liquefaction Process, 1919.
2. Mochida, I. and Sakamishi, K. *Advances in Catalysis*, **40**, 1994, 39-85.
3. a) Artok, L.; Davis, A.; Mitchell, G. D. and Schobert, H. H. *Energy & Fuels*, **1993**, *7*, 67-77.
4. b) Garg, D. and Givens, E. N. *Fuel Process. Technol.*, **8**, 1984, 123-34.
5. a) Hirschon, A. S.; Wilson Jr., R. B. *Coal Science II*, ACS Sym. Ser., **1991**, 273-83.
6. b) Hirschon, A. S.; Wilson Jr., R. B. *Fuel*, **71**, 1992, 1025-31.
7. a) O. Yamada, T. Suzuki, J. Then, T. Ando and Y. Watanabe, *Fuel Process. Technol.*, **11**, 1985, 297-311.
8. b) T. Suzuki, T. Ando and Y. Watanabe, *Energy & Fuels*, **1**, 1987, 299-300.
9. c) S. Weller, *Energy Fuels*, **8**, 1994, 415-420.
10. Song, C. and Saini, A. K. *Energy & Fuels*, **9**, 1995, 188-9.
11. a) Bockrath, B. C.; Finseth, D. H. and Illig, E. G. *Fuel Process. Technol.*, **12**, 1986, 175.
12. b) Ruether, J. A.; Mima, J. A.; Koronsky, R. M. and Ha, B. C. *Energy & Fuels*, **1**, 1987, 198.
13. c) Kamiya, Y.; Nobusawa, T. and Futamura, S. *Fuel Process. Technol.*, **18**, 1988, 1.
14. a) Schmidt, E. and Song, C. *Prepr. Pap. - Am. Chem. Soc., Div. Fuel Chem.*, **35**, 1994, 733-737.

- b) Song, C.; Schmidt, E. and Schobert, H. H. *DOE Coal Liquefaction and Gas Conversion, Contractors' Review Meeting in Pittsburgh*, (September 7-8, 1994), 593-604.
9. Farcasiu, M.; Smith, C.; Pradhan, V. R. and Wender, I. *Fuel Processing Technology*, **29**, 1991, 199-208.
10. a) Song, C., Parfitt, D.S.; and Schobert, H.H., *Energy & Fuels*, **8**, 1994, 313-9.
 a) Song, C.; Nomura, M. and Miyake *Fuel*, **65**, 1986, 922-6.
 c) Song, C.; Nomura, M. and Ono, T. *Prepr. Pap. - Am. Chem. Soc. Div. Fuel Chem.*, **36(2)**, 1991, 586-96.

Table 1: Effect of S and H₂O on hydrocracking of NMBB at 350 °C.

Experiment #	105	95	107-1/ 109-1	94/96/ 108/110	97	98	100	102
Catalyst Precursors*	S [1.4 wt %]	H ₂ O	ATTM	ATTM+ H ₂ O	Mo(CO) ₆	Mo(CO) ₆ + H ₂ O	Mo(CO) ₆ +S	Mo(CO) ₆ +S+H ₂ O
Products [mol %]								
Tetralin			6.6	8.0	3.5		20.6	13.5
Naphthalene	4.4	2.4	25.6	40.0	1.6	1.5	55.4	58.8
2-MTHN ^a				0.1			1.4	0.8
1-MTHN			0.4	0.6			1.7	1.1
2-Methylnaphthalene				0.16			1.9	1.4
1-Methylnaphthalene			1.7	2.9			5.7	5.8
Bibenzyl	0.2		4.7	6.5	0.5		21.2	15.8
4-Methylbibenzyl	3.7	1.9	33.2	50.2	3.8	1.1	74	71.1
TH-NMBB		1.6	5.8	5.3	45.5		2.1	3.1
Conversion [wt %]	4.1	3.7	42.4	60.0	50.8	1.3	94.3	88.2

^aMethyltetrahydronaphthalene. *when S was added, the atomic ratio S:Mo was 4:1.

Table 2: Effect of Mo-based catalyst precursors on hydrocracking reactions of NMBB at 400 °C.

Experiment #	21	78	91	92	106
Catalyst Precursors*	Non-catalytic run	S [1.2 wt %]	ATTM	ATTM+H ₂ O	Mo(CO) ₆
Products [mol %]					
Toluene	0.3	1.4	4.2	3.9	1.5
Tetralin	0.2	0.8	21.8	6.8	49.5
Naphthalene	0.6	24.8	58.1	42.9	10.5
2-MTHN ^a			0.7	0.6	1.2
1-MTHN			1.7	0.5	5.2
2-Methylnaphthalene			1.0	1.3	
1-Methylnaphthalene		1.7	6.8	5.6	0.9
Bibenzyl		2.4	14.5	11.1	12.7
4-Methylbibenzyl	1.3	22.1	77.3	53.1	58.5
Conversion [wt %]	3.9	26.1	93.0	63.2	79.6

^aMethyltetrahydronaphthalene, *when S was added, the atomic ratio S:Mo was 4:1.

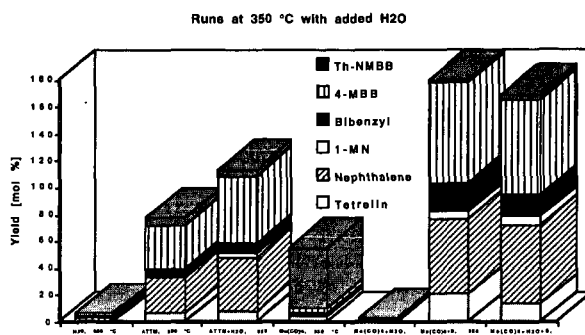


Figure 1. Effect of S and water on hydrocracking of NMBB.

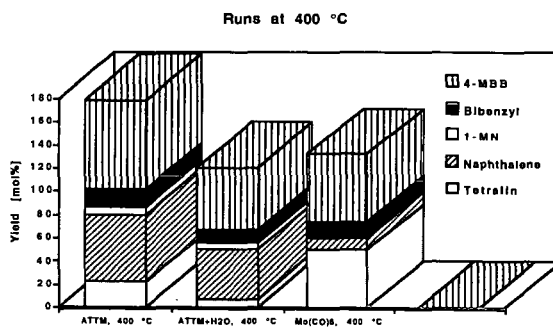


Figure 2: Effect of Mo-based catalysts on hydrocracking of NMBB.

CATALYTIC CONVERSION OF POLYCYCLIC AROMATIC HYDROCARBONS:
MECHANISTIC INVESTIGATIONS OF HYDROGEN TRANSFER FROM AN IRON-
BASED CATALYST TO ALKYLARENES.

Tom Autrey, John C Linehan, Donald M Camaioni, Tess R Powers,
Eric F McMillan and James A Franz

Pacific Northwest Laboratory, P.O. Box 999, Richland, WA 99352 USA

Key Words. Catalysis, mechanism, hydrogen transfer

Introduction.

The utility of iron-based nanophase catalysts in the liquefaction of coal and coal model compounds has been demonstrated to increase the efficiency of liquefaction during the early stages of catalytic coal hydrotreatment.¹ Despite numerous model compound studies, the mechanism of "liquefaction" remains controversial. Wei and coworkers²⁻⁵ proposed a hydrogen atom - ipso displacement pathway, however, this pathway alone cannot explain the observed selectivity.⁶ Farcasiu and co-workers⁷ proposed a mechanism in which the alkyl-arene moiety is activated to undergo bond scission by electron transfer to the catalyst. However, a key step in this pathway, unimolecular scission of the radical cation, has been argued to be kinetically and thermodynamically unfavorable.⁸

We recently reported a beneficial characteristic of the Fe/S catalysts, generated in situ by the reaction of sulfur with iron oxyhydroxides produced by the RTDS process: *scission of strong carbon-carbon bonds without addition of hydrogen gas and with minimum formation of light gases.*^{6,9} We investigated a series of mono-, di-, and trimethyldiphenylmethanes and found that in all cases the benzyl group is preferentially displaced. We proposed a variant of the Farcasiu mechanism⁷ in which a hydrogen atom is transferred to the ipso position of the radical cation, which then scissions a benzyl cation. Back electron transfer from the reduced catalyst surface to the benzyl cation would give the benzyl radical.⁶ We refer to this radical ion mechanism as "ET/HT". The mechanism is consistent with (1) the proposed redox properties of the catalyst,⁷ (2) the observed "dealkylation" selectivity, benzyl >> methyl, and (3) the low yield of transalkylation products.

Recent examination of the structure - reactivity relationships for the methylated diphenylmethanes shows the rate of catalytic-induced bond scission correlates not only with the ease of arene oxidation but also correlates with the stability of the ipso radical adduct.¹⁰ To accommodate the observed selectivity for benzyl scission >> methyl scission by a radical pathway, we proposed a reversible hydrogen atom transfer between the catalyst surface and the arenes, in which case, the rate of back hydrogen transfer from the ipso and nonipso adducts must be fast compared to scission of methyl radical.

In the present study, we designed and prepared model compounds to differentiate between the ET/HT radical ion pathway and the reversible hydrogen atom transfer pathway.

Experimental.

Materials. All catalytic experiments used the RTDS-prepared, 6-line ferrihydrite catalyst precursor.¹¹ 9,10-dihydrophenanthrene (DHP), xanthene, and *o*-hydroxydiphenylmethane were purchased from Aldrich. The DHP was distilled and recrystallized from methanol/dichloromethane. 1,2-ditolyethanol was available from a previous study.¹² *o*- and *p*-benzylidiphenyl ether were prepared by the same method used for our synthesis of the alkylidiphenylmethanes.¹³ The isomers were separated on a Chromatotron® eluting with pentane.

Thermolysis Studies. The model compound (15 mg), the 6-line ferrihydrite (3 mg), the sulfur (3 mg), and the DHP solvent (100 mg) were loaded into the glass tubes and sealed under vacuum. The thermolysis was carried out in sealed 5-mm o.d. borosilicate glass tubes immersed in a fluidized sand bath regulated at 400°C for 1 h. The GC and GC/MS analysis were carried out as described previously.¹¹

Results and Discussion.

Given the parallel structure - reactivity trends for ion, radical, and radical-ion intermediates in the alkylarene series previously examined, we prepared a new series of model compounds to discriminate between the ion, radical, and radical ion hydrogen transfer pathways. A comparison of diphenyl ether analogs with our diphenylmethane model compounds was suggested as an approach to obtain insight into the proposed multi-step ET/HA transfer step or a free radical pathway.¹⁴ The cation formed by ipso addition of H-atom to the radical cation of diphenyl ether (DPE) was suggested to be more resistant to bond scission than the analogous cation obtained from diphenylmethane (DPM) because of the differences in the stability of the leaving group, $\text{PhO}^+ \ll \text{PhCH}_2^+$, while the

opposite selectivity was predicted for a radical pathway, $\text{PhO}\cdot > \text{PhCH}_2\cdot$. Unfortunately, while the β -scission of a phenoxy cation from DPE is expected to be significantly slower than the β -scission of a benzyl cation from DPM the first step, oxidation of the DPE, is faster than oxidation of DPM.¹⁵ Thus, an "external" comparison of DPM and DPE derivatives could complicate direct kinetic comparisons. To alleviate this concern, we used model compounds that had both the $\text{PhO}\cdot$ and $\text{PhCH}_2\cdot$ substituents in a single molecule — xanthone (XA), *p*-benzylbiphenyl ether (pBDPE), and *o*-benzylbiphenyl ether (oBDPE). This approach avoids complications caused by differences in oxidation potential of diphenylmethane and diphenyl ether and takes advantage of the selectivity differences between scission of $\text{PhO}\cdot$ and $\text{PhCH}_2\cdot$.¹⁶ Thus, the appearance of PhCH_2Ph would be consistent with a carbon-oxygen ($\text{PhCH}_2\text{Ph-OPh}$) free radical bond scission pathway, and the appearance of PhOPh would be consistent with an apparent carbon-carbon ($\text{PhCH}_2\text{-PhOPh}$) cationic bond scission pathway.

Thermolysis of pBDPE in DHP- Fe/S at 400 °C leads to ca. 70% consumption of the starting material in 60 minutes with the formation of DPM, DPE, toluene and phenol. The ratio of DPM/DPE (i.e. carbon-oxygen/carbon-carbon bond scission) is 8:1.

This result offers significant insight into the mechanism of catalytic-induced bond scission. The selectivity of the 8:1 ratio for scission of benzyl over phenoxy radical from pBDPE is significantly less than expected for β -scission of $\text{PhCH}_2(+)$ over $\text{PhO}(+)$.¹⁷ Therefore, we have considerably less confidence with the involvement of a cationic intermediate formed either by acidic proton transfer or multi-step ET/HA pathways for promoting bond scission. What is interesting about these results is that the selectivity is the opposite of the relative stabilities of the benzyl and phenoxy radicals. Therefore, bond cleavage must not be the rate-limiting step for reaction of this molecule. The selectivity is consistent with rate-limiting formation of the ipso adducts. The stability of the ipso adduct, (a), leading to formation of DPE and the benzyl radical is 3±2 kcal/mol¹⁸ more stable than the ipso adduct, (b), leading to formation of DPM and the phenoxy radical (Scheme 1).

Thermolysis of oBDPE under the same reaction conditions again yields DPM, DPE, toluene and phenol, however, the ratio of DPM/DPE is 1:1. The apparent lower selectivity observed from the catalytic thermolysis of oBDPE could be due to a competing neophyl-like phenyl migration, 1,5 addition, in Scheme 2. These $\text{Ar}_1\text{-5}$ radical rearrangements are known to occur,¹⁹ especially when heteroatom termini are involved.^{20,21} Tautomerization of the phenol, followed by unimolecular scission,²² can yield diphenylmethane by an alternative pathway. The expected side product from this radical rearrangement pathway, 9-phenylxanthene — formed from addition of the diphenylmethyl radical to the *ortho*-position, 1,6 addition, followed by disproportionation—is detected in the thermolysis of oBDPE. This provides further evidence for the presence of the precursor to the neophyl rearrangement pathway under the reaction conditions.²³

Thermolysis of xanthene under the same catalytic reaction conditions yields little bond scission after 60 minutes, no detectable 2-methyldiphenyl ether, and only traces of 2-bond scission products, toluene and phenol. Here, the absence of significant quantities of scission products in the xanthene thermolysis is probably due to competing reversible reactions that regenerate the starting material. Because the leaving group is "attached," little bond scission is observed.

Unimolecular Scission of Radical Ions. Early mechanistic studies demonstrated the preference for catalytic-induced scission of diarylmethane linkages over the thermally labile bibenzyl linkages in 4-(1-naphthylmethyl)biphenyl (NMBB). Farcasiu and coworkers invoked single electron oxidation of the arene followed by a unimolecular scission to yield naphthalene and 4-methylbiphenyl (referred to as -A- bond cleavage).⁷ However, the observed selectivity is the opposite of that expected based on reactions in solution or reactions in the gas phase based upon fragmentation reactions of the NMBB radical cation in a mass spectrometer.⁸ Almost as surprising as radical cation cleavage at the diarylmethane -A- bond is the suggestion that the positive charge is carried on the naphthyl group,²⁴ not the benzyl group, given the difference between stabilization of benzylic cation and a benzylic radical. To favor -A- bond scission over -D- bond scission, the catalyst must uniquely stabilize the naphthyl cation and/or destabilize the benzyl cation. This novel unimolecular scission pathway is reported to be supported by atom superposition and electron delocalization molecular orbital (ASED-MO) methods, however, AM1 and MNDO theoretical methods indicate cleavage of the -D- bond is favored.²⁵

NMBB probably is not the best model compound to test the unimolecular radical cation dissociation mechanism. Although the bond dissociation energy (BDE) for biphenyl radical cation, at about 30 kcal/mol, is substantially weaker than the bibenzyl bond, we expect that -D- bond scission in the NMBB radical cation will be a minimum of 40 kcal/mol, given that oxidation of 1-methylnaphthalene is ca. 10 kcal/mol more favorable than oxidation of *p*-xylene, and conservatively assuming no barrier for the ET process that

generates the radical cation. A barrier of this magnitude probably cannot compete with bimolecular reactions of the radical cation or alternative free radical pathways, Scheme 3. A more judicious choice of model compounds, for example one with a much lower radical cation BDE, could provide support for the proposed electron transfer pathway if the bond were broken more rapidly than purely thermal pathways allow.

We used 1,2-*p*-ditolyethanol (DTE) as a probe for the electron transfer mechanism. Diphenylethanol radical cation has a BDE of 15 kcal/mol and therefore is expected to dissociate ca. 8 orders of magnitude faster than the NMBB radical cation at 400°C, and will be more likely to compete with other pathways. Thermolysis of DTE in DHP for 60 minutes at 400°C results in ca. 50% conversion to yield 4,4'-*p*-dimethylbibenzyl, *p*-xylene, 4-methylbenzylalcohol, 4-methylbenzaldehyde and a trace of toluene. The ratio of toluene to *p*-xylene is 1:25. The 4,4'-*p*-dimethylbibenzyl is formed by a reduction pathway that competes with unimolecular scission. Since the 4,4'-*p*-dimethylbibenzyl is thermally stable under the reaction conditions, the xylene is predominately formed from unimolecular thermal scission of the starting material.

Thermolysis of DTE in DHP containing the Fe/S catalyst for 60 minutes at 400°C results in complete conversion to yield 4,4'-*p*-dimethylbibenzyl, *p*-xylene, and toluene. The *p*-xylene is most likely formed from the thermal background and reduction of the alcohol and aldehyde since no oxygen-containing products are detected. The most significant finding is the ratio of toluene to *p*-xylene has increased to 1:1. The presence of the Fe/S catalyst pathway apparently increases the yield of toluene! Toluene is not a product expected from single electron oxidation of the diphenylethanol.¹² The formation of toluene under the catalytic conditions is more rationally explained by an ipso hydrogen displacement pathway. Hydrogen atom addition to the phenyl ring α - to the hydroxy group leads to the β -scission of a stabilized ketyl radical. As we have previously observed efficiency of bond scission is strongly dependent on the stability leaving group.¹⁰

If the radical cation of DTE was formed under the reaction conditions, instantaneous unimolecular scission of the bibenzyl bond would have occurred to yield *p*-xylene as the major product. While we are convinced DTE is an improved probe molecule for investigating the radical ion pathway, we would like to investigate better models, e.g. the methyl ether of DTE, that are not expected to be reduced under the reaction conditions. We are confident that electron transfer from the alkylarene to the catalytic surface does not occur, otherwise we would have observed much higher yields of xylene. Admittedly, oxidation of this xylene derivative will be more endergonic than oxidation of the naphthyl moiety in NMBB, however, the selective catalytic pathways seem to operate even for single ring model compounds.^{6,9} We cannot guess what the ASSED-MO methods would find for single electron transfer cleavage pathways of DTE, but experiments¹² and AM1 calculations²⁶ suggest highly efficient bibenzyl bond scission.

Summary and Conclusions.

The results of our model compound studies suggest that free radical hydrogen transfer pathways from the catalyst to the alkylarene are responsible for the scission of strong carbon-carbon bonds. There are two requisites for the observed selective bond scission. First, and most importantly is the stability of the ipso adduct precursor leading to displacement, the more stable the adduct the more probable bond scission. This explains why benzyl radical displacement > phenoxy radical displacement in benzyldiphenyl ether and explains why $\text{PhCH}_2\text{CH}_2\text{PhCH}_2$ radical > naphthylmethyl radical from NMBB. Second, given "equal" ipso adduct precursor stabilities, e.g. methylphenylmethane, the stability of the departing radical determines the selectivity. This explains benzyl radical > methyl radical in the methylated diphenylmethanes and explains why α -hydroxyphenethyl radical > methyl radical in 1,2-ditolyethanol.

We have assumed little physical interaction between the molecules and the catalytic surface and have been able to satisfactorily explain most of the observed selectivity. However, for NMBB we expect a higher selectivity for -A- bond scission relative to -B- bond scission, given the ca. 6 kcal/mol difference between the radical adduct formed by the hydrogen atom addition to 1-methylnaphthalene and *p*-xylene. It is possible that physical properties play a role in lowering the selectivity in NMBB bond scission. Also, we realize that catalysts prepared by other methods may contain different activity sites and operate by different mechanisms.

Acknowledgment

This work was supported by the U.S. Department of Energy, Office of Basic Energy Research, Chemical Sciences Division, Process and Techniques Branch. The work was conducted at Pacific Northwest Laboratory, which is operated by Battelle Memorial Institute for the U. S. Department of Energy under Contract DE-AC06-76RL0 1830. We thank Dean Matson for our supply of the world's best catalytic precursors. Support for TRP and EFM was provided through AWU-NW under grant DE-FG06-89ER-75522 with the U.S. Department of Energy.

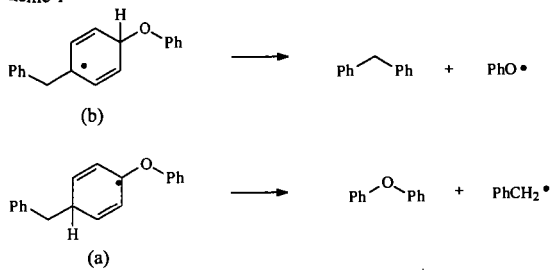
Glossary of Acronyms.

BDE	bond dissociation energy
RTDS	Rapid Thermal Decomposition of Precursors in Solution
DHP	9,10-dihydrophenanthrene
pBDPE	p-benzylidiphenyl ether
oBDPE	o-benzylidiphenyl ether
DPM	diphenylmethane
DPE	diphenyl ether
DTE	1,2-ditolylethanol
NMBB	4-(1-naphthylmethyl)bibenzyl

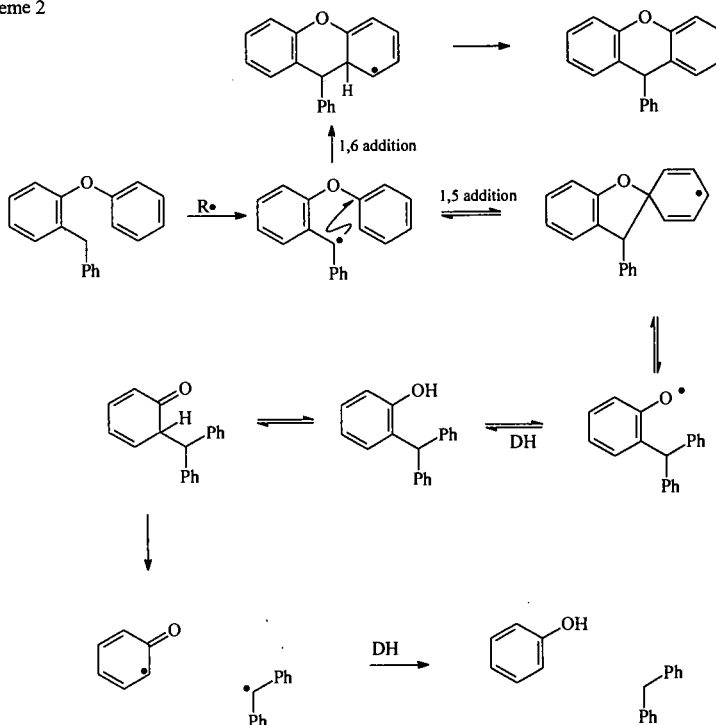
References and Notes.

1. See the first 21 papers in *Energy & Fuels*, **1994**, 1, and references therein.
2. Wei, X-Y, Ogata, E., Niki, E., *Bull. Chem. Soc. Jpn.*, **1992**, 65, 1114.
3. Wei, X-Y, Ogata, E., Niki, E., *Chemistry Letters*, **1991**, 2199.
4. Wei, X-Y, Ogata, E., Zong, Z-M., Niki, E. *Energy Fuels* **1992**, 6, 868.
5. Wei, X-Y, Zong, Z-M., *Energy Fuels* **1992**, 6, 236.
6. Franz, J.A.; Camaioni, D. M.; Alnajjar, M. S.; Autrey, T.; Linehan, J. C. *Am Chem Soc, Div Fuel Chem. Preprints*, **1995**, 40(2) 203. Anaheim, CA.
7. Farcasiu, M.; Smith, C.; Pradhan, V. R.; Wender, I. *Fuel Proc. Tech.* **1991**, 29, 199.
8. Penn, J. H.; Wang, J-h. *Energy Fuels* **1994**, 8, 421.
9. Linehan, J. C.; Matson, D. W.; Darab, J. G.; Autrey, S. T.; Franz, J. A.; Camaioni, D. M. *Am Chem Soc, Div Fuel Chem. Preprints*, **1994**, 39(3) 720. Washington D. C.
10. Autrey, T.; Camaioni, D. M.; Linehan, J. C.; Wartob, H. W.; Franz, J. A. in preparation. To be submitted to *Energy Fuels*.
11. Matson, D. W.; Linehan, J. C.; Darab, J. G.; Buehler, M. F. *Energy Fuels* **1994**, 8, 10.
12. Camaioni, D. M.; Franz, J. A. *J. Org. Chem.* **1984**, 49, 1607.
13. See reference 9 for general preparation. A few drops of sulfuric acid was added to a solution of diphenylether and benzyl alcohol in methylene chloride. The reaction was stirred at room temperature for 24 h. Distillation under vacuum yielded both the ortho and para isomers.
14. McMillen, D. M.; Malhotra, R. *Am Chem Soc, Div Fuel Chem. Preprints*, **1995**, 40(2) 221. Anaheim, CA.
15. IP of DPE (8.09eV) DPM (8.55eV) Lias, S. G.; Bartmass, J. E.; Liebman, J. L.; Holmes, J. L.; Levin, R. D.; Mallard, W. G. *J Chem. Phys. Ref. Data*, **1988**, 17, suppl.
16. * designates either radical or radical ion.
17. Personal communication with Ripu Malhotra; the difference in appearance potential for oxidation of $\text{PhO} \cdot \rightarrow \text{PhO}^+(\cdot)$ and $\text{PhCH}_2 \cdot \rightarrow \text{PhCH}_2^+(\cdot)$ is ca. 34 kcal/mol. Assuming a ΔBDE PhO-H and $\text{PhCH}_2\text{-H}$ of 3-4 kcal/mol this predicts a selectivity of several orders of magnitude even at 400°C.
18. McMillen, D. F.; Golden, D. M. *Ann. Rev. Phys. Chem.*, **1982**, 33, 493.
19. Winstein, S.; Heck, R.; Lapporte, S.; Baird, R. *Experientia*, **1956**, 12, 138.
20. Kochi, J. K.; Gilliom, R. D. *J. Am. Chem. Soc.* **1964**, 86, 5251.
21. DeTar, D. F.; Hlynsky, A. J. *Am. Chem. Soc.* **1955**, 77, 4411.
22. McMillen, D. F.; Ogier, W. C.; Ross, D. S. *J. Org. Chem.* **1981**, 46, 3322.
23. Thermolysis of o-bismethyldiphenyl ether appears to give o-xylene under the catalytic conditions. This product can only come from a Ar₁-CS neophyl rearrangement.
24. Fragmentation of NMBB by 70 eV electron impact in a mass spectrometer leads to a fragmentation pattern that has the charge on the -D- bond scission products, no charge is detectable on the naphthalene fragment: MS m/z 322 (M⁺, 50); 231(100); 215 (40); 127 (0); 91 (15).
25. Ades, H. F.; Companion, A. L. Subbaswamy, K. R. *Energy Fuels* **1994**, 8, 71.
26. Camaioni, D. M. *J. Am. Chem. Soc.* **1990**, 112, 9475.

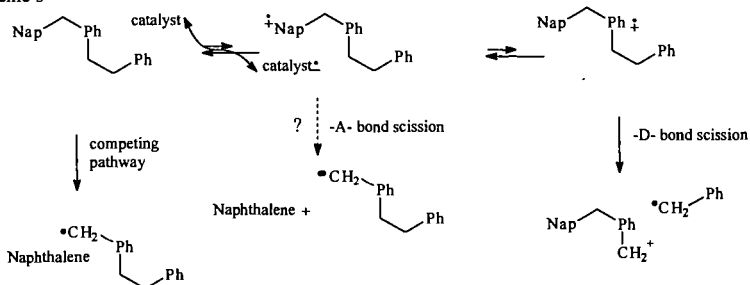
Scheme 1



Scheme 2



Scheme 3



EFFECT OF MODIFIER Pd METAL ON HYDROCRACKING OF POLYAROMATIC COMPOUNDS OVER Ni-LOADED Y-TYPE ZEOLITE AND ITS APPLICATION AS HYDRODESULFURIZATION CATALYSTS

Takema Wada, Satoru Murata, and Masakatsu Nomura,
Department of Applied Chemistry, Faculty of Engineering, Osaka University,
2-1 Yamada-oka, Suita, Osaka 565, Japan

Keywords: hydrocracking, hydrodesulfurization, metal-supported zeolite catalyst

INTRODUCTION

Coal tar obtained from coal carbonization is a treasure of polyaromatic hydrocarbons, where more than 400 kinds of aromatic compounds are found to be contained. Naphthalene's content in coal tar is about 9.0 %, being used as starting materials for phthalic anhydride, dye stuff, pharmaceutical products and synthetic resins. On the other hands, phenanthrene and pyrene are contained in the yield of 5.0 % and 2.1 %, respectively, being used only for production of carbon black and antiseptics of timbers. Application of these three or four ring aromatic compounds for starting materials of fine chemicals is not yet developed so extensively. The development of new catalysts being able to convert these aromatics into mono or diaromatic compounds is one of objectives for utilization of polyaromatics. Hydrocracking of polyaromatic compounds is believed to proceed via formation of terminal-naphthenic ring of starting aromatic compounds, followed by cleavage of the naphthenic ring to produce alkylated aromatic compounds which has less numbers of ring than starting aromatics. Accordingly, hydrogenation of aromatic rings and cracking of resulting naphthenic rings are key steps of hydrocracking reaction, so that dual functional catalysts such as metal-supported acid catalysts are considered to be one of the best catalysts.^{1,2} Zeolite has controlled pore structures and strong acidity enough to crack naphthenic rings, being characteristics in exchanging metal species with ease. We have been studying the hydrocracking of polyaromatic compounds over Ni-loaded zeolite catalysts (ZSM-5, mordenite, and Y-type) and found the fact that pore size of zeolite exerts an interesting effect on product distribution.³ We also conducted computer-simulation for diffusion phenomena of the polyaromatic hydrocarbons in the pore of these zeolites and found that diffusion ability of the substrate affects strongly the product distribution.⁴ Recently we found that modifying of Ni-loaded Y-type zeolite by Pd-loading enhanced hydrocracking ability of the catalyst. In this report, we would like to refer to the results of both hydrocracking reaction of pyrene and hydrodesulfurization of dibenzothiophene using Pd-modified Ni-loaded Y-type zeolite.

Experimental Section

Preparation of metal-supported zeolites

The NH_4 -substituted Y-type zeolite (50 g) was stirred in 1000 ml of aqueous solution of $\text{Ni}(\text{NO}_3)_2$ (0.25 M) at 90 °C for 96 h, then being filtered and dried at 110 °C to obtain the nickel cation substituted zeolites. As to the Pd supported one, NH_4 -substituted Y-type zeolite (15 g) was treated in aqueous solution (200 ml) of $[\text{Pd}(\text{NH}_3)_4](\text{NO}_3)_2$ (0.025 M) at 40 °C for 24 h. As to Ni-Pd-Y catalysts, NH_4 -substituted Y-type zeolite was treated with aqueous $[\text{Pd}(\text{NH}_3)_4](\text{NO}_3)_2$ solution, followed by aqueous $\text{Ni}(\text{NO}_3)_2$ solution. The resulting cation exchanged zeolites were calcined in a stream of air at 500 °C for 4 h, being submitted to the reduction with H_2 atmosphere at 450 °C for 1 h. The content of nickel and palladium in each zeolite was determined by using a Rigaku Denki System 3270 type fluorescence X-ray analyzer, this being summarized in Table 1.

Hydrotreatment of pyrene or dibenzothiophene

The substrate (1 g) and the catalyst (0.5 g) were placed in a 70 ml SUS 316 autoclave, which were pressurized to 70 kg/cm² with hydrogen, being followed by heating up to 350 °C with the rate of 8 °C / min. Reaction time is the duration being kept at 350 °C. After the gaseous product was collected, its aliquot was submitted to GC analysis with a Shimadzu GC-3BT (active carbon column, 2 m) and a Shimadzu GC-8AIT (silica gel column, 60/80 mesh, 3 m). The liquid product was recovered by washing the inside of the autoclave with CH_2Cl_2 . According to the analysis by a JEOL JMS-DX-303HF type GC-MS, components of liquid products were assigned, their quantitative analyses being conducted by a Shimadzu GC-14APFSC (CBP-1 capillary column, f 0.5 mm x 25 m). The carbon deposited on the catalyst was calculated based on the microanalysis of the recovered catalyst.

Results and Discussion

Hydrocracking reaction of pyrene

In a previous study, we conducted hydrocracking reaction of phenanthrene and pyrene over three

different Ni-supported zeolite catalysts such as Ni-loaded ZSM-5, mordenite, and Y-type zeolite at 350 °C for 1 h at 70 kg/cm² of hydrogen and found that pore size of zeolites is controlling product distribution. Conversion of the substrates depended also on the size of these zeolites. By the use of Ni-loaded Y-type zeolite (Ni-Y) catalyst, phenanthrene was completely converted to gases and one- or two-ring compounds, while in the case of pyrene both hydrogenated pyrene and unreacted one still remained in the product. This results could be interpreted by the fact that the pore size of Y-type zeolite is larger than the molecular size of phenanthrene, however, it is somewhat smaller than that of pyrene. In order to improve the activity of Ni-Y catalyst, we examined modifying of Ni-Y catalyst by loading second metal species.

We prepared Pd-modified Ni-Y (Ni-Pd-Y) catalyst by ion exchange of NH₄-substituted Y-type zeolite with aqueous [Pd(NH₃)₄]²⁺ solution followed by Ni²⁺ solution. Concentration of metal species on the resulting zeolite is summarized in Table 1. To examine catalytic activity of Pd metal itself, we also prepared Pd-loaded Y-type (Pd-Y) zeolite. Using these three catalysts, hydrocracking of pyrene was conducted in a 70 mL autoclave at 350 °C for 1 h at 70 kg/cm² of hydrogen, the results being shown in Figure 1. In the presence of Pd-Y or Ni-Pd-Y catalyst, pyrene was completely converted to gases (from methane to butane) and derivatives of benzene or cyclohexane, especially in the case using Ni-Pd-Y catalyst, yield of gases reached to 70%. Amounts of carbon deposited on the catalyst were 9.1% for Ni-Y, 9.6% for Pd-Y, and 7.0% for Ni-Pd-Y catalyst. Figure 2 summarizes the distribution of mono-ring compounds produced from hydrocracking of pyrene over three catalysts. In the case using Ni-Y catalyst, the selective formation of each compound was not observed, while, the yield of cyclohexanes was higher than that of benzenes in the case using Pd-Y and Ni-Pd-Y catalysts. No C₇- and C₈-benzenes and C₇-cyclohexanes was observed in products obtained from the reaction using Ni-Pd-Y catalyst. These results indicated that activity of Ni-Pd-Y catalyst toward hydrogenation and cracking reaction is the highest among three catalysts. This finding agrees well with the fact that the ratio of *i*-butane to *n*-butane (2.1) of gaseous products in the reaction using Ni-Pd-Y catalyst was slightly higher than that (1.8) from the reaction using Ni-Y catalyst. This higher activity of Ni-Pd-Y catalyst might be partly due to the decrease of carbon deposited on the catalyst, this often leading to deactivation of the catalyst.

Effects of reaction temperature and duration on the extent of hydrocracking were also investigated, the results being shown in Figure 3. In the reaction at 350 °C for 0 min, 25% of pyrene was still remained and main products were hydrogenated pyrenes (60%). With the reaction time being longer than 30 min, no pyrene was recovered and gases and mono-ring compounds became main products. In the reaction at lower temperature such as 325 °C, conversion of pyrene was still higher than that in the reaction using Ni-Y catalyst at 350 °C. These results suggested that modifying of Ni-Y catalyst by Pd can reduce the reaction temperature of hydrocracking of pyrene compared with Ni-Y catalyst.

Hydrosulfurization of dibenzothiophene

In a previous chapter, we found that modifying of Ni-Y catalyst by Pd-loading resulted in very high activity for hydrogenation or hydrocracking of polyaromatic hydrocarbons. So, we tried to apply this modified catalyst for hydrosulfurization (HDS) of dibenzothiophene (DBT). HDS reaction of DBT was conducted at 300 °C for 1 h under 70 kg/cm² of H₂. Figure 4 shows the product distribution of HDS reaction by using Ni-Y and Ni-Pd-Y catalysts. In the case using Ni-Y catalyst, 15% of DBT was recovered along with 12% yield of sulfur-containing compounds, while, using Ni-Pd-Y catalyst, DBT was almost converted to gases and monoring compounds and no sulfur-containing compound was observed in the liquid products. These results suggest that high activity of Ni-Pd-Y catalyst is much more effective for HDS reaction. Now, we are conducting characterization of this active catalyst.

This work was supported by Grant-in-Aid for Scientific Research No. 07242249 from the Ministry of Education, Science and Culture, Japan.

4. REFERENCES

- 1) Hayes Jr., H. W.; Parcher, J. F.; Halmer, N. E. *Ind. Eng. Chem. Process Des. Dev.*, **1983**, 22, 401.
- 2) Lapinas, A. T.; Klein, M. T.; Gates, B. C.; Macris, A.; Lyons, J. E. *Ind. Eng. Chem. Res.*, **1987**, 26, 1026.
- 3) Matsui, H.; Akagi, K.; Murata, S.; Nomura, M. *J. Jpn. Petrol. Inst.*, in contribution.
- 4) Matsui, H.; Akagi, K.; Murata, S.; Nomura, M. *Energy Fuels*, in press.

Table 1. The catalyst employed in this study

	Contents (wt%)	
	Ni	Pd
Ni-Y	5.5	-
Ni-Pd-Y	3.3	3.6
Pd-Y	-	3.7

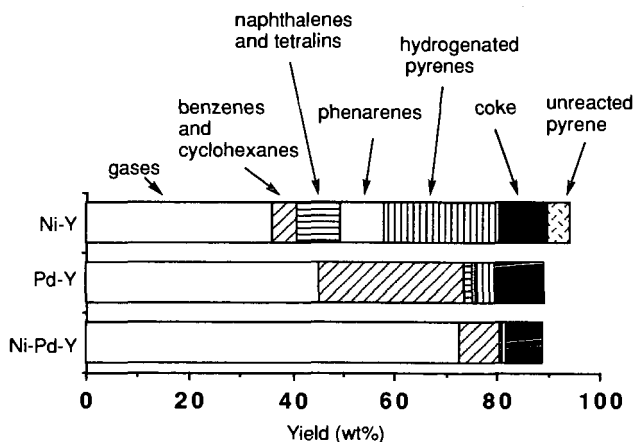


Figure 1. Hydrocracking of pyrene over metal-supported Y-type zeolites at 350 °C for 1 h

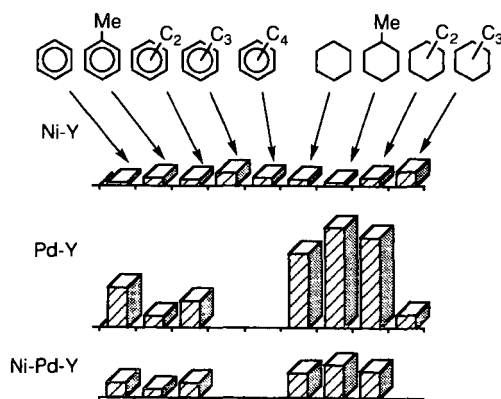


Figure 2. Distribution of mono-ring compounds in hydrocracking of pyrene over three metal-supported Y-type zeolite catalysts at 350 °C for 1 h under 70 kg/cm² of H₂

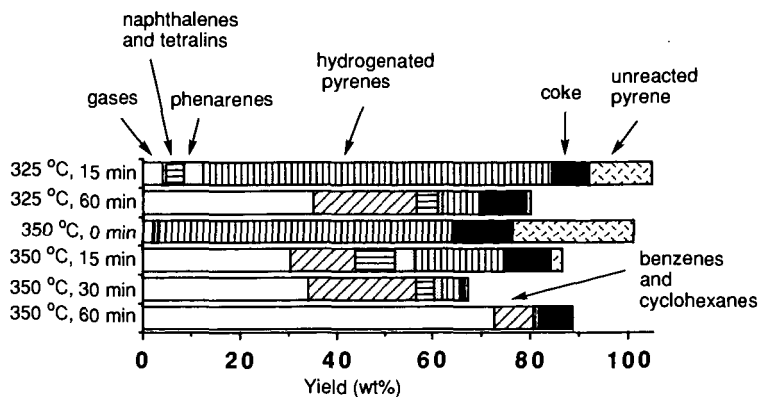


Figure 3. Hydrocracking of pyrene over Ni-Pd-Y catalyst

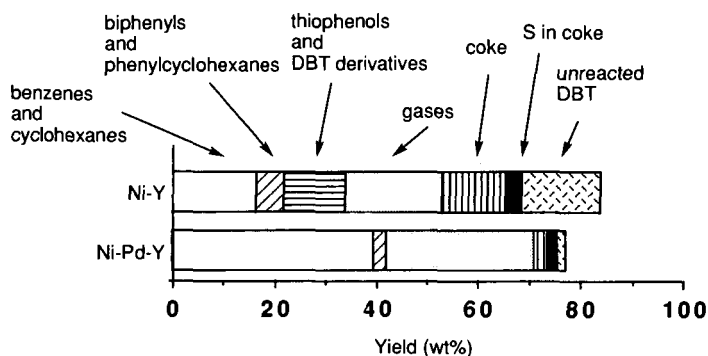


Figure 4. Hydrodesulfurization of DBT over metal-supported Y-type zeolite at 350 °C for 1h

SELECTIVE HYDRODESULFURIZATION OF 4,6-DIMETHYLBENZOTHIOPHENE IN THE MAJOR PRESENCE OF NAPHTHALENE OVER MOLYBDENUM BASED BINARY AND TERTIARY SULFIDES CATALYSTS

Takaaki ISODA*, Shinichi NAGAO, Xiaoliang MA,
YOZO KORAI and Isao MOCHIDA

* Institute of Advanced Material Study, Kyushu University,
Kasugakouen 6-1, Kasuga, Fukuoka 816, Japan

Keywords : Selective HDS, Ru-CoMo / Al_2O_3 , 4,6-dimethyldibenzothiophene

INTRODUCTION

It has been clarified in previous papers (1) that the sufficient desulfurization of the refractory sulfur species in the diesel fuel such as 4-methyldibenzothiophene and 4,6-dimethyldibenzothiophene (4,6-DMDBT) should be achieved in its sulfur level of 0.05 % which is currently regulated (2). Such refractory species have been proved to be desulfurized through the hydrogenation of one or both phenyl rings in the substrate to moderate the steric hindrance of methyl groups located in the neighbours of the sulfur atom (3). Hydrogenation of neighboring phenyl rings should competitive with the aromatic partners in the hydrogenation step, being severely hindered (4). The diesel fuel tends to be more aromatic due to crude of more aromaticity and more blending of the craked oil.

In the present study, the catalytic activities of CoMo and NiMo of different contents of Co or Ni and Ru-CoMo / Al_2O_3 were examined for the desulfurization of 4,6-DMDBT in decane and decane with naphthalene to find selective catalysts which desulfurize 4,6-DMDBT in the presence of naphthalene through preferential hydrogenation through its phenyl ring. The key step is assumed to be the hydrogenation step of 4,6-DMDBT in the competition with naphthalene. Ru was the selected as the third component of metal promoter which was added to CoMo / Al_2O_3 , since sulfur atom in 4,6-DMDBT can be a preferable anchor to the noble metal sulfide in competition with the aromatic hydrocarbon (5-6). Characterization of Ru-CoMo / Al_2O_3 using XPS, XRD and HR-EM to find the origin of the selectivity for the desulfurization in the aromatic hydrocarbons.

EXPERIMENTALS

Chemicals and Catalysts ; 4,6-DMDBT was synthesized according to the reference (7). Commercially available $(\text{NH}_4)_2\text{MoO}_4$, $\text{Co}(\text{NO}_3)_2 \cdot 6\text{H}_2\text{O}$, $\text{Ni}(\text{NO}_3)_2 \cdot 6\text{H}_2\text{O}$ and $\text{RuCl}_3 \cdot 3\text{H}_2\text{O}$ were used as catalyst precursor salts. Commercially available Al_2O_3 was selected as the catalyst support.

The precursor salt was impregnated onto Al_2O_3 according to an incipient wetness impregnation procedure. Impregnation additives such as HCl, H_3PO_4 , malic acid and citric acid are used in the impregnation solution. Contents of metal oxides supported were as follows; Co(0 - 3 wt%)-Mo(15 wt%) / Al_2O_3 , Ni(0 - 5 wt%)-Mo(15 wt%) / Al_2O_3 , Ru(0.75 wt%)-Co(0.25wt%)-Mo(15 wt%) / Al_2O_3 , respectively.

After the impregnation, the catalyst was dried at 160°C, calcined at 420°C under air flow, and presulfurized at 360°C for 2h by flowing H_2S (5vol %) in H_2 under atmospheric pressure just before its use.

Reaction ; HDS of 4,6-DMDBT in decane with naphthalene was performed in a 50 ml batch-autoclave at 300°C under 2.5MPa H_2 pressure for 0.5 - 2.5h, using 1.5g catalyst and 10g substrate including solvent. The concentrations of 4,6-DMDBT and naphthalene were 0.1 and 10 wt %, respectively. After the reaction, products were qualitatively and quantitatively analyzed by GC-MS, GC-FID (Yanaco G-3800 and G-100) and GC-FPD(Yanaco G-3800 and 50ml OV-101).

XPS ; X-ray photoelectron spectra (XPS) was taken on a ESCA 1000 (Shimadzu co.) with Mg K_{α} radiation energy of 1253.6 eV. The binding energy was identified according to the references (8-11).

XRD ; X-ray diffraction (XRD) was taken on a X-ray diffraction meter (Rigaku co.) with Cu target electrode at 40 KV voltage. X-ray diffraction was performed according to the procedure described by International Center for Diffraction Data (12).

HREM ; High resolution electron micrographs (HREM) of catalysts were taken on JEM -2000 EX (Jeol co.) at 200 KV acceleration voltage at magnification of 150 to 500K.

RESULTS

Inhibition with Naphthalene of HDS Reaction over NiMo and CoMo catalysts

Fig.1(A) illustrates HDS activity of NiMo catalysts for 4,6-DMDBT in decane and decane with 10 wt% naphthalene at 300°C under 2.5MPa H₂ for 2h. The catalysts gave 95 - 100% conversion of 4,6-DMDBT in decane regardless of Ni content which increased very much the desulfurization compared to that over Mo / Al₂O₃ in decane. Naphthalene of 10 wt% reduced the conversion to 45% on Mo / Al₂O₃ and Ni(1)-Mo / Al₂O₃, and 77% on Ni(5)-Mo / Al₂O₃. Significant retardation by naphthalene was observed over Ni-Mo / Al₂O₃ especially when Ni content was low.

Fig.2 shows the HDS products from 4,6-DMDBT over Mo and NiMo / Al₂O₃. NiMo / Al₂O₃ produced B_{4,6} as the major product and A_{4,6} as the second major while Mo / Al₂O₃ did A_{4,6} as the major and B_{4,6} as the second major in decane. Overall desulfurization was certainly enhanced by addition of Ni through the hydrogenation. Naphthalene of 10 wt% reduced very much the desulfurization over Mo / Al₂O₃ and Ni(1)-Mo / Al₂O₃. Mo / Al₂O₃ and Ni-Mo / Al₂O₃ with less content of Ni suffered large reduction of both products by 10 wt% naphthalene. Large amount of Ni increased the B_{4,6} overcoming the inhibition of naphthalene while A_{4,6} suffered very much the retardation regardless of Ni content.

Fig.1(B) shows conversion of naphthalene to tetralin and decalin. Ni of 1 wt% or more addition accelerate very much the hydrogenation of naphthalene, giving 100% tetralin and 25% decalin, while Mo / Al₂O₃ provided 80% conversion to tetralin without decalin.

Table I summarizes the yield of minor products, hydrogenated one (H) and desulfurized one without hydrogenation (C_{4,6}). Addition of Ni increased the yield of C_{4,6} and reduced that of H.

Fig.3(A) illustrates the HDS of 4,6-DMDBT over CoMo / Al₂O₃ in decane and decane with 10 wt% naphthalene. The CoMo catalysts allowed 100% conversion of 4,6-DMDBT regardless of Co content under the present conditions in decane. Naphthalene of 10 wt% reduced the conversion to 75% in Co(0.25)Mo / Al₂O₃, 87% over Co(1)Mo / Al₂O₃, and 68% over Co(3)Mo / Al₂O₃. It should be noted that Co(1)Mo / Al₂O₃ suffered the smallest retardation by naphthalene.

Fig.4 shows yields of products from 4,6-DMDBT over CoMo / Al₂O₃ of different Co contents. B_{4,6} was the major product, of which yield increased markedly by addition of Co to Mo, reaches the maximum of 80% by Co of 1wt% in decane and 60% in decane with 10 wt% naphthalene. Addition of Co increased very sharply the yield of B_{4,6} the major product, 1 wt% of Co giving the maximum yield. A_{4,6} the second major product, was produced most over Mo / Al₂O₃. Addition of Co reduced it sharply in decane. Yield of A_{4,6} decreased markedly in decane with 10% naphthalene over Mo / Al₂O₃, while addition of 0.25 and 1 wt% of Co slightly increased it.

Activity of Ru-CoMo / Al₂O₃

Fig.5 (A) illustrates HDS conversion of 4,6-DMDBT in decane or decane with 10wt % naphthalene over Ru(0.75 wt%) added Co(0.25 wt%)-Mo, Co(3 wt%)-Mo and Ni (5 wt%)-Mo / Al₂O₃, respectively, by 2h. High HDS conversions of 95 - 100 % were obtained over all three catalysts in decane. Naphthalene of 10 wt% in decane reduced the HDS conversion over the catalysts, however the extent reduction depended in the amounts of Co or Ni. Co content of 0.75 wt% exhibited 22% reduction while Co and Ni of 3 and 5 wt% severe suffered 30 and 39 % reduction, respectively.

Hydrogenation conversion of coexistent naphthalene is shown in Fig.5 (B). Ru-NiMo / Al₂O₃ provide the highest conversions of naphthalene to tetralin and decalin of 100% and 20%, respectively, while the conversions were 90% and 10%, respectively, over Ru-Co(0.25 wt%)-Mo / Al₂O₃. Hence, Ru-CoMo / Al₂O₃ with 0.25 wt% Co exhibited the highest HDS activity of 4,6-DMDBT by minimum hydrogenation of co-existence naphthalene.

Hydrodesulfurization and Hydrogenation Selectivities

Fig. 6 compares the conversions of 4,6-DMDBT hydrodesulfurization and naphthalene hydrogenation over NiMo, CoMo and additive with Ru(0.75 wt%)-Co(0.25 wt%)-Mo(15 wt%) / Al₂O₃ at 300°C for 0.5h and 2h where 0.1 wt% 4,6-DMDBT and 10 wt% naphthalene were present in decane. There were found two kinds of the catalysts: one exhibited a larger conversion of naphthalene with much less conversion of 4,6-DMDBT, and the others were large conversions of 4,6-DMDBT. The first group of catalyst contained NiMo, the second one contained Ru-CoMo and Ru-CoMo with additive H₃PO₄ and HCl.

In order to compare the reaction selectivity between the HDS for sulfur compound and hydrogenation (HGN) for aromatic hydrocarbon, relative selectivity was introduced according to the equation (1). Selectivity ratio is shown as follows:

$$\text{Selectivity ratio of 4,6-DMDBT} = \frac{(\text{Reaction mole ratio of 4,6-DMDBT over NiMo / Al}_2\text{O}_3 \text{ or Ru-CoMo / Al}_2\text{O}_3)}{(\text{Reaction mole ratio of 4,6-DMDBT over CoMo / Al}_2\text{O}_3)} \quad (1)$$

Fig. 7 shows the selectivity ratio of 4,6-DMDBT calculated from data of Fig. 6 versus conversion of naphthalene. It clarified hydrogenation activity for naphthalene decreased with increasing the selectivity ratio of 4,6-DMDBT over these catalysts. Particular Ru-CoMo-HCl / Al₂O₃ showed the highest hydrodesulfurization selectivity for 4,6-DMDBT, giving ratio of 1.41, while giving ratio of 1.28, 1.12 and 1.0 over Ru-CoMo / Al₂O₃, Ru-CoMo-P / Al₂O₃ and CoMo / Al₂O₃, respectively. NiMo / Al₂O₃ was inferior to CoMo / Al₂O₃ for hydrodesulfurization selectivity of 4,6-DMDBT, giving ratio of 0.38. Especially, Ru-CoMo-HCl / Al₂O₃ showed as 1.7 times higher selectivity for hydrodesulfurization of 4,6-DMDBT as that of NiMo / Al₂O₃, while 0.4 times lower hydrogenation activity of naphthalene.

XPS Analysis

Fig. 8 shows XPS of Mo 3d in the Ru(x)-Co(y)-Mo(15wt%) / Al₂O₃ (0 ≤ x, y ≤ 1 wt %) catalysts before and after presulfiding. Before sulfiding, two Mo 3d_{3/2} and 3d_{5/2} peaks were found at 235 and 232 eV of binding energies (8-11), indicating MoO₃ species in all catalysts regardless of their compositions. Sulfiding sharply the peaks to 225 and 222 eV, respectively in Mo / Al₂O₃ and CoMo / Al₂O₃, indicating the Mo(II) species (8-11). Ru-CoMo / Al₂O₃ and Ru-Mo / Al₂O₃ exhibited two peaks at 222 and 218 eV with a very small peak at 225 eV, indicating major presence of Mo 3d_{5/2} of Mo(0) at 218 eV after the sulfiding. These results indicated two kinds of Mo species, such as MoS₂ and metal Mo existed on sulfided Ru-CoMo / Al₂O₃ catalyst.

XRD Analysis

Fig. 9 shows XRD spectra of a series of Ru(x)-Co(y)-Mo(15 wt%) / Al₂O₃ (0 ≤ x, y ≤ 1 wt %) before presulfiding. There were two large peaks ascribed to alumina of 45.7° and 66.5°, respectively, with all catalysts. Three sharp peaks were identified with MoO₃ of 23.4°, 25.6° and 27.3°, respectively, over the Mo based on catalysts. The intensity of these three peaks increased with increasing content of Ru on CoMo / Al₂O₃ indicating the large crystals of MoO₃ in the presence of Ru. The peaks of 33.7° and 53.9° were identified to RuO₂, while no peak was ascribed to Co oxide. No definite peaks related to Mo, Ru and Co species were found after the sulfiding.

HREM

Fig. 10 shows HREM micrographs of sulfided Ru(0.75 wt%)-Co(0.25 wt%)-Mo(15 wt%) / Al₂O₃. Fig. 10 (a) and (b) shows MoS₂ layers and RuS₂ crystals as dotted spots, respectively, under 20K magnification which were typically observed on Ru-CoMo / Al₂O₃. Large magnification of (a) under 50K clarified large length and thickness of MoS₂ layers.

DISCUSSION

Fig. 11 illustrates the reaction pathway of 4,6-DMDBT in decane over Mo sulfide based on catalysts. There were two desulfurization routes, one is the desulfurization through the hydrogenation of one phenyl group; i.e., hydrodesulfurization route, and the other is desulfurization without apparent hydrogenation; i.e., direct-desulfurization route. The former reaction route is strongly hindered by the dominant presence of naphthalene.

In earlier works, it has been proposed desulfurization active site of sulfided CoMo and NiMo catalysts were anion-vacancy at edge plane of MoS_2 (13). Voorhoeve and Stuver proposed "Intercalation model" which Ni and Co located edge plane of MoS_2 (14), Delmon proposed "Contact synergy model" which high activity brought contact between tiny Co_8S_9 and MoS_2 crystal (15), and Topsøe insisted the mechanism of high activity by "Co-Mo-S phase model" which located on edge plane of MoS_2 (16). Additive co-catalysts, such as Ni or Co brought the high activity of MoS_2 .

The role of Ru addition to Mo sulfide based on catalysts are classified two categories, reduction of hydrogenation activity for aromatic hydrocarbon and promotion of hydrogenation selectivity for sulfur compound. In addition XPS spectra indicated additive Ru in CoMo catalyst was easily reduced MoS_2 to metal Mo. Hence hydrogenation activity of aromatic hydrocarbon was controlled by additive Ru, and it suggests competitive reaction of 4,6-DMDBT with naphthalene on hydrogenation active site was relieved. Crystals of RuS_2 and (Co)- MoS_2 were found existing separately by HREM, it may be suggest 4,6-DMDBT takes precedence over the hydrogenation of naphthalene on the RuS_2 , and hydrogenated 4,6-DMDBT was completely desulfurized over (Co)- MoS_2 .

In order to design of the higher selective hydrodesulfurization catalyst, it will be necessary to high dispersion of Ru on the surface of support, and optimization of the amount of CoMo and Ru on catalyst. Other side of the aspect, it will be worthwhile to try the hybridization of $\text{Ru} / \text{Al}_2\text{O}_3$ and $\text{CoMo} / \text{Al}_2\text{O}_3$.

LITERATURE CITED

- (1) Isoda, T., Ma, X., Mochida, I., *J.Jpn. Pet. Inst.*, **37**, 368 (1994).
- (2) Takatuka, T., Wada, Y., Suzuki, H., Komatsu, S., Morimura, Y., *J.Jpn. Pet. Inst.*, **35**, 197 (1992).
- (3) Isoda, T., Ma, X., Mochida, I., *J.Jpn. Pet. Inst.*, **37**, 506 (1994).
- (4) Isoda, T., Ma, X., Nagao, S., Mochida, I., *J.Jpn. Pet. Inst.*, **38**, 25 (1995).
- (5) Isoda, T., Kisamori, M., Ma, X., Mochida, I., Abstract of Symposium on Jpn. Pet. Inst., p.42, 17 - 18 May 1994, Japan.
- (6) Isoda, T., Ma, X., Nagao, S., Mochida, I., Abstract of Symposium on Jpn. Pet. Inst., p.316, 26 - 27 Oct. 1994, Japan.
- (7) Gerdil, R., Lucken, E., *J.Am. Chem. Soc.*, **87**, 213 (1965).
- (8) Chung, P.L., David, M.H., *J. Phys. Chem.*, **88**, 456 (1984).
- (9) Gajardo, P., Mathieux, A., Grange, P., Delmon, B., *Appl. Catal.*, **3**, 347 (1987).
- (10) Walton, R.A., *J. Catal.*, **44**, 488 (1976).
- (11) Ledoux, M.J., Hantzer, S., Guille, J., *Bull. Soc. Chem. Belge.*, **26**, 855 (1987).
- (12) International centre for diffraction data, "Inorganic Phases", (1989).
- (13) Prins, R., De Beer, V.H.J., Somorjai, G., *Catal. Rev. Sci. Eng.*, **31**, 1 (1989).
- (14) Voorhoeve, R.J.H., Stuver, J.C.M., *J. Catal.*, **23**, 228 (1971).
- (15) Grange, P., Delmon, B., *J. Less Common Met.*, **36**, 353 (1974).
- (16) Topsøe, N.Y., Topsøe, H., *J. Catal.*, **84**, 386 (1983).

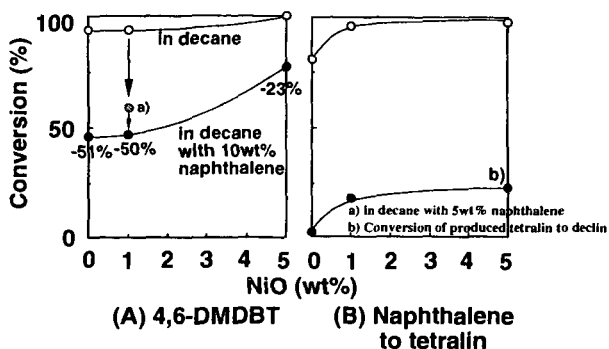


Fig.1 Inhibition with naphthalene of HDS reaction over NiMo catalysts. (300°C-2.5MPa, 4,6-DMDBT 0.1wt% + Nap 10wt% in decane, Catalyst content; 15 wt%)

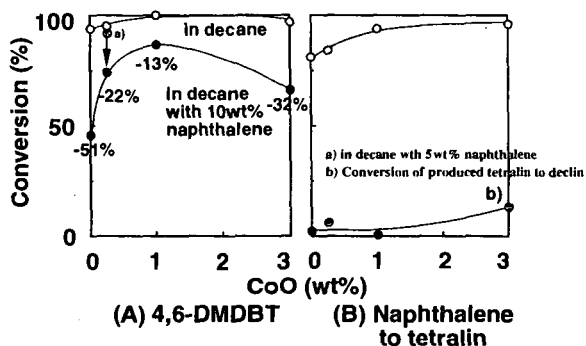


Fig.3 Inhibition with naphthalene of HDS reaction over CoMo catalysts.

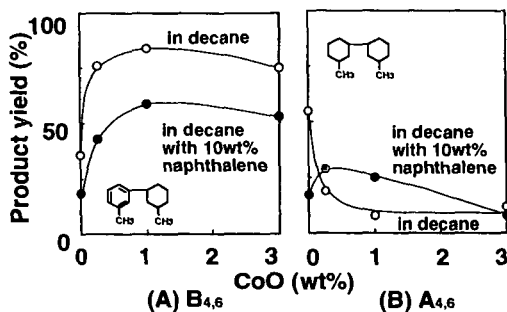


Fig.4 Major products from 4,6-DMDBT over CoMo catalysts.

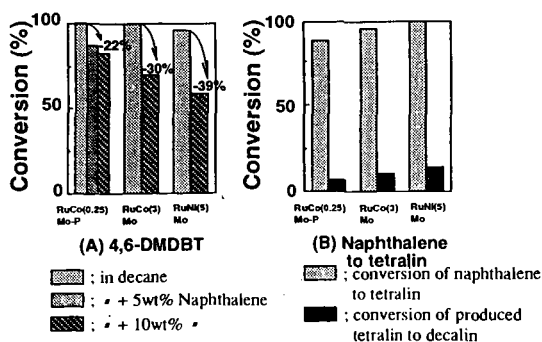


Fig.5 Inhibition with naphthalene for the HDS reaction of 4,6-DMDBT over Ru(0.75)-Co(0.25)-Mo-P, Ru(0.75)-Co(3)-Mo and Ru(0.75)-Ni(5)-Mo / Al₂O₃. (300°C-2.5MPa-2h, 4,6-DMDBT 0.1wt% + Nap 10wt% in decane, Catalyst content; 15 wt%)

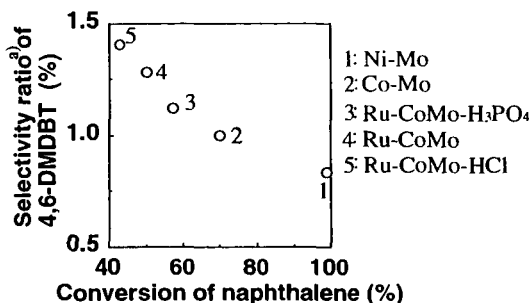


Fig.7 Effect of the additive on the HDS selectivity ratio of 4,6-DMDBT

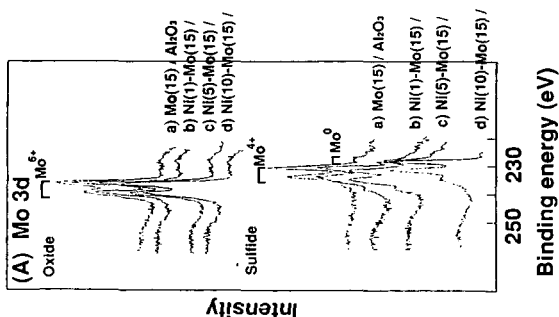


Fig.8 XPS spectra of MoS₂ based on catalysts before and after presulfiding

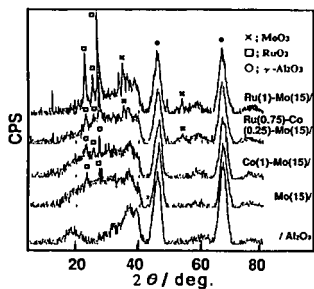
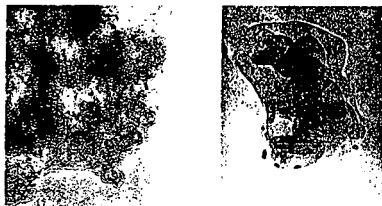


Fig.9 XRD spectra of MoS₂ based on catalyst before presulfiding

(a)

(b)



(c)

(a) (b) under 20K magnification
(c) " " 50K "



Fig.10 HREM micrographs of sulfide
Ru(0.75)-Co(0.25)-Mo(15) / Al₂O₃

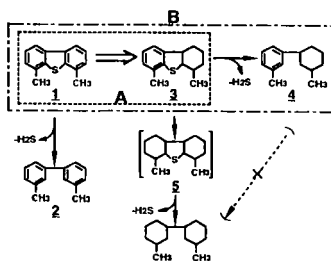


Fig.11 Reaction pathway of 4,6-Dimethyldibenzothiophene over Mo sulfide based on catalyst. (300°C-2.5MPa)

**SELECTIVE HYDRODESULFURIZATION OF 4,6-DIMETHYL-
DIBENZOTHIOPHENE IN THE DOMINANT PRESENCE OF
NAPHTHALENE OVER HYBRID CoMo / Al₂O₃
AND Ru / Al₂O₃ CATALYSTS**

Takaaki ISODA*, Shinichi NAGAO, Xiaoliang MA,
YOZO KORAI and Isao MOCHIDA

* Institute of Advanced Material Study, Kyushu University, Kasugakouen 6-1,
Kasuga, Fukuoka 816, Japan

Keywords : selective HDS, Ru / Al₂O₃ catalyst, 4,6-dimethyldibenzothiophene

INTRODUCTION

It has been revealed that significant desulfurization of refractory 4-methyldibenzothiophene and 4,6-dimethyldibenzothiophene (4,6-DMDBT) is very essential to achieve the low sulfur level of gas oil requested by the current regulation (1). Their direct desulfurization through the interaction of their sulfur atom with the catalyst surface is sterically hindered by its neighbouring methyl groups. The substrate is found kinetically to be hydrogenated at one of its phenyl rings prior to the desulfurization in order to reduce the steric hindrance through non-planar configuration (2-4). NiMo / Al₂O₃ was reported to be superior to CoMo / Al₂O₃ in the deep desulfurization, because of its higher hydrogenation activity (2). However, such a hydrogenation route suffers severe inhibition by aromatic species in their dominant presence (3), because 4,6-DMDBT must compete with the aromatic species to the hydrogenation sites on the catalysts. The aromatic species up to 30 wt % in the gas oil was that completely stop the desulfurization of the particular substrate (3). The catalyst for the selective hydrogenation of 4,6-DMDBT in the dominant aromatic partners is most wanted to achieve its extensive desulfurization in the gas oil, although there have been reported activities of various transition metal sulfides for HDS of dibenzothiophene (5), and hydrogenation of aromatic hydrocarbons (6).

The present authors have reported that different hydrogenation selectivity for 4,6-DMDBT and naphthalene over mixed sulfides of molybdenum and other transition metals (7). Ru-CoMo / Al₂O₃ catalyst which was impregnated from aqueous HCl of Co, Mo and Ru salts showed four times higher hydrogenation selectivity for 4,6-DMDBT than NiMo / Al₂O₃ catalyst (8). In the present study, HDS of 4,6-DMDBT in decane containing a significant amount of naphthalene was examined over a hybrid of CoMo / Al₂O₃ and Ru / Al₂O₃ to design the selective hydrogenation and successive desulfurization of 4,6-DMDBT in an aromatic moiety. Its activity was compared to those of CoMo / Al₂O₃, NiMo / Al₂O₃ and Ru / Al₂O₃ in their single use.

EXPERIMENTALS

Chemicals and Catalysts ; 4,6-DMDBT was synthesized according to the reference (9). Commercially available (NH₄)₂MoO₄, Co(NO₃)₂·6H₂O, and RuCl₃·3H₂O were used as catalyst precursor salts. Al₂O₃ as the catalyst support was commercially available.

The precursor salt was impregnated onto Al₂O₃ according to an incipient wetness impregnation procedure. Content weight of metal oxide on each catalyst as follows ; Co(0.25 wt%)-Mo(15 wt%) / Al₂O₃, Ni(1 wt%)-Mo(15 wt%) / Al₂O₃ and Ru(6 wt%) / Al₂O₃, respectively. After the impregnation, the catalyst was dried at 160°C, calcined at 420°C under air flow, and presulfurized at 360°C for 2h by flowing H₂S (5 vol %) in H₂ under atmospheric pressure just before its use.

Reaction ; HDS of 4,6-DMDBT in decane with naphthalene was performed in a 50ml batch-autoclave at 300°C under 2.5MPa H₂ pressure for 1.0 - 2.5h, using 1.5g catalyst and 10g substrate including solvent. The concentrations of 4,6-DMDBT and naphthalene were 0.1 and 10 wt %, respectively. After the reaction, products were qualitatively and quantitatively analyzed by GC-MS, GC-FID (Yanaco G-3800 and G-100) and GC-FPD (Yanaco G-3800 and 50ml OV-101).

RESULTS

HDS Activity of 4,6-DMDBT

Fig. 1(A) and (B) illustrates the conversion of 4,6-DMDBT and naphthalene versus reaction time, respectively, over CoMo / Al₂O₃, NiMo / Al₂O₃, Ru / Al₂O₃ and a hybrid of CoMo / Al₂O₃ and Ru / Al₂O₃ at 300°C. CoMo / Al₂O₃ exhibited an excellent activity for HDS of 4,6-DMDBT, giving conversions of 46% by 1h and 74% by 2h as shown in Fig. 1(A). The particular NiMo / Al₂O₃ was inferior to CoMo / Al₂O₃, giving conversions of 24% by 1h and 47% by 2h. Ru / Al₂O₃ was very inactive for HDS, giving conversions of 6% by 1h and 8% by 2h. The hybrid showed the highest activity for HDS of 4,6-DMDBT among the catalyst examined, giving conversions of 71% by 1h, 87% by 2h and 90% by 2.5h, when 20 wt% of Ru / Al₂O₃ and 15 wt% CoMo / Al₂O₃ were used. NiMo / Al₂O₃ showed high activity for the hydrogenation of naphthalene, giving conversion of 90% by 1h. Tetralin and decalin were the products, their yields of the latter produced being 6% by 1h and 18% by 2h, respectively. CoMo / Al₂O₃ and its hybrid with Ru / Al₂O₃ exhibited similar activities, being much inferior to NiMo / Al₂O₃ to give conversion of 61 and 77% by 1h, respectively. Decalin of 80% produced by 1h over CoMo / Al₂O₃, 5% by 1h over the hybrids. Ru / Al₂O₃ was very inactive, giving a conversion of 10% by 1h and 23% by 2h.

Products from 4,6-DMDBT

Fig. 2(A) and (B) illustrates the product yields from 4,6-DMDBT over the CoMo / Al₂O₃, NiMo / Al₂O₃, Ru / Al₂O₃ and a hybrid of CoMo / Al₂O₃ and Ru / Al₂O₃ at 300°C. The major products were hydrodesulfurization products B_{4,6} and A_{4,6}, respectively. B_{4,6} and A_{4,6} were produced through the hydrogenation of one or both phenyl ring in 4,6-DMDBT. In addition, hydrogenation products of H and desulfurized product C_{4,6} were also found in minor yields, being produced through the hydrogenation of one phenyl ring and successive direct sulfur elimination, respectively, by the yields over CoMo / Al₂O₃, NiMo / Al₂O₃, Ru / Al₂O₃ and hybrids with 10 and 20 wt% Ru / Al₂O₃, respectively, as summarized in Table 1. CoMo / Al₂O₃ and the hybrid provided B_{4,6} by the yields of 24 and 35%, respectively, by 1h, while the yields of H were 3 and 10% by 1h, respectively. The yield of H decreased beyond 1h over CoMo / Al₂O₃ and hybrids, indicating its consecutive reaction pathway. Large yield of A_{4,6} over the hybrid was noted, being produced of A_{4,6} 43% and 45% by 2h over hybrid with Ru / Al₂O₃ 10 wt% and 20 wt%, respectively, while giving conversions of 29% and 11% by 2h over CoMo / Al₂O₃ and NiMo / Al₂O₃, respectively. Yield of C_{4,6} were 0 to 2%, respectively over these catalysts, indicating very minor contribution of direct elimination of sulfur from 4,6-DMDBT as reported previously (2).

The particular Ru / Al₂O₃ was inferior in the desulfurization to CoMo / Al₂O₃ and the hybrid, however it produced more H, giving its yield of 6% by 1h, and 8% by 2h. Longer reaction time beyond 1h increased the yield, although no definite product of desulfurization was found.

DISCUSSION

Fig. 3 illustrates the hydrodesulfurization scheme of 4,6-DMDBT carries two methyl groups on 4 and 6 carbons neighbouring sulfur atom. Because two methyl groups on the sulfur atom, sterically hinder the interaction of sulfur through its Pz orbital with the sulfur vacancy of sulfide catalyst, the direct elimination of sulfur atom is strongly hindered. The hydrogenation of one of two phenyl rings breaks the co-planarity of the dibenzothiophene skeleton, moderating the steric hindrance of the methyl groups in the neighbors of the sulfur atom. Furthermore the hydrogenation of the neighboring phenyl ring increases electron density of the sulfur atom enhance its elimination through electron density interaction with the active site. Thus, it is very essential to hydrogenate the phenyl ring of 4,6-DMDBT for the accelerate of its desulfurization.

The hydrogenation of 4,6-DMDBT at one of its phenyl ring certainly competes the hydrogenation active site with aromatic partners of dominant presence in the diesel oil as observed in the present study. The selective hydrogenation of 4,6-DMDBT is very essential to accelerate its desulfurization. NiMo / Al₂O₃ exhibited preferable hydrogenation of naphthalene on the conversion-base to that of 4,6-DMDBT in the dominant presence of the former substrate. While CoMo / Al₂O₃ and the hybrid of CoMo / Al₂O₃ and Ru / Al₂O₃ did similar or slightly preferable selectivity to 4,6-DMDBT, respectively. Thus, the latter catalyst promoted the largest desulfurization activity of 4,6-DMDBT with the smallest hydrogenation of naphthalene.

The products for 4,6-DMDBT are classified into three categories, hydrogenation, direct-desulfurization and desulfurization through the hydrogenation. Ru / Al₂O₃ produce more hydrogenation product of 4,6-DMDBT than CoMo / Al₂O₃ and the hybrid catalyst, because of its inscutive desulfurization reactivity, while the hybrid catalyst gave the largest yield of bicyclohexyl which is the desulfurized product of both rings hydrogenated. Based on the above discussion, the hybrid catalyst performed the selective desulfurization of 4,6-DMDBT in the dominant presence of naphthalene through the selective hydrogenation of substrate over Ru / Al₂O₃ and the desulfurization of hydrogenated products over CoMo / Al₂O₃. High activity of NiMo / Al₂O₃ for the non-selective hydrogenation rules out the efficiency of its hybrid with Ru / Al₂O₃.

The origin of selectivity for 4,6-DMDBT may be worthwhile for speculation, although no sufficient evidence is available at moment. π orbital localized on the sulfur atom in 4,6-DMDBT may interact preferable to d orbital of the sulfide catalyst to that of the naphthalene ring, being free from the steric hindrance of its methyl groups. Such a π -M interaction may be expected more strongly with Ru than Ni, Co or Mo because of the higher polarizability of noble Ru, allowing the higher selectivity of Ru / Al₂O₃ to 4,6-DMDBT than naphthalene.

LITERATURE CITED

- (1) Takatuka, T., Wada, Y., Suzuki, H., Komatsu, S., Morimura, Y., *J.Jpn. Pet. Inst.*, 35, 197(1992).
- (2) Isoda, T., Ma, X., Mochida, I., *J.Jpn. Pet. Inst.*, 37, 368 (1994).
- (3) Isoda, T., Ma, X., Mochida, I., *J.Jpn. Pet. Inst.*, 37, 506 (1994).
- (4) Isoda, T., Ma, X., Nagao, S., Mochida, I., *J.Jpn. Pet. Inst.*, 38, 25 (1995).
- (5) Lacroix, M., Boutarfa, N., Guillard, C., Vrinat, M., Breyse, M., *J. Catal.*, 120, 473 (1989).
- (6) Des Los Reyes, J.A., Vrinat, M., Geantet, C., Breyse, M., Grimblot, J., *J. Catal.*, 142, 455 (1993).
- (7) Isoda, T., Kisamori, M., Ma, X., Mochida, I., Abstract of Symposium on Jpn. Pet. Inst., p.42, 17 - 18 May 1994, Japan.
- (8) Isoda, T., Ma, X., Nagao, S., Mochida, I., Abstract of Symposium on Jpn. Pet. Inst., p.316, 26 - 27 Oct. 1994, Japan.
- (9) Gerdil, R., Lucken, E., *J.Am. Chem. Soc.*, 87, 213 (1965).

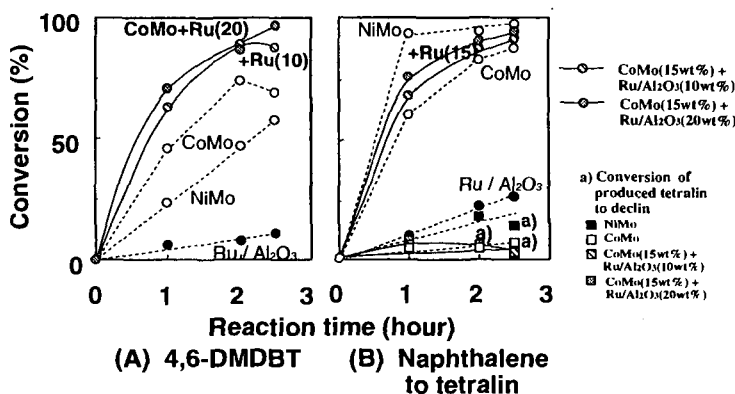


Fig.1 Conversions of 4,6-DMDBT and naphthalene over a hybrids of CoMo / Al₂O₃ and Ru / Al₂O₃. (300°C-2.5MPa, 4,6-DMDBT 0.1wt% + Nap 10wt% in decane, Catalyst content; 15 wt%, (CoMo / Al₂O₃) / (Ru / Al₂O₃) = 1.0 and 2.0)

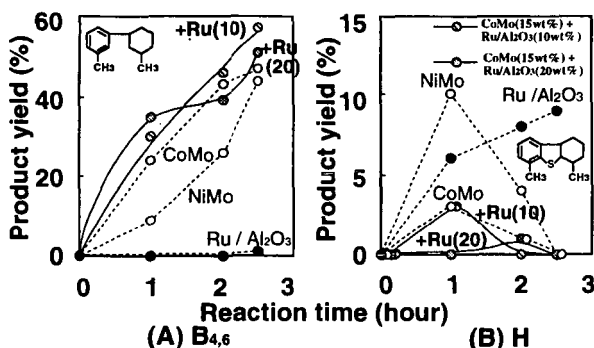


Fig.2 Products from 4,6-DMDBT over a hybrids of CoMo / Al₂O₃ and Ru / Al₂O₃.

Table1 Product distribution of 4,6-Dimethyldibenzothiophene over NiMo, CoMo, Ru / Al₂O₃ and a hybrid of CoMo / Al₂O₃ and Ru / Al₂O₃.

Catalyst	Conversion ^{a)} of 4,6-DMDBT (1) A _{4,6} (%) ^{b)}	Conversion ^{a)} of 4,6-DMDBT (1) C _{4,6} (%) ^{c)}
Co-Mo / Al ₂ O ₃	29	1
Ni-Mo / Al ₂ O ₃	12	5
Ru / Al ₂ O ₃	0	0
Co-Mo / Al ₂ O ₃ + Ru / Al ₂ O ₃ (10wt%)	43	0
Co-Mo / Al ₂ O ₃ + Ru / Al ₂ O ₃ (20wt%)	45	2

a) reaction condition: 300°C-2.5MPa-2h, 4,6-DMDBT 0.1wt% and Nap 10wt%

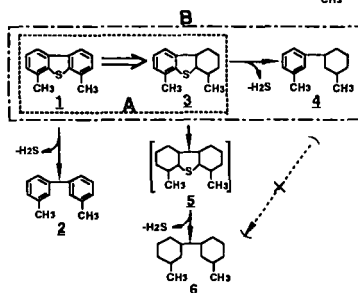
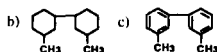


Fig.3 Reaction Pathway of 4,6-Dimethyldibenzothiophene over Mo Sulfide Based on Catalyst. (300°C-2.5MPa)

HYDRODEOXYGENATION OF O-CONTAINING POLYCYCLIC MODEL COMPOUNDS USING NOVEL ORGANOMETALLIC CATALYST PRECURSORS

Stephen R. Kirby, Chunshan Song and Harold H. Schobert
Fuel Science Program, 209 Academic Projects Bldg.
Penn State University, PA 16802

Keywords: Deoxygenation, catalyst, liquefaction.

INTRODUCTION

Oxygenated compounds are present in virtually all coals [1]. Phenols (and related hydroxyl compounds) have been identified as components of coal-derived distillates [2,3]. Ethers and related compounds, connecting structural units within the coal matrix, have been proposed as sites for the depolymerization of the coal [4] and also ethers, together with carboxyls and phenolics, have been implicated in the facilitation of retrogressive, crosslinking, repolymerization reactions [5,6].

Low-rank coals (i.e. lignites and subbituminous coals) include significantly more oxygen-containing groups than coals of higher rank [7]. With the increase in the extraction of lower rank coals in the U.S. and research into their use as liquefaction feedstocks [5,8,9], the importance of oxygen functionality removal from coal and coal-derived liquids is all the more apparent.

The removal of these functionalities from the distillate products of coal liquefaction can be both complicated and expensive, and often leads to substantial reductions in distillate yields [3]. Therefore, deoxygenation during the liquefaction process would be beneficial. This goal may be attainable with the use of sulphided bimetallic catalysts dispersed onto the coal using an organometallic precursor [10,11].

Model compound studies using multi-ring systems, or those of comparable molecular weight, were performed to investigate the capabilities of these catalysts. The model compounds selected represent a variety of oxygen functionalities, possibly present in coals of differing rank [12-14], contained within polycyclic systems. They include: anthrone (carbonyl); dinaphthyl ether (aryl-aryl ether); xanthene (heterocyclic ether); and 2,6-di-*t*-butyl-4-methylphenol (hydroxyl).

EXPERIMENTAL

All experiments were performed in a 22ml capacity microreactor. A 0.5g sample of model compound was loaded into the reactor. Solvent was added in a 1:2 weight ratio to model compound and catalyst precursors were added at 2.46mol% concentration (unless otherwise stated). The catalyst precursors used were $(\text{NH}_4)_2\text{MoS}_4$ (ATTM), $[\text{Ph}_4\text{P}]_2[\text{Ni}(\text{MoS}_4)_2]$ (Ni-Mo1) and $\text{Cp}_2\text{Co}_2\text{Mo}_2(\text{CO})_2\text{S}_4$ (CoMo-T2).

Air was removed by flushing the reactor three times with H_2 to 1000psi. The reactor was then repressurized to 1000psi H_2 . Reactions were performed at 300°C, 350°C and 400°C for 30 minutes. All reactions were carried out in a fluidized sand bath equipped with a vertical oscillator driving at a setting of 55 (~250 strokes per minute). At the end of the reaction the microreactor was quenched in cold water.

Tridecane (0.25g) was added to the microreactor as an internal standard. The microreactor contents were then extracted with acetone and diluted for analysis.

Capillary gas chromatography (GC) connected to a flame ionization detector (Perkin Elmer-8500) and gas chromatography / mass spectrometry (Hewlett Packard-5890) were used for the quantitative and qualitative analysis of the product distribution, respectively.

RESULTS AND DISCUSSION

Product distributions have been grouped as oxygen-containing and deoxygenated for the purposes of this article. The conversions of anthrone, dinaphthyl ether, xanthene and 2,6-di-*t*-butyl-4-methylphenol are shown in Figures 1-4, and the product distribution of dinaphthyl ether is given in Figure 5.

Generally, the addition of any catalyst to a system under the conditions studied increases the total conversion. For example, at 400°C dinaphthyl ether undergoes 26% thermal conversion; this yield is increased to 72% in the presence of ATTM, 88.5% with Ni-Mo1, and 100% using CoMo-T2. However, any improvement in the product quality, especially deoxygenation and ring reduction, in the presence of these catalysts is also important, and the variation of these factors for the different oxygen functional groups will be the main focus of this discussion.

Anthrone

Under non-catalytic conditions anthrone converts to anthracene through thermal reaction of the carbonyl oxygen. Anthracene then reacts further to form a variety of hydrogenated ring species, such as di- and tetrahydroanthracene.

In the presence of ATTM, the formation of oxygen-containing compounds in the products at 350°C and 400°C (substituted naphthols and phenols) suggest hydrogenation of

the carbonyl oxygen to a hydroxyl group before extensive conversion to anthracene. Reduction in the yields of these oxygen functionalities in the ATTM reaction at 400°C may indicate the possibility of an increase in the conversion of these species to non-oxygenated products.

Conversion of anthrone to oxygen-free products is increased considerably using the CoMo-T2 catalyst precursor. This implies that CoMo-T2 has the capability to increase the conversion of carbonyls without additional phenol or naphthol production. This may be achieved by either rapid C=O cleavage prior to ring hydrogenation, rapid phenol conversion to oxygen-free products, or by the prevention of initial hydroxyl group formation. From the reactions of 2,6-di-*t*-butyl-4-methylphenol with CoMo-T2, it can be seen that this catalyst, although removing some hydroxyl functionality, does not promote the ready conversion of phenols to non-oxygen containing species.

Variations in the oxygen-free products of anthrone conversion are also apparent for the different catalyst precursors. Ni-Mo1 appears to promote the formation of 1,2,3,4-tetrahydroanthracene (THA), whereas CoMo-T2 demonstrates the facilitation of 9,10-dihydroanthracene (DHA) production. ATTM seems to have equal affinity for the formation of both products. Ni-Mo1 and ATTM both exhibit an increase in the formation of 1,2,3,4,5,6,7,8-octahydroanthracene (OHA) at 400°C (0% under catalyst-free conditions to 11.8% and 11.3% respectively), which only appears in very low yields with CoMo-T2 (1.5%). This reduction in OHA yield for the CoMo-T2 precursor is comparable to increases in anthracene and DHA production, suggesting selective hydrogenation of the 9- and 10- positions (i.e. the carbonyl carbon).

Dinaphthyl Ether

Under non-catalytic conditions naphthalene is the major product of dinaphthyl ether (DNE) hydrogenation, with low yields of 2-naphthol, although total conversion is very small (26%). Oxygen functionality removal is increased in the presence of all the catalyst precursors, although to a lesser extent than for anthrone.

ATTM increases DNE conversion to oxygen-free products (63.6% at 400°C) with the balance of the products being phenols, naphthols (1.8%) and ring-reduced derivatives of the starting material. Phenol and naphthol yields decrease from 350°C to 400°C, again implying that ATTM facilitates hydroxyl group removal.

High conversions to tetralin and naphthalene are achieved in the presence of CoMo-T2 (51.6% and 40.2% respectively at 400°C). Phenols and naphthols are present in larger yields than for anthrone, suggesting the cleavage of a single C-O bond followed by hydrogenation of the phenoxy (or naphthoxy) group. Ring-reduced derivatives of DNE produced at 350°C are absent at 400°C and naphthol yields decrease across the same temperature range. These reductions in oxygen compound yields are accompanied by increases in tetralin, naphthalene and alkylbenzene formation.

The product distributions (O : non-O) of reactions of ATTM, Ni-Mo and CoMo-T2 with DNE (Figures 2 and 5) distinctly show the latter precursor to be the most favourable for C-O-C bond cleavage to oxygen-free products.

Xanthene

In the absence of a catalyst xanthene is totally unreactive. Addition of ATTM or CoMo-T2 produces noticeable reaction at 350°C and 400°C.

At 350°C the products from both precursors are phenols, cycloalkyl- and long-chain alkylbenzenes formed by C-O and C-C bond cleavage. However, at 400°C ATTM produces an increase in oxygen-free products with no increase in phenols, although conversion to non-oxygen containing species is low (24.9%).

Increases in oxygen-free product yields are also achieved with CoMo-T2 at 400°C, but with accompanying increases in phenol formation. This gain in phenols may be attributed to the formation of short-chain (C1-C2) alkylphenols from longer chain alkylphenols, implying that CoMo-T2 favours C-C cleavage over C-OH.

The comparably large conversion to oxygen-free products and phenols reinforces the ability of CoMo-T2 to cleave ether linkages, and inability to remove hydroxyl groups. However, the low conversions of xanthene illustrate the unreactive nature of the starting material.

2,6-Di-*t*-butyl-4-methylphenol (DBMP)

Under non-catalytic reaction conditions the conversion of DBMP involves the cleavage of one, or both, of the *t*-butyl groups to produce 2-butyl-4-methylphenol (BMP) and ultimately 4-methylphenol (100% at 400°C). No reaction occurs at 300°C in the absence of a catalyst. When a catalyst is present the removal of the butyl groups becomes more favourable and formation of the above products takes place.

At 350°C with ATTM, almost all the starting material has reacted and only a small portion remains as BMP (13.5%). The major product, 4-methylphenol, then undergoes catalytic hydrogenation and hydroxyl removal to form toluene and methylcyclohexane. At 400°C these reactions proceed to a greater extent, resulting in greater yields of both products (46.5% and 20.2% respectively).

In the presence of CoMo-T2, DBMP appears to lose both butyl groups so rapidly that no 2-*t*-butyl-4-methylphenol is isolated, so 4-methylphenol is the only product at

300°C. At 350°C it exhibits some further conversion to methylcyclohexane (1.6%) and at 400°C toluene and methylcyclohexane are produced.

DBMP is a reactive compound through loss of its butyl groups. However, the hydroxyl group C-OH bond is very resistant to reaction and is only cleaved, to a substantial degree, in the presence of the ATTM precursor. CoMo-T2 removes the OH-group, but only to a small extent.

Investigations using the Ni-Mo1 precursor are not as advanced as those for ATTM and CoMo-T2. Presentation of these results is planned for future articles.

CONCLUSIONS

From the non-catalytic data shown there is a clear order of starting material reactivity : 2,6-di-*t*-butyl-4-methylphenol > anthrone > dinaphthyl ether > xanthene. However, the reactivity order of the oxygen functionalities in the presence of the various catalysts is different. For non-catalytic conditions the order appears to be : carbonyl > aryl-aryl ether > substituted phenol ≈ heterocyclic ether. In the presence of ATTM this sequence changes slightly to : carbonyl > substituted phenol ≈ aryl-aryl ether > heterocyclic ether and for reactions involving CoMo-T2 the reactivity order appears to be : carbonyl > aryl-aryl ether > heterocyclic ether > substituted phenol.

These differences in reactivity order emphasize the effect of the nature of the oxygen functionality on the deoxygenating capabilities of the catalysts and that different catalysts can have different roles in promoting hydrodeoxygenation and reduction, depending on the nature of the starting material. They also highlight the undesirability of phenolic and heterocyclic ether structures in liquefaction systems. Both these structures types are quite unreactive under liquefaction conditions and any reaction has a tendency to form high yields of single-ring phenols.

When applied to coals, these findings suggest that coals differing from each other in the form of which oxygen functional groups are dominant, may show quite different kinds of liquefaction products, depending on which catalyst precursor was chosen.

ACKNOWLEDGEMENTS

The authors wish to express their appreciation to the U.S. Department of Energy, Pittsburgh Energy Technology Centre for supporting this work, Dr. E. Schmidt for synthesizing the catalyst precursors and Mr. R.M. Copenhagen for the fabrication of the microreactors.

REFERENCES

1. C. Song, L. Hou, A. K. Saini, P. G. Hatcher and H. H. Schobert, (1993). *Fuel Processing Technology*, **34** 249-276.
2. R. E. Pauls, M. E. Bambacht, C. Bradley, S. E. Scheppele and D. C. Cronauer, (1990). *Energy & Fuels*, **4** 236-242.
3. C. Burgess, (1994). "Direct Coal Liquefaction: A Potential Route to Thermally Stable Jet Fuel", pp. 167.
4. L. Artok, O. Erbatur and H. H. Schobert, (in press).
5. C. Song, H. H. Schobert and P. G. Hatcher, (1992). *Energy & Fuels*, **6** 326-328.
6. M. A. Serio, E. Kroo, S. Charpenay, R. Basilakis, P. R. Solomon, D. F. McMillen, A. Satyam, J. Manion and R. Malhotra, (1993). Proceedings of Contractors' Review Conference: "Coal Liquefaction and Gas Conversion": "The Dual Role of Oxygen Functions in Coal Pretreatment and Liquefaction: Crosslinking and Cleavage Reactions", Pittsburgh, PA, 15-44.
7. S. M. Solum, R. J. Pugmire and D. M. Grant, (1989). *Energy & Fuels*, **3** 187-193.
8. C. Song and H. H. Schobert, (1992). *Am. Chem. Soc. Div. Fuel Chem. Prepr.*, **37** 42.
9. L. Huang, C. Song and H. H. Schobert, (1992). *Am. Chem. Soc. Div. Fuel Chem. Prepr.*, **37** 223.
10. C. Song and H. H. Schobert, (1993). "Novel Bimetallic Dispersed Catalysts for Temperature-Programmed Coal Liquefaction", Penn State University DE-AC22-92PC92122-TPR-1.
11. C. Song, D. S. Parfitt and H. H. Schobert, (1993). *Catalysis Letters*, **21** 27-34.
12. L. M. Stock, (1989). *Accounts of Chemical Research*, **22** 427-433.
13. R. Hayatsu, R. E. Winans, R. G. Scott, L. P. Moore and M. H. Studier, (1978). *Fuel*, **57** (2), 541.
14. J. H. Shinn, (1984). *Fuel*, **63** (3), 1187.

Figure 1. Yield of oxygenated and deoxygenated products of anthrone as a function of temperature and catalyst precursor.

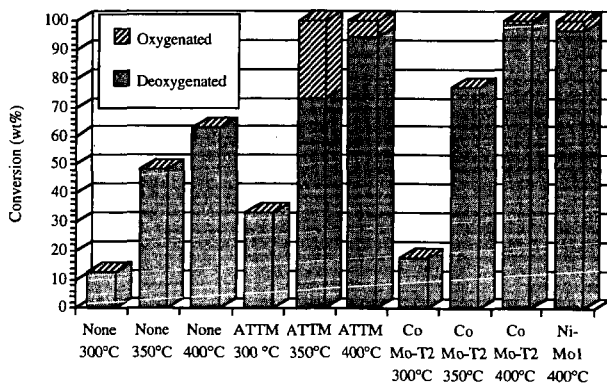


Figure 2. Yield of oxygenated and deoxygenated products from dinaphthyl ether as a function of temperature and catalyst.

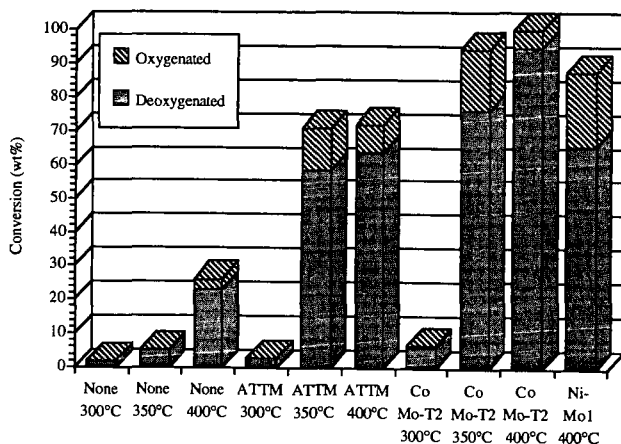


Figure 3. Yield of oxygenated and deoxygenated products of xanthene as a function of temperature and catalyst.

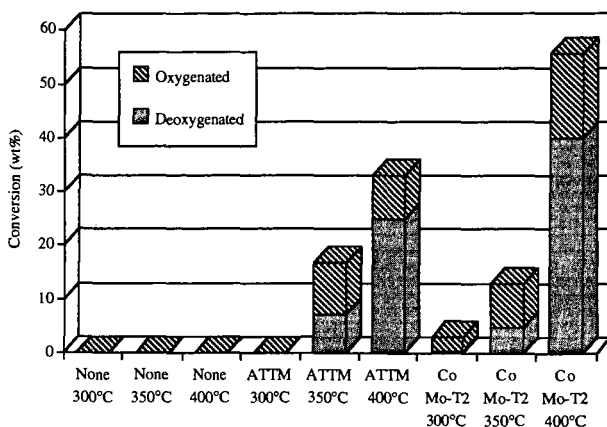


Figure 4. Yield of oxygenated and deoxygenated products of 2,6-di-*t*-butyl-4-methylphenol as a function of temperature and catalyst.

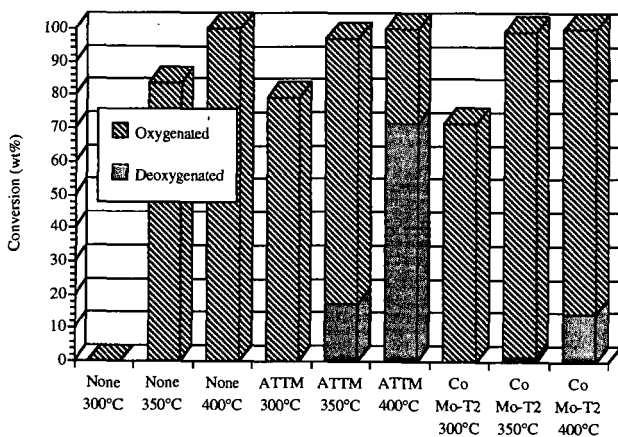


Figure 5. Product distribution of dinaphthyl ether under liquefaction conditions.

React. temp. (°C)	300	350	400	300	350	400	400	300	350	400
Cat. Precursors	None	None	None	ATTM	ATTM	ATTM	Ni-Mo	CoMo-T2	CoMo-T2	CoMo-T2
Products (wt%)										
Tetralin		1.2		1.3	30.5	24.4	24.6	4.4	47.2	51.6
Naphthalene	1.9	4.1	22.9	1.4	26.1	38.3	39.1	1.9	28.6	40.2
THDNE					7.4	6.3	12.0	0.3	7.5	0.3
OH DNE					1.7		3.2		2.6	
THnaphthol					2.3	1.0	4.1		5.9	3.5
2-Naphthol			3.2		0.6	0.8	2.1	0.3	1.5	0.5
Methylphenol					0.3		0.4		0.6	0.7
Alkylbenzenes					1.9	0.9	2.0		0.5	3.1
Conv. (wt%)	1.9	5.3	26.1	2.7	70.7	71.9	87.6	6.9	94.3	100

SYNTHESIS AND REACTIVITY OF NEW BIMETALLIC OXYNITRIDES

S. Ramanathan, C. C. Yu and S. T. Oyama
Department of Chemical Engineering, Virginia Polytechnic
Institute and State University, Blacksburg, VA 24061

Keywords: Bimetallic oxynitrides, Hydrodenitrogenation,
Hydrosulfurization

ABSTRACT

A new series of catalysts, transition metal bimetallic oxynitrides of the form $M_1M_2O_xN_y$ ($M_1 = V, Nb$ and Cr , $M_2 = Mo$), was prepared. The catalysts were synthesized by nitriding the bimetallic oxide precursors in an ammonia gas stream at 1000 cm^3/min ($6.8 \times 10^2 \mu mol s^{-1}$) using a heating rate of 5 K/min ($8.3 \times 10^{-2} K s^{-1}$). The catalysts were characterized by x-ray diffraction, CO chemisorption and surface area measurements. The activity of these catalysts for hydroprocessing was studied in a three-phase trickle bed reactor operated at 3.1 MPa and 643 K. The liquid feed consisted of 3000 ppm sulfur (dibenzothiophene), 2000 ppm nitrogen (quinoline), 500 ppm oxygen (benzofuran), 20 wt% aromatics (15 wt% tetralin and 5 wt% amylbenzene) and balance aliphatics (tetradecane). The activities of the bimetallic oxynitrides were compared to a commercial Ni-Mo/ Al_2O_3 (Shell 324) catalyst tested at the same conditions. The bimetallic oxynitrides were found to be active for the hydrodenitrogenation (HDN) of quinoline. In particular, V-Mo-O-N exhibited higher HDN activity than the commercial Ni-Mo/ Al_2O_3 catalyst. The hydrosulfurization (HDS) activity of the bimetallic oxynitrides ranged from 9-25% with V-Mo-O-N showing the highest HDS activity among the oxynitrides tested.

INTRODUCTION

Monometallic nitrides have been investigated extensively since the 50's and 60's [1,2]. However, in order to take advantage of the catalytic properties of the carbides and nitrides, it is important to prepare these materials in high surface area form. Conventional powder metallurgy methods such as direct nitridation or carburization of metal or metal oxide powders resulted in compounds of typically low surface area ($< 10 m^2 g^{-1}$). Significant progress has been made in the preparation of these materials in high surface area form in the last decade and a half [3-6]. One of the techniques developed during this period was the temperature programmed reaction [7] method of preparing high surface area compounds from oxide precursors. The technique offers the advantage of lower synthesis temperatures than the conventional methods. In addition, the transformation of the oxide to the carbide/nitride phase is direct, bypassing the metal phase, which is the most prone to sintering. However, most of the work on the temperature programmed reaction is focused on the synthesis of monometallic carbides and nitrides. There is little work reported on the preparation of high surface area mixed transition metal nitrides/oxynitrides in the literature.

Transition metal carbides and nitrides were found to be active for a number of hydrocarbon reactions [8]. One of the major applications of transition metal carbides and nitrides has been in hydroprocessing. Removal of nitrogen and sulfur from petroleum feedstocks is gaining importance with the need to process heavier resources. Nitrogen removal is always accompanied by the consumption of excess hydrogen due to the difficulty involved in the C-N bond scission. The development of catalysts that are selective to C-N cleavage is an important goal, and this paper reports an investigation on a new class of catalysts which is different in structure and properties from the conventional Ni-Mo/ Al_2O_3 and Co-Mo/ Al_2O_3 hydrotreating catalysts.

After the initial results by Schlatter, et al., [9] on quinoline HDN, most of the hydroprocessing work has been concentrated on molybdenum nitride catalysts, both supported and unsupported [10-14]. This paper reports a new family of nitrides, where the nitrogen is partially exchanged by oxygen and a second transition metal is also introduced in the interstitial compound.

SYNTHESIS AND CHARACTERIZATION

The bimetallic oxynitrides were prepared by nitriding the bimetallic oxide precursors using the temperature programmed reaction technique [15]. The oxide precursor was loaded in a quartz reactor placed in a furnace (Hoskins 500W). Ammonia reactant gas was passed over the oxide bed at a flow rate of 1000 cm³/min (680×10² μmols⁻¹). The temperature of the reactor bed was ramped linearly at 5 K/min (8.3×10⁻² Ks⁻¹) to the final synthesis temperature (T_{max}) and held at that temperature for a period of time (t_{hold}). The effluent gases from the reactor were analyzed by an on-line mass spectrometer (Ametek/Dycor, MA100). Once the reaction was completed, the gas flow was switched to helium and the reactor was quickly cooled down to room temperature by removing the furnace. The catalysts were passivated at room temperature in a 0.5% O₂/He gas mixture before exposure to the atmosphere. A summary of the synthesis conditions used in the preparation of these materials is presented in Table 1.

The bulk phase purity of the samples was identified by x-ray diffraction (XRD) (Siemens Model D500 with a CuKα monochromatized radiation source). Figure 1 presents the XRD patterns of the passivated bimetallic oxynitrides. The patterns did not show any features of the starting oxide material and moreover, all the patterns indicate that the oxynitrides have a face centered cubic arrangement. In addition, the line-broadening of the peaks indicates the presence of small crystallites. Elemental analysis indicated that the actual composition of the catalysts was V_{2.0}Mo_{1.0}O_{1.7}N_{2.4}, Nb_{2.0}Mo_{2.6}O_{3.0}N_{4.2} and Cr_{1.0}Mo_{1.3}O_{2.3}N_{1.4}. N₂ physisorption and CO chemisorption measurements were carried out to obtain the specific surface area and the number of exposed surface metal atoms. Prior to surface adsorption measurements, the catalysts were activated in a flow of 10% H₂/He gas mixture at 738 K for 2 h. The surface areas, CO uptakes and the number densities are summarized in Table 2. The number densities indicated in Table 2 reveal that only a maximum of 14% of the total metal atoms are available for the chemisorbing molecule. These values are typical of the interstitial compounds due to the prior occupation of the sites by N and O, which were not removed during the activation process.

REACTIVITY

Experimental runs consisted of testing a series of oxynitride catalysts for their activity in hydrodenitrogenation (HDN), hydrodesulfurization (HDS) and hydrodeoxygenation (HDO). The reactions were carried out in a three-phase trickle-bed reactor at 3.1 MPa and 643 K. Typically about 0.2-1 g of the catalyst was loaded, corresponding to a total surface area of 30 m². Prior to catalytic testing, the oxynitrides were activated in flowing hydrogen at 723 K for 3 hours. The commercial Ni-Mo/Al₂O₃ catalyst was sulfided in a flow of 10% H₂S/H₂ gas mixture. After the activation process, the reactors were cooled down to 643 K and hydrogen was pressurized to 3.1 MPa. Hydrogen flow to the reactor was maintained at 150 cm³(NTP)/min (100 μmols⁻¹) using mass flow controllers. Liquid feed rate was set at 5 cm³h⁻¹ using high-pressure liquid pumps. The gas and liquid passed over the catalyst bed in a cocurrent upflow mode and out

to the liquid sampling valve. The liquid feed composition used in all the experiments was 3000 ppm S (dibenzothiophene), 2000 ppm N (quinoline), 500 ppm O (benzofuran), 20 wt% aromatics (15 wt% tetralin and 5 wt% amylbenzene) and balance aliphatics (tetradecane). The reactions were carried out for a period of 60 hours. The liquid samples were analyzed off-line by gas chromatography.

The activity of the catalysts was compared on the basis of equal surface areas of 30 m² loaded in the reactor. Figure 2 shows a comparison of the activities of the catalysts for HDN, HDS and HDO at 3.1 MPa and 643 K. Clearly, the oxynitrides show considerable activity for the HDN of quinoline. In fact, V-Mo-O-N exhibited higher activity than the commercial sulfided Ni-Mo/Al₂O₃ catalyst. All the catalysts showed similar product distribution and the major hydrodenitrogenated product was propylcyclohexane. The HDN activity of the catalysts was stable even after 60 hours on-stream. The HDS activity of the oxynitrides ranged from 9-25%, with V-Mo-O-N displaying the highest HDS activity among the oxynitrides tested. The oxynitrides showed high initial HDS activities, but they deactivated after about 25 h on-stream. The major product from the HDS of dibenzothiophene was biphenyl. The oxynitrides were also active for the removal of oxygen from benzofuran. The HDO activity ranged from 12-32% and the major deoxygenated product was ethylcyclohexane. In fact, the V-Mo-O-N showed higher overall activity than the corresponding monometallic nitrides [16]. The commercial Ni-Mo/Al₂O₃ catalyst showed high activities for the removal of sulfur and oxygen from the liquid feed.

X-ray diffraction patterns of the spent catalysts indicated that the bulk phase purity of the samples was preserved. The patterns did not show extraneous oxide or sulfide peaks indicating that the oxynitrides were stable towards heteroatoms even after prolonged exposure at elevated temperatures.

CONCLUSIONS

A new series of catalysts, bimetallic oxynitrides of transition metals, was prepared in high surface area form. They were found to be active for the hydrodenitrogenation of quinoline. Interestingly, V-Mo-O-N displayed higher HDN activity than the commercial Ni-Mo/Al₂O₃ catalyst. The new catalysts were found to be sulfur resistant under the reaction conditions. The bimetallic oxynitrides displayed better activity and stability than the monometallic nitrides.

ACKNOWLEDGMENT

Support for this work by Akzo Nobel and the Department of Energy, Office of Basic Energy Sciences is appreciated.

REFERENCES

1. Toth, L. E., "Transition Metal Carbides and Nitrides", Academic Press, New York, 1971.
2. Juza, R., in *Advances in Inorganic Chemistry and Radiochemistry*, (H. J. Emeléus and A. G. Sharpe, Eds.), Vol. 9, p. 81, Academic Press, New York, 1966.
3. Volpe, L., Oyama, S. T., and Boudart, M., "Preparation of Catalysts III", p. 147, 1983.
4. Volpe, L., and Boudart, M., *J. Solid State Chem.* **59**, 332 (1985).
5. Volpe, L., and Boudart, M., *J. Solid State Chem.* **59**, 348 (1985).
6. Ledoux, M. J., Guille, J., Hanzter, S., Marin, S., and Pham-Huu, C., *Extended Abstracts, Proceedings MRS Symposium*, Boston, Nov 26-Dec 1, p. 135, 1990.
7. Oyama, S. T., Ph.D. Dissertation, Stanford University, 1981.

8. Oyama, S. T., *Catal. Today*, **15**, 179 (1992).
9. Schlatter, J. C., Oyama, S. T., Metcalfe, J. M., III., and Lambert, J. M., Jr., *Ind. Eng. Chem. Res.*, **27**, 1648 (1988).
10. Lee, K. S., Abe, H., Reimer, J. A., and Bell, A. T., *J. Catal.*, **139**, 34 (1993).
11. Abe, H., and Bell, A. T., *Catal. Lett.*, **18**, 1 (1993).
12. Colling, W. C., and Thompson, L. T., *J. Catal.*, **146**, 193 (1994).
13. Nagai, M., and Miyao, T., *Catal. Lett.*, **15**, 105 (1992).
14. Nagai, M., Miyao, T., and Tuboi, T., *Catal. Lett.*, **18**, 9 (1993).
15. Yu, C. C., and Oyama, S. T., *J. Sol. St. Chem.*, **116**, 205 (1995).
16. Yu, C. C., Ramanathan, S., Sherif, F., and Oyama, S. T., *J. Phy. Chem.*, **98**, 13038 (1994).

Table 1. Summary of the Synthesis Conditions

Catalyst	Final Temperature T_{max} / K	Soak Period t_{hold} / h
V-Mo-O-N	1037	0.5
Nb-Mo-O-N	1063	0.3
Cr-Mo-O-N	1013	0.3

Table 2. Results of Surface Adsorption Measurements

Catalyst	CO Uptake $\mu\text{mol g}^{-1}$	Surface Area m^2g^{-1}	Number Density $\times 10^{15} \text{ cm}^{-2}$
V-Mo-O-N	167	74	0.14
Nb-Mo-O-N	11.2	121	0.0056
Cr-Mo-O-N	163	90	0.11

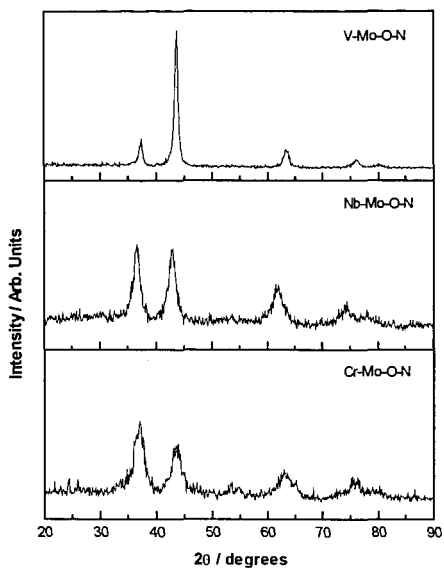


Figure 1. X-ray diffraction patterns of the fresh catalysts.

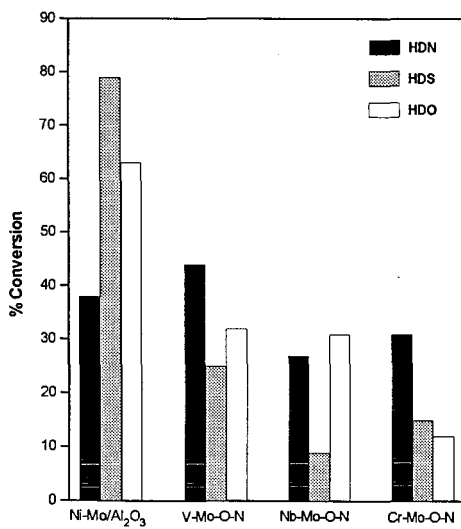


Figure 2. Comparison of the HDN, HDS and HDO activities of the catalysts at 3.1 MPa and 643 K.

SYNTHESIS OF MESOPOROUS MOLECULAR SIEVES AND THEIR APPLICATION FOR CATALYTIC CONVERSION OF POLYCYCLIC AROMATIC HYDROCARBONS

Kondam Madhusudan Reddy and Chunshan Song

Fuel Science Program, Department of Materials Science and Engineering
The Pennsylvania State University, University Park, PA 16802, USA

Keywords: Mesoporous molecular sieves, Al-MCM-41, hydrogenation, isopropylation, hydrocracking, polycyclic aromatic hydrocarbons

INTRODUCTION

Molecular sieves such as Y and ZSM-5 are widely used catalysts in acid-catalyzed reactions for the production of fuels, petrochemicals, and fine chemicals [1-3]. Despite their enormous use as environmentally safe catalysts, they are limited to convert relatively small molecules as their pore size is restricted to micropore size range (usually 1.4 nm). However, with the growing demand of technologies for treating heavier feeds, as well as for synthesizing large molecules for producing commodities and fine chemicals, it is necessary to develop catalysts with wider pores. Recently, Mobil workers have reported a new series of mesoporous molecular sieves [4,5]: MCM-41 is one of the members of this extensive family of mesoporous series possessing a hexagonal array of uniform mesopores. Many reports have since appeared on synthesis and characterization of these new materials [6-10]. However, information on their catalytic activity is still very limited. The pore dimensions of these materials can be tailored (in the range of 1.5-10.0 nm or more) through the choice of surfactant and auxiliary chemicals as templates and the crystallization conditions in the synthesis procedure. The BET surface area of these materials is more than 1000 m²/g with high sorption capacities of 0.7 cc/g and greater. Moreover, these materials can be synthesized in a large range of framework Si/Al ratios and therefore can develop acid sites of different strength. Hence, these new mesoporous aluminosilicate molecular sieves, Al-MCM-41, might open new possibilities in developing catalysts for processing large molecules.

As part of our ongoing project on liquefaction of coal and upgrading of coal liquids, we intend to use these mesoporous aluminosilicates molecular sieves as catalysts to upgrade the coal derived oils to transportation fuels, particularly thermally stable jet fuels. We have studied the synthesis and characterization of these materials [11]. In this paper, we report some of the results on the synthesis and their application for the catalytic conversion of model polycyclic aromatic hydrocarbon compounds.

EXPERIMENTAL

The mesoporous aluminosilicate molecular sieves, Al-MCM-41, were synthesized hydrothermally in 100 ml Teflon lined autoclaves from a mixture of reactants with the following composition: 50SiO₂-xAl₂O₃-2.19(TMA)₂O-15.62(CTMA)Br-3165H₂O; where x=0.5, 1.0 and 2.0. The details of synthesis are given elsewhere [11]. Three series of samples with varying Si/Al ratios, and using three different aluminum sources (aluminum isopropoxide, pseudo boehmite and aluminum sulfate) were synthesized. Some synthesis parameters and their physical characteristics are shown in Table 1. The Al-MCM-41 samples were characterized by chemical analysis, X-ray diffraction, nitrogen adsorption, thermogravimetric analysis, and solid state NMR.

Prior to catalytic runs, the organic template from the as-synthesized solids was removed by calcining the samples in a tubular furnace at 550 °C for one hour in nitrogen and 6 hours in air flow. The calcined samples were exchanged with ammonium nitrate. The protonated form was then obtained by calcining these ammonium exchanged samples at 550 °C for 3 hours. Finally, 3wt% Pt was loaded by wet impregnation, with a required amount of hexachloro platonic acid (Aldrich) solution and the sample in a beaker and evaporating the water at room temperature while stirring it overnight. The Pt loaded samples were then calcined in air at 450 °C for 3 hours.

Mesoporous molecular sieve catalysts were tested for the following reactions: 1) hydrogenation of naphthalene and phenanthrene, 2) isopropylation of naphthalene and 3) hydrocracking of 1,3,5-triisopropyl benzene. A 30 cc stainless-steel tubing bomb batch reactor was used for all the experiments. During the reaction, reactors were heated in a fluidized sand-bath under vertical shaking (240 cycles/min.). All the chemicals were used as supplied. The standard reactor charge was 0.10 g of catalyst and 1.0 g of reactant and other reaction conditions are given in appropriate Tables. At the end of the reaction, the reactor was quenched in cold water. After collecting the reaction products in acetone solution, they were analyzed by GC (Perkin-Elmer 8500) using DB-17 fused silica capillary column. The products were identified by GC-MS (HP).

RESULTS AND DISCUSSIONS

Three series of Al-MCM-41 samples using three different aluminum sources, aluminum isopropoxide, pseudo boehmite (Catapal B), and aluminum sulfate, with Si/Al ratios 50, 25, and 12.5 were synthesized. Details are shown in Table 1. The crystallinity, the incorporation of aluminum in framework and the acidity were studied by XRD, nitrogen sorption, thermal analysis of n-butylamine on samples, ²⁷Al MAS NMR. The results on the synthesis and characterization were reported in our earlier paper [11]. X-ray diffraction patterns showed that all the samples are well crystallized and phase pure with a very strong peak and three weak peaks [1,2]. A typical XRD pattern of Al-MCM-41 is shown in Figure 1. It was observed from nitrogen sorption and XRD studies that the samples prepared with aluminum sulfate are less crystalline compared to the

other two series of samples prepared with different aluminum sources. However, the incorporation of aluminum framework was found to be efficient with aluminum isopropoxide and aluminum sulfate, compared to pseudo boehmite. The aluminum incorporation was characterized by increase in the interplanar spacings from XRD and ^{27}Al MAS NMR. The acidity due to the presence of aluminum in the framework was determined by a thermal analysis of *n*-butylamine on samples. As the aluminum incorporation is higher in samples prepared with aluminum sulfate and aluminum isopropoxide, they have shown better acidity compared to other samples prepared with pseudo boehmite [11].

Catalytic test results in the reactions of hydrogenation of naphthalene and phenanthrene, isopropylation of naphthalene, and hydrocracking of 1,3,5-trisopropylbenzene are presented in Tables 2-5. The initial observation is that they are active in these reactions with good conversions. However, reactions occurred non-selectively as expected, because of the no shape-selective nature of mesoporous materials with wide pores.

In the case of hydrogenation of naphthalene, conversion was almost hundred percent with all the catalysts (see Table 2). There was a large amount of unconverted tetralin observed for the MCM-41 catalysts prepared with pseudo boehmite, whereas for other MCM-41 catalysts the conversion of tetralin to decalin was almost complete. The *t*-decalin/*c*-decalin ratios for all the MCM-41 catalysts are low and in case of the MCM-41 catalyst prepared with pseudo boehmite the ratio is lower compared to the earlier results reported on mordenite [12,13]. These results indicate that in this reaction, the isomerization of *c*-decalin to *t*-decalin probably takes place on acid sites. If that is the case, MCM-41 samples are less acidic as compared to mordenite, hence the *t*-decalin/*c*-decalin ratio is low for these materials. Moreover this ratio is lower for the MCM-41 catalyst prepared with pseudo boehmite because of the poor incorporation of aluminum in the framework, leading to poor acidity.

Table 3 shows the product analyses in hydrogenation of phenanthrene over three different MCM-41 catalysts. They were all active but product selectivities were different compared to earlier results reported [14]; especially sym-octahydroanthracene was formed less, which is an isomerized product from sym-octahydrophenanthrene. This isomerization was believed to be occurring on acid sites [14]. Hence MCM-41 catalysts are not as acidic as other zeolites, especially the MCM-41 catalyst prepared with pseudo boehmite. Similar observations were reported by earlier authors [6,8].

The product analyses of isopropylation of naphthalene using propylene are presented in Table 4. The alkylation over zeolites is known to occur on acid sites. The MCM-41 catalyst prepared with pseudo boehmite was not as active as the other two MCM-41 catalysts. It indicates that the catalyst prepared with pseudo boehmite is less acidic, which again confirms the poor incorporation of aluminum in the framework compared to the other two catalysts. From the product analyses it is also clear that tri and tetra isopropyl naphthalene are formed in large quantities which is a clear indication of non selective nature of these mesoporous materials compared to other zeolites [12, 13]. Non selective nature of these mesoporous materials can also be verified from the α and β substituted product selectivities, which are different from the results obtained on mordenite and Y zeolites [12,13].

Table 3 also shows the effect of Pt loading in the reaction of isopropylation of naphthalene. Both Pt and non Pt containing catalyst showed more or less similar activity, however, selectivities were different. The Pt loaded catalyst yielded more tri and tetra substituted isopropyl naphthalenes, which indicates that the alkylation processes seems to be more efficient with Pt loaded catalysts. This may be due to the bifunctional nature of the catalyst. In zeolite catalysis, it is a known fact that the bifunctional catalysts are more susceptible to the coke formation. In these experiments, because of less reaction time and with limited availability of propylene, deactivation due to coke has not been noticed. However, with continuous supply of propylene for longer reaction times there might be a noticeable difference in catalyst stabilities with and without Pt loading.

In alkylation reactions over zeolites, the type of alkylating agent is known to have an effect. For example, the alkylation with alcohols was found to be less efficient compared with respective alkenes [13]. This could be due to the water formation in the reactions with alcohol and water, that may be suppressing the activity of acid sites. Similar results were observed with these mesoporous molecular sieves. The conversion of naphthalene to isopropyl naphthalenes was found to be less when isopropanol was used as an alkylating agent compared to propylene.

Apart from the hydrogenation and alkylation, hydrocracking is an important reaction in the process of upgrading the heavy oils. Zeolites are known to be good hydrocracking catalysts with good activity, selectivity, and stability. Table 5 shows the results of hydrocracking of bulky molecule, 1,3,5 trisopropylbenzene over mesoporous molecular sieves. Both Pt/Al-MCM-41 and H/Al-MCM-41 were found to be active in this reaction. The main products on H/Al-MCM-41 were mono and di substituted isopropylbenzenes. However, the conversion of Pt loaded catalyst is 100% and products were of lower molecular weight, mainly C_3 - C_5 hydrocarbons. This may be due to the hydrogenation reaction thus leading to further cracking. The conversion of 1,3,5 trisopropylbenzene was negligible without catalyst at similar conditions.

CONCLUSIONS

We observed that mesoporous molecular sieve catalysts are capable of converting bulky polycyclic aromatic hydrocarbons. Due to the large size of mesopores relative to the substrate molecules, however, reactions are found to be occurring non-selectively. The efficiency of the mesoporous

molecular sieves can be significantly different depending on their synthesis method, especially with the source of aluminum used. The catalysts prepared with aluminum isopropoxide and aluminum sulfate were found to be more active compared to the ones prepared with pseudo boehmite. The Pt loading and type of alkylating agent are influential in the conversion of polycyclic aromatic compounds, as reflected in the product selectivities.

ACKNOWLEDGMENTS

We are grateful to Dr. H. H. Schobert for his encouragement and support. Financial support was provided by US Department of Energy and US Air Force. We wish to thank Mr. W. E. Harrison III of USAF and Dr. S. Rogers of DOE for their support, and Dr. A. Schmitz for assistance in performing out catalytic runs and GC analysis.

REFERENCES

1. J. E. Naber, K. P. deJong, W. H. J. Stork, H. P. C. E. Kuipers, and M. F. Post, *Stud. in Surf. Sci. and Catal.*, 84 (1994) 2197.
2. W. F. Hoelderich, M. Hesse, and F. Naumann, *Angew. Chem. Int. Ed. Eng.*, 27 (1988) 226.
3. W. O. Haag, *Stud. in Surf. Sci. and Catal.*, 84 (1994) 1375.
4. C. T. Kresge, M. E. Leonowicz, W. J. Roth, J. C. Vartuli, and J. S. Beck, *Nature*, 359 (1992) 710.
5. J. S. Beck, J. C. Vartuli, W. J. Roth, M. E. Leonowicz, C. T. Kresge, K. D. Schmitt, C. T. W. Chu, D. H. Olson, E. W. Sheppard, S. B. McCullen, J. B. Higgins, and J. C. Schlenker, *J. Am. Chem. Soc.*, 114 (1992) 10834.
6. C.-Y. Chen, S. L. Burkett, H.-X Li and M. Davis, *Microporous Mater.* 2 (1993) 17.
7. C.-Y. Chen, H.-X Li, and M. Davis, *Microporous Mater.*, 2 (1993) 27.
8. A. Corma, V. Fornes, M. T. Navarro and J. Perez-Pariente, *J. Catal.* 148 (1994) 569.
9. M. Janicke, D. Kumar, G. D. Stucky, and B. F. Chmelka, *Stud. in Surf. Sci. and Catal.*, 84 (1994) 243.
10. R. B. Borade, and A. Clearfield, *Catalysis Letters*, 31 (1995) 267.
11. K. M. Reddy, and C. Song, submitted for publication.
12. C. Song, and S. Kirby, *Microporous Mater.*, 2 (1994) 467.
13. A. D. Schmitz, and C. Song, *Fuel Chemistry Division Preprints of 208th ACS Symp.*, Washington D. C., 1994, p.986.
14. C. Song, and K. Moffatt, *Microporous Mater.*, 1994, 2(5), 459.

Figure 1. A typical X-ray powder diffraction pattern of Al-MCM-41 molecular sieves

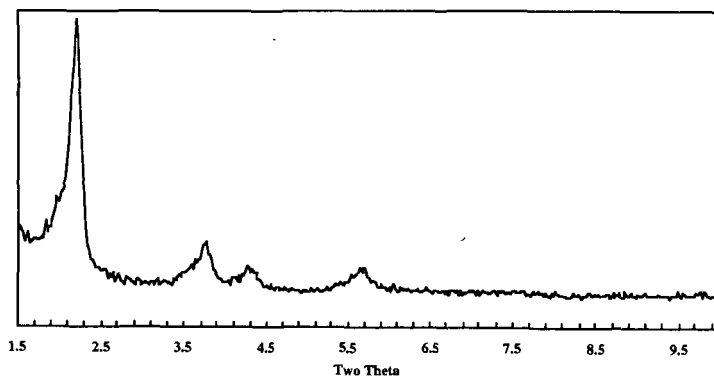


Table 1. Synthesis and physical characteristics of mesoporous molecular sieves

Sample	Source of Al	SiO ₂ /Al ₂ O ₃ (mole ratio)		BET surface Area (m ² /g)	Pore Size from sorption (Å)
		Input	Output		
MRK9a	Al isopropoxide	100	88.4	1147	27.67
MRK9b	Al isopropoxide	50	53.8	1206	28.02
MRK10a	Catapal B	100	95.5	1010	21.92
MRK10b	Catapal B	50	44.3	----	----
MRK11a	Al sulfate	100	164.6	834	25.38
MRK11b	Al sulfate	50	87.4	----	----

Table 2. Naphthalene hydrogenation over Pt/MCM-41 catalysts

Reaction conditions: 0.1 g catalyst, 1.0 g naphthalene, 1000 psi H₂ pressure
200 °C temperature and 1 hour reaction time

Catalyst	naphthalene conv. (%)	Product distribution (wt%)				<i>t</i> - <i>c</i> - decalins
		tetralin	<i>t</i> -decalin	<i>c</i> -decalin	total decalins	
MRK9b	100.0	0.18	33.15	66.67	99.82	0.497
MRK10b	99.7	25.50	18.01	56.48	74.49	0.319
MRK11b	100.0	0.00	32.25	67.75	100.00	0.476

Table 3. Hydrogenation of phenanthrene over Pt/MCM-41 catalysts

Reaction conditions: 0.1 g catalyst, 1.0 g phenanthrene, 1500 psi H₂ pressure
300 °C temperature and 2 hours reaction time

	Product distribution (wt%)		
	MRK9b	MRK10b	MRK11b
Phenanthrene Conv. (%)	79.61	88.00	66.63
1,2,3,4-tetrahydrophenanthrene (THP)	7.03	6.84	14.69
9,10-dihydrophenanthrene (DHP)	41.59	45.47	54.29
sym-octahydrophenanthrene (sym-OHP)	14.82	31.25	13.25
sym-octahydroanthracene (sym-OHA)	16.70	1.40	7.71
unsym-octahydrophenanthrene (unsym-OHP)	15.27	12.99	9.51
tetradecahydrophenanthrenes (TDHP)	3.94	2.03	0.00
sym-OHA/sym-OHP	1.41	0.07	0.09

Table 4. Isopropylation of naphthalene over MCM-41 catalysts

Reaction conditions: 0.1 g catalyst, 1.0 g naphthalene, 150 psi propylene
200 °C temperature and 2 hours reaction time

Catalyst	Product distribution (wt%)			
	H/MRK9b	Pt/MRK9b	Pt/MRK10b	Pt/MRK11b
naphthalene Conv. (%)	92.48	96.62	37.41	90.25
2-isopropyl naphthalene	11.82	9.13	24.59	11.57
1-isopropyl naphthalene	16.27	9.88	56.13	20.24
diisopropyl naphthalenes	42.11	39.25	16.41	42.19
triisopropyl naphthalenes	25.37	34.26	2.51	22.35
tetraisopropyl naphthalenes	4.41	7.46	0.29	3.63
2,6-diisopropyl naphthalenes	3.18	4.87	0.80	2.09
2,7 di isopropyl naphthalenes	3.96	3.83	0.77	2.09

Table 5. Hydrocracking of 1,3,5-triisopropylbenzene over MCM-41 catalysts

Reaction conditions: 0.1 g catalyst, 1.0 g triisopropylbenzene, 1500 psi H₂ pressure
350 °C temperature and 2 hours reaction time

Catalyst	Product distribution (wt%)		
	no catalyst	H/MRK9b	Pt/MRK9b
1,3,5-triisopropylbenzene Conv. (%)	1.02	67.69	100.0
isopropylbenzene	0.00	19.56	0.0
1,3-diisopropylbenzene	94.20	63.09	0.0
1,4-diisopropylbenzene	3.30	7.71	0.0
others, mainly C ₃ -C ₅ hydrocarbons	4.10	9.63	100.0

ZEOLITE-CATALYZED RING-SHIFT ISOMERIZATION OF
sym-OCTAHYDROPHENANTHRENE INTO *sym*-OCTAHYDROANTHRACENE.
EXPERIMENTAL RESULTS AND CALCULATED EQUILIBRIUM COMPOSITIONS

Wei-Chuan Lai, Chunshan Song*, Adri van Duin[§] and J. W. de Leeuw[§]

Fuel Science Program, 209 Academic Projects Building,
The Pennsylvania State University, University Park, Pennsylvania 16802, U.S.A

[§]Division of Marine Biogeochemistry, Netherlands Institute of Sea Research (NIOZ),
P.O. Box 59, 1790 AB Den Burg, The Netherlands

Keywords: Zeolites, isomerization, octahydrophenanthrene, octahydroanthracene

INTRODUCTION

Phenanthrene and its derivatives are abundant in coal-derived liquids from coal carbonization, pyrolysis, and liquefaction; however, they are used in industries only to a limited extent despite of considerable efforts [Song and Schobert, 1993]. On the other hand, their isomers, anthracene and its derivatives such as *sym*-octahydroanthracene (*sym*-OHA), are more useful materials for industrial applications. Anthracene and its derivatives may be used as the starting materials for the manufacturing of anthraquinone (an effective pulping accelerator), pyromellitic dianhydride (PMDA, the monomer for polyimides such as Du Pont's Kapton), and dyestuffs [Song and Schobert, 1993, 1995]. Thus, it is desirable to convert phenanthrenes to anthracenes.

There has been much research on the catalytic hydroprocessing of phenanthrene under high H₂ pressures and at temperatures generally in excess of 623 K [Nakatsuji et al., 1978; Haynes et al., 1983; Salim and Bell, 1984; Lee and Satterfield, 1993; Girgis and Gates, 1994; Landau et al., 1994; Korre et al., 1995]. However, relatively little information about the ring-shift isomerization of phenanthrenes into anthracenes at lower temperatures is available. It has been shown in our earlier exploratory work that some chemically modified mordenites and Y-zeolites may selectively promote the transformation of *sym*-octahydrophenanthrene (*sym*-OHP) into *sym*-OHA [Song and Moffatt, 1993, 1994]. Cook and Colgrove (1994) reported the acid catalyzed isomerization of phenanthrene, anthracene, and *sym*-OHA under FCC conditions (755 K). The objective of this work is to clarify the effects of reaction conditions and catalyst properties on the catalytic isomerization of *sym*-OHP into *sym*-OHA. In addition, the Molecular Mechanics (MM3) [Allinger et al., 1990] calculations were performed to find the equilibrium compositions of *sym*-OHP and *sym*-OHA, and to establish the upper limit of the catalytic conversion. We wish to establish activity and selectivity data that could point to an inexpensive way of making anthracene derivatives from phenanthrene derivatives.

EXPERIMENTAL

The *sym*-OHA and *sym*-OHP chemicals were obtained from Aldrich Chemical Company and TCI America, respectively, and were used as received. Their purities were analyzed in our laboratory using gas chromatography (GC) and gas chromatography-mass spectrometry (GC-MS). The catalysts used in the catalytic isomerization reactions include: two hydrogen mordenites (HML8 and HM30A) and two noble metal loaded mordenites (Pt/HM30A and Pd/HM30A). Pt/HM30A and Pd/HM30A were prepared by incipient wetness impregnation method; i.e., the salt of platinum and palladium were dispersed into the mordenites by incipient wetness impregnation of corresponding aqueous H₂PtCl₆ or H₂PdCl₄ dissolved in hydrochloric acid. The noble metal loading on the support was kept at nominally 6 wt%. The metal-loaded catalysts were calcined in air at 723 K for 2 h after being dried in vacuum oven. The details of the preparation and properties of the catalysts are described elsewhere [Song and Moffatt, 1994; Schmitz et al., 1994].

Catalytic isomerization reactions were carried out in 28-mL horizontal type stainless steel tubing bomb reactors, which were charged with 0.6 mmole of *sym*-OHP or *sym*-OHA (0.112 g), 1 ml of 1,3,5-trimethylbenzene solvent, and 0.2 g of catalyst, at 473–573 K for 0.15–12 h under an initial pressure of 0.79 MPa UHP N₂ or H₂. The uniformity of concentration and temperature inside the reactor was obtained by agitating the reactor vertically at 240 cycles/min. After the reaction, the gas products were collected in a gas bag, and the liquid products were recovered by washing with acetone. The recovered catalyst was stored in a vial for thermogravimetric analysis performed later. The gaseous products were quantitatively analyzed using a Perkin-Elmer Autosystem GC equipped with two detectors, a thermal conductivity detector (TCD) and a flame ionization detector (FID). The liquid products were analyzed on an HP 5890II GC coupled with an HP 5971A Mass Selective Detector (MSD) and quantified by a Perkin-Elmer GC 8500 equipped with an FID. More details for the analytical procedures may be found elsewhere [Song et al., 1994].

RESULTS AND DISCUSSION

Calculated equilibrium compositions from MM3. The equilibrium compositions of *sym*-OHP and *sym*-OHA at three temperatures were calculated to establish the theoretical upper limit of the catalytic conversion. The procedures are as follows. Calculations on the various conformers present in an equilibrium mixture containing only *sym*-OHA and *sym*-OHP were first performed. In order to obtain the raw geometries for the molecules and to find the different conformers present, the DELPHI-molecular mechanics program was used with the MM3 force field. The obtained minimized geometries were used as starting points for the MM3 program, using the MM3 force field (both the 1992 versions). Only slight differences were found between the optimized DELPHI- and MM3-geometries. Five and six different conformers were found for *sym*-OHA and *sym*-OHP,

respectively, as shown in Table 1. Table 1 also shows the calculated heats of formation and entropies for the different conformations of *sym*-OHA and *sym*-OHP at 298 K. The literature value of the heat of formation of *sym*-OHA is -8.89 kcal/mol [Pedley et al., 1986]. The good agreement between the literature value (-8.89 kcal/mol) and the calculated one (-9.17 kcal/mol, in Table 1) indicates that the MM3 force field should be applicable to problems like these. From these data, the Gibbs free energy of *sym*-OHA and *sym*-OHP at 298 K could be obtained. In similar fashion, the Gibbs free energies of these compounds at 473, 523, and 573 K may be calculated by correcting the heats of formation and entropies in Table 1 for temperatures. From these free energies, the equilibrium composition of the *sym*-OHA/*sym*-OHP mixture was calculated. It should be noticed that one may get different MM3 calculation results from using different estimated thermodynamic parameters of *sym*-OHA and *sym*-OHP. It was found that the error in the MM3 calculations using current parameters for such kind of mixture compositions is about 10%. The calculated mixture compositions will be presented later and compared with experimental data following the presentation of experimental results.

Effectiveness of HML8. HML8 was studied more extensively than other catalysts in this work, because it was found to be the best among several zeolitic catalysts in our previous work at 523 K for 2 h [Song and Moffatt, 1993, 1994]. Table 2 presents the results of *sym*-OHP isomerization over HML8 with *sym*-OHP as the starting material at three different temperatures (473, 523, and 573 K) under N₂ environment. The purity analysis results of the starting material was also presented in Table 2. It can be seen that the as-received reactant contains about 91% of *sym*-OHP, 2.9% of *sym*-OHA, 5.5% in total of various hydrogenated phenanthrenes (*asym*-OHP, 9,10-DHP, 1,2,3,4,4a,10a-HHP, and 1,2,3,4-THP), and 0.6% of other impurities. The purity analysis is important, because without this information it is possible that impurities are mistaken as products. The reactivities of 9,10-DHP and 1,2,3,4,4a,10a-HHP will be briefly discussed first. 9,10-DHP does not react to a great extent except under severe conditions, e.g., 573 K for 1 h; on the other hand, 1,2,3,4,4a,10a-HHP reacts quickly even at a lower temperature, 473 K. The main reaction of 9,10-DHP, which accounts for about 2.7% of the starting reactant, was believed to be dehydrogenation to phenanthrene under current reaction conditions. The supporting evidence is from the fact that the sum of 9,10-DHP and phenanthrene was relatively constant (about 2.8) for most of the reaction conditions. Other researchers also suggested the hydrogenation of 9,10-DHP to 1,2,3,4-THP [Lemberton and Guisnet, 1984] and *asym*-OHP [Nakatsuji et al., 1978]; however, these hydrogenation reactions are less likely under the current reaction conditions judging from the deficiency of hydrogen and the overall product distribution of 1,2,3,4-THP and *asym*-OHP. To verify this, experiments need to be performed with 9,10-DHP as the sole reactant. For 1,2,3,4,4a,10a-HHP, the main reactions were believed to include dehydrogenation to 1,2,3,4-THP, and ring-contraction isomerization and ring-opening cracking.

The major reaction of interest in this work is the isomerization of *sym*-OHP to *sym*-OHA; Table 2 shows that HML8 was an effective catalyst for this reaction because it could afford over 90% selectivity with reasonable conversion (about 50%). In order to approach equilibrium conditions, relatively long residence times have been employed, e.g., 12 h at 473 K, 4 h at 523 K, and 1 h at 573 K. From Table 2, the reactions seemed to have reached the asymptotic equilibrium after 12 h at 473 K, 2 h at 523 K, and 0.25 h at 573 K. In other words, the yield of *sym*-OHA reached its maximum at those reaction conditions, and longer reaction times at 523 K and 573 K only served to decrease the *sym*-OHA yield because of enhanced competitive side-reactions or secondary reactions such as ring-opening cracking and subsequent dealkylation (to form mainly alkyltetralins), conventional ring-contraction isomerization, and dehydrogenation. The selectivity towards *sym*-OHA suffered severely when the reaction temperature was increased to 573 K, when side-reactions became significant.

Table 3 compares the pseudo-equilibrium yields from MM3 calculations and experimental results at three temperatures. There exists discrepancy between the calculated data and the experimental results. The MM3 calculations indicate that the reaction temperature has a moderate effect on the equilibrium ratio of *sym*-OHA to *sym*-OHP. For example, the ratio changes from 2.56 to 1.95 when the temperature is increased from 473 K to 573 K. However, the experiments show that although the reaction temperature affects the reaction rate and selectivity, the equilibrium ratio is not sensitive to the reaction temperature. For example, the equilibrium ratios are all close to 1.3 for the temperature range studied. Table 3 shows that the pseudo-equilibrium yields of *sym*-OHA from experiments are considerably lower than the calculated equilibrium yield from MM3 method. There might be some explanations for the discrepancy. The calculation assumes that *sym*-OHP and *sym*-OHA are the only reacting species in the reaction system. However in the real experimental system since there are other reactants as well as by-products, the actual equilibrium state now depends on more simultaneous chemical reactions. For the current reaction system, at higher temperatures, e.g., 523 K and 573 K, there are significant side reactions as can be seen from the smaller *sym*-OHA selectivity or the decreasing sum of *sym*-OHP and *sym*-OHA. Other simultaneous reactions might include the reactions due to the solvent used (1,3,5-trimethylbenzene) as well. Since many reactions are involved, the composition is a resultant of all the operative reactions and is determined by the thermodynamic equilibrium for the total system. In short, the presence of such simultaneous reactions have shifted the equilibrium state of *sym*-OHA and *sym*-OHP.

Some experiments using pure *sym*-OHA (rather than *sym*-OHP) as starting material were also performed to check the reversibility of the ring-shift isomerization and to confirm the experimentally obtained pseudo-equilibrium composition (Table 3). The results of *sym*-OHA isomerization over HML8 with *sym*-OHA as the starting material at three temperatures under N₂ environment are given

in Table 4. The results demonstrate the reversibility of the ring-shift isomerization. Besides, it was shown again that HML8 was quite selective for the ring-shift isomerization except under severe conditions. From Table 4, the reactions seemed to have reached pseudo-equilibrium after 4 h at 473 K, 0.5 h at 523 K, and 0.15 h at 573 K judging from the fact that the yield of *sym*-OHP reached its maximum at those reaction conditions. The pseudo-equilibrium compositions of *sym*-OHA and *sym*-OHP and their ratios reported in Table 4 are very close to those reported earlier (see Tables 2 and 3); for example, the equilibrium ratio is not sensitive to the reaction temperature and is close to 1.3. From the data in Tables 2-4, on the basis of reaction rate alone, it appears desirable to operate the reaction at a high temperature level such as 573 K. However, an examination of the reaction selectivity reveals that the selectivity towards *sym*-OHA drops rapidly at 573 K due to significant side-reactions. Taking both rate and selectivity into consideration, it seems that 523 K for 0.5 h might be the desirable condition for the *sym*-OHP isomerization over HML8.

Effectiveness of HM30A. HM30A was used to examine the possible effect of dealumination on the ring-shift isomerization in comparison to HML8. The $\text{SiO}_2/\text{Al}_2\text{O}_3$ molar ratios of HML8 and HM30A are 17 and 35, respectively. Table 5 presents the results of *sym*-OHP isomerization over HM30A with *sym*-OHP as the starting material at two temperatures (473 and 523 K) under N_2 . Tables 2 and 5 suggest that both catalysts reacted comparably near the pseudo-equilibrium condition at 473 K for 12 h; this could be seen from the similar conversion level, selectivity, and *sym*-OHA to *sym*-OHP ratio. However, at 523 K, they behaved slightly different. The H-mordenites with relatively larger $\text{SiO}_2/\text{Al}_2\text{O}_3$ ratio, i.e., HM30A, seem to exhibit higher activity for *sym*-OHP conversion but lower selectivity towards *sym*-OHA plus THA. The comparison of selectivity could be seen at similar conversion level, 51.9%, where the selectivity is 91.9% and 83.5% for HML8 and HM30A, respectively. In short, HM30A shows promising results at 473 K in terms of both activity and selectivity, but is not as selective as HML8 at 523 K. More experiments with additional catalysts will be needed to clarify the effect of dealumination on the ring-shift isomerization.

Effectiveness of Pt/HM30A and Pd/HM30A. The motivation of using these two noble metal loaded mordenites on the ring-shift isomerization comes from the promising activity and selectivity results of HM30A at 473 K as well as our study on conformational isomerization of *cis*-decalin using the same two catalysts [Lai and Song, 1995]. It was found that Pt- and Pd-loaded mordenites are very effective catalysts under H_2 atmosphere for the conformational isomerization of *cis*-decalin even at 473 K. Because of their high activity and selectivity on the isomerization of naphthalene derivatives, Pt/HM30A and Pd/HM30A were also used in this study. Table 6 presents the results of isomerization over these two catalysts with *sym*-OHP or *sym*-OHA as the starting material at 473 K under 0.79 MPa of H_2 or N_2 .

The effect of noble metals can be seen by comparing the results of HM30A (PS42, in Table 5) and those of Pt- and Pd-loaded HM30A (PS47 and PS48, respectively, see Table 6). Mordenites loaded with noble metal exhibits much higher activity but lower selectivity towards hydrogenated anthracenes. The activity for *sym*-OHP conversion is: Pd/HM30A > Pt/HM30A > HM30A. The lower selectivity towards *sym*-OHA for both Pd/HM30A and Pt/HM30A is due to the significant dehydrogenation reactions to form THA and THP or even phenanthrene under N_2 environments. The results are not beyond expectation because both Pt and Pd are well known active metals for dehydrogenation and hydrogenation. Hydrogenation was not apparent because of the H_2 deficient environment, since reactions were performed under N_2 . The dehydrogenation activity drops in the order Pd > Pt.

As can be seen from Table 6, changing the gas environment from N_2 to H_2 significantly affects the final product distribution because the dehydrogenation under N_2 was replaced with hydrogenation under H_2 . Figure 1 presents the temporal plots of major products from *sym*-OHP isomerization using Pt/HM30A and Pd/HM30A at 473 K under excess H_2 (8 mmole). Figure 1 provides information about the reaction pathways. For example, for the catalyst Pt/HM30A, it can be seen that *sym*-OHA was the primary product; its yield reached a maximum at 0.3 h and then decreased due to enhanced hydrogenation. On the other hand, PHA and PHP appeared to be the secondary products resulting from hydrogenation of OHA or OHP. Table 6 shows that for Pt/HM30A after 0.3-h reaction time, the ratio of *sym*-OHA to *sym*-OHP approached a constant value of 1.28, which was very close to the pseudo-equilibrium mole ratio determined from the study of HML8 and HM30A. All these results suggest that *sym*-OHA formation be the major primary reaction and hydrogenation of OHP and OHA did not occur until *sym*-OHA and *sym*-OHP reached pseudo-equilibrium. In addition, it was demonstrated that Pt/HM30A shows promising activity and selectivity at 473 K under H_2 . Optimal products may be reached in a short period of time, e.g., 0.15-0.3 h. Longer reaction time under H_2 environment beyond the pseudo-equilibrium stage is not beneficial to the production of *sym*-OHA, due to pronounced hydrogenation to form deeper hydrogenation products such as perhydrophenanthrene and perhydroanthracene.

The other noble metal catalyst, Pd/HM30A, showed slightly different results. Pd again shows higher activity but lower selectivity towards hydrogenated anthracenes. Its superior hydrogenation ability might have changed the reaction pathways. For example, instead of being a secondary product only, PHP might as well be a primary product too. The hydrogenation and isomerization reactions might have proceeded in parallel instead of in series for Pd/HM30A under H_2 environment. The supporting evidence is that the ratio of *sym*-OHA to *sym*-OHP did not approach the pseudo-equilibrium mole ratio until very late in the reaction when *sym*-OHP was almost completely consumed. The results seem to suggest that such strong ability of dehydrogenation and

hydrogenation might make Pd a less favorable catalyst for the ring-shift isomerization of *sym*-OHP. The results of *sym*-OHA isomerization over Pt/HM30A and Pd/HM30A with *sym*-OHA as the starting material under H₂ environment, are also given in Table 6. The results demonstrate the reversibility of the ring-shift isomerization and the important role of deeper hydrogenation.

SUMMARY

The MM3 calculations were performed to find the equilibrium compositions of *sym*-OHP and *sym*-OHA and were compared to experimental results using four catalysts including HML8, HM30A, Pt/HM30A, and Pd/HM30A. The MM3 calculations showed a moderate effect of the reaction temperature on the equilibrium ratio of *sym*-OHA to *sym*-OHP. However, the experiments showed that although the reaction temperature affected the reaction rate and selectivity, the equilibrium ratio was not sensitive to the reaction temperature. The presence of simultaneous side reactions was believed to have shifted the equilibrium state. The rate and selectivity of the isomerization reactions depended on both the metal and support type of the catalysts, but the equilibrium ratio was not sensitive to the catalysts used and was close to a constant value of 1.3. The activity for *sym*-OHP conversion is: Pd/HM30A > Pt/HM30A > HML8 ≈ HM38. Longer reaction time beyond the pseudo-equilibrium stage was not beneficial to the production of *sym*-OHA, especially for Pd/HM30A and Pt/HM30A due to the pronounced hydrogenation or dehydrogenation. Pt/HM30A showed promising activity and selectivity at 473 K under H₂ with optimal reaction time of 0.15–0.3 h. The desirable condition for HML8 was 523 K for 0.5 h. HM30A showed promising results at 473 K, but was not as selective as HML8 at 523 K. Too strong an ability of dehydrogenation and hydrogenation might make Pd/HM30A a less favorable catalyst for the ring-shift isomerization of *sym*-OHP.

ACKNOWLEDGMENTS

We are grateful to Dr. T. Golden and Dr. V. Schillinger for providing the mordenites samples, and to Dr. A. Schmitz of PSU for preparing the noble metal catalysts. C.S. would like to thank Prof. H. H. Schobert and Prof. P. B. Weisz for their encouragement.

REFERENCES

- Allinger, N. L.; Li, F.; Yan, L.; Tai, J. C. J. *Computational Chem.* **1990**, *11*, 868–895.
- Cook, B. R.; Colgrove, S. G. *Prepr.-Am. Chem. Soc., Div. Pet. Chem.* **1994**, *39* (3), 372–378.
- Girgis, M. J.; Gates, B. C. *Ind. Eng. Chem. Res.* **1994**, *33*, 1098–1106.
- Haynes, H. W. Jr.; Parcher, J. F.; Helmer, N. E. *Ind. Eng. Chem. Process Des. Dev.* **1983**, *22*, 401–409.
- Korre, S. C.; Klein, M. T.; Quann, R. J. *Ind. Eng. Chem. Res.* **1995**, *34*, 101–117.
- Lai, W.-C.; Song, C. *Prepr.-Am. Chem. Soc., Div. Fuel Chem.* **1995**, *40*, in press.
- Landau, R. N.; Korré, S. C.; Neurock, M.; Klein, M. T. In *Catalytic Hydroprocessing of Petroleum and Distillates*. M. C. Oballa and S. S. Shih, Eds., Marcel Dekker, Inc.: New York, **1994**, pp421–432.
- Lee, C. M.; Satterfield, C. N. *Energy & Fuel* **1993**, *7*, 978–980.
- Lemberton, J.-L.; Guisnet, M. *Appl. Catal.* **1984**, *13*, 181–192.
- Nakatsui, Y.; Kubo, T.; Nomura, M.; Kikkawa, S. *Bull. Chem. Soc. Jpn.* **1978**, *51*, 618–624.
- Pedley, J. B.; Naylor, R. D.; Kirby, S. B. *Thermochemical Data of Organic Compounds*. **1986**, Chapman and Hall: London.
- Salim, S. S.; Bell, A. T. *Fuel* **1984**, *63*, 469–476.
- Schmitz, A. D.; Bowers, G.; Song, C. In *Advanced Thermally Stable Jet Fuels*. Technical Report, U.S. Department of Energy, DE-FG22-92PC92104-TPR-9, October **1994**, H. H. Schobert et al., Eds., pp37–42.
- Song, C.; Moffatt, K. *Prepr.-Am. Chem. Soc., Div. Pet. Chem.* **1993**, *38* (4), 779–783.
- Song, C.; Schobert, H. H. *Fuel Processing Technology* **1993**, *34*, 157–196.
- Song, C.; Lai, W.-C.; Schobert, H. H. *Ind. Eng. Chem. Res.* **1994**, *33*, 534–547.
- Song, C.; Moffatt, K. *Microporous Materials* **1994**, *2*, 459–466.
- Song, C.; Schobert, H. H. *Prepr.-Am. Chem. Soc., Div. Fuel Chem.* **1995**, *40* (2), 249–259.

Table 1. The calculated heats of formation and entropies at 298 K

Conformation	ΔH_f (kcal/mole)	S (cal/mol·K)
<i>sym</i> -octahydroanthracene		
double chair (symmetric)	-9.17	105.54
double chair (asymmetric)	-9.17	105.54
boat-chair	-6.08	109.27
double boat (symmetric)	-3.00	107.48
double boat (asymmetric)	-3.03	107.47
<i>sym</i> -octahydrophenanthrene		
double chair (symmetric)	-7.98	106.33
double chair (asymmetric)	-7.57	106.89
boat-chair I	-5.05	108.78
boat-chair II	-4.83	108.76
double boat (symmetric)	-1.72	108.82
double boat (asymmetric)	-1.62	108.71

Table 2. *sym*-OHP isomerization over HML8 with *sym*-OHP as the starting material

Expt. no.	Temp. (K)	Time (h)	Products (wt% of feed)								X ^c (%)	Sel. ^d (%)	Ratio <i>sym</i> -OHA/ <i>sym</i> -OHP
			<i>sym</i> -OHA	THA ^a	<i>sym</i> -OHP	<i>asym</i> -OHP ^a	9,10-DHP ^a	HHP ^a	THP ^a	Phen. ^a	Others ^b		
		0.0 ^e	2.90		91.04	0.32	2.67	1.74	0.77	0.07	0.50		0.03
PS6	473	0.50	14.70	0.11	77.99	0.35	2.78	0.43	1.40	0.15	2.10	91.2	0.19
PS8	473	1.00	28.10	0.21	64.38	0.34	2.59	0.52	1.20	0.20	2.45	95.3	0.44
PS9	473	2.00	42.30	0.26	50.35	0.36	2.57	0.22	1.16	0.20	2.58	97.5	0.84
PS14	473	4.00	49.64	0.33	42.25	0.35	2.60	0.04	1.21	0.17	3.41	96.5	1.17
PS15	473	6.00	51.44	0.45	40.20	0.33	2.54	0.04	1.29	0.16	3.55	96.4	1.28
PS41	473	12.0	52.15	0.42	40.07	0.35	2.62	0.04	1.24	0.17	2.94	97.4	1.30
PS10	523	0.25	35.90	0.48	55.62	0.36	2.53	0.51	1.21	0.20	3.18	94.5	0.65
PS1	523	0.50	48.76	1.00	40.70	0.30	2.53	0.12	1.67	0.33	4.59	93.1	1.20
PS3	523	2.00	49.32	1.30	39.11	0.22	2.23	0.03	1.65	0.49	5.65	91.9	1.26
PS18	523	4.00	47.74	1.56	38.42	0.13	1.95		1.88	0.75	7.57	88.2	1.24
PS13	573	0.15	44.96	1.21	41.20	0.20	2.20	0.12	2.03	0.60	7.48	86.8	1.09
PS7	573	0.25	45.50	1.95	36.58	0.10	1.50	0.27	2.26	0.80	11.04	84.5	1.24
PS4	573	0.50	42.67	2.13	35.64	0.15	1.75	0.12	3.70	1.12	12.72	75.6	1.20
PS5	573	1.00	33.62	3.20	27.19	0.10	0.80	0.12	3.98	1.53	29.46	53.1	1.24

^a THA = 1,2,3,4-tetrahydroanthracene; *asym*-OHP = 1,2,3,4,4a,9,10,10a-octahydrophenanthrene;

9,10-DHP = 9,10-dihydrophenanthrene; HHP = 1,2,3,4,4a,10a-hexahydrophenanthrene;

THP = 1,2,3,4-tetrahydrophenanthrene; Phen. = phenanthrene.

^b Others include products of ring-contraction isomerization and ring-opening cracking and subsequent dealkylation.

^c X = conversion of *sym*-OHP (weight % of feed).

^d Selectivity to *sym*-OHA plus THA, defined as the percentage of *sym*-OHP conversion.

^e This row presents the purity of as-received *sym*-OHP.

Table 3. Pseudo-equilibrium composition of the *sym*-OHA/*sym*-OHP mixture

Temperature (K)	MM3 calculation		Experimental data ^a	
	OHA : OHP	Ratio	OHA : OHP ^b	Ratio
473	71.9% : 28.1%	2.56	52.2% : 40.1%	1.30
523	68.7% : 31.3%	2.19	49.3% : 39.1%	1.26
573	66.1% : 33.9%	1.95	45.5% : 36.6%	1.24

^a Data from Table 2: 12 h at 473 K, 2 h at 523 K, and 0.25 h at 573 K.

^b Other products make up the remainder.

Table 4. *sym*-OHA isomerization over HML8 with *sym*-OHA as the starting material

Expt. no.	Temp. (K)	Time (h)	Products (wt% of feed)						X ^a (%)	Sel. ^b (%)	Sel. ^c (%)	Ratio <i>sym</i> -OHA/ <i>sym</i> -OHP
			<i>sym</i> -OHA	THA	<i>sym</i> -OHP	HHP	THP	Others				
PS27	473	1.00	61.44	0.23	35.52	0.18	0.08	2.54	38.6	92.1	92.8	1.73
PS28	473	4.00	55.07	0.40	41.22	0.14	0.10	3.07	44.9	91.7	92.3	1.34
PS33	473	8.00	55.42	0.39	40.56	0.16	0.09	3.38	44.6	91.0	91.5	1.37
PS25	523	0.25	56.18	0.67	37.95	0.25	0.20	4.75	43.8	86.6	87.6	1.48
PS26	523	0.50	53.36	0.76	40.69	0.27	0.30	4.62	46.6	87.2	88.5	1.31
PS32	523	2.00	51.38	1.04	39.91	0.19	0.57	6.91	48.6	82.1	83.6	1.29
PS29	573	0.15	50.91	1.26	39.15	0.23	0.92	7.53	49.1	79.8	82.1	1.30
PS30	573	0.25	45.97	1.67	36.39	0.18	1.57	14.22	54.0	67.4	70.6	1.26
PS31	573	0.50	40.65	2.28	32.36	0.16	2.52	22.03	59.4	54.5	59.0	1.26

^a X = conversion of *sym*-OHA (weight % of feed, *sym*-OHA).

^b Selectivity to *sym*-OHP, defined as the percentage of *sym*-OHA conversion.

^c Selectivity to *sym*-OHP plus HHP and THP, defined as the percentage of *sym*-OHA conversion.

Table 5. *sym*-OHP isomerization over HM30A with *sym*-OHP as the starting material

Expt. no.	Catalyst type	Temp. (K)	Time (h)	Products (wt% of feed)								X ^a (%)	Sel. ^b (%)	Ratio <i>sym</i> -OHA/ <i>sym</i> -OHP
				<i>sym</i> -OHA	THA	<i>asym</i> -OHP	9,10-DHP	HHP	THP	Phen.	Others			
			0.00 ^c	2.90		91.04	0.32	2.67	1.74	0.77	0.50			0.03
PS42	HM30A	473	12.00	52.57	0.64	39.03	0.30	2.39	0.14	1.40		52.0	96.7	1.35
PS16	HM30A	523	0.50	44.47	1.72	39.19	0.21	1.55	0.14	2.34	1.05	9.33	83.5	1.13
PS17	HM30A	523	1.00	42.87	2.06	35.90	0.12	1.20	0.11	2.54	1.29	13.91	76.2	1.19

Table 6. Ring-shift isomerization over noble metal loaded mordenites with *sym*-OHP or *sym*-OHA as the starting material at 473 K under 0.79 MPa of H₂ or N₂

Catalyst	Pt/HM30A							Pd/HM30A				
Time (h)	0.00 ^f	0.30	0.15	0.30	1.00	2.00	2.00	0.30	0.15	0.30	2.00	2.00
Starting reactant		OHP	OHP	OHP	OHP	OHP	OHA	OHP	OHP	OHP	OHP	OHA
0.79-MPa N ₂ or H ₂		N ₂	H ₂	H ₂	H ₂	H ₂	H ₂	N ₂	H ₂	H ₂	H ₂	H ₂
Expt. no.		PS47	PS45	PS43	PS36	PS39	PS38	PS48	PS46	PS44	PS37	PS40
Products (wt% of feed)												
<i>sym</i> -OHA	2.90	42.52	47.82	48.07	40.62	34.76	37.21	38.10	30.17	26.53	8.01	4.03
THA		7.77				0.20	0.05	9.00				
PHA ^a			2.57	3.70	9.94	12.63	12.06		10.00	16.72	33.77	40.11
<i>sym</i> -OHP	91.04	33.07	40.16	38.28	31.72	27.13	29.44	29.99	36.17	24.80	6.47	3.21
<i>asym</i> -OHP	0.32	1.14	2.62	3.53	3.67	3.65	3.61	1.95	4.23	3.47	1.55	0.82
9,10-DHP	2.67	0.71	0.01		0.03	0.13	0.14	1.47	0.01			
HHP	1.74	0.02	0.02	0.06	0.06	0.03		0.02	0.02	0.08		
THP	0.77	10.45			0.12	0.91	0.36	12.66				
Phenanthrene	0.06	3.35						5.20				
PHP ^a		0.08	5.25	5.06	11.53	15.12	13.24	0.07	16.94	25.34	45.85	47.40
Others	0.50	0.89	1.55	1.30	2.31	5.44	3.89	1.54	2.46	3.06	4.35	4.43
X (%) ^b		58.0	50.9	52.8	59.3	63.9	62.8	61.1	54.9	66.2	84.6	96.0
Selectivity ^c (%)		81.7	93.3	92.6	80.3	69.9		72.4	67.9	60.9	46.0	
Selectivity ^d (%)							46.9					3.3
Selectivity ^e (%)							74.5					53.6
<i>sym</i> -OHA/ <i>sym</i> -OHP	0.03	1.29	1.19	1.26	1.28	1.28	1.26	1.27	0.83	1.07	1.24	1.26

^a PHA = perhydroanthracene; PHP = perhydrophenanthrene.

^b X = conversion of *sym*-OHP or *sym*-OHA (weight % of feed).

^c Selectivity to *sym*-OHA plus THA and PHA, defined as the percentage of *sym*-OHP conversion.

^d Selectivity to *sym*-OHP, defined as the percentage of *sym*-OHA conversion.

^e Selectivity to hydrogenated phenanthrenes, defined as the percentage of *sym*-OHA conversion.

^f This column presents the purity of as-received *sym*-OHP.

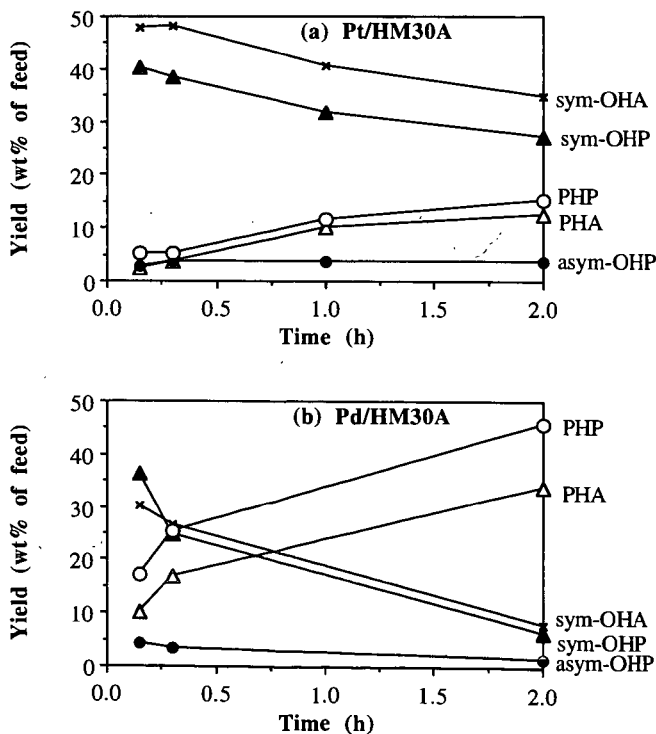


Figure 1. Temporal plots of major products from *sym*-OHP isomerization at 473 K under H₂.

ADAMANTANES FROM PETROLEUM, WITH ZEOLITES

L. Deane Rollmann, Larry A. Green, Robert A. Bradway,
and Hye Kyung C. Timken

Mobil Research and Development Corporation, Paulsboro Research
Laboratory, PO Box 480, Paulsboro, NJ 08066

Keywords: Adamantane, zeolite, hydrocracking

ABSTRACT

Circumstances have been found under which adamantanes are significantly concentrated and, it is believed, formed in a petroleum refinery, and catalysts have been identified which are effective in recovering these compounds from a complex mixture of similarly boiling hydrocarbons. In an example detailed below, nearly 10% adamantanes, largely methyl-substituted derivatives, were found in and isolated from a refinery stream by selectively removing the non-adamantanes with a Pt-containing zeolite Beta catalyst.

INTRODUCTION

Despite their discovery in the early 1930's in the heavy Hodonin crude of eastern Europe (1), adamantanes occasioned relatively little interest until a facile chemical synthesis was reported, in 1957 (2). Although notable as part of the diamondoids found in certain natural gas condensates (3, 4), adamantanes appear never to exceed about 0.02-0.04% in crudes (5), a concentration too low for economic recovery.

Unsubstituted adamantane was first prepared by the AlCl_3 -catalyzed isomerization of hydrogenated cyclopentadiene dimer, tetrahydrocyclopentadiene (THDCP), an approach which was quickly expanded to include a number of methyl adamantanes (6). Solid acid catalysts such as silica-alumina (7) and HY zeolite (8) were also able to effect the THDCP-adamantane transformation, but none was apparently competitive in yield and stability with AlCl_3 and/or AlBr_3 .

In the present context, the most significant post-1960 advance in the synthesis of adamantanes was a change in feedstock, from THDCP to a variety of tricyclic perhydroaromatics (9). The effective catalyst was an AlX_3 -HX-hydrocarbon mixture, where X = chloride or bromide. The products were methyl or polymethyl adamantanes, each having the same molecular weight as the feed tricycloalkane, often in a yield of some 60% or more. An example is shown in Figure 1. Subsequent work showed that numerous acid catalysts would convert tricyclic naphthenes (tricycloalkanes) into methyl adamantanes, namely, chlorinated $\text{PV}/\text{Al}_2\text{O}_3$ (11), silica-alumina (12), silica-alumina with Group VIII metal (13), and REX/REY, usually with Group VIII metal (14).

Based on the chemical synthesis work, potential precursors to adamantanes exist in a crude in the form of high boiling polycyclic naphthenes and aromatics. In a modern refinery, these precursors, boiling above about 300°C, commonly encounter acid catalysts in both a fluid catalytic cracking (FCC) unit and in a hydrocracker (HDC). Thus, the present experiments focused on HDC recycle streams.

EXPERIMENTAL

Two zeolites were used in the experiments, Beta (15) and "ultrastable" Y (USY) (16). Framework $\text{SiO}_2/\text{Al}_2\text{O}_3$ ratios were approximately 50 for Beta and 200 for "ultrastable" Y (USY). For better comparison with the USY, a sample of the Beta catalyst was dealuminated to a similar framework $\text{SiO}_2/\text{Al}_2\text{O}_3$ ratio and designated "low activity" Beta (LoAct-Beta). In the experiments, all catalysts contained alumina binder, all were 24/60 mesh, all contained 0.5% Pt or Pd, and all were brought to initial operating conditions (232°C and 2.5 mPa) in flowing hydrogen. The experiments were conducted in a downflow tubular reactor, at 2.5 mPa, with a H_2 /hydrocarbon (H_2/HC) mole ratio of 3 - 4, at temperatures of 230° - 330°C, and at 1 - 4 WHSV (weight hourly space velocity). Day-to-day catalyst aging was not significant in these experiments.

Gas chromatography (gc) results were obtained with a 60m DB-1 capillary column (J&W Scientific, 0.25 mm id, 0.25 μ film). The gc-mass spec analyses were performed on a Kratos Model MS80RFA, with a Hewlett Packard Series II 5890 gc and a 30m DB-5HT column (0.32 mm id, 0.1 μ film). Ionization was by electron impact.

RESULTS AND DISCUSSION

Refinery streams selected for testing are shown in Table 1. Since most methyl and ethyl adamantanes boil between 180°C and 240°C, streams were selected to bracket that range, namely, a 135° - 210°C HDC heavy naphtha, a 175° - 375°C HDC recycle stream, a 175° - 260°C portion of the HDC recycle stream, and a 120° - 245°C hydrotreated kerosene, all from a refinery sourced largely with heavy crude. In addition, a 175° - 290°C analog of the above HDC recycle stream was obtained from a refinery sourced with light, conventional crude. Crude type was a consideration since, in general, heavy crudes are enriched in polycyclic alkanes relative to light, "conventional" crudes (17).

Isolation of adamantanes. The adamantanes shown in Figure 2a were obtained when the heavy crude HDC recycle stream described in Table 1 was passed over the Pt/LoAct-Beta catalyst at 325°C and 1.2 WHSV. Approximately 90% of the feed, which boiled above 175°C, was converted to lower boiling, mostly gasoline-range hydrocarbon. The remaining high-boiling material contained over 70% adamantane and methyl adamantanes. Gas chromatography (gc) and gc-mass spec showed the presence of diamantanes as well.

Comparison of Figures 2a and 2b showed the striking similarity between this potential refinery product and a mixture of naturally occurring adamantanes recovered from a deep gas condensate (4). Despite the understandable difference in carbon-number and isomer distribution, every major peak in the product from Pt/LoAct-Beta corresponded to a peak in the condensate adamantanes. Gc-mass spec confirmed the molecular weights indicated in Figure 2.

Adamantanes free from diamantanes were obtained by using a lower boiling portion of the HDC recycle stream. When the above experiments were repeated with a 175° - 260°C fraction of the HDC stream, this time using the high-activity Pt/Beta (50 SiO₂/Al₂O₃ ratio) at 260°C and 2.0 WHSV, conversion to lighter hydrocarbon was 86%. The product "mixed methyl adamantanes" (MMA's) were virtually indistinguishable from those obtained with full-range HDC recycle, and material boiling higher than the MMA's (e.g., diamantanes) was < 0.1% of the product.

MMA yield was substantial. With the 175° - 260°C feed, 9.1 g of MMA was obtained from 100 g of feed, representing 32% of the 3RN's. A second experiment, under slightly milder conditions, yielded 9.3 g of MMA, or 33%. The product MMA, separated from lower boiling hydrocarbons by distillation, was a colorless liquid with a density of 0.89 g/cc.

That the MMA's were associated with the recycle stream was further affirmed by a "blank" experiment with Pt/Beta and the 135° - 210°C HDC heavy naphtha, at 255°C and 1.9 WHSV. The product containing only 0.6% MMA's, essentially all of which were bridgehead-methyl isomers boiling between 180° and 200°C.

Yield of adamantanes was much lower in a refinery operating on light, conventional crude. When a 1:1 blend of the light crude HDC recycle and the HDC heavy naphtha in Table 1 was processed over high-activity Pt/Beta, the product contained only 0.9 % MMA's.

A final experiment was conducted to probe for adamantanes in the crude supply to the heavy crude refinery. The feed was the hydrotreated kerosene, a stream which had never contacted a zeolite catalyst but which, given its 120° - 245°C boiling range, should contain any MMA's in the crude. As shown in Table 1, it analyzed 0.6% 3RN's. When processed over both Pd/Beta and Pt/Beta, the products contained 0.4% MMA's. This result strongly suggests that, while some portion of adamantanes did enter the refinery with the crude, the bulk was being formed, either in the HDC (and possibly FCC) unit or in these noble metal/zeolite experiments.

Formation of adamantanes. A model compound was used to probe possible formation of adamantanes over Pt and Pd/Beta catalysts under the conditions of these experiments. Based on the adamantane literature and on commercial

availability, perhydrofluorene (PHF) was the selected for most of the experiments. Boiling at 253°C, it should convert to 1,3,5-TriMA, as depicted in Figure 1.

The PHF to 1,3,5-TriMA conversion process was largely absent over zeolite Beta, for reasons which will be discussed below. Dissolved at 10% in HDC heavy naphtha and processed over high-activity Pt/Beta at 265°C and 1.6 WHSV, the yield of MMA's based on PHF was less than 5%. (PHF was 100% converted.) The very small amount of new MMA's in the product had methyl or ethyl groups on non-bridgehead carbons, and little or none of the "end" product, 1,3,5-TriMA, was formed. A similarly low MMA yield was obtained with phenanthrene, a molecule which might be expected to hydrogenate and isomerize to 1,3,5,7-TetMA over a noble metal/zeolite catalyst.

Choice of zeolite. Beta was selected for the first experiments because it is a member of a class called "large-pore" zeolites (18), a class which includes zeolite Y. The Beta pores, like those of Y, are formed from 12-membered rings of linked silicon and aluminum oxide tetrahedra. The opening of those pores in Beta is an elliptical 6.4 x 7.6 Å, while those of Y are a circular 7.4 Å (19). Unsubstituted adamantane, a spherical molecule with a Van der Waals diameter of 7.4 Å, is known to penetrate the pores of zeolite Y (8), but should have difficulty penetrating Beta, whose critical pore dimension is only 6.4 Å. Thus Beta was the zeolite of choice for isolating adamantanes. It is noteworthy, with respect to this approach to adamantanes, that MMA's had been isolated earlier by hydrocracking narrow-boiling, laboratory crude extracts over 10% Pt-on-diatomite, at temperatures of about 430°C (20).

Zeolite Y, while also effective in isolating adamantanes, was much more effective than Beta in generating them, as shown by experiments with PHF. When the PHF experiment described earlier was repeated over Pd/Y at 590°C and 1.7 WHSV, the product contained 3.5% MMA's which, when corrected for the heavy naphtha contribution, represented an approximately 27% yield based on PHF. Gc-mass spec showed four new non-bridgehead products, all C13 MMA's, and 1,3,5-TriMA was enhanced in concentration relative to the other bridgehead isomers. PHF, a C13 molecule, was 100% converted.

The PHF experiments demonstrated size-selective differentiation between zeolites Y and Beta, and they strongly suggested that some portion of the adamantanes isolated from these refinery streams were formed in the HDC unit and were only being concentrated in the experiments with Pt and Pd/Beta.

Higher severe experiments with Pd/Beta further demonstrated the size-discriminating ability of this zeolite. When the contact time between HDC heavy naphtha and Pd/Beta was increased, the smallest of the MMA's were converted, namely, unsubstituted adamantane and 1-MA. The larger MMA's presumably could not enter the pores of zeolite Beta and were essentially unconverted. With Pd/Y, at the same HDC heavy naphtha conversion levels, the relative reactivity relationships were reversed. The larger MMA's were preferentially converted.

CONCLUSIONS

These results show that adamantanes, while present in crudes, can both be formed and concentrated in certain refinery operations, most notably in an HDC unit, and that their amount depends on crude source, catalyst, refinery configuration, and operating conditions. A level of some 10% adamantanes is not unexpected in the 175° - 260°C portion of the HDC recycle stream in a refinery sourced by heavy crude. These adamantanes can be isolated very effectively from such streams by mild hydrocracking over large-pore zeolite catalysts, such as zeolite Beta.

ACKNOWLEDGEMENTS

Special thanks go to W. Weimar and F. Daugherty for excellent laboratory assistance and to M. Granchi, B. Hagee, M. Nicholas, K. Peters, R. Quann, and W. Rogers for helpful input and advice. Samples of deep gas diamondoids were provided by C. Chen and D. Whitehurst.

REFERENCES

1. Landa, S., and Machacek, V., Coll. Czech. Chem. Comm., **5**, 1 (1933).
2. Schleyer, P. von R., J. Am. Chem. Soc., **79**, 3292 (1957).
3. Sokolova, I. M., Berman, S. S., Abryutina, N. N., and Petrov, A. A., Khim. Technol. Topl. Masel, **5**, 7 (1989). Chem. Abst., **111**, 81021.

4. Wingert, W. S., *Fuel*, **71**, 37 (1992).
5. Petrov, A. A., "Petroleum Hydrocarbons," (Springer-Verlag, Berlin, 1984) p. 93.
6. Fort, R. C., Jr., and Schleyer, P. von R., *Chem. Rev.*, **64**, 277 (1964).
7. Plate, A. F., Nikitina, Z. K., and Burtseva, T. A., *Neftekhimiya*, **1**, 599 (1961). *Chem. Abstr.*, **57**, 4938a.
8. Lau, G. C., and Maier, W. F., *Langmuir*, **3**, 164 (1987).
9. Schneider, A., Warren, R. W., and Janoski, E. J., *J. Am. Chem. Soc.*, **86**, 5365 (1964).
10. Schneider, A., Warren, R. W., and Janoski, E. J., in "Proceedings, 7th World Pet. Cong., Mexico City," **5**, 427 (1967).
11. Johnston, D. E., McKervey, M. A., and Rooney, J. J., *J. Am. Chem. Soc.*, **93**, 2798 (1971).
12. Bagni, E. I., and Sanin, P. I., US Patent 3,637,876 (January 25, 1972).
13. Landa, S., and Podrouzhkova, V., *Petrol. Chem. USSR*, **14**, 135 (1974).
14. Honna, K., Shimizu, N., and Kurisaki, K., US Patent 3,944,626 (March 16, 1976).
15. Wadlinger, R. L., Kerr, G. T., and Rosinski, E. J., US Patent 3,308,069 (1967).
16. Breck, D. W., "Zeolite Molecular Sieves," (R. F. Krieger, Malabar, FL, 1989) p. 507.
17. Tissot, B. P., and Welte, D. H., "Petroleum Formation and Occurrence," (Springer-Verlag, New York, ed. 2, 1984) p. 390.
18. Higgins, J. B., LaPierre, R. B., Schlenker, J. L., Rohrman, A. C., Wood, J. D., Kerr, G. T., and Rohrbaugh, W. J., *Zeolites*, **8**, 446 (1988).
19. Meier, W. M., and Olson, D. H., *Zeolites*, **12**, 1 (1992).
20. Yakubson, Z. V., Arefev, O. A., and Petrov, A. A., *Neftekhimiya*, **13**, 345 (1973). *Chem. Abstr.*, **79**, 116756.

Table 1.
Boiling ranges and three-ring naphthene (3RN) contents of
refinery streams tested for adamantanes.

<u>Stream</u>	<u>Boiling Range, °C</u>	<u>3RN *</u>
Heavy crude HDC recycle stream	175 - 375	24
Fraction boiling below 260° (46 %)	175 - 260	28
Heavy crude HDC heavy naphtha	135 - 210	1.2
Heavy crude hydrotreated kerosene	120 - 245	0.6
Light crude HDC recycle stream	175 - 290	3.4

* By mass spectrometry

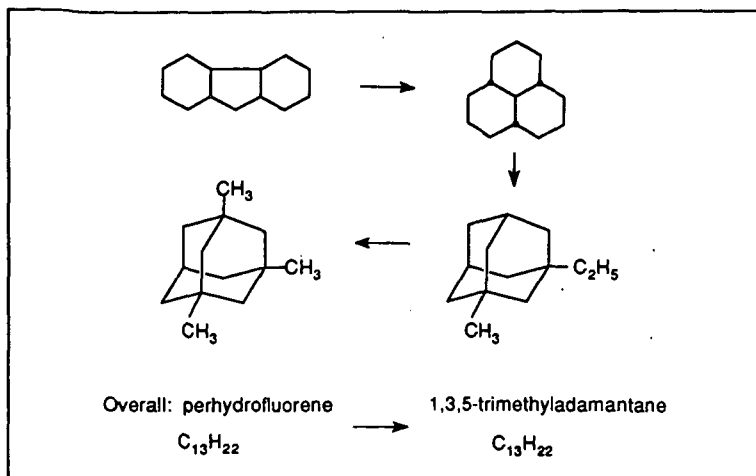


Figure 1. A simplified reaction scheme for the preparation of 1,3,5-trimethyladamantane from perhydrofluorene (10).

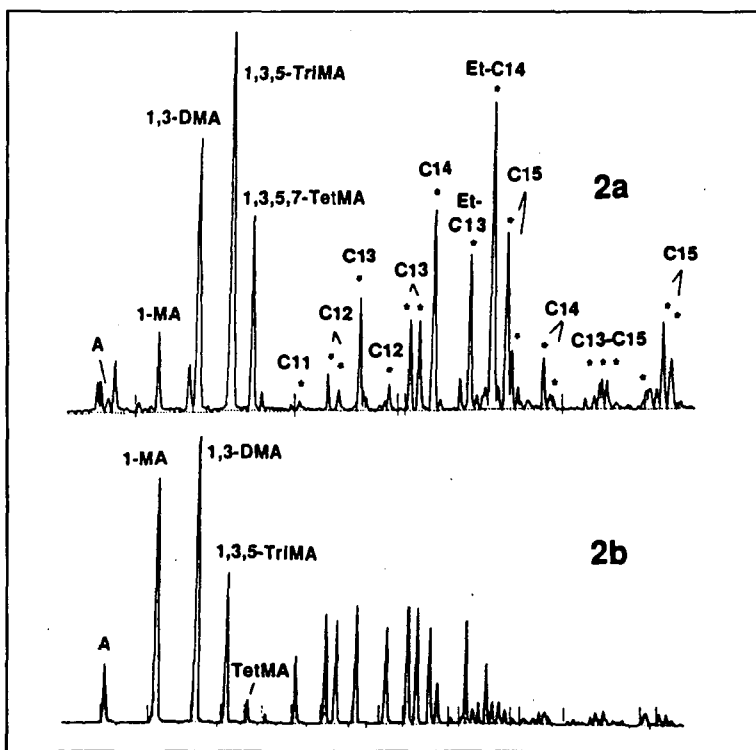


Figure 2. (a) Gc trace showing adamantanes isolated from 175° - 375°C heavy crude HDC recycle by processing over Pt/Beta. (b) Adamantanes recovered from a deep gas condensate. Asterisks in 2a indicate peaks which match those in 2b and which have MMA molecular weights by gc-mass spec.

ZEOLITE-CATALYZED CONFORMATIONAL ISOMERIZATION OF *cis*-DECAHYDRONAPHTHALENE. REACTION PATHWAYS AND KINETICS.

Wei-Chuan Lai and Chunshan Song*

Fuel Science Program, 209 Academic Projects Building,
The Pennsylvania State University, University Park, Pennsylvania 16802, U.S.A.

Keywords: Zeolites, isomerization, decahydronaphthalene, kinetics

INTRODUCTION

It was shown in literature that decalin (DHN) may be one of the potential endothermic jet fuels that can serve as the primary heat sink to cool the hot surfaces and system components [Donath and Hess, 1960; Lander and Nixon, 1987; Taylor and Rubey, 1987]. Commercial decalin solvents from industrial hydrogenation processes consist of almost equimolar mixtures of *cis*- and *trans*-DHN. Although the physical properties of these two isomers are similar, their chemical properties are different. One example is their difference in thermal stability at high temperatures. We have previously shown that as jet fuel components, *trans*-DHN is superior to *cis*-DHN for high temperature application because the former is much more stable at high temperatures [Song et al., 1992]. The excellent thermal stability at high temperatures is desirable for future high Mach aircraft. Besides, *trans*-DHN has the desirable ability of inhibiting the solid deposit formation from jet fuels and their components at high temperatures [Song et al., 1994a]. For example, adding 50 vol% *trans*-DHN to a JP-8P fuel, *n*-tetradecane, and *n*-butylbenzene thermally stressed at 723 K for 4 h significantly reduced the deposit formation from 3.1 to 0.1 wt%, from 3.0 to 0.1 wt%, and from 5.6 to 0.0 wt%, respectively. Although *cis*-DHN also has some potential industrial applications, it is desirable to convert *cis*-DHN to *trans*-DHN for fuel stability consideration at high temperatures.

There has been much research on the catalytic hydrocracking or dehydrogenation of decalin under high pressures and at temperatures generally in excess of 673 K [Ritchie and Nixon, 1967; Shabtai et al., 1979; Constant et al., 1986; Mostad et al., 1990a,b; Nimz, 1990; Sousa-Aguiar et al., 1994]. However, relatively little information about the conformational isomerization of *cis*-DHN into *trans*-DHN at lower temperatures is available. Petrov et al. (1977) reported the isomerization of *cis*- and *trans*-DHN on a nickel catalyst in the temperature range of 393-453 K. They claimed that the isomerization took place only in the presence of hydrogen. Our earlier exploratory work has shown that some mordenites and chemically modified zeolites may promote the isomerization of *cis*-DHN into *trans*-DHN at 523 K for 2 h under N₂ environment [Song and Moffatt, 1993, 1994]. This work extended previous exploratory studies on the catalytic isomerization of *cis*-DHN to *trans*-DHN. The objective of this work is to examine the effects of reaction conditions as well as catalyst properties on the catalytic reaction. An overall kinetic model for the catalytic reaction was proposed and empirical equations were presented to predict the selectivity.

EXPERIMENTAL

The chemicals, *cis*-DHN, *trans*-DHN, and DHN (an almost equimolar mixture of *cis*- and *trans*-DHN) were obtained from Aldrich Chemical Company and were used as received. Their purities (>99%) were analyzed in our laboratory using gas chromatography (GC) and gas chromatography-mass spectrometry (GC-MS). The six catalysts used in the catalytic isomerization reactions include: a hydrogen Y zeolite (HY), a metal ion-exchanged Y zeolite (LaHY), a hydrogen mordenite (HM30A), and three noble metal loaded mordenites (Pt/HM30A, Pd/HM30A, and Pt/HM20A). The noble metal loaded mordenites were prepared by dispersing the salt of platinum or palladium into the mordenites by incipient wetness impregnation method. The noble metal loading on the support was kept at nominally 6 wt%. The details of the preparation and properties of the catalysts are described elsewhere [Song and Moffatt, 1994; Schmitz et al., 1994].

Catalytic isomerization reactions were carried out in 28-mL horizontal type stainless steel tubing bomb reactors, which were charged with 1 g of *cis*-DHN, *trans*-DHN, or DHN (7.23 mmol) and 0.2 g of catalyst, at 473-548 K for 0.15-8 h under an initial pressure of 0.79 MPa UHP N₂ or H₂. The reactor was agitated vertically at 240 cycles/min to ensure the uniformity of concentration and temperature inside the reactor. After the reaction, the gas products were collected in a gas bag and were quantitatively analyzed using a Perkin-Elmer Autosystem GC equipped with two detectors, a thermal conductivity detector (TCD) and a flame ionization detector (FID). The liquid products were recovered by washing with acetone and were analyzed on an HP 5890II GC coupled with an HP 5971A Mass Selective Detector (MSD) and quantified by a Perkin-Elmer GC 8500 equipped with an FID. The catalyst was recovered and stored in a vial for thermogravimetric analysis performed later. More analytical details may be found elsewhere [Song et al., 1994b].

RESULTS AND DISCUSSION

Calculated composition of equilibria. The equilibrium compositions of *trans*-DHN and *cis*-DHN at several temperatures were calculated to establish the theoretical upper limit of the catalytic conversion. The equilibrium constant (*K*) is related to the Gibbs energy change (ΔG^0) by Eq. (1)

$$\ln K = -\frac{\Delta G^0}{RT} \quad (1)$$

Using the data in Reid et al. (1987) for a binary mixture system of *cis*-DHN and *trans*-DHN, we have determined the general expression for the equilibrium constant as a function of temperature as shown in Eq. (2)

$$R \ln K = \frac{15370}{T} + 14.83 \ln T - 0.0365 T + 1.885 \times 10^{-5} T^2 - 4.49 \times 10^{-9} T^3 - 85.2 \quad (2)$$

where R is the gas constant (8.314 J/mol-K) and T is the temperature in K. The computed heat of reaction, equilibrium constant, and composition are shown in Table 1. It should be noticed that because of the exponential nature of Equation 1, the calculated results highly depend on the thermodynamic parameters used. For example, if the Gibbs energy was off by just 5-10%, the estimation error for the equilibrium constant at 473 K may be as large as 16-35%. The calculated mixture compositions will be compared with experimental data following the presentation of experimental results.

Effectiveness of zeolitic catalysts. Table 2 shows the products distribution from catalyzed isomerization of *cis*-DHN using 1-g commercial DHN (an almost equimolar mixture of *cis*- and *trans*-isomers) as starting reactant at 473 or 523 K under an initial pressure of 0.79 MPa UHP H_2 or N_2 . Pt- and Pd-loaded mordenites, i.e., Pt/HM30A, Pt/HM20A, and Pd/HM30A, are very effective catalysts under H_2 atmosphere for the conformational isomerization of *cis*-DHN to *trans*-DHN even at low temperature, 473 K. The conversion selectivity towards *trans*-DHN reached nearly 100%; in other words, there were almost no side-products accompanying the isomerization. Take Pt/HM30A as an example. The experimental final product composition of 92.3% *trans*-DHN and 7.3% *cis*-DHN at 473 K as shown in Table 2 is very close to the calculated equilibrium composition (95.3% *trans*-DHN, 4.7% *cis*-DHN), which is shown in Table 1. Although Pt- and Pd-loaded mordenites were effective catalysts under H_2 atmosphere, they became less effective under N_2 atmosphere (see Table 2). Pt/HM30A is a better catalyst than Pd/HM30A at 473 K under N_2 atmosphere in terms of conversion and *trans*-DHN selectivity although they are almost equally effective under H_2 . It is interesting to look at the yield change of tetralin, which initially existed as an impurity (0.7 wt%), under different gas environment. Tetralin was completely hydrogenated into decalin under H_2 environment because of the hydrogenation ability of Pt and Pd. On the other hand, the noble metals under N_2 served to dehydrogenate the decalin to tetralin and thus increased the yield of tetralin.

For the other three catalysts studied, HY, LaHY, and HM30A, they are much less effective than Pt- and Pd-loaded mordenites, and do not react at all at 473 K. It is also interesting to note that although the effectiveness of Pt- and Pd-loaded mordenites depends on the gas environment (H_2 or N_2), H_2 has no impact on the performance of LaHY. The data in Table 3 seems to show that the hydrogen Y zeolite (HY) performed about as well as the metal ion-exchanged Y zeolite (LaHY), and HM30A is the least effective one among the catalysts studied.

Reaction pathways and kinetic data. We further investigated the performance of LaHY and HY intending to get the kinetic data. These isomerization reactions were carried out using 1 g of *cis*-DHN instead of DHN mixture, and 0.2 g of catalyst, at 508-548 K for 0.15-8 h under an initial pressure of 0.79 MPa UHP N_2 . The experimental results are shown in Table 3. Isomerization is the dominant reaction under the conditions employed. The dominant products are two types of isomers: *trans*-DHN (from conformational isomerization) with as high as 81% selectivity (defined as the ratio of molar yield of the product to the conversion), and other decalin isomers from ring-opening or ring-contraction isomerization. Although cracking products are not shown in Table 3, they are in general small (less than 4% selectivity) except under severe conditions such as at 538-548 K for 1 h. There was no apparent dehydrogenation reaction from decalin to tetralin observed judging from the gradually decreasing yield of tetralin, which initially existed as an impurity in *cis*-DHN (0.27 wt%).

Figure 1 presents the *trans*-DHN selectivity vs *cis*-DHN conversion plots for LaHY and HY catalysts at four different temperatures. There are a few features that may be pointed out from examining Table 3 and Figure 1. First, the more complete data in Table 3 seem to indicate that HY performs slightly better than LaHY in terms of criteria such as activity and selectivity. This observation is somewhat different from what we said earlier that they perform equally well judging from the data in Table 2 where commercial decalin was used as the starting material. Second, selectivity towards *trans*-DHN decreases with increasing temperature. This is not unexpected since the isomerization from *cis*-DHN to *trans*-DHN is exothermic, 13212 J/mol (95 J/g or 3.16 kcal/mol) at 523 K (our calculation in Table 1). Third, the product (*trans*-DHN) selectivity decreases with increasing conversion level under isothermal condition, and displays a concave downward behavior, which could be empirically fitted by a second degree polynomial as demonstrated later. The trend of selectivity vs conversion in Figure 1 provided useful information about the reaction pathways. It implied that the reactions proceeded through a parallel-consecutive network [Bond, 1987].

Based on the previous observations, a simple reaction pathway model for the catalytic reaction of *cis*-DHN to products was proposed. It should be noted that readers interested in more detailed mechanisms from *cis* to *trans* isomers may refer to the review by Weitkamp (1968). The overall reaction is modeled as the parallel-consecutive kinetic scheme shown in Figure 2. The isomerization between *cis*- and *trans*-DHN was known to be a reversible process; thus the interconversion between them was also included in Figure 2. However, our experimental data using both *cis*- and *trans*-DHN have shown that the forward reaction from *cis*- to *trans*-DHN is much faster than the backward reaction, i.e., $k_1 \gg k_{-1}$. In addition, for the reaction conditions studied, the reactions were taken to be approximately first order. With these assumptions, the rate equations may be written as the following:

$$\frac{dA}{dt} = -(k_1 + k_2) A \quad (3)$$

$$\frac{dB}{dt} = k_1 A - k_3 B \quad (4)$$

$$\frac{dC}{dt} = k_2 A + k_3 B \quad (5)$$

Equations 3-5 may be solved to give

$$A/A_0 = \exp [-(k_1+k_2) t] = \exp [-k t] \quad (6)$$

$$B/A_0 = [k_1/(k_1+k_2-k_3)] [\exp (-k_3 t) - \exp (-k t)] \quad (7)$$

$$C = A_0 - A - B \quad (8)$$

Because we are mainly interested in the yield of *trans*-DHN and only limited data are available in the current work, we did not intend to find all the kinetic parameters. Instead, we used the experimental data to find the lumped rate constant k (equal to k_1+k_2 in Eq. 6) and then developed empirical equations to predict the product yield of *trans*-DHN. The procedures are described as follows. First, the rate constant k was determined by using Eq. (6) for all the experiments shown in Table 3. Then, the rate constant (k) was correlated by the Arrhenius law as shown in Eq. (9)

$$k = A^* e^{-E_a/RT} \quad (9)$$

where A^* (h^{-1}) is the frequency (or preexponential) factor, E_a is the apparent activation energy (kcal/mol), and R is the gas constant ($\text{kcal mol}^{-1} \text{K}^{-1}$). The E_a and A values determined from Arrhenius plots are as follows:

$$\text{for HY} \quad E_a = 49.9 \text{ kcal/mol} \quad \text{and} \quad A^* = 6.03 \times 10^{20} \text{ h}^{-1} \quad (10)$$

$$\text{for LaHY} \quad E_a = 54.6 \text{ kcal/mol} \quad \text{and} \quad A^* = 3.36 \times 10^{22} \text{ h}^{-1} \quad (11)$$

Third, empirical equations were developed to predict the product yield of *trans*-DHN. Based on the results in Figure 1, we proposed that the selectivity of *trans*-DHN could be presented by a second degree polynomial as shown in Eq. (12)

$$\text{Selectivity of } \textit{trans}\text{-DHN} = a_1 + a_2 X + a_3 X^2 + a_4 T + a_5 X T \quad (12)$$

where X is the *cis*-DHN conversion, T is the temperature in K, and a_i ($i=1,\dots,5$) are the empirical parameters to be found. Using the data in Table 3, we have determined the parameters a_i as follows:

$$\text{for HY} \quad \text{Sel.} = 1.938 + 0.779 X - 0.285 X^2 - 0.00228 T - 0.0012 X T \quad (13)$$

$$\text{for LaHY} \quad \text{Sel.} = 1.534 + 2.745 X - 0.082 X^2 - 0.00146 T - 0.0054 X T \quad (14)$$

In order to check the reliability of these equations in predicting the conversion and selectivity, predictions based on equations 6, 10, 11, 13, and 14 are compared with experimental results. Figures 3 and 4, respectively compare the experimental selectivity and yield of *trans*-DHN to the values predicted from the empirical equations for both catalysts. The line corresponding to exact agreement is drawn as a diagonal. It is clear from Figures 3 and 4 that the predicted values are generally in good agreement with experimental values over a wide range of conversion.

SUMMARY

This work presented some exploratory studies on the effects of reaction conditions as well as catalyst properties on the catalytic isomerization of *cis*-DHN to *trans*-DHN. The theoretical equilibrium compositions of *trans*-DHN and *cis*-DHN at several temperatures were calculated and compared with experimental data. The catalytic reactions were studied under N_2 or H_2 environment using HY, LaHY, HM30A, Pt/HM30A, Pd/HM30A, and Pt/HM20A. Pt- and Pd-loaded mordenites are very effective catalysts under H_2 atmosphere for the conformational isomerization of *cis*-DHN to *trans*-DHN at 473 K; however, they are less effective under N_2 atmosphere. Pt/HM30A is a better catalyst than Pd/HM30A at 473 K under N_2 atmosphere in terms of conversion and *trans*-DHN selectivity although they are almost equally effective under H_2 . HY, LaHY, and HM30A are much less effective than Pt- and Pd-loaded mordenites, and their performance was not affected by H_2 . Besides, they do not react at all at 473 K. HY performs slightly better than LaHY, and HM30A is the least effective one among the catalysts studied. Selectivity towards *trans*-DHN decreases with both increasing temperature and increasing conversion level (under isothermal condition). A simple reaction pathways model containing parallel-consecutive kinetic scheme was proposed. The E_a and A^* values for the *cis*-DHN conversion were determined from Arrhenius plots. Empirical equations capable of predicting product yields were also developed. In short, equations 6, 10, 11, 13, and 14 may be used to predict reaction conversion and major products.

ACKNOWLEDGMENTS

We are grateful to Prof. H. H. Schobert and Prof. P. B. Weisz for their encouragement and support, and to Ms. Cindy Chan of PSU for carrying out many of the catalytic experiments. Funding was provided by U.S. Department of Energy and U.S. Air Force. We wish to thank Mr. W. E. Harrison III of USAF and Dr. S. Rogers of DOE for their support.

REFERENCES

- Bond, G. C. *Heterogeneous Catalysis: Principles and Applications*. Second Edition. 1987, Oxford University Press: Oxford, pp 52-53.
- Constant, W. D.; Price, G. L.; McLaughlin, E. *Fuel* **1986**, 65, 8-16.
- Donath, E. E.; Hess, M. *Chemical Engineering Progress*. April 1960, 56 (4), 68-71.
- Lander, H. R.; Nixon, A. C. *Prepr.-Am. Chem. Soc., Div. Pet. Chem.* **1987**, 32 (2), 504-511.
- Mostad, H. B.; Riis, T. U.; Ellestad, O. H. *Applied Catalysis* **1990a**, 58, 105-117.
- Mostad, H. B.; Riis, T. U.; Ellestad, O. H. *Applied Catalysis* **1990b**, 63, 345-364.
- Nimz, M. *Zeolites* **1990**, 10, 297-300.
- Petrov, L.; Angelova, L.; Shopov, D. *Bokl. Bolg. Akad. Nauk* **1977**, 30 (1), 85-88.
- Reid, R. C.; Prausnitz, J. M.; Poling, B. E. *The Properties of Gases & Liquids*. Fourth Edition. 1987, McGraw-Hill Book Company: New York, N.Y.
- Ritchie, A. W.; Nixon, A. C. *Prepr.-Am. Chem. Soc., Div. Pet. Chem.* **1967**, 12 (3), 117.
- Roberts, R. M.; Madison, J. J. *J. Am. Chem. Soc.* **1959**, 81, 5839-5839.
- Schmitz, A. D.; Bowers, G.; Song, C. In *Advanced Thermally Stable Jet Fuels*. Technical Report, U.S. Department of Energy, DE-FG22-92PC92104-TPR-9, October 1994, H. H. Schobert et al., Eds., pp37-42.
- Shabtai, J.; Ramakrishnan, R.; Oblad, A. G. In *Thermal Hydrocarbon Chemistry*; Oblad, A. G.; Davis, H. G.; Eddinger, R. T., Eds.; Advances in Chemistry Series 183; American Chemical Society: Washington, D. C., **1979**; pp 297-328.
- Song, C.; Lai, W.-C.; Schobert, H. H. *Prepr.-Am. Chem. Soc., Div. Fuel Chem.* **1992**, 37 (4), 1655-1663.
- Song, C.; Moffatt, K. *Prepr.-Am. Chem. Soc., Div. Pet. Chem.* **1993**, 38 (4), 779-783.
- Song, C.; Lai, W.-C.; Schobert, H. H. *Ind. Eng. Chem. Res.* **1994a**, 33, 548-557.
- Song, C.; Lai, W.-C.; Schobert, H. H. *Ind. Eng. Chem. Res.* **1994b**, 33, 534-547.
- Song, C.; Moffatt, K. *Microporous Materials* **1994**, 2, 459-466.
- Sousa-Aguiar, E. F.; Pinhel da Silva, M.; Murta Valle, M. L.; Forte da Silva, D. *Prepr.-Am. Chem. Soc., Div. Pet. Chem.* **1994**, 39 (3), 356-359.
- Taylor, P. H.; Rubey, W. A. *Prepr.-Am. Chem. Soc., Div. Pet. Chem.* **1987**, 32 (2), 521-525.
- Weitkamp, A. W. In *Advances in catalysis and Related Subjects*. D. D. Eley, H. Pines, and P. B. Weisz, Eds. Academic Press: New York and London. **1968**, Volume 18, pp1-110.

Table 1. Calculated heat of reaction, equilibrium constant and composition for a binary mixture system of *cis*-decalin and *trans*-decalin

Temperature (K)	Heat of reaction ΔH (J/mol)	Equilibrium constant ^a	Composition (wt %)	
			<i>cis</i> -DHN	<i>trans</i> -DHN
473	-13205.8	20.5	4.65%	95.35%
508	-13210.1	16.3	5.79%	94.21%
523	-13212.0	14.9	6.30%	93.70%
538	-13213.7	13.7	6.82%	93.18%
548	-13214.6	12.9	7.17%	92.83%
573	-13215.7	11.4	8.06%	91.94%
623	-13210.6	9.1	9.87%	90.13%
673	-13192.9	7.6	11.69%	88.31%
723	-13160.2	6.4	13.48%	86.52%

a) Equilibrium constant for the reaction: *cis*-DHN \leftrightarrow *trans*-DHN

$$K = \frac{[\text{trans-DHN}]}{[\text{cis-DHN}]}$$

Table 2. Catalyzed isomerization of *cis*-decalin (starting reactant is 1-g commercial decalin) under an initial pressure of 0.79 MPa UHP H₂ or N₂

Catalyst type	Temp. (K)	Time (h)	Gas	Product (wt % of feed)				<i>trans/cis</i> ratio	X ^c (%)	Sel. ^d
				<i>trans</i> -DHN	<i>cis</i> -DHN	Tetralin	Others ^b			
		0.0 ^a		48.34	50.62	0.70	0.34			
Pt/HM30A	473	2.0	H ₂	92.34	7.25	0	0.41	12.7	43.4	1.00
Pd/HM30A	473	2.0	H ₂	92.31	7.23	0	0.46	12.8	43.4	1.00
Pt/HM20A	473	8.0	H ₂	91.50	7.95	0	0.55	11.5	42.7	1.00
Pt/HM30A	473	2.0	N ₂	62.40	33.46	2.26	1.88	1.9	17.2	0.82
Pd/HM30A	473	2.0	N ₂	54.50	42.43	1.84	1.23	1.3	8.2	0.75
LaHY	473	2.0	N ₂	48.29	50.73	0.68	0.30	0.95	0	-
HY	523	2.0	N ₂	65.92	19.04	0.60	14.44	3.5	31.6	0.56
LaHY	523	2.0	N ₂	65.15	18.82	0.61	15.42	3.5	31.8	0.53
LaHY	523	2.0	H ₂	65.79	16.73	0.59	16.89	3.9	33.9	0.52
HM30A	523	2.0	N ₂	53.02	31.60	0.38	15.00	1.7	19.0	0.25

a) This row presents the purity of as-received commercial decalin including 0.34% *n*-decane.

b) Unreacted *n*-decane plus products of ring-contraction and ring-opening reactions.

c) Conversion of *cis*-decalin (weight % of feed).

d) Selectivity to *trans*-decalin, defined as a fraction of *cis*-decalin conversion.

Table 3. Catalyzed isomerization of *cis*-decalin (starting reactant is 1-*g* *cis*-decalin) under an initial pressure of 0.79 MPa UHP N₂

Catalyst: 0.2 g of LaHY													
temperature (K)	508	508	508	508	523	523	523	523	538	538	538	548	548
residence time ^a (min)	60	120	240	480	30	60	120	120	9	18	60	9	18
reaction time ^b (min)	54	114	234	474	25	55	115	115	4	13	55	5	14
product yield ^c (wt %)													
<i>trans</i> -DHN	7.4	11.5	22.7	43.0	20.4	29.0	47.7	46.3	11.7	32.7	50.4	24.2	37.9
<i>cis</i> -DHN	90.5	85.2	70.8	42.8	72.0	60.1	29.4	32.5	83.5	51.4	10.2	61.2	31.2
<i>trans</i> -/ <i>cis</i> -DHN ratio	0.08	0.13	0.32	1.00	0.28	0.48	1.62	1.42	0.14	0.64	4.94	0.40	1.21
<i>cis</i> -DHN conversion ^c	9.1	14.4	28.8	56.8	27.6	39.5	70.2	67.1	16.1	48.2	89.4	38.4	68.4
rate constant, <i>k</i> (h ⁻¹)	0.11	0.08	0.09	0.11	0.78	0.55	0.63	0.58	2.62	3.02	2.45	5.83	4.92
<i>trans</i> -DHN selectivity	0.80	0.79	0.79	0.76	0.73	0.73	0.68	0.69	0.72	0.68	0.56	0.63	0.55

Catalyst: 0.2 g of HY													
temperature (K)	508	508	508	523	523	523	538	538	538	538	548	548	548
residence time ^a (min)	120	240	480	30	60	120	9	18	30	60	9	18	30
reaction time ^b (min)	114	234	474	25	55	115	4	13	25	55	5	14	26
product yield ^c (wt %)													
<i>trans</i> -DHN	21.1	47.6	57.0	23.1	46.1	52.7	20.7	34.6	51.9	54.5	35.8	47.8	50.3
<i>cis</i> -DHN	73.9	37.8	23.0	69.3	36.8	25.6	71.6	51.1	19.4	7.4	45.9	23.1	10.2
<i>trans</i> -/ <i>cis</i> -DHN ratio	0.28	1.26	2.48	0.33	1.25	2.06	0.29	0.68	2.67	7.35	0.78	2.07	4.93
<i>cis</i> -DHN conversion ^c	25.8	61.8	76.6	30.3	62.9	74.0	28.0	48.5	80.3	92.2	53.7	76.5	89.4
rate constant, <i>k</i> (h ⁻¹)	0.16	0.25	0.18	0.87	1.08	0.70	4.91	3.06	3.89	2.78	9.16	6.19	5.17
<i>trans</i> -DHN selectivity	0.81	0.77	0.74	0.76	0.73	0.71	0.73	0.71	0.64	0.59	0.67	0.62	0.56

a) Reactor residence time in sand bath preheated to reaction temperature.

b) Corrected reaction time (reactor residence time minus heat-up time).

c) Based on the initial amount of *cis*-DHN.

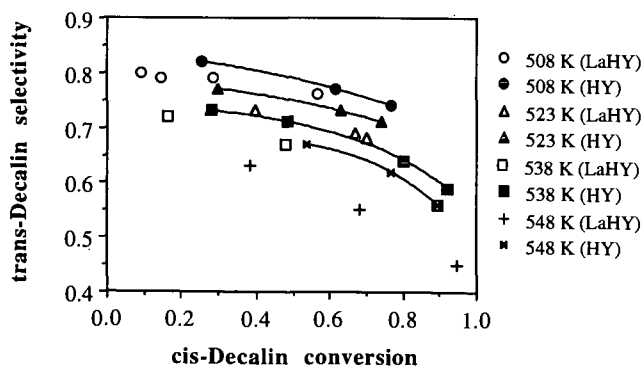


Figure 1. *trans*-Decalin selectivity vs *cis*-decalin conversion plots for LaHY and HY catalysts at four different temperatures.

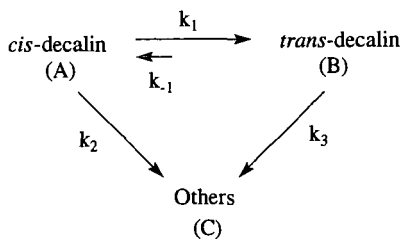


Figure 2. Proposed overall reaction pathways for the catalytic reaction of *cis*-decalin.

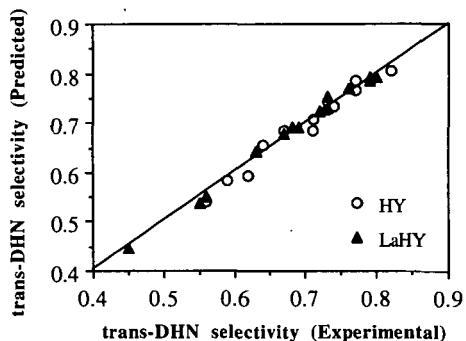


Figure 3. Predicted versus measured values of *trans*-decalin selectivity for the catalytic isomerization of *cis*-decalin using HY and LaHY at 508-548 K for 9-480 min.

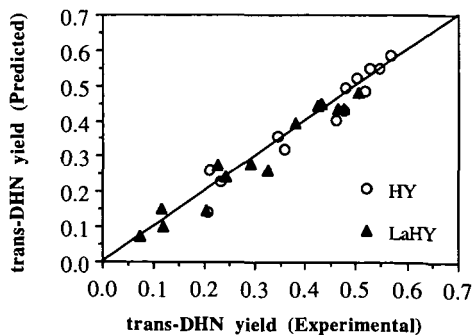


Figure 4. Predicted versus measured values of *trans*-decalin yield for the catalytic isomerization of *cis*-decalin using HY and LaHY at 508-548 K for 9-480 min.